Enclosure 5 to TN E-28473

Non-proprietary Versions of
SAR Appendix B Drawings,
SAR Appendix B.2.13.11, and
SAR Chapters B.3, B.5, and B6

NON-PROPRIETARY

AREVA

TRANSNUCLEAR INC.

NUHOMS®-MP197 TRANSPORT PACKAGING SAFETY ANALYSIS REPORT

Revision 7

TRANSNUCLEAR INC.
7135 Minstrel Way • Suite 300 • Columbia, MD 21045

PROPRIETARY AND SECURITY RELATED INFORMATION WITHHELD UNDER 10 CFR 2.390

ALL DIMENSIONS ARE NOMINAL UNLESS A SPECIFIC TOLERANCE IS INDICATED WITH THE DRAWING DIMENSION

DIMENSIONS ARE IN INCHES AND DEGREES UNLESS OTHERWISE SPECIFIED. DIMENSIONING IN ACCORDANCE WITH ASME Y14.5M.

INTERPRET WELD SYMBOLS PER ANSI / AWS 2.4

U.S. Patent No. 4,780,269
Transnuclear, Inc.

TRANSNUCLEAR
AN AREVA COMPANY

SAFETY ANALYSIS REPORT
TN TAD
TRANSPORTATION OVERPACK
TRANSPORT CONFIGURATION

DRAWING NO.	SCALE	SHEET	REVISION
TNTAD-TO -71-1	NONE	1 OF 2	0

PROPRIETARY AND SECURITY RELATED INFORMATION WITHHELD UNDER 10 CFR 2.390

PROPRIETARY AND SECURITY RELATED INFORMATION WITHHELD UNDER 10 CFR 2.390

ALL DIMENSIONS ARE NOMINAL UNLESS A SPECIFIC TOLERANCE IS INDICATED WITH THE DRAWING DIMENSION

DIMENSIONS ARE IN INCHES AND DEGREES UNLESS OTHERWISE SPECIFIED. DIMENSIONING IN ACCORDANCE WITH ASME Y14.5M.

INTERPRET WELD SYMBOLS PER ANSI / AWS 2.4

U.S. Patent No. 4,780,269
Transnuclear, Inc.

TRANSNUCLEAR
AN AREVA COMPANY

SAFETY ANALYSIS REPORT
TN TAD
TRANSPORTATION OVERPACK
PARTS LIST

DRAWING NO.	SCALE	SHEET	REVISION
TNTAD-TO -71-2	NONE	1 OF 2	

DRAWING NO. TNTAD-TO -71-2 SHEET 1 OF 2

PROPRIETARY AND SECURITY RELATED INFORMATION WITHHELD UNDER 10 CFR 2.390

PROPRIETARY AND SECURITY RELATED INFORMATION WITHHELD UNDER 10 CFR 2.390

ALL DIMENSIONS ARE NOMINAL UNLESS A SPECIFIC TOLERANCE IS INDICATED WITH THE DRAWING DIMENSION

DIMENSIONS ARE IN INCHES AND DEGREES UNLESS OTHERWISE SPECIFIED. DIMENSIONING IN ACCORDANCE WITH ASME Y14.5M.

INTERPRET WELD SYMBOLS PER ANSI / AWS 2.4

U.S. Patent No. 4,780,269
Transnuclear, Inc.

TRANSNUCLEAR
AN AREVA COMPANY

SAFETY ANALYSIS REPORT
TN TAD
TRANSPORTATION OVERPACK
GENERAL ARRANGEMENT

DRAWING NO.	SCALE	SHEET	REVISION
TNTAD-TO -71-3	NONE	1 OF 1	0

PROPRIETARY AND SECURITY RELATED INFORMATION WITHHELD UNDER 10 CFR 2.390

ALL DIMENSIONS ARE NOMINAL UNLESS A SPECIFIC TOLERANCE IS INDICATED WITH THE DRAWING DIMENSION

DIMENSIONS ARE IN INCHES AND DEGREES UNLESS OTHERWISE SPECIFIED. DIMENSIONING IN ACCORDANCE WITH ASME Y14.5M.

INTERPRET WELD SYMBOLS PER ANSI / AWS 2.4

U.S. Patent No. 4,780,269
Transnuclear, Inc.

TRANSNUCLEAR
AN AREVA COMPANY

SAFETY ANALYSIS REPORT
TN TAD
TRANSPORTATION OVERPACK
CASK BODY ASSEMBLY

DRAWING NO.	SCALE	SHEET	REVISION
TNTAD–TO –71–4	NONE	1 OF 1	0

PROPRIETARY AND SECURITY RELATED INFORMATION WITHHELD UNDER 10 CFR 2.390

ALL DIMENSIONS ARE NOMINAL UNLESS A SPECIFIC TOLERANCE IS INDICATED WITH THE DRAWING DIMENSION

DIMENSIONS ARE IN INCHES AND DEGREES UNLESS OTHERWISE SPECIFIED. DIMENSIONING IN ACCORDANCE WITH ASME Y14.5M.

INTERPRET WELD SYMBOLS PER ANSI / AWS 2.4

U.S. Patent No. 4,780,269
Transnuclear, Inc.

TRANSNUCLEAR
AN AREVA COMPANY

SAFETY ANALYSIS REPORT
TN TAD
TRANSPORTATION OVERPACK
CASK BODY DETAILS

DRAWING NO.	SCALE	SHEET	REVISION
TNTAD–TO –71–5	NONE	1 OF 4	0

PROPRIETARY AND SECURITY RELATED INFORMATION WITHHELD UNDER 10 CFR 2.390

PROPRIETARY AND SECURITY RELATED INFORMATION WITHHELD UNDER 10 CFR 2.390

PROPRIETARY AND SECURITY RELATED INFORMATION WITHHELD UNDER 10 CFR 2.390

PROPRIETARY AND SECURITY RELATED INFORMATION WITHHELD UNDER 10 CFR 2.390

ALL DIMENSIONS ARE NOMINAL UNLESS A SPECIFIC TOLERANCE IS INDICATED WITH THE DRAWING DIMENSION

DIMENSIONS ARE IN INCHES AND DEGREES UNLESS OTHERWISE SPECIFIED. DIMENSIONING IN ACCORDANCE WITH ASME Y14.5M.

INTERPRET WELD SYMBOLS PER ANSI / AWS 2.4

U.S. Patent No. 4,780,269
Transnuclear, Inc.

This drawing may not be disclosed to others in whole or in part, nor used for other than the transaction for which it was provided to Transnuclear, Inc.

TRANSNUCLEAR
AN AREVA COMPANY

SAFETY ANALYSIS REPORT
TN TAD
TRANSPORTATION OVERPACK
LID ASSEMBLY & DETAILS

DRAWING NO.	SCALE	SHEET	REVISION
TNTAD-TO-71-6	NONE	1 OF 1	0

PROPRIETARY AND SECURITY RELATED INFORMATION WITHHELD UNDER 10 CFR 2.390

ALL DIMENSIONS ARE NOMINAL UNLESS A SPECIFIC TOLERANCE IS INDICATED WITH THE DRAWING DIMENSION

DIMENSIONS ARE IN INCHES AND DEGREES UNLESS OTHERWISE SPECIFIED. DIMENSIONING IN ACCORDANCE WITH ASME Y14.5M.

INTERPRET WELD SYMBOLS PER ANSI / AWS 2.4

U.S. Patent No. 4,780,269
Transnuclear, Inc.

TRANSNUCLEAR
AN AREVA COMPANY

SAFETY ANALYSIS REPORT
TN TAD
TRANSPORTATION OVERPACK
REGULATORY PLATE .

DRAWING NO.	SCALE	SHEET	REVISION
TNTAD-TO -71-7	NONE	1 OF 1	0

PROPRIETARY AND SECURITY RELATED INFORMATION WITHHELD UNDER 10 CFR 2.390

ALL DIMENSIONS ARE NOMINAL UNLESS A SPECIFIC TOLERANCE IS INDICATED WITH THE DRAWING DIMENSION

DIMENSIONS ARE IN INCHES AND DEGREES UNLESS OTHERWISE SPECIFIED. DIMENSIONING IN ACCORDANCE WITH ASME Y14.5M.

INTERPRET WELD SYMBOLS PER ANSI / AWS 2.4

U.S. Patent No. 4,780,269
Transnuclear, Inc.

TRANSNUCLEAR
AN AREVA COMPANY

SAFETY ANALYSIS REPORT
TN TAD
TRANSPORTATION OVERPACK
IMPACT LIMITER ASSEMBLY

DRAWING NO.	SCALE	SHEET	REVISION
TNTAD–TO –71–8	NONE	1 OF 1	0

PROPRIETARY AND SECURITY RELATED INFORMATION WITHHELD UNDER 10 CFR 2.390

ALL DIMENSIONS ARE NOMINAL UNLESS A SPECIFIC TOLERANCE IS INDICATED WITH THE DRAWING DIMENSION

DIMENSIONS ARE IN INCHES AND DEGREES UNLESS OTHERWISE SPECIFIED. DIMENSIONING IN ACCORDANCE WITH ASME Y14.5M.

INTERPRET WELD SYMBOLS PER ANSI / AWS 2.4

U.S. Patent No. 4,780,269
Transnuclear, Inc.

TRANSNUCLEAR
AN AREVA COMPANY

SAFETY ANALYSIS REPORT
TN TAD
TRANSPORTATION OVERPACK
IMPACT LIMITER DETAILS

DRAWING NO.	SCALE	SHEET	REVISION
TNTAD-TO -71-9	NONE	1 OF 1	0

PROPRIETARY AND SECURITY RELATED INFORMATION WITHHELD UNDER 10 CFR 2.390

ALL DIMENSIONS ARE NOMINAL UNLESS A SPECIFIC TOLERANCE IS INDICATED WITH THE DRAWING DIMENSION

DIMENSIONS ARE IN INCHES AND DEGREES UNLESS OTHERWISE SPECIFIED. DIMENSIONING IN ACCORDANCE WITH ASME Y14.5M.

INTERPRET WELD SYMBOLS PER ANSI / AWS 2.4

U.S. Patent No. 4,780,269
Transnuclear, Inc.

TRANSNUCLEAR
AN AREVA COMPANY

SAFETY ANALYSIS REPORT
NUHOMS®TN44B
TAD TRANSPORTABLE CANISTER FOR BWR FUEL
MAIN ASSEMBLY

DRAWING NO.	SCALE	SHEET	REVISION
NUH44B-71-1	NONE	1 OF 4	0

PROPRIETARY AND SECURITY RELATED INFORMATION WITHHELD UNDER 10 CFR 2.390

PROPRIETARY AND SECURITY RELATED INFORMATION WITHHELD UNDER 10 CFR 2.390

PROPRIETARY AND SECURITY RELATED INFORMATION WITHHELD UNDER 10 CFR 2.390

DRAWING NO. NUH44B-71-2 SHEET 1 OF 4

PROPRIETARY AND SECURITY RELATED INFORMATION WITHHELD UNDER 10 CFR 2.390

ALL DIMENSIONS ARE NOMINAL UNLESS A SPECIFIC TOLERANCE IS INDICATED WITH THE DRAWING DIMENSION

DIMENSIONS ARE IN INCHES AND DEGREES UNLESS OTHERWISE SPECIFIED. DIMENSIONING IN ACCORDANCE WITH ASME Y14.5M.

INTERPRET WELD SYMBOLS PER ANSI / AWS 2.4

U.S. Patent No. 4,780,269
Transnuclear, Inc.

This drawing copy not to be distributed to others by sale or by gift, or used for other than Transnuclear purposes without written permission of Transnuclear, Inc.

TRANSNUCLEAR
AN AREVA COMPANY

SAFETY ANALYSIS REPORT
NUHOMS® TN44B
TAD TRANSPORTABLE CANISTER FOR BWR FUEL
BASKET-SHELL ASSEMBLY

DRAWING NO.	SCALE	SHEET	REVISION
NUH44B-71-2	NONE	1 OF 4	0

PROPRIETARY AND SECURITY RELATED INFORMATION WITHHELD UNDER 10 CFR 2.390

PROPRIETARY AND SECURITY RELATED INFORMATION WITHHELD UNDER 10 CFR 2.390

PROPRIETARY AND SECURITY RELATED INFORMATION WITHHELD UNDER 10 CFR 2.390

PROPRIETARY AND SECURITY RELATED INFORMATION WITHHELD UNDER 10 CFR 2.390

ALL DIMENSIONS ARE NOMINAL UNLESS A SPECIFIC TOLERANCE IS INDICATED WITH THE DRAWING DIMENSION

DIMENSIONS ARE IN INCHES AND DEGREES UNLESS OTHERWISE SPECIFIED. DIMENSIONING IN ACCORDANCE WITH ASME Y14.5M.

INTERPRET WELD SYMBOLS PER ANSI / AWS 2.4

U.S. Patent No. 4,780,269
Transnuclear, Inc.

TRANSNUCLEAR
AN AREVA COMPANY

SAFETY ANALYSIS REPORT
NUHOMS® TN44B
TAD TRANSPORTABLE CANISTER FOR BWR FUEL
SHELL ASSEMBLY

DRAWING NO.	SCALE	SHEET	REVISION
NUH44B-71-3	NONE	1 OF 4	0

PROPRIETARY AND SECURITY RELATED INFORMATION WITHHELD UNDER 10 CFR 2.390

PROPRIETARY AND SECURITY RELATED INFORMATION WITHHELD UNDER 10 CFR 2.390

PROPRIETARY AND SECURITY RELATED INFORMATION WITHHELD UNDER 10 CFR 2.390

DRAWING NO. NUH448-71-10 SHEET 1 OF 5

PROPRIETARY AND SECURITY RELATED INFORMATION WITHHELD UNDER 10 CFR 2.390

ALL DIMENSIONS ARE NOMINAL UNLESS A SPECIFIC TOLERANCE IS INDICATED WITH THE DRAWING DIMENSION

DIMENSIONS ARE IN INCHES AND DEGREES UNLESS OTHERWISE SPECIFIED. DIMENSIONING IN ACCORDANCE WITH ASME Y14.5M.

INTERPRET WELD SYMBOLS PER ANSI / AWS 2.4

U.S. Patent No. 4,780,269
Transnuclear, Inc.

TRANSNUCLEAR
AN AREVA COMPANY

SAFETY ANALYSIS REPORT
NUHOMS® TN44B
TAD TRANSPORTABLE CANISTER FOR BWR FUEL BASKET ASSEMBLY

DRAWING NO.	SCALE	SHEET	REVISION
NUH448-71-10	NONE	1 OF 5	0

PROPRIETARY AND SECURITY RELATED INFORMATION WITHHELD UNDER 10 CFR 2.390

PROPRIETARY AND SECURITY RELATED INFORMATION WITHHELD UNDER 10 CFR 2.390

PROPRIETARY AND SECURITY RELATED INFORMATION WITHHELD UNDER 10 CFR 2.390

PROPRIETARY AND SECURITY RELATED INFORMATION WITHHELD UNDER 10 CFR 2.390

PROPRIETARY AND SECURITY RELATED INFORMATION WITHHELD UNDER 10 CFR 2.390

ALL DIMENSIONS ARE NOMINAL UNLESS A SPECIFIC TOLERANCE IS INDICATED WITH THE DRAWING DIMENSION

DIMENSIONS ARE IN INCHES AND DEGREES UNLESS OTHERWISE SPECIFIED. DIMENSIONING IN ACCORDANCE WITH ASME Y14.5M.

INTERPRET WELD SYMBOLS PER ANSI / AWS 2.4

U.S. Patent No. 4,780,269
Transnuclear, Inc.

TRANSNUCLEAR
AN AREVA COMPANY

SAFETY ANALYSIS REPORT
NUHOMS® TN44B
TAD TRANSPORTABLE CANISTER FOR BWR FUEL
TRANSITION RAILS

DRAWING NO.	SCALE	SHEET	REVISION
NUH44B-71-11	NONE	1 OF 2	0

PROPRIETARY AND SECURITY RELATED INFORMATION WITHHELD UNDER 10 CFR 2.390

Appendix B.2.13.11
MP197TAD TO Evaluation of the Fuel Assemblies under Impact Loads

The information on pages
B.2.13.11.i through B.2.13.11-20 is
Proprietary Information Withheld
Pursuant to 10 CFR 2.390

Chapter B.3
Thermal Evaluation

CONTENTS

B.3.1 Description of Thermal Design Criteria B.3-2
B.3.1.1 Design Features B.3-3
B.3.1.2 Content's Decay Heat B.3-4
B.3.1.3 Summary Tables of Temperatures B.3-4
B.3.1.4 Summary Tables of Maximum Pressures B.3-5
B.3.2 Material Properties and Component Specifications B.3-6
B.3.2.1 Material Properties for MP197TAD TO B.3-6
B.3.2.2 Material Properties for TN44B DSC B.3-12
B.3.2.3 Component Specifications B.3-19
B.3.3 Thermal Evaluation under Normal Conditions of Transport B.3-20
B.3.3.1 Thermal Models B.3-20
B.3.3.2 Heat and Cold B.3-39
B.3.3.3 Maximum Normal Operating Pressure B.3-40
B.3.3.4 Thermal Evaluation for Loading/Unloading Operations B.3-44
B.3.4 Thermal Evaluation under Hypothetical Accident Conditions B.3-46
B.3.4.1 Initial Conditions B.3-46
B.3.4.2 Fire Test Conditions B.3-47
B.3.4.3 Maximum Temperatures and Pressure B.3-51
B.3.4.4 Maximum Thermal Stresses B.3-53
B.3.4.5 Accident Conditions for Fissile Material Packages for Air Transport B.3-53
B.3.5 References B.3-54
B.3.6 Appendices B.3-56
B.3.6.1 Macros for Heat Transfer Coefficient B.3-57
B.3.6.2 Mesh Sensitivity B.3-61
B.3.6.3 Acceptance Criteria for Coating Damages for MP197TAD TO B.3-61
B.3.6.4 Justification of Hot Gaps B.3-61

LIST OF TABLES

Table B.3- 1 TN44B DSC Shell Nominal Dimensions B.3-64
Table B.3- 2 Peaking Factors for TN44B Fuel B.3-65
Table B.3- 3 List of Homogenized Multiple Plates in TN44B DSC Model B.3-66
Table B.3- 4 Effective Density for TN44B Basket B.3-67
Table B.3- 5 Effective Specific Heat for the TN44B Basket B.3-68
Table B.3- 6 Effective Axial Conductivity for TN44B Basket B.3-69
Table B.3- 7 Effective Radial Conductivity for TN44B Basket B.3-70
Table B.3- 8 Maximum Temperatures of MP197TAD TO Components/TN44B DSC Shell for NCT (100°F and Insolation) B.3-71
Table B.3- 9 Maximum Fuel Cladding and Basket Component Temperatures for NCT B.3-72
Table B.3- 10 Maximum/Minimum MP197TAD TO and TN44B DSC Component Temperatures for NCT B.3-73
Table B.3- 11 Maximum Temperatures of MP197TAD TO Components and TN44B DSC Shell for Cold NCT B.3-74
Table B.3- 12 Average Component Temperatures for NCT B.3-75
Table B.3- 13 List of the Gaps and Thermal Properties for HAC Analysis B.3-76
Table B.3- 14 Maximum Temperatures of MP197TAD TO Components / TN44B DSC Shell for HAC B.3-77
Table B.3- 15 Time Intervals for Short Term Exposure of Seals to High Temperatures B.3-78
Table B.3- 16 Maximum Fuel Cladding and Basket Component Temperatures for HAC B.3-79
Table B.3- 17 Summary of the MP197TAD TO/TN44B DSC Maximum Temperatures for HAC . B.3-80
Table B.3- 18 MP197TAD TO Cavity Pressure for NCT and HAC B.3-81
Table B.3- 19 Maximum Internal Pressures of TN44B DSC in MP197TAD TO for NCT and HAC B.3-82
Table B.3- 20 Maximum Internal Pressures of TN44B DSC in MP197TAD TO for NCT and HAC B.3-83

LIST OF FIGURES

Figure B.3– 1 Location of TN44B DSC within TAD Transport Overpack B.3-84
Figure B.3– 2 Finite Element Model of MP197TAD TO with TN44B DSC, Longitudinal Section... B.3-85
Figure B.3– 3 Finite Element Model of TAD TO with TN44B DSC, Cross Section B.3-86
Figure B.3– 4 MP197TAD TO Finite Element Model, Cask Components B.3-87
Figure B.3– 5 MP197TAD TO Finite Element Model, TN44B DSC Shell and Impact Limiter Components B.3-88
Figure B.3– 6 Gaps in MP197TAD TO Model B.3-89
Figure B.3– 7 Gaps in MP197TAD TO and TN44B DSC Assembly Model B.3-90
Figure B.3– 8 Typical Boundary Conditions for MP197TAD TO Model B.3-91
Figure B.3– 9 Temperature Profiles for MP197TAD TO with TN44B DSC NCT, 100°F, Insolation, 22 kW B.3-92
Figure B.3– 10 Schematic View of Cask and Personnel Barrier B.3-93
Figure B.3– 11 Sub-Model for Helium Gap Effective Conductivity Calculation B.3-94
Figure B.3– 12 Thermal Model of TN44B DSC, Cross Sectional View B.3-95
Figure B.3– 13 Thermal Model of TN44B DSC, Longitudinal View B.3-96
Figure B.3– 14 TN44B DSC Model – Gaps between Rail Sections B.3-97
Figure B.3– 15 TN44B DSC Model – Axial Gaps at DSC End Plates B.3-98
Figure B.3– 16 Typical Boundary Conditions for TN44B DSC Model B.3-99
Figure B.3– 17 Finite Element Model of FANP 9x9-2 Fuel Assembly B.3-100
Figure B.3– 18 Basket Slice Models and Boundary Conditions B.3-101
Figure B.3– 19 Bounding Temperature Profiles for TN44B DSC under NCT B.3-102
Figure B.3– 20 Impact Limiter Crush Areas for MP197TAD TO (Side, End and Corner Drop)..... B.3-103
Figure B.3– 21 Impact Limiter Crush Areas for MP197TAD TO (Slap Down Drop) B.3-104
Figure B.3– 22 Finite Element Model of MP197TAD TO with Deformed Impact Limiters B.3-105
Figure B.3– 23 Typical Boundary Conditions for MP197TAD TO during Fire Conditions B.3-106
Figure B.3– 24 Typical Boundary Conditions for MP197TAD TO during Smoldering/Cool-Down Periods B.3-107
Figure B.3– 25 Time-Temperature Histories for MP197TAD TO / TN44B, HAC Rear Impact Limiter Punctured B.3-108
Figure B.3– 26 Time-Temperature Histories for MP197TAD TO / TN44B, HAC Front Impact Limiter Punctured B.3-109
Figure B.3– 27 Temperature Profiles for MP197TAD TO with TN44B DSC under HAC B.3-110
Figure B.3– 28 Temperature Profiles for TN44B DSC under HAC B.3-111

Chapter B.3
Thermal Evaluation

NOTE: References in this chapter are shown as [1], [2], etc., and refer to the reference list in Section B.3.5.

This chapter presents the thermal evaluation which demonstrates that the NUHOMS®-MP197 TAD Transportation Overpack (MP197TAD TO) meets the thermal requirements of 10 CFR 71 [5] for transportation of BWR spent fuel assemblies (FA) within the TN44B DSC.

The maximum heat load for TN44B DSC allowed for transportation in MP197TAD TO is 22 kW. This evaluation demonstrates that TN44B DSC component temperatures are within material temperature limits and fuel cladding temperatures meet the thermal requirements of ISG-11 [6].

B.3.1 Description of Thermal Design Criteria

The MP197TAD TO is designed to passively reject decay heat under normal conditions of transport (NCT) and hypothetical accident conditions (HAC) while maintaining packaging temperatures and pressures within specified limits. Objectives of the thermal analyses performed for this evaluation include:

a) Determination of maximum component temperatures with respect to MP197TAD TO material limits to ensure components perform their intended safety functions,

b) Determination of temperature distributions to support the calculation of thermal stresses,

c) Determination of the MP197TAD TO cavity gas temperature to support containment pressure calculations, and

d) Determination of the maximum fuel cladding temperature.

Chapter B.1 presents the principal design bases for the MP197TAD TO.

Several thermal design criteria are established for the MP197TAD TO to ensure that the package meets all its functional and safety requirements. These are:

- Maximum fuel cladding temperature limits of 752°F (400°C) for NCT and 1,058°F (570°C) for HAC are considered for the FAs with an inert cover gas as concluded in ISG-11 [6].
- Containment of radioactive material and gases is a major design requirement. Seal temperatures must be maintained within specified limits to satisfy the leak tight containment requirement. Based on [14], maximum long-term and short-term seal temperature limits of 400°F (204°C) and 482°F (250°C), respectively are considered for the Fluorocarbon seals (Viton O-rings). The study in [15] shows that the Fluorocarbon seals (Viton O-rings) are leak tight (no leakage above 10^{-7} cc/sec) at 470°F (243°C) for 10 hours, and at 500°F (260°C) for 3 hours.
- Maintain the stability of the neutron shield resin, a maximum allowable temperature of 320°F (160°C) is considered for the neutron shield [13] for NCT.
- Prevent melting of the gamma shield (lead) under NCT, an allowable maximum temperature of 621°F (327.5°C – melting point of lead) is considered for the gamma shield [4].
- A temperature limit of 320°F (160°C) is considered for wood to prevent excessive reduction in structural properties at elevated temperatures [16].
- In accordance with 10 CFR 71.43(g) [5] the maximum temperature of the accessible packaging surfaces in the shade is limited to 185°F (85°C).

The NCT ambient temperature range is –20°F to 100°F (-29°C to 38°C) per 10 CFR 71.71(b) [5]. In general, all the thermal criteria are associated with maximum temperature limits and not minimum temperatures. All materials can be subjected to the minimum environment temperature of -40°F (-40°C) without adverse effects as required by 10 CFR 71.71 (c)(2) [5].

Thermal performance of MP197TAD TO is evaluated based on finite element analyses using ANSYS computer code [21].

The following thermal design criteria are established for TN44B DSC to satisfy the functional and safety requirements.

- Maximum fuel cladding temperature limits of 752°F (400°C) for NCT and 1,058°F (570°C) for HAC are considered for the fuel assemblies with an inert cover gas as concluded in ISG-11 [6].
- The maximum TN44B DSC cavity internal design pressures are summarized below:

Operating condition	TN44B DSC
Normal Conditions of Transport (NCT) (3% rods ruptured) [8]	15 psig
Hypothetical Accident Conditions (HAC) (100% rods ruptured) [8]	100 psig

B.3.1.1 Design Features

B.3.1.1.1 MP197TAD TO

The MP197TAD TO consists of multiple shells which conduct the decay heat to the cask outer surface. The thermal design feature of the cask is the conduction path created by the aluminum boxes that contain the neutron shielding material as described in Chapter B.5. The neutron shielding material is provided by a resin compound cast into long slender aluminum boxes placed around the TO outer structural shell and enclosed within a steel shell (shield shell). The aluminum boxes are designed to fit tightly against the steel shell surfaces, thus improving the heat transfer across the neutron shield.

Heat dissipates from the packaging outer surfaces via natural convection and radiation. The outer surface of the shield shell is painted white to improve the thermal radiation exchange with ambient.

The design of the steel-encased wood impact limiters is described in Chapter B.1. These components are included in the thermal analysis because of their contribution as a thermal insulator. The impact limiters provide protection to the lid and bottom regions from the external heat input due to fire during the HAC thermal event.

A personnel barrier prevents access to the outer surfaces of the cask body. The barrier, which consists of a stainless steel mesh attached to stainless steel tubing, encloses the cask body between the impact limiters, and has an open area fraction of approximately 80%.

The gaps considered in the thermal model of MP197TAD TO are described in Section B.3.3.1.1.

B.3.1.1.2 TN44B DSC

The TN44B DSC design is similar to the 61BT DSC design documented in Appendix K, of the Standardized NUHOMS® System UFSAR [1].

The TN44B DSC consists of a shell assembly, which provides confinement and shielding, and an internal basket assembly which locates and supports the fuel assemblies.The basket structure consists of 9 and 2 compartment fuel cell subassemblies held in place by basket rails. The compartment subassemblies are held together by welded stainless plates wrapped around the fuel compartments, which also retain the aluminum and/or neutron absorbing plates sandwiched between the fuel compartments. The aluminum and neutron absorbing plates provide the necessary criticality control and heat conduction paths from the fuel cells to the perimeter of subassemblies. The aluminum plates retained between the subassemblies provide the heat conduction paths from the subassemblies to the perimeter of the basket. The space between the fuel compartments assembly and the DSC shell is bridged by aluminum/stainless steel transition rails.

No convection heat transfer is considered within the basket for conservatism. Radiation heat transfer is considered implicitly between the fuel rods and the fuel compartment in calculation of transverse effective fuel conductivity. No other radiation heat transfer is considered within the TN44B DSC models.

The decay heat from the DSC is carried to the inner shell of the MP197TAD TO cask via conduction, convection, and radiation. Convection heat transfer in the annulus between the DSC outer shell and the cask inner shell is not considered in the thermal evaluation for conservatism.

B.3.1.2 Content's Decay Heat

The maximum decay heat load for TN44B DSC for off-site transport in MP197TAD TO is 22.0 kW. The permitted heat load for TN44B DSC is listed in Chapter B.1. The total maximum decay heat load per FA within the TN44B DSC is 0.54 kW. Possible asymmetry of decay heat load (within specified FA and TN44B DSC limits) means reduction of heat load in a particular FA resulting in reduction of local and maximum temperatures of fuel cladding and TN44B DSC components.

A description of the detailed analyses of MP197TAD TO and TN44B DSC for NCT and HAC is provided in Section B.3.3 and Section B.3.4.

Summaries of the maximum temperatures and pressures are provided in Section B.3.1.3 and Section B.3.1.4, respectively. The thermal evaluation concludes that for the maximum heat load of 22 kW all design criteria listed in Section B.3.1 are satisfied.

B.3.1.3 Summary Tables of Temperatures

The maximum and minimum MP197TAD TO and TN44B DSC component temperatures for NCT are summarized in Table B.3- 10. The component temperatures remain within the allowable range for NCT.

The maximum MP197TAD TO and TN44B DSC shell temperatures for cold conditions at -20°F and -40°F ambient without insolance are presented in Table B.3- 11. These temperatures are used for the structural evaluation of MP197TAD TO.

The maximum accessible surface temperatures under shade are 119°F and 140°F for impact limiter shell and personnel barrier as calculated in Section B.3.3.1.2 and are below the allowable limit of 185°F for NCT.

The maximum transient temperatures of the MP197TAD TO and TN44B DSC components and the time at which they occur are summarized in Table B.3- 17 for HAC. The resins and wood are assumed to be decomposed or charred after fire accident. Therefore, the maximum temperatures for these components are irrelevant for HAC. The maximum fuel cladding, gamma shield and seal temperatures remain below the allowable limits and ensure the integrity of the fuel cladding and the containment boundary for HAC.

B.3.1.4 Summary Tables of Maximum Pressures

The maximum internal pressures inside MP197TAD TO cavity are calculated in Section B.3.3.3.1 for NCT and Section B.3.4.3 for HAC. The maximum internal pressures of the MP197TAD TO cavity are summarized in Table B.3- 18. The maximum pressures inside TN44B DSC cavity are are calculated in Section B.3.3.3.2 and listed in Table B.3- 20. These pressures remain below the design pressures for NCT and HAC.

B.3.2 Material Properties and Component Specifications

B.3.2.1 Material Properties for MP197TAD TO

The following tables provide the thermal properties of materials used in the analysis of the MP197TAD TO with TN44B DSC.

1. SA-240, Type 304 Stainless Steel [9]

Temperature (°F)	Thermal Conductivity, k (Btu/hr-in-°F)	Density, ρ (lbm/in^3)	Specific Heat, C_p (Btu/lb$_m$-°F)
70	0.717	0.284	0.116
100	0.725		0.117
200	0.775		0.121
300	0.817		0.125
400	0.867		0.128
500	0.908		0.131
600	0.942		0.132
700	0.983		0.134
800	1.025		0.136
900	1.058		0.137
1000	1.092		0.138

2. SA-240 Type 316 [9]

Temperature (°F)	k (Btu/hr-in-°F)	ρ (lbm/in^3)	C_p (Btu/lb$_m$-°F)
70	0.683	0.284	0.120
100	0.692		0.121
200	0.733		0.124
300	0.775		0.126
400	0.817		0.129
500	0.850		0.130
600	0.892		0.132
700	0.933		0.134
800	0.967		0.135
900	1.008		0.137
1000	1.042		0.138

3. SA-182-F6NM [9]

Temperature (°F)	k (Btu/hr-in-°F)	ρ (lbm/in^3)	C_p (Btu/lb$_m$-°F)
70	1.183	0.284	0.105
100	1.183		0.107
200	1.192		0.112
300	1.200		0.117
400	1.208		0.122
500	1.208		0.128
600	1.217		0.135
700	1.217		0.142
800	1.225		0.150
900	1.225		0.157
1000	1.225		0.166

4. Aluminum, Type 6063 [9]

Temperature (°F)	k (Btu/hr-in-°F)	ρ (lb$_m$/in^3)	C_p (Btu/lb$_m$-°F)
70	10.067	0.098	0.213
100	10.025		0.215
150	9.975		0.218
200	9.917		0.221
250	9.875		0.223
300	9.842		0.226
350	9.833		0.228
400	9.800		0.230

5. Gamma Shield, ASTM B29 Lead [19]

Temperature (°F)	k (Btu/hr-in-°F)	ρ (lb$_m$/in^3)	C_p (Btu/lb$_m$-°F)
-100	1.767	0.413	0.030
-10	1.733	0.411	0.030
80	1.700	0.409	0.031
260	1.637	0.406	0.032
440	1.579	0.402	0.033
620	1.512	0.398	0.034

6. Neutron Shield Resin (Vyal B) [13]

Temperature (°F)	k (Btu/hr-in-°F)	ρ (lb$_m$/in^3)	C_p (Btu/lb$_m$-°F)
104	0.039	0.06	0.256
140			0.260
176			0.282
212			0.301
284			0.358
320			0.380

7. Trunnion Plug Resin [(1)] (Polypropylene) [4]

Temperature (°F)	k (Btu/hr-in-°F)	ρ (lb$_m$/in^3)	C_p (Btu/lb$_m$-°F)
All temperatures	0.0067	0.03	0.46

[(1)] The material of trunnion plug is stainless steel. See Section B.3.3.1.1 for discussion.

8. Wood [16]

Minimum thermal conductivity, k_{min} = 0.0019 Btu/hr-in-°F for NCT and cool-down period, see Section 3.2, Item 8		
Maximum thermal conductivity, k_{max} = 0.0378 Btu/hr-in-°F during fire period, see Section 3.2, Item 8		
Temperature (°F)	**ρ (lb_m/in^3) (1)**	**C_p (Btu/lb_m-°F)**
100	0.007	0.312
200	0.006	0.363
300	0.005	0.414
400	0.005	0.466
500	0.004	0.517
600	0.004	0.568

(1) The wood density is calculated based on thermal diffusivity using $\alpha = \frac{k}{\rho c_P}$ with

k = conductivity =0.0019 (Btu/hr-in-°F),
ρ = density (lbm/in^3), and
c_P = specific heat (Btu/lbm-°F).

9. Helium [17]

Temperature (K)	k (W/m-K)	Temperature (°F)	k (Btu/hr-in-°F)
300	0.1499	80	0.0072
400	0.1795	260	0.0086
500	0.2115	440	0.0102
600	0.2466	620	0.0119
800	0.3073	980	0.0148
1000	0.3622	1340	0.0174
1050	0.3757	1430	0.0181

The above data are calculated base on the following polynomial function from [17]

$k = \sum C_i \, T_i$ for conductivity in (W/m-K) and T in (K)

For 300 < T < 500 K		for 500< T < 1050 K	
C0	-7.761491E-03	C0	-9.0656E-02
C1	8.66192033E-04	C1	9.37593087E-04
C2	-1.5559338E-06	C2	-9.13347535E-07
C3	1.40150565E-09	C3	5.55037072E-10
C4	0.0E+00	C4	-1.26457196E-13

No density or specific heat is considered for helium for conservatism.

10. Air [17]

Temperature (K)	k (W/m-K)	Temperature (°F)	k (Btu/hr-in-°F)
250	0.02228	-10	0.0011
300	0.02607	80	0.0013
400	0.03304	260	0.0016
500	0.03948	440	0.0019
600	0.04557	620	0.0022
800	0.05698	980	0.0027
1000	0.06721	1340	0.0032

The above data are calculated base on the following polynomial function from [17]

$k = \sum C_i \, T_i$ for conductivity in(W/m-K) and T in (K)

For 250 < T < 1050 K	
C0	-2.2765010E-03
C1	1.2598485E-04
C2	-1.4815235E-07
C3	1.7355064E-10
C4	-1.0666570E-13
C5	2.4766304E-17

No density or specific heat is considered for air in the thermal models for conservatism. Specific heat, viscosity, density and Prandtl number of air are used to calculate heat transfer coefficients described in Section B.3.3.1.1 based on the following data from [17].

$c_p = \sum A_i \, T_i$ for specific heat in (kJ/kg-K) and T in (K)

For 250 < T < 1050 K	
A0	0.103409E+1
A1	-0.2848870E-3
A2	0.7816818E-6
A3	-0.4970786E-9
A4	0.1077024E-12

$\mu = \sum B_i \, T_i$ for viscosity (N-s/m^2)×10^6 and T in (K)

For 250 < T < 600 K		For 600 < T < 1050 K	
B0	-9.8601E-1	B0	4.8856745
B1	9.080125E-2	B1	5.43232E-2
B2	-1.17635575E-4	B2	-2.4261775E-5
B3	1.2349703E-7	B3	7.9306E-9
B4	-5.7971299E-11	B4	-1.10398E-12

$\rho = P / RT$ for density (kg/m^3) with P=101.3 kPa; R = 0.287040 kJ/kg-K; T = air temp in (K),

$\mathrm{Pr} = c_p \, \mu / k$ Prandtl number.

11. Effective Conductivity for Helium Gap between DSC and MP197TAD TO Inner Shell
(See Section B.3.3.1.3 for justification)

Temperature (°F)	$k_{_eff}$ (Btu/hr-in-°F)
45	0.0080
92	0.0084
138	0.0090
183	0.0097
230	0.0104
248	0.0108
294	0.0116
341	0.0126
388	0.0136
435	0.0148
482	0.0160
530	0.0173
578	0.0187
626	0.0202
674	0.0217
722	0.0233
771	0.0251

12. Effective Conductivity for Cask Slide Rails
(See Section B.3.3.1.3 for justification)

Slide rail thickness = 0.12 in
Gap thickness = 0.01 in

Temp (°F)	k_eff[1] (Btu/hr-in-°F)
70	0.076
100	0.079
200	0.087
300	0.095
400	0.104
500	0.113
600	0.122
700	0.131
800	0.139
900	0.147
1,000	0.154

[1] The above effective conductivities are considered in the model for the Cartesian x and y coordinates, covering the cross sectional plane of the cask slide rail. The conductivity of the rail in the axial direction (Cartesian z coordinate in the model) remains equal to the conductivity of Nitronic 60.

Thermal radiation at the external surfaces of the packaging is considered for thermal analysis. The outer surface of the neutron shield shell is painted white. Reference [18] gives an emissivity between 0.92 and 0.96 and a solar absorptivity between 0.09 and 0.23 for white paints. To account for dust and dirt and to bound the problem, the thermal analysis uses a solar absorptivity of 0.3 and an emissivity of 0.9 for the white painted surfaces.

The outer surfaces of the impact limiter shells are uncoated stainless steel. An emissivity of 0.587 is considered for these surfaces based on [12]. Solar absorptance values of 0.39 and 0.47 are given in [24] for rolled and machined stainless steel plates. For conservatism, it is assumed that the solar absorptivity of stainless steel is equal to emissivity.

The emissivity of rolled stainless steel plates is 0.587 as considered in [12]. The MP197TAD TO inner shell is stainless steel. The emissivity value of 0.587 is considered for both the TN44B DSC shell and the MP197TAD TO inner shell in the calculation of thermal radiation exchange between these shells.

After fire, the cask outer surfaces will be partially covered in soot. Based on [18], emissivity and solar absorptivity of soot are 0.95. The HAC thermal analysis conservatively assumes an absorptivity of 1.0 and an emissivity of 0.9 for the post fire, cool-down period.

B.3.2.2 Material Properties for TN44B DSC

An emissivity of 0.2 is considered conservatively for the stainless steel compartment walls in the calculation of the transverse effective conductivity for the homogenized fuel assemblies.

A conservative emissivity of 0.74 is considered for Zircaloy cladding based on data in [26].

The tables below provide the thermal properties of materials used in the analysis of the NUHOMS® TAD TN44B DSC.

13. Bounding BWR Fuel with Helium Backfill

The effective thermal properties are the lowest calculated values among the various BWR fuel assembly types that may be stored in the TN44B DSC. The calculation of the fuel assembly effective properties is discussed in Section B.3.3.1.5.

Fuel in Helium

Temperature (°F)	k, Transverse (Btu/hr-in-°F)	k, Axial (Btu/hr-in-°F)	ρ (lb_m/in^3)	C_p (Btu/lb_m-°F)
200	0.0142	0.037	0.095	0.0575
300	0.0165			
400	0.0194			
500	0.0226			
600	0.0260			
700	0.0305			
800	0.0343			

14. SA-240, Type 304 Stainless Steel [9]

Temperature (°F)	k (Btu/hr-in-°F)	ρ (lbm/in^3)	C_p (Btu/lb_m-°F)
70	0.717	0.284	0.116
100	0.725		0.117
200	0.775		0.122
300	0.817		0.125
400	0.867		0.128
500	0.908		0.131
600	0.942		0.133
700	0.983		0.135
800	1.025		0.136
900	1.058		0.137
1000	1.092		0.138

15. SA-240 Type 316 [9]

Temperature (°F)	k (Btu/hr-in-°F)
70	0.683
100	0.692
200	0.733
300	0.775
400	0.817
500	0.850
600	0.892
700	0.933
800	0.967
900	1.008
1000	1.042
1100	1.083
1200	1.117
1300	1.150
1400	1.192

16. Aluminum, Type 1100 [9]

Temperature (°F)	k (Btu/hr-in-°F)	ρ (lb_m/in^3)	C_p (Btu/lb_m-°F)
70	11.092	0.098	0.214
100	10.983		0.216
150	10.833		0.219
200	10.708		0.222
250	10.608		0.224
300	10.517		0.227
350	10.442		0.229
400	10.375		0.232

17. Aluminum, Type 6061 [9]

Temperature (°F)	k (Btu/hr-in-°F)	ρ (lb_m/in^3)	C_p (Btu/lb_m-°F)
70	8.008	0.098	0.213
100	8.075		0.215
150	8.167		0.218
200	8.250		0.221
250	8.317		0.223
300	8.383		0.226
350	8.442		0.228
400	8.492		0.230

18. Borated Stainless Steel [27]

Temperature (°F)	k (Btu/hr-in-°F)	ρ (lb_m/in^3) (1)	C_p (Btu/lb_m-°F) (1)
77	0.657	0.278	0.116
194	0.705		
302	0.743		
392	0.773		
500	0.810		

Note (1) Based on 95% bounding values from [27].

19. Helium [17]

Temperature (K)	k (W/m-K)	Temperature (°F)	k (Btu/hr-in-°F)
300	0.1499	80	0.0072
400	0.1795	260	0.0086
500	0.2115	440	0.0102
600	0.2466	620	0.0119
800	0.3073	980	0.0148
1000	0.3622	1340	0.0174
1050	0.3757	1430	0.0181

The above data are calculated base on the following polynomial function from [17]

$k = \sum C_i \, T_i$ for conductivity in (W/m-K) and T in (K)

For 300 < T < 500 K		for 500< T < 1050 K	
C0	-7.761491E-03	C0	-9.0656E-02
C1	8.66192033E-04	C1	9.37593087E-04
C2	-1.5559338E-06	C2	-9.13347535E-07
C3	1.40150565E-09	C3	5.55037072E-10
C4	0.0E+00	C4	-1.26457196E-13

20. Effective Conductivity for Homogenized Center Plates in Nine-Compartments Assembly

Center Plates in Nine-Comp. Assembly - ANSYS MAT 3 and 13 listed in Table B.3- 3						
AL	0.9375	in	See Section B.3.3.1.5 for calculation methodology.			
SST Wrap	0.210	in				
Borated SST	0.4375	in				
Contact Gap	0.060	in				
t_total	1.645	in				
	Al-1100 (2)	Helium Gap (3)	SST	Borated SST (1)	Homogenized Plates	
Temp (°F)	k (Btu/hr-in-°F)	k (Btu/hr-in-°F)	k (Btu/hr-in-°F)	k (Btu/hr-in-°F)	$k_{eff,\ across}$ (Btu/hr-in-°F)	$k_{eff,along}$ (Btu/hr-in-°F)
200	10.708	0.0082	0.775	0.707	0.198	6.390
300	10.517	0.0090	0.817	0.742	0.216	6.296
400	10.375	0.0098	0.867	0.776	0.235	6.230
500	10.233	0.0107	0.908	0.810	0.255	6.164
600	10.092	0.0117	0.942	0.810	0.275	6.087
700	9.950	0.0125	0.983	0.810	0.292	6.012
800	9.808	0.0133	1.025	0.810	0.308	5.937
900	9.667	0.0141	1.058	0.810	0.325	5.860
1000	9.525	0.0149	1.092	0.810	0.340	5.784

Notes:
(1) Interpolated from data of 95% borated stainless steel conductivity (Item 18 in this Section). The conductivity at 500°F used for temperature beyond 500°F.
(2) Extrapolated from data in [9] shown under item 16 in this Section.
(3) Interpolated from data in [17] shown under item 19 in this Section.

21. Effective Conductivity for Homogenized Middle Plates in Nine-Compartments Assembly

Middle Plates in Nine-Comp. Assembly - ANSYS MAT 4 and 14 listed in Table B.3- 3						
AL	0.1875	in	See Section B.3.3.1.5 for calculation methodology.			
SST Wrap	0	in				
Borated SST	0.4375	in				
Contact Gap	0.030	in				
t_total	0.655	in				
	Al-1100 (2)	Helium Gap(3)	SST	Borated SST (1)	Homogenized Plates	
Temp (°F)	k (Btu/hr-in-°F)	k (Btu/hr-in-°F)	k (Btu/hr-in-°F)	k (Btu/hr-in-°F)	$k_{eff,\ across}$ (Btu/hr-in-°F)	$k_{eff,along}$ (Btu/hr-in-°F)
200	10.708	0.0082	0.775	0.707	0.152	3.538
300	10.517	0.0090	0.817	0.742	0.166	3.507
400	10.375	0.0098	0.867	0.776	0.180	3.489
500	10.233	0.0107	0.908	0.810	0.196	3.471
600	10.092	0.0117	0.942	0.810	0.210	3.430
700	9.950	0.0125	0.983	0.810	0.222	3.390
800	9.808	0.0133	1.025	0.810	0.233	3.349
900	9.667	0.0141	1.058	0.810	0.244	3.309
1000	9.525	0.0149	1.092	0.810	0.255	3.268

Notes:
(1) Interpolated from data of 95% borated stainless steel conductivity (item 18 in this Section). The conductivity at 500°F used for temperature beyond 500°F.
(2) Extrapolated from data in [9] shown under item 16 in this Section.
(3) Interpolated from data in [17] shown under item 19 in this Section.

22. Effective Conductivity for Homogenized Corner Plates in Nine-Compartments Assembly

Middle Plates in Nine-Comp. Assembly - ANSYS MAT 5 and 15 listed in Table B.3- 3						
AL	0	in	See Section B.3.3.1.5 for calculation methodology.			
SST Wrap	0.105	in				
Borated SST	0.4375	in				
Contact Gap	0.020	in				
t_total	0.5625	in				
	Al-1100 (2)	Helium Gap (3)	SST	Borated SST (1)	Homogenized Plates	
Temp (°F)	k (Btu/hr-in-°F)	k (Btu/hr-in-°F)	k (Btu/hr-in-°F)	k (Btu/hr-in-°F)	$k_{eff,\ across}$ (Btu/hr-in-°F)	$k_{eff,along}$ (Btu/hr-in-°F)
200	10.708	0.0082	0.775	0.707	0.176	0.695
300	10.517	0.0090	0.817	0.742	0.191	0.730
400	10.375	0.0098	0.867	0.776	0.207	0.766
500	10.233	0.0107	0.908	0.810	0.224	0.800
600	10.092	0.0117	0.942	0.810	0.238	0.806
700	9.950	0.0125	0.983	0.810	0.251	0.814
800	9.808	0.0133	1.025	0.810	0.263	0.822
900	9.667	0.0141	1.058	0.810	0.274	0.828
1000	9.525	0.0149	1.092	0.810	0.285	0.834

Notes:
(1) Interpolated from data of 95% borated stainless steel conductivity (item 18 in this Section). The conductivity at 500°F used for temperature beyond 500°F.
(2) Extrapolated from data in [9] shown under item 16 in this Section.
(3) Interpolated from data in [17] shown under item 19 in this Section.

23. Effective Conductivity for Homogenized Center Plates in Two-Compartments Assembly

Center Plates in Two-Comp. Assembly - ANSYS MAT 6 and 16 listed in Table B.3- 3						
AL	1.125	in	See Section B.3.3.1.5 for calculation methodology.			
SST Wrap	0	in				
Borated SST	0.4375	in				
Contact Gap	0.040	in				
t_total	1.6025	in				
	Al-1100 (2)	Helium Gap (3)	SST	Borated SST(1)	Homogenized Plates	
Temp (°F)	k (Btu/hr-in-°F)	k (Btu/hr-in-°F)	k (Btu/hr-in-°F)	k (Btu/hr-in-°F)	$k_{eff,\ across}$ (Btu/hr-in-°F)	$k_{eff,along}$ (Btu/hr-in-°F)
200	10.708	0.0082	0.775	0.707	0.285	7.711
300	10.517	0.0090	0.817	0.742	0.311	7.586
400	10.375	0.0098	0.867	0.776	0.338	7.496
500	10.233	0.0107	0.908	0.810	0.367	7.405
600	10.092	0.0117	0.942	0.810	0.393	7.306
700	9.950	0.0125	0.983	0.810	0.417	7.207
800	9.808	0.0133	1.025	0.810	0.438	7.107
900	9.667	0.0141	1.058	0.810	0.460	7.008
1000	9.525	0.0149	1.092	0.810	0.480	6.908

Notes:
(1) Interpolated from data of 95% borated stainless steel conductivity (item 18 in this Section). The conductivity at 500°F used for temperature beyond 500°F.
(2) Extrapolated from data in [9] shown under item 16 in this Section.
(3) Interpolated from data in [17] shown under item 19 in this Section.

24. Effective Conductivity for Homogenized Corner Plates in Two-Compartments Assembly

Corner Plates in Two-Comp. Assembly - ANSYS MAT 7 and 17 listed in Table B.3- 3						
AL	0	in	See Section B.3.3.1.5 for calculation methodology.			
SST Wrap	0.105	in				
Borated SST	0.4375	in				
Contact Gap	0.030	in				
t_total	0.5725	in				
	Al-1100 (2)	Helium Gap (3)	SST	Borated SST(1)	Homogenized Plates	
Temp (°F)	k (Btu/hr-in-°F)	k (Btu/hr-in-°F)	k (Btu/hr-in-°F)	k (Btu/hr-in-°F)	$k_{eff,\ across}$ (Btu/hr-in-°F)	$k_{eff,along}$ (Btu/hr-in-°F)
200	10.708	0.0082	0.775	0.707	0.129	0.683
300	10.517	0.0090	0.817	0.742	0.141	0.717
400	10.375	0.0098	0.867	0.776	0.153	0.752
500	10.233	0.0107	0.908	0.810	0.166	0.786
600	10.092	0.0117	0.942	0.810	0.178	0.792
700	9.950	0.0125	0.983	0.810	0.188	0.800
800	9.808	0.0133	1.025	0.810	0.198	0.808
900	9.667	0.0141	1.058	0.810	0.207	0.814
1000	9.525	0.0149	1.092	0.810	0.217	0.820

Notes:
(1) Interpolated from data of 95% borated stainless steel conductivity (item 18 in this Section). The conductivity at 500°F used for temperature beyond 500°F.
(2) Extrapolated from data in [9] shown under item 16 in this Section.
(3) Interpolated from data in [17] shown under item 19 in this Section.

25. Effective Conductivity for Homogenized Comp./Wrap Plates in Two-Comp. Assembly

Comp./Wrap Plates in Two-Comp. Assembly - ANSYS MAT 2 and 12 listed in Table B.3- 3						
AL	0	in	See Section B.3.3.1.5 for calculation methodology.			
SST Wrap	0.2925	in				
Borated SST	0	in				
Contact Gap	0.010	in				
t_total	0.3025	in				
	Al-1100 (2)	Helium Gap (3)	SST	Borated SST (1)	Homogenized Plates	
Temp (°F)	k (Btu/hr-in-°F)	k (Btu/hr-in-°F)	k (Btu/hr-in-°F)	k (Btu/hr-in-°F)	$k_{eff,\ across}$ (Btu/hr-in-°F)	$k_{eff,along}$ (Btu/hr-in-°F)
200	10.708	0.0082	0.775	0.707	0.189	0.750
300	10.517	0.0090	0.817	0.742	0.206	0.790
400	10.375	0.0098	0.867	0.776	0.223	0.838
500	10.233	0.0107	0.908	0.810	0.242	0.879
600	10.092	0.0117	0.942	0.810	0.259	0.911
700	9.950	0.0125	0.983	0.810	0.276	0.951
800	9.808	0.0133	1.025	0.810	0.292	0.992
900	9.667	0.0141	1.058	0.810	0.308	1.024
1000	9.525	0.0149	1.092	0.810	0.323	1.056

Notes:
(1) Interpolated from data of 95% borated stainless steel conductivity (item 18 in this Section). The conductivity at 500°F used for temperature beyond 500°F.
(2) Extrapolated from data in [9] shown under item 16 in this Section.
(3) Interpolated from data in [17] shown under item 19 in this Section.

26. Effective Conductivity for Homogenized Long Aluminum Plates

Long Aluminum Plates Homogenized with Gaps - ANSYS MAT 8 and 18 listed in Table B.3-3					
AL	0.500	in	See Section B.3.3.1.5 for calculation methodology.		
SST	0	in			
Contact Gap	0.020	in			
t_total	0.520	in			
	Al-1100 (1)	Helium Gap (2)	SST	Homogenized Plates	
Temp (°F)	k (Btu/hr-in-°F)	k (Btu/hr-in-°F)	k (Btu/hr-in-°F)	$k_{eff,\ across}$ (Btu/hr-in-°F)	$k_{eff,along}$ (Btu/hr-in-°F)
200	10.708	0.0082	0.775	0.208	10.297
300	10.517	0.0090	0.817	0.229	10.113
400	10.375	0.0098	0.867	0.250	9.976
500	10.233	0.0107	0.908	0.273	9.840
600	10.092	0.0117	0.942	0.296	9.704
700	9.950	0.0125	0.983	0.316	9.568
800	9.808	0.0133	1.025	0.336	9.432
900	9.667	0.0141	1.058	0.356	9.295
1000	9.525	0.0149	1.092	0.375	9.159

Notes:
(1) Extrapolated from data in [9] shown under item 16 in this Section.
(2) Interpolated from data in [17] shown under item 19 in this Section.

27. Effective Conductivity for Homogenized Short Al /Rail 45 Plates

Short Aluminum / R45 Rail Plates - ANSYS MAT 9 and 19 listed in Table B.3- 3					
AL	0.500	in	See Section B.3.3.1.5 for calculation methodology.		
SST R45	0.250	in			
Contact Gap	0.020	in			
t_total	0.770	in			
	Al-1100 (1)	Helium Gap (2)	SST	Homogenized Plates	
Temp (°F)	k (Btu/hr-in-°F)	k (Btu/hr-in-°F)	k (Btu/hr-in-°F)	$k_{eff,\ across}$ (Btu/hr-in-°F)	$k_{eff,along}$ (Btu/hr-in-°F)
200	10.708	0.0082	0.775	0.273	7.205
300	10.517	0.0090	0.817	0.298	7.094
400	10.375	0.0098	0.867	0.325	7.019
500	10.233	0.0107	0.908	0.352	6.940
600	10.092	0.0117	0.942	0.380	6.859
700	9.950	0.0125	0.983	0.405	6.781
800	9.808	0.0133	1.025	0.429	6.702
900	9.667	0.0141	1.058	0.452	6.621
1000	9.525	0.0149	1.092	0.475	6.540

Notes:
(1) Extrapolated from data in [9] shown under item 16 in this Section.
(2) Interpolated from data in [17] shown under item 19 in this Section.

B.3.2.3 Component Specifications

The components for which thermal technical specification are necessary are the MP197TAD TO containment seals and poison plates used in TN44B DSC basket.

B.3.2.3.1 MP197TAD TO

The seals used in the packaging are the Fluorocarbon seals (Viton O-rings). The seals will have a minimum and maximum temperature rating of -40°F and 400°F for long term, respectively and a maximum temperature rating 482°F for short term conditions.

B.3.2.3.2 TN44B DSC

The TN44B DSC design allows for the use of borated stainless steel as neutron absorber materials. The borated stainless steel is subjected to the following minimum thermal conductivity, which are used in the DSC thermal analyses.

Temperature (°F)	Conductivity (Btu/hr-in-°F)
77	0.657
194	0.705
302	0.743
392	0.773
500	0.810

B.3.3 Thermal Evaluation under Normal Conditions of Transport

The NCT ambient conditions are used for the determination of the maximum fuel cladding temperature, the maximum MP197TAD TO and TN44B DSC temperatures, the containment pressure, and the thermal stresses. These steady state environmental conditions correspond to maximum daily averaged ambient temperature of 100°F and to 10 CFR 71.71(c) (1) [5] insolation averaged over a 24 hour period.

Ambient conditions for NCT are taken from 10 CFR 71 [5] and applied to the boundaries of the cask model. These conditions are listed in the following table.

Normal Conditions of Transport

Case #	Ambient temperature (°F)	Insolance	Purpose
1	100	Yes	Maximum Component Temperatures
2	-20	No	Cold conditions for Structural Analysis
3	-40	No	Maximum Thermal Stress
4	100	No	Maximum Accessible Surface Temperature

B.3.3.1 Thermal Models

The MP197TAD TO loaded with a TN44B DSC is analyzed based on finite element models developed using the ANSYS computer code [21]. ANSYS is a comprehensive thermal, structural and fluid flow analysis package. ANSYS is capable of solving steady state and transient thermal analysis problems in one, two, or three dimensions. Heat transfer via a combination of conduction, radiation, and convection can be modeled by ANSYS.

Two finite element models are developed for analyses of the MP197TAD TO loaded with TN44B DSC.

a) A half-symmetric, three-dimensional finite element model is developed using ANSYS [21], version 8.1 for analyses of the MP197TAD TO loaded with TN44B DSC. The model contains the cask shells, cask bottom plate, cask lid, impact limiters, TN44B DSC shell, and DSC end plates without the basket. The canister dimensions correspond to nominal TN44B DSC dimensions listed in Table B.3- 1. SOLID70 elements are used to model the components including the gaseous gaps. Impact limiter gussets and bottom trunnion plug plates are modeled using SHELL57 elements. Surface elements SURF152 are used for applying the insolation boundary conditions. The models are run with steady state conditions for NCT evaluations.

b) A half-symmetric, three-dimensional finite element model of the TN44B DSC is developed using ANSYS version 10.0 [21]. This model contains the DSC shell, the DSC cover plates, shield plugs, aluminum rails, basket plates, and homogenized fuel assemblies. Radiation along the gap between the DSC shell and the basket rails is conservatively neglected. Only SOLID70 elements are used in the TN44B DSC model.

The TN44B DSC shell temperatures for NCT are retrieved from the MP197TAD TO model analyzed with 22 kW. However, the TN44B DSC model used in determining the maximum fuel cladding and basket component temperartures are based on a heat load of 24 kW. Also, the

bounding DSC shell temperature profiles are used for the TN44B DSC model. This is conservative since it increases the maximum fuel cladding and basket component temperatures.

B.3.3.1.1 MP197TAD TO Model

The following assumptions are considered in the MP197TAD TO model:

- TN44B DSC is centered axially in the transport overpack. This assumption reduces the axial heat transfer and maximizes the canister shell temperature, which in turn results in higher fuel cladding temperature.
- Heat load is simulated by heat flux distributed uniformly over the basket length on the radial inner surface of the DSC shell.
- Since the transport operation occurs in horizontal position, the lower halves of the overpack cylindrical surfaces are not exposed to insolance. No solar heat flux is considered over these surfaces. To remove any uncertainty about the solar impact on the vertical surfaces, the entire surface areas of vertical surfaces are considered for application of the solar heat flux.
- No convection is considered within the overpack cavity.
- No convection is considered between the overpack ends and the thermal shields.
- No heat transfer is considered within the bearing block.
- Radiation heat exchange is considered between the canister and the overpack inner shell by calculating effective conductivities for helium in this region.

The following gaps are considered in the MP197TAD TO model:

a) 0.12" diametrical gap between cask lid and upper part of cask body flange
b) 0.48" diametrical gap between cask lid and lower part of cask body flange
c) 0.09" radial gap between top shield plug and canister shell
d) 0.25" diametrical gap between bottom shield plug and canister shell
e) 0.01" radial gaps between neutron shield boxes and surrounding shells
f) 0.015" radial gap between gamma shield and overpack outer shell
g) 0.06" axial gap between canister lifting device spacer and cask lid
h) 0.06" axial gap between cask lid and cask flange
i) 0.06" axial gap between ram closure plate and overpack bottom plate
j) 0.06" axial gaps between the canister bottom shield plug and bottom cover plates
k) 0.06" axial gaps between the canister inner top cover and the adjacent top shield plug and outer top cover plate

The assumed gaps "a" through "d" are equal or larger than the nominal cold gaps. These gaps are conservative since the hot gaps at thermal equilibrium would be smaller.

The 0.01" radial gaps between the neutron shield boxes and the surrounding shells (gap "e") is based on assumptions in Section 3.4.1.1 of this SAR.

The gap "f" of 0.015" assumed between gamma shield and cask outer shell is justified in Section B.3.6.4.1 .

The axial gaps of 0.06" (gaps "g" and "i") between the canister lifting device spacer / cask lid, cask lid / cask body flange and ram closure plate / cask bottom plate account for thermal resistance between bolted components.

The axial gaps of 0.06" (gaps "j" and "k") between canister end plates maximize the radial heat transfer through canister shell toward the overpack to bound the maximum component temperatures conservatively.

An axial gap of 0.25" is considered between the impact limiter spacers and the cask top or bottom end surfaces. This gap is much larger than a common gap considered between bolted components. Since this gap increases the thermal resistance in this area and maximizes the canister shell temperature, it is conservative.

The trunnion plugs are modeled using polypropylene thermal properties. Stainless steel is considered as the material of the trunnion plugs in the final design of MP197TAD TO. Since these plugs are covered by the impact limiters, they do not provide a major conduction path. Therefore, change of their material properties does not affect any maximum temperatures.

The width of MP197TAD TO slide rail is 3". For conservatism, a gap of 0.01" is considered between the MP197TAD TO slide rails and the canister shell at 168° and 192° orientations. The conductive effect of the slide rails at 142° and 218° orientations are conservatively omitted in this analysis.

In the transport configuration, MP197TAD TO is supported on two saddles on a transport skid and is secured in place by two straps. The immediate critical component affected by the skid saddles and straps is the neutron shield resin. The effects of the skid straps/saddles on the critical component temperatures of a transport cask are expected to be insignificant and therefore, the fin effect of the skid straps and the conduction heat transfer through skid saddles are not considered in this evaluation. Instead, it is assumed that these effects are greater than or equivalent to the free convection and radiation from shield shell outer surface.

Decay heat load is applied as a uniform heat flux over the inner surface of the DSC shell covering the basket length. The decay heat flux applied in the MP197TAD TO model is calculated as follows.

$$q'' = \frac{Q}{\pi\ D_i\ L_b} = 2.091\ Btu/hr-in^2$$

where
q" = decay heat flux (Btu/hr-in^2),

Q = decay heat load (Btu/hr) (to convert from kW multiply by 3412.3) = 75,071 Btu/hr
D_i = TN44B DSC inner diameter = 64.75 in,
L_b = Basket length = 176.5 in.

Radiation and conduction between the DSC and the MP197TAD TO inner shell is considered by calculating effective conductivity for the helium gap between the components, as described in Section B.3.3.1.3.

Insolance is applied as a heat flux over the MP197TAD TO outer surfaces using average insolence values from 10 CFR 71 [5]. The insolance values are averaged over 24 hours and multiplied by the surface absorptivity factor to calculate the solar heat flux. The solar heat flux values used in the MP197TAD TO model are summarized below.

Solar Heat Flux

Surface Material	Shape	Insolance over 12 hrs[5] (gcal/cm^2)	Solar Absorptivity	Total solar heat flux averaged over 24 hrs (Btu/hr-in^2)
Stainless Steel	Curved	400	0.587 (1)	0.2505
	Flat vertical	200	0.587 (1)	0.1252
White Paint (shield shell)	Curved	400	0.30	0.1280

(1) Solar absorptivity of stainless steel is taken equal to its emissivity. See Section B.3.2.1 for justification.

Convection and radiation heat transfer from the overpack outer surfaces are combined together as total heat transfer coefficients. The total heat transfer coefficients are calculated using free convection correlations from [17] and incorporated in the model using ANSYS macros listed in Appendix B.3.6.1.

The total heat transfer coefficient, h_t, is used to combine the convection and radiation heat transfer together.

$$h_t = h_r + h_c \quad \text{Btu/hr-in}^2\text{-°F}$$

where,

h_r = radiation heat transfer coefficient (Btu/hr-in^2-°F),
h_c = free convection heat transfer coefficient (Btu/hr-in^2-°F).

The radiation heat transfer coefficient, h_r, is given by the equation:

$$h_r = \varepsilon F_{w\infty}\left[\frac{\sigma(T_w^4 - T_{amb}^4)}{T_w - T_{amb}}\right] \quad \text{Btu/hr-in}^2\text{-°F}$$

where,

ε = surface emissivity,
$F_{w\infty}$ = view factor from MP197TAD TO outer surface to ambient = 1,
σ = 0.1714×10^{-8} Btu/hr-ft^2-°R^4,
T_w = surface temperature (°R),
T_{amb} = ambient temperature (°R).

Surface emissivity values are discussed in Section B.3.2.1.

The natural convection coefficients are calculated using handbook correlations [17] and are incorporated in the model using ANSYS macros. These correlations are described below.

For horizontal cylinders:

$$Ra = Gr\,\mathrm{Pr} \quad ; \quad Gr = \frac{g\,\beta\,(T_w - T_\infty)\,D^3}{\nu^2} \quad .$$

$$Nu_l = \frac{2f}{\ln(1 + 2f / Nu^T)}$$

with

$$Nu^T = 0.772\,\overline{C}_l\,Ra^{1/4} \quad ,$$

$$f = 1 - \frac{0.13}{(Nu^T)^{0.16}},$$

$\overline{C}_l = 0.515$ for gases [17].

$$Nu_t = \overline{C}_t\,Ra^{1/3},$$

$\overline{C}_t = 0.103$ for air with $\mathrm{Pr} \approx 0.71$ [17].

$$Nu = \left[(Nu_l)^m + (Nu_t)^m\right]^{1/m} \qquad with \quad m = 10 \quad for \;\; 10^{-10} < Ra < 10^7,$$

$$h_c = \frac{Nu\,k}{D}.$$

The above correlations are incorporated in ANSYS model via macro "HTOT_HCL.mac" listed in Section B.3.6.1.

For vertical flat surfaces:

$$Ra = Gr\,\mathrm{Pr} \quad ; \quad Gr = \frac{g\,\beta\,(T_w - T_\infty)\,L^3}{\nu^2} \quad .$$

$$Nu_l = \frac{2.0}{\ln(1 + 2.0 / Nu^T)}$$

with

$Nu^T = \overline{C}_l\,Ra^{1/4}$; $\overline{C}_l = 0.515$ for gases [17].

$$Nu_t = C_t^V\,f\,Ra^{1/3} / \left(1 + 1.4 \times 10^9\,\mathrm{Pr}/Ra\right) \qquad \text{with}$$

$$C_t^V = \frac{0.13\,\mathrm{Pr}^{0.22}}{(1 + 0.61\,\mathrm{Pr}^{0.81})^{0.42}}, \qquad f = 1.0 + 0.078\left(\frac{T_w}{T_\infty} - 1\right).$$

$$Nu = \left[(Nu_l)^m + (Nu_t)^m\right]^{1/m} \qquad with \quad m = 6 \quad for \;\; 1 < Ra < 10^{12},$$

$$h_c = \frac{Nu\,k}{L}.$$

The above correlations are incorporated in ANSYS model via macro "HTOT_VPL.mac" listed in Section B.3.6.1.

The following parameters are used in the above correlations.

g = gravitational constant = 9.81 (m/s^2),
β = expansion coefficient = 1/T (1/K),
T = absolute temperature (K),
ν = kinematic viscosity (m^2/s),
L = height of the vertical surface (in),

D = diameter of the horizontal cylinder (in),

k = air thermal conductivity (W/m-K),

Pr = Prandtl number,

T_∞= ambient temperature.

During transportation, the DSC shell rests on four slide rails in the cask. These rails are Nitronic 60 stainless steel plates welded to the inner shell of the cask. The thickness of the slide rail is 0.12". The angle between the lower rail and the vertical plane is 12 degree. Considering this configuration as shown in Figure B.3– 1, the distance between the centerline of the TN44B DSC and the centerline of the cask is calculated as follows.

$$R_2^{\,2} = R_1^{\,2} + x^2 - 2\,R_1\,x\,Cos(\alpha)$$

With,

$R_1 = D_{i,\,cask}/2 - t_{rail}$,
$R_2 = D_{o,\,can}/2$,
$\alpha = 12°$,
x = Distance between the canister and cask centerlines,
$D_{i,\,cask}$ = Inner diameter of cask,
$D_{o,\,can}$ = TN44B DSC outer diameter,
t_{rail} = cask slide rail thickness = 0.12".

For TN44B DSC within the Overpack, the calculated value for x is 0.26". In the ANSYS model, the canister is shifted down by the amount of x in the Cartesian y-direction within the MP197TAD TO cavity.

To simplify the model, the assumed helium gap 0.01" between the canister and slide rail is integrated into the slide rail material at 168° and 192° orientations. The effects of the other overpack slide rails are conservatively omitted. The effective conductivity of the slide rail is calculated in Section B.3.3.1.3.

The material properties used in the MP197TAD TO model are listed in Section B.3.2.1.

The seal O-rings are not explicitly considered in the models. The maximum seal temperatures are retrieved from the models by selecting the nodes at the locations of the corresponding seal O-rings.

The geometry of the MP197TAD TO model and the gaps are shown in Figure B.3– 2 through Figure B.3– 7. Mesh sensitivity of the MP197TAD TO model is discussed in Appendix B.3.6.2.1.

Typical boundary conditions for MP197TAD TO model under NCT are shown in Figure B.3– 8.

B.3.3.1.2 Calculation of Maximum Accessible Surface Temperature

A personnel barrier installed on the transport skid between the two impact limiters limits the accessible packaging surfaces to the impact limiter and barrier outer surfaces. The personnel barrier has an open area of at least 80%. Heat transfer between the overpack and barrier will be minimal due to the small radiation view factor between the cask and the barrier. Due to large distance between the barrier and cask outer surface, the free convection heat transfer remains undisturbed. The transport configuration is shown in Chapter B.1.

The MP197TAD TO model described in Section B.3.3.1.1 is run with a heat load of 22 kW, 100°F ambient temperature and no insolance to bound the maximum accessible surface temperature under shade.

The maximum accessible surface temperature of impact limiters under these conditions is 119°F. The maximum temperature of the shield shell outer surface is 270°F. The maximum temperature of the personnel barrier is calculated based on the maximum temperature of the shield shell outer surface using the following methodology.

The personnel barrier is exposed to thermal radiation from the overpack shield shell and dissipates heat via thermal radiation and natural convection to ambient. Since the personnel barrier is far apart from the overpack shield shell, it is not exposed to the hot air streams from the overpack.

The heat balance for the personnel barrier is shown schematically in Figure B.3– 10. The following conservative assumptions are considered to simplify the heat balance.

- Convection heat dissipation from the barrier is omitted completely.
- Radiation heat dissipation to ambient from barrier surfaces facing the cask is omitted.
- The maximum cask outer surface temperature is considered for the cask entire outer surface facing the barrier.
- An emissivity of 0.9 is considered for the Overpack shield shell outer surface.

The heat balance for the personnel barrier is as follows.

$$q_{in,rad} = q_{out,rad}$$

$$q_{in,rad} = \frac{\sigma\left(T_{shell}{}^4 - T_{PB}{}^4\right)}{\dfrac{1-\varepsilon_{shell}}{\varepsilon_{shell}\,A_{shell}} + \dfrac{1}{F_{PB-shell}\,A_{PB}} + \dfrac{1-\varepsilon_{PB}}{\varepsilon_{PB}\,A_{PB}}},$$

$q_{out,rad} = q_{1,rad,amb} + q_{2,rad,amb}$, $q_{1,rad,amb} = 0$ (conservatively, omitted in this analysis),

$$q_{2,rad,amb} = \frac{\sigma\left(T_{PB}{}^4 - T_{\infty}{}^4\right)}{\dfrac{1-\varepsilon_{PB}}{\varepsilon_{PB}\,A_{PB}} + \dfrac{1}{F_{PB-\infty}\,A_{PB}}},$$

σ = Stefan-Boltzmann constant = 0.119E-10 (Btu/hr-in^2-°R^4),
T_{shell} = maximum cask shield shell temperature (°R),
T_{PB} = maximum personnel barrier temperature (°R),

T_∞ = ambient temperature = 100 °F = 560 °R,
ε_{shell} = emissivity of painted shield shell = 0.9,
ε_{PB} = emissivity of personnel barrier = 0.587 (see discussion in Section B.3.2.1),
$F_{PB\text{-}shell}$ = view factor from personnel barrier to overpack shield shell,
$F_{PB\text{-}\infty}$ = view factor from personnel barrier (not facing overpack) to ambient = 1.0,
A_{PB} = surface area of personnel barrier (in^2),
A_{shell} = surface area of overpack shield shell (in^2).

The dimensions of the overpack shield shell (D_{shell}) and personnel barrier (l_{PB}) are 92.75" and 51.88", respectively as shown in the drawings in Chapter B.1.

$$\frac{A_{shell}}{A_{PB}} = \frac{\pi D_{shell}/2}{l_{PB}} = \frac{\pi \times 92.75/2}{51.88} = 2.808.$$

The view factor of a long strip element to a parallel cylinder is given in [17], Chapter 7, Appendix B, Page 7.80 as follows. The dimensions are defined in Figure B.3– 10.

$$F_{d1-2} = \frac{Y}{X^2 + Y^2}$$

with
Y = y/r, X = x/r,
y = 56" (See the drawings in Appendix B.1.4.1),
r = 92.75/2 = 46.375" (See the drawings in Appendix B.1.4.1).

Integration of the above incremental view factor over the length of the strip barrier gives the view factor of the strip to the cask.

$$F_{1-2} = \frac{1}{l_{PB}} \int_0^{l_{PB}} \left(\frac{Y}{X^2 + Y^2} \right) dx$$

Considering $L = l_{PB}/r$ and $dX = dx/r$, gives the view factor of the personnel barrier to the cask.

$$F_{1-2} = \frac{1}{L} \int_0^{L} \left(\frac{Y}{X^2 + Y^2} \right) dX = \frac{1}{L} \left(\tan^{-1} \frac{L}{Y} \right) = \frac{r}{l_{PB}} \tan^{-1} \left(\frac{l_{PB}}{y} \right)$$

The view factor of the personnel barrier mesh to the cask shield shell is calculated as follows:

$$F_{1-2} = \frac{r}{l_{PB}} \tan^{-1} \left(\frac{l_{PB}}{y} \right) = \frac{46.375}{51.88} \tan^{-1} \left(\frac{51.88}{56} \right) = 0.668.$$

Since the personnel barrier has an open area of 80% (f = 0.8), a factor of 0.2 is considered to calculate the view factor of the personnel barrier mesh to the cask.

$$F_{PB-shell} = F_{1-2} \times (1 - f) = 0.668 \times (1 - 0.8) = 0.134.$$

The substitution of the above values in the heat balance of the personnel barrier gives the maximum temperature of the personnel barrier as 140°F.

B.3.3.1.3 Effective Thermal Properties in MP197TAD TO Model

1) Effective Conductivity for Helium Gap between the DSC and the MP197TAD TO Inner Shell

Effective conductivities are calculated for helium between the DSC and the MP197TAD TO inner shell to account for conduction and radiation between these components.

The effective conductivity of helium within the gap between the DSC shell and MP197TAD TO inner shell is calculated based on a detailed sub-model of this region. This sub-model considers a 10" high, 30 degree segment of the shells. Radiation between surfaces is modeled using /AUX12 processor. Figure B.3– 11shows the sub-model of the DSC shell and the MP197TAD TO inner shell.

The following assumptions are considered in calculation of this effective conductivity.

- Conductivity of helium for the gas between the shells,
- Stainless steel conductivity for the shells,
- Emissivity of 0.587 for the shells,
- Diametrical gap size of 0.75",
- Heat flux of 2.813 Btu/hr-in2 equivalents to 29.2 kW,
- Inner diameter of the MP197TAD TO Inner Shell is considered as 70.5",
- Outer diameter of the TN44B DSC is considered as 69.75".

Helium is also used as backfill gas for TN44B in MP197TAD TO. The TN44B DSC shell and the MP197TAD TO inner shell are made of stainless steel with an emissivity of 0.587 as noted in Section B.3.2.1. The diametrical gap between TN44B DSC and MP197TAD TO cask inner shell is 0.75", which is identical to the above parameter.

The effect of heat flux and the temperature gradient caused by the applied heat flux cancel each other out in the equation for calculation of effective conductivity as shown below. Therefore, the effective conductivity for the gap between the canister shell and the cask inner shell is relatively insensitive to the heat flux.

Since the parameters used in calculation of effective conductivity for the gap between DSC and inner shell are identical to those for the gap between TN44B DSC and MP197TAD TO inner shell, the calculated effective conductivity is applicable for this evaluation.

In the DSC/MP197TAD TO sub-model, a heat flux of 2.813 Btu/hr-in^2 equivalent to 29.2 kW is applied on the radial surface of the innermost shell (DSC shell) and fixed temperature boundary conditions are applied over the radial surface of the outermost shell (MP197TAD TO inner shell).

The nodes of the gap between the DSC shell and MP197TAD TO inner shell build up the radiation super element (MATRIX50). To avoid convergence problems, the heat flux or fixed temperature boundary conditions are not applied directly on the nodes of the radiation super element. Instead the heat flux is applied on the innermost nodes of the DSC shell and the fixed temperatures are applied on the outermost nodes of the MP197TAD TO shell.

The effective conductivity is calculated as follows.

$$k_{eff} = \frac{(q_{react} \times 360/30)\ \ln(D_{i,TC}/D_{o,DSC})}{2\pi \times 10 \times (T_{DSC} - T_{TC})}$$

Where,
q_{react} = reaction solution retrieved from the model (Btu/hr)
$D_{i,TC}$ = inner diameter of inner shell = 70.5"
$D_{o,DSC}$ = outer diameter of DSC = 69.75"
T_{TC} = temperature of the inner shell innermost nodes (°F)
T_{DSC} = average temperature of DSC shell (°F)

Due to high conductivity of the metallic shells, the temperature gradient across the shells is very small (< 1°F). Therefore the actual temperature gradient across the gap is slightly lower than the temperature gradient between the shells ($T_{DSC} - T_{TC}$) considered in the above equation. This results in a slightly underestimated effective conductivity across the gap, which is conservative for the purpose of this calculation.

The average temperature of the DSC shell is retrieved from the model using "ETABLE" commands in ANSYS [21]. The fixed temperature boundary condition applied on the outermost node of TC shell is considered as TC temperature.

The calculated effective conductivity shown in Section B.3.2.1, material # 11 and is applied only in radial direction for the gap between the TN44B DSC shell and the cask inner shell. The conductivity in axial direction is set equal to helium conductivity for conservatism.

2) Effective Conductivity for MP197TAD TO Slide Rails

A helium gap of 0.01" is considered between the slide rail and DSC shell to account for the contact resistance. For simplification of the model, this gap is integrated into the slide rail model and an effective conductivity is calculated for this component. The calculated effective conductivity for the slide rail is applied conservatively in all directions.

The gap and the slide rail built up serial thermal resistances along the rail height. The effective conductivity through these serial pieces is:

$$k_{eff} = \frac{t_{rail} + t_{gap}}{\dfrac{t_{rail}}{k_{rail}} + \dfrac{t_{gap}}{k_{He}}}$$

Where,
k_{eff} = effective conductivity (Btu/hr-in-°F)
t_{rail} = thickness of TC slide rail = 0.12"
t_{gap} = thickness of gap = 0.01"
k_{rail} = conductivity of TC slide rails (Nitronic 60)
k_{He} = conductivity of helium (Btu/hr-in-°F)

The calculated effective conductivity for the slide rail is listed in Section B.3.2.1, material # 12 for reference.
The effective conductivities listed in Section B.3.2.1, material # 12 are considered in the model for the Cartesian x and y coordinates, covering the cross sectional plane of the cask slide rail.

The conductivity of the rail in the axial direction (Cartesian z coordinate in the model) remains equal to the conductivity of Nitronic 60. The conductivity of stainless steel SA-240, Type 304 shown in Section B.3.2.1 is used for Nitronic 60.

B.3.3.1.4 TN44B DSC Model

The maximum decay heat load for the TN44B DSC during transport in the MP197TAD TO is 22 kW. The maximum decay heat load per fuel assembly is 0.54 kW for the TN44B basket. The maximum decay heat load for the TN44B DSC during transport is summarized in the following table.

Maximum Decay Heat Load

No of FA	Max Decay Heat (kW/FA)	Total
44	0.54	22 (1)
Total Heat Load		**22** (1)

(1) Adjust payload to maintain the total TN44B DSC heat load within the specified limit.

The following assumptions and conservatism are considered for TN44B DSC model:

- The maximum heat load of 0.545 kW per assembly is considered for the TN44B DSC with a maximum heat load of 24 kW per DSC.
- The fuel assemblies contained in the TN44B basket are intact fuel assemblies.
- No convection is considered within the DSC cavity.
- Only helium conduction is considered from the basket upper surface to the DSC top shield plug.
- Heat transfer between the basket and the top shield plug is conservatively modeled as conduction through helium.
- Radiation is considered only implicitly between the fuel rods and the fuel compartment walls in the calculation of effective fuel conductivity in Section B.3.3.1.5. No other radiation heat exchange is considered within the DSC.
- Active fuel length for BWR fuel assemblies is 144" [29] and starts about 7.5" from the bottom of the basket [29]. The total length of the basket assembly is 176.5".

The following gaps are considered in the TN44B DSC model at thermal equilibrium:

- 0.50" diametrical hot gap between the basket outer surface and the DSC inner surface. This assumed gap is larger than the nominal diametrical cold gap and is therefore conservative regarding the maximum temperatures.
- 0.50" diametrical hot gap between the shield plugs and the DSC inner surface. This assumed gap is larger than the maximum diametrical cold gap of 0.25".
- 0.125" axial gap between the bottom of the basket and the DSC bottom inner cover plate. This assumed gap is considered conservatively to reduce the axial heat dissipation and maximize DSC component temperatures in the hot section.

- 0.125" gap in axial direction between the aluminum rail pieces. These axial gaps considered between the rail pieces are larger than the tolerances considered for the rails and are therefore conservative.
- 0.01" gap between any two adjacent plates or components in the cross section of the basket for calculation of effective conductivities of multiple plates retained between fuel compartments. The locations of these multiple plates are shown in Figure B.3–12.
- 0.01" gap on either side of aluminum thermal plates for calculation of effective conductivities of aluminum plates.
- 0.01" axial gap between DSC shield plugs and DSC cover plates.
  The above 0.01" gaps account for the total contact resistances between the adjacent plates.

The geometry of the model and the gaps are shown in Figure B.3– 13 through Figure B.3– 15.

Decay heat load is applied as heat generation boundary conditions over the elements representing homogenized fuel assemblies. The base heat generation rates used in this analysis is calculated as follows.

$$\dot{q}'''_{base} = \frac{q}{a^2\ L_a} = 0.3326 \text{ Btu/hr-in}^3$$

Where,
q = Decay heat load per assembly = 1,860 Btu/hr (0.545 kW),
a = Width of the homogenized fuel assembly = 6.25",
L_a =Active fuel length = 144".
The base heat generation rate is multiplied by peaking factors along the axial fuel length to represent the axial decay heat profile. A correction factor is used to avoid degradation of decay heat load due to imperfections in application of peaking factors.

$$\dot{q}''' = \dot{q}'''_{base} \times PF \times CF$$

Where,
PF = Peaking Factor,
CF = correction factor = 1.006.

Axial decay heat profile for BWR fuel assemblies is the same as the one described in Appendix T, Section T.4.6.4 [30]. The peaking factors from Appendix T Section T.4.6.4 [30] are converted to match the regions defined for the fuel assemblies in the TN44B DSC model. These peaking factors are listed in Table B.3- 2.

The active fuel length for fuel assembly LaCrosse is only 85", which is significantly shorter than the other fuel assemblies considered for storage/transport in the TN44B DSC. The heat load of this fuel assembly should be lower than the longer fuel assemblies to maintain the same temperature distribution in the TN44B DSC. Since conduction and effective conductivities are the only heat transfer paths considered in the TN44B DSC model, the temperatures are directly proportional to the fuel assembly heat load and inversely proportional to the active fuel length and effective fuel conductivity.

The transverse and axial effective conductivities of fuel assembly LaCrosse are higher than those for the bounding fuel assembly. Therefore, the following equations determine the reduction in

heat load for fuel assembly LaCrosse to maintain the TN44B DSC temperatures at the same level as those determined for the bounding fuel assembly.

$$\left(\frac{q}{L_a\, k_{eff}}\right)_{LaCrosse} = \left(\frac{q}{L_a\, k_{eff}}\right)_{BoundingFA}$$

$$q_{LaCrosse} = q_{boundingFA}\,\frac{L_{a,LaCrosse}}{L_{a,BoundingFA}}\cdot\frac{k_{eff,LaCrosse}}{k_{eff,boundingFA}} > q_{boundingFA}\,\left(\frac{85}{144}\right) \approx 0.59\, q_{boundingFA}$$

$$= 0.59 \times 1860\ \ (\text{Btu/hr}) = 1098\ \ (\text{Btu/hr})$$

With,

k_{eff} = effective fuel assembly conductivity (Btu/hr-in-°F),

q = Decay heat load per assembly defined for each loading zone (Btu/hr),

$q_{boundingFA}$ = Decay heat load per assembly for bounding FA =1860 Btu/hr= 0.545 kW,

L_a =Active fuel length (in),
= 144" for bounding fuel assembly,
= 85" for LaCrosse fuel assembly.

The contribution of higher effective conductivity for LaCrosse fuel assemblies ($k_{eff,\,LaCrosse}$ / $k_{eff,\,bounding\,FA}$) is omitted in the above equation for conservatism. The heat load for LaCrosse fuel assembly should be reduced to 59% of the heat load for bounding fuel assembly to maintain the TN44B DSC temperatures at the same level calculated for the bounding fuel assembly. The maximum decay heat load per assembly for LaCrosse fuel assembly in the TN44B DSC is limited to 1098 Btu/hr (0.32 kW).

Axial Heat Flux Profile

The thermal analyses consider the effect of the decay heat flux varying axially along a fuel assembly. The axial heat flux profile for a BWR fuel assembly is shown in Appendix T, Figure T.4-37 [30] and is based on data from an operating BWR facility.

As noted in Appendix T, Section T.4.6.4 [30], the heat flux profile of Figure T.4-37 is based on a maximum bundle-average burnup of 40,000 MWd/MTU. The maximum bundle-average burnup allowed in TN44B DSC is 62,000 MWd/MTU, which is considerably higher than 40,000 MWd/MTU. Reference [35] shows that at a higher burnup, the heat flux shape tends to flatten with a reduction in the maximum axial peaking factor in the middle region, and the flux shape becomes more pronounced in the fuel end regions. The reduction of the maximum axial peaking factor in a more flattened heat flux shape will result in lower fuel cladding temperatures. Therefore, the application of a heat flux shape from a lower burnup spent fuel (40,000 MWd/MTU) on a higher burnup spent fuel (62,000 MWd/MTU) is conservative. These peaking factors are shown schematically below for reference.

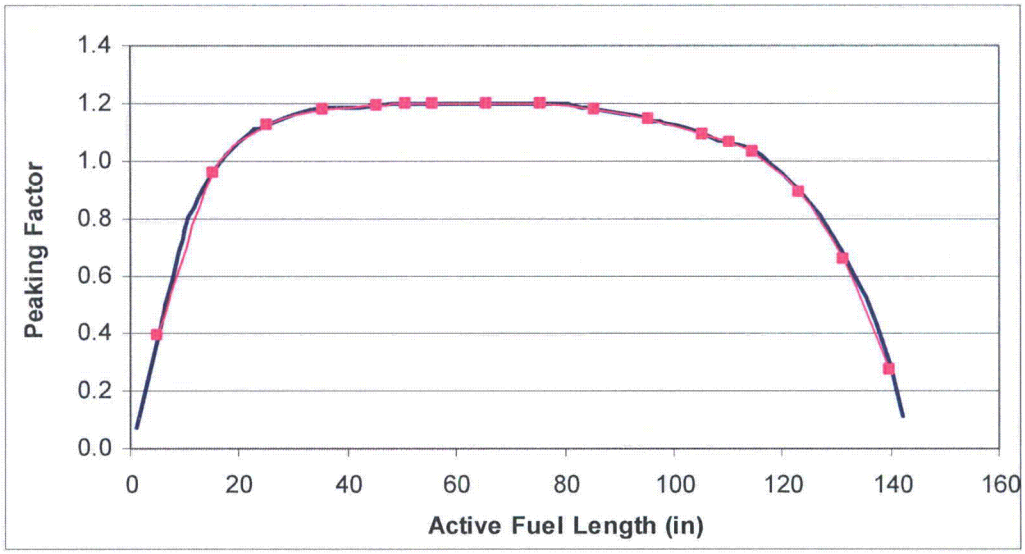

Typical boundary conditions for the TN44B DSC model are shown in Figure B.3– 16.

The material properties are shown in Section B.3.2.2.

B.3.3.1.5 Effective Thermal Properties in TN44B Basket

1) Effective Conductivity for Homogenized Plates in TN44B Basket

Multiple plates retained between two fuel compartments or between a fuel compartment and a basket rail are considered as one homogenized material in the TN44B DSC model. A list of the homogenized multiple plates are shown in Table B.3- 3.

The multiple plates built up parallel thermal resistances along their length and serial thermal resistances across their thickness. The gaps considered between the paired plates and their adjacent basket plates at the cross section account for the contact resistance between the plates.

The effective conductivities of the paired plates are calculated as follows:

$$k_{eff,along} = \frac{k_{poison} \times t_{poison} + k_{Al} \times t_{Al} + k_{SS} \times t_{SS} + k_{Gap} \times t_{Gap}}{t_{poison} + t_{\mathrm{Al}} + t_{\mathrm{SS}} + t_{\mathrm{Gap}}}$$ along the length (parallel resistances)

$$k_{eff,across} = \frac{t_{poison} + t_{\mathrm{Al}} + t_{\mathrm{SS}} + t_{\mathrm{Gap}}}{\frac{\mathrm{t}_{poison}}{\mathrm{k}_{poison}} + \frac{t_{Al}}{k_{Al}} + \frac{t_{SS}}{k_{SS}} + \frac{t_{Gap}}{k_{Gap}}}$$ across the thickness (serial resistances)

Where,

k_{poison} = conductivity of borated stainless steel poison plate (Btu/hr-in-°F)
t_{poison} = thickness of borated stainless steel poison plate (in)
k_{Al} = conductivity of aluminum (Btu/hr-in-°F)
t_{Al} = thickness of aluminum plate (in)
k_{SS} = conductivity of stainless steel (Btu/hr-in-°F)
t_{SS} = thickness of stainless steel plate (in)

k_{Gap} = conductivity of helium (Btu/hr-in-°F)
t_{Gap} = total thickness of helium gaps among multiple plates (in)
For conservatism, the conductivity of borated stainless steel is reduced by 5% for calculation of effective conductivities.

The calculated effective conductivity values for the homogenized multiple plates are listed in Section B.3.2.2 item 20 through 27.

2) Effective Thermal Properties for BWR Fuel Assemblies in TN44B DSC

The BWR fuel assemblies that are considered for transport in the TN44B DSC including design data for each fuel assembly are listed in Chapter B.1. This section includes calculation of the bounding properties among all BWR fuel assemblies allowed to be transported in the TN44B DSC with maximum total decay heat load of 22 kW per DSC.

The thermal properties of Zircaloy and UO_2 pellet are presented in Appendix T, Section T.4.2 of [30]. Thermal conductivity of un-irradiated UO_2 for temperatures below 750K (890°F) is bounded by k = 4 W/(m·K) = 0.1926 Btu/(hr·in·°F) = 0.0032 Btu/(min·in·°F), as shown in Figures A-2.1 through A-2.4 in [26]. This value was used in the calculation.

As discussed in [32], response 4.1, the irradiated UO_2 conductivity is lower by approximately a factor of two compared to the un-irradiated UO_2 conductivity. Using irradiated UO_2 conductivity decreases the effective fuel conductivity in the transverse direction. However, the transverse fuel effective conductivity with the irradiated UO_2 conductivity at the operating temperature of 700°F is only 3% lower than the one with un-irradiated UO_2 conductivity.

The sensitivity runs in [32], response 4.1 show that fuel cladding temperature changes due to irradiation is insignificant (within 1°F), which is negligible. These results show that the fuel cladding temperatures are not sensitive to the conductivity of UO_2. Therefore, use of un-irradiated UO_2 fuel pellet conductivity is reasonable for the irradiated UO_2.

Axial Fuel Effective Thermal Conductivity

The axial fuel conductivity is assumed to be limited to the cladding conductivity weighted by its fractional area as required in NUREG 1536 [33].

$K_{axl} = (K_{zirc})(A_{zirc}/A_{eff})$

K_{zirc} = conductivity of Zircaloy,

A_{eff} = cross section area of fuel compartment (6.25") x (6.25") = 39.063 in^2,

A_{zirc} = number of fuel rods × cross sectional area of one fuel rod cladding.

The bounding axial effective conductivity for the TN44B fuel assemblies is listed in Section B.3.2.2, Item #13.

Transverse Fuel Effective Thermal Conductivity

The transverse fuel effective thermal conductivity is determined by creating a two-dimensional finite element model of the fuel assembly centered within a fuel compartment. The outer surfaces, representing the fuel compartment walls, are held at a constant temperature, and heat generating boundary condition is applied to the fuel pellets within the model. A maximum fuel

assembly temperature is then determined. The isotropic effective thermal conductivity of a heat generating square, such as the fuel assembly, can be calculated as described in [34]:

$$K_{eff} = 0.29468 \times \frac{q''' \cdot a^2}{(T_c - T_o)}$$

q''' = heat load per unit volume of fuel assembly, Btu/hr·in^3,
a = width of fuel compartment opening = 6.25",
T_c = maximum temperature of fuel assembly, °F,
T_o = compartment wall temperature, °F.

where:

$$q''' = \frac{q}{a^2 L_a}$$

q = decay heat load per assembly, Btu/hr,
L_a = active fuel length = 144 in.

In determining the temperature dependent effective fuel conductivities an average temperature, equal to $(T_c + T_o)/2$, is used for the fuel temperature.

Two dimensional, finite element model of fuel assembly was developed using ANSYS code [21]. PLANE55 elements were used to model components such as the fuel pellets, fuel cladding, and the helium back fill gas. The gap between the fuel cladding and the fuel pellets is also included in the model.

Heat generated in the fuel pellets dissipates by conduction and radiation to the fuel compartment walls. Convection is not considered in the model. Radiation between the fuel rods, guide tubes, channel, and basket walls was simulated using the radiation super-element processor (AUX12). LINK32 elements were used for modeling of radiating surfaces in creating the radiation super-element and were unselected prior to the solution of the model. The compartment walls are not modeled as a solid entity but using LINK32 elements. For these elements aligned with the outermost nodes of the model are given the emissivity of the compartment walls.

An emissivity of stainless steel of 0.20 is applied to the LINK32 elements on compartment walls. The bounding emissivity of 0.74 is considered for Zircaloy cladding and applied to the LINK32 elements on cladding walls.

The finite element model of bounding fuel assembly FANP 9x9-2 is shown in Figure B.3– 17.

The following heat generation is applied to the fuel pellets in the model:

$$q''' = \frac{q/N}{n\left(\frac{\pi}{4} d_p^{\,2}\right) L_a}$$

q''' = heat generation, Btu/(min·in^3·°F),
q = total decay heat load per assembly, Btu/min,
N = number of Fuel Assemblies = 44,

n = number of fuel rods per fuel assembly,
d_p = pellet outer diameter, in,
L_a = active fuel length, in.

The reaction solution (q_{react}) after solving the 2D model is equal to the heat generated per unit length of the active fuel.

$$q_{react} = \frac{q}{L_a}$$

Substitution it to the equation for K_{eff} gives

$$K_{eff} = 0.29468 \times \frac{q_{react}}{(T_c - T_o)}$$

The above equation is used to calculate the transverse effective fuel conductivity for the FA model.

The models were run with a series of isothermal boundary conditions applied to the nodes representing the fuel compartment walls.

The bounding transverse effective conductivity for the TN44B fuel assemblies is listed in Section B.3.2.2, Item #13.

Fuel Effective Density and Specific Heat

Volume average density and weight average specific heat are calculated to determine the effective density and specific heat for the fuel assembly. The equations to determine the effective density ρ_{eff} and specific heat $C_{p\,eff}$ are shown below.

$$\rho_{eff} = \frac{\sum \rho_i V_i}{V_{assembly}} = \frac{\rho_{UO2}\ V_{UO2} + \rho_{Zr4}\ V_{Zr4}}{a^2 L_a}$$

$$C_{p_{eff}} = \frac{\sum \rho_i V_i C_{Pi}}{\sum \rho_i V_i} = \frac{\rho_{UO2}\ V_{UO2}\ C_{P\,UO2} + \rho_{Zr4}\ V_{Zr4}\ C_{P\,Zr4}}{\rho_{UO2}\ V_{UO2} + \rho_{Zr4}\ V_{Zr4}}$$

where

ρ_{UO2}, ρ_{Zr4} = density of fuel pellets and cladding,
V_{UO2}, V_{Zr4} = volume of fuel pellets and cladding,
$c_{p\,UO2}$, $c_{p\,Zr4}$ = specific heat of fuel pellets and cladding.

The bounding values for fuel effective density and fuel effective specific heat are listed in Section B.3.2.2, Item #13.

3) Effective Thermal Properties of Homogenized TN44B Basket

The TN44B basket effective density, thermal conductivity and specific heat are calculated for use in the transient analyses of the TN44B DSC. The calculation of these thermal effective properties are based on the basket components' weight data provided in Chapter B.2.

Dimensions of Homogenized TN44B

Basket OD (in) (1)	64.75
Basket length (in)	176.5

Notes:
(1) Basket OD here includes the gap between the basket and the DSC shell.

The basket effective density $\rho_{eff\,basket}$, and specific heat $c_{p\,eff\,basket}$ are calculated as volumetric and weight average, respectively using the following equations.

$$\rho_{eff\,basket} = \frac{\sum W_i}{V_{basket}} = \frac{W_{steel} + W_{Al} + W_{poison} + W_{fuel}}{L_{basket} \cdot \pi \cdot D_{basket}^{\ 2} / 4}$$

$$c_{p\,eff\,basket} = \frac{\sum W_i \cdot c_{pi}}{\sum W_i} = \frac{W_{steel} \cdot c_{p\,steel} + W_{Al} \cdot c_{p\,Al} + W_{poison} \cdot c_{p\,poison} + W_{fuel} \cdot c_{p\,fuel}}{W_{steel} + W_{Al} + W_{poison} + W_{fuel}}$$

Where
W_i = weight of basket components
V_{basket} = total basket volume
L_{basket} = basket length = 176.5"
D_{basket} = basket OD = 64.75",
$c_{p\,i}$ = specific heat of basket materials.

The following assumptions are used in the calculation of the basket effective density and specific heat calculation:

- These specific heat and density values are listed in Section B.3.2.2.
- For aluminum at T > 400°F specific heat is conservatively assumed equal to value at 400°F.
- For borated stainless steel at T>500°F, specific heat is conservatively assumed equal to value at 500°F.
- Conservatively, helium is not included in density and specific heat calculation.

The calculated effective density and effective specific heat for the TN44B basket are summarized in Table B.3- 4 and Table B.3- 5, respectively.

To calculate the effective thermal conductivities, a 33.625" long slice of the TN44B basket is created by selecting the nodes and elements of the basket from the finite element model described in Section B.3.3.1.4. The slice model is shown in Figure B.3– 18

To calculate the axial effective conductivity of the basket, constant temperature boundary conditions are applied at the top and bottom of the slice model. No heat generation is considered for the fuel elements in this case. The axial effective conductivity is calculated using the equation below.

$$k_{basket,axl} = \frac{Q_{axl} \times L}{A_{slice} \times \Delta T} \times 0.95$$

Where:

Q_{axl} = Amount of heat leaving the upper face of the slice model retrieved using the reaction solution of the uppermost nodes (Btu/hr),
L = Length of the model = 33.625",
A_{slice} = Surface area of the upper (or bottom) face of the basket slice model
$= \pi/8 \times D_{basket}{}^2 = 1646\ in^2$
$\Delta T = (T_2 - T_1)$ =Temperature difference between upper and lower faces of the model (°F),
T_2 = Constant temperature applied on the upper face of the model (°F),
T_1 = Constant temperature applied on the lower face of the model (°F).

Only 95% of the estimated axial effective conductivity is considered for conservatism.

Typical applied boundary conditions for the calculation of the axial effective conductivity are shown in Figure B.3– 18.

In determining the temperature dependent axial effective conductivities an average temperature, equal to $(T_1 + T_2)/2$, is used for the basket temperature. The axial effective conductivities for the TN44B basket are listed in Table B.3- 6.

The basket slice models are also used to calculate the transverse effective conductivity of the basket. For this purpose, constant temperature boundary conditions are applied on the outermost nodes of the slice model and heat generating conditions are applied over the fuel elements.

The heat generation rates for the slice model of the TN44B basket are calculated based on the heat load of 0.545 kW per assembly and a peaking factor of 1.2 for BWR assemblies.

The following equation is given in [31] for long solid cylinders with uniformly distributed heat sources.

$$T = T_o + \frac{q''' r_o^2}{4k}\left[1 - \left(\frac{r}{r_o}\right)^2\right]$$

with:
T_o = Temperature at the outer surface of the cylinder (°F),
T = Maximum temperature of cylinder (°F),
q''' = Heat generation rate (Btu/hr-in^3),
r_o = Outer radius = $D_{basket}/2$ = 32.375" for TN44B basket including the gap to the DSC shell,
r = Inner radius = 0 for slice model,
k = Thermal Conductivity (Btu/hr-in-°F).

The above equation is rearranged to calculate the transverse effective conductivity of the basket as follows.

$$\dot{q} = \frac{Q_{rad}}{V}$$

$$k_{basket,rad} = \frac{Q_{rad} \cdot r_0^2}{4 \cdot V \cdot \Delta T} \times 0.95 = \frac{0.95\, Q_{rad}}{2\pi \cdot L \cdot \Delta T}$$

With:

Q_{rad} = Amount of heat leaving the periphery of the slice model retrieved using the reaction solution of the outermost nodes (Btu/hr),
L = Length of the slice model = 33.625",
V = Volume of the slice model = $(\pi r_0^2 L)/2$,
$\Delta T = (T_{max} - T_o)$ = Difference between maximum and the outer surface temperatures in (°F).
Only 95% of the estimated radial effective conductivity is considered for conservatism.

Since the surface area of the fuel assemblies at the basket cross section is much larger than the other components, assuming a uniform heat generation is a reasonable approximation to calculate the radial effective conductivity.

Typical boundary conditions for the calculation of the transverse effective conductivity are shown in Figure B.3– 18.

In determining the temperature dependent transverse effective conductivities an average temperature, equal to $(T_{max}+T_o)/2$, is used for the basket temperature.

The radial effective conductivities of the TN44B basket are listed in Table B.3- 7.

B.3.3.2 Heat and Cold

Table B.3- 8 presents the maximum temperatures for MP197TAD TO components and TN44B DSC shell for NCT.

As shown in Table B.3- 8, the maximum TN44B DSC shell temperatures within the MP197TAD TO with 22 kW heat load for NCT are 422°F at the ends and 419°F at the mid-section, where the peaking factors are at their highest level.

However, the maximum fuel cladding and basket component temperatures within the TN44B DSC for NCT are analyzed with a heat load of 24 kW. A conservative DSC shell temperature profile with a maximum canister shell temperature of 468°F is used in this evaluation. This bounds the maximum DSC shell temperature of 422°F obtained with TN44B DSC in MP197TAD TO with 22kW heat load.

Based on the above conservatism, the thermal analysis results for TN44B DSC with 24kW heat load and higher DSC shell temperatures represent the bounding fuel cladding and basket component temperatures for NCT with 22kW and lower DSC shell temperatures. The estimated maximum component temperatures for TN44B DSC under NCT are summarized in Table B.3- 9.

As calculated in Section B.3.3.1.2, the maximum accessible surface temperatures for impact limiter and personnel barrier are 119°F and 140°F, respectively. These temperatures are well below the limit of 185°F defined in Section B.3.1.

The thermal analysis of NCT demonstrates that the MP197TAD TO with up to 22 kW heat load meets all applicable requirements. The maximum temperatures of MP197TAD TO and TN44B DSC are summarized in Table B.3- 10 for -40°F and 100°F ambient temperatures.

The maximum temperatures calculated using conservative assumptions are well below specified limits. The seal O-rings are not explicitly considered in the models. The maximum seal temperatures are retrieved from the models by selecting the nodes at the locations of the corresponding seal O-rings in the MP197TAD TO model. The maximum seal temperature is

324°F, which is well below the long-term limit of 400°F specified for continued seal function in Section B.3.1.

The maximum wood temperature for is 305°F which is below the considered limit of 320°F specified in Section B.3.1 for structural analysis.

The maximum temperature of gamma shield (lead) is 333°F, which is well below the lead melting point of 621°F specified in Section B.3.1.

The highest volumetric average resin temperature in the neutron shield at the hottest cross section is 281°F. The Vyal B resin temperature is well below the temperature limit of 320°F specified in Section B.3.1 and no degradation of the neutron resin is expected.

The temperature distributions of MP197TAD TO with TN44B DSC for NCT with 100°F ambient and insolation are shown in Figure B.3– 9.

The temperature distributions of TN44B DSC with 24 kW and bounding DSC shell temperature profile used in this evaluation are shown in Figure B.3– 19.

Under the minimum ambient temperature of -40°F (-40°C) for NCT, the resulting packaging component temperatures will approach -40°F if no credit is taken for the decay heat load. Since the package materials, including containment structures and the seals, continue to function at this temperature, the minimum temperature condition has no adverse effect on the performance of the MP197TAD TO.

The maximum component temperatures for ambient temperatures of -40°F and -20°F with maximum decay heat and no insulation are calculated for TN44B DSC to use for structural evaluations. These temperatures are listed in Table B.3- 11.

The average temperatures of inner shell, lifting device spacers and helium gas in MP197TAD TO cavity, and the average temperatures of TN44B DSC shell for NCT are listed in Table B.3-12. These temperatures are used to evaluate the maximum internal pressures and thermal expansion in MP197TAD TO cavity.

Thermal stresses for the MP197TAD TO loaded with TN44B DSC are discussed in Chapter B.2. The maximum normal operating pressure for the MP197TAD TO is discussed in Section B.3.3.3. The performance of the MP197TAD TO loaded with TN44B DSC for HAC is discussed in Section B.3.4.

B.3.3.3 Maximum Normal Operating Pressure

B.3.3.3.1 MP197TAD TO Operating Pressure

The following assumptions are considered to determine the maximum pressures within the MP197TAD TO cavity during NCT when the MP197TAD TO is loaded with TN44B DSC:

- All dimensions used in calculating the maximum pressures are nominal.
- 98% of the MP197TAD TO cavity free volume is conservatively used in calculating the maximum pressures.

- The spacer at the top of the MP197TAD TO cask lid is assumed as solid disc with diameter equal to the MP197TAD TO inner diameter. This conservatively decreases the free volume of the cask cavity.
- The initial temperature of helium backfill in the cask cavity is assumed to be 70°F.
- The maximum initial pressure of the helium backfill in the cask cavity is 3.5 (2.5±1) psig.
- The maximum helium temperature is conservatively assumed as the average temperature for calculating the HAC TAD TO cask cavity pressure.
- The average temperatures for helium in the TAD TO cask cavity calculated for 100°F daily average ambient temperature are conservatively increased by 16°F for both NCT and HAC.

The average helium temperatures in the cask cavity are retrieved from the MP197TAD TO model described in Section B.3.3.1.1. The dimensions and temperatures used in calculating the pressures in the MP197TAD TO cavity during NCT and HAC are listed below.

$OD_{Canister}$ = Outer diameter of the TN44B DSC = 66.25",
$L_{Canister}$ = Length of the TN44B DSC = 196.25",
$T_{avg,he,NCT}$ = Average temperature of helium for NCT = 324°F,
$T_{avg,he,HAC}$ = Average temperature of helium for HAC = 367°F,
ID_{Shell} = Inner diameter of MP197TAD TO inner shell = 67",
L_{Cavity} = Total MP197TAD TO cavity length = 206"
L_{Spacer} = Length of the canister lifting device spacer = 6.25"
L_{TO} = Available MP197TAD TO cavity length = L_{Cavity}-L_{Spacer} = 206 - 6.25 = 199.75".

The free volume of the MP197TAD TO cask cavity determined based on these dimensions is:

$$V_{free,cc} = \frac{\pi}{4} * \left[(ID_{Shell}^2 * L_{TO}) - (OD_{Canister}^2 * L_{Canister}) \right]$$

The number of moles of helium in the cask cavity is calculated using the ideal gas law is:

$$n_{he,Initial} = \frac{P_{initial} * (6894.8 Pa/psi) * V_{free,cc} * (1.6387 * 10^{-5} m^3/in^3)}{R * T_{avg,He} (5/9 K/^oR)}$$

The maximum normal operating pressure in the MP197TAD TO cavity for NCT is calculated as:

$$P_{NCT} = \frac{\left(1.4504 * 10^{-4} \frac{psia}{Pa}\right) * (n_{he,initial}) * R * T_{avg,he,NCT} * (5/9 K/^oR)}{0.98 * V_{free,cc} * (1.6387 * 10^{-5} m^3/in^3)}$$

where,

$P_{initial}$ = Initial pressure in the MP197TAD TO cask cavity, $psia$

$V_{free,cc}$ = Free volume of MP197TAD TO cask cavity, in^3

R = Universal gas constant, $8.314 J/(mol-K)$

$T_{avg,He}$ = Initial average temperature of helium, K

$n_{he,initial}$ = Number of moles of helium in MP197TAD TO cask cavity, $g-moles$

The maximum normal operating pressure in the cask cavity of the MP197TAD TO loaded with the TN44B DSC at 22 kW heat load is 12.8 psig and is shown in Table B.3- 18.

B.3.3.3.2 TN44B DSC Internal Pressure

This section describes the methodology used to determine maximum internal pressures during transport within the TN44B DSC. The following assumptions and conservatisms are used in determining the maximum internal pressure for the TN44B DSC during transport in MP197TAD TO:

- The average helium temperature in the TN44B DSC cavity is based on a heat load of 24 kW.

The calculations account for the DSC free volume, the quantities of DSC backfill gas, fuel rod fill gas, and fission products and the average DSC cavity gas temperature. The internal pressures are then calculated using the ideal gas law as follows.

$$P = \frac{nRT}{V}$$

where:
n = Total number of moles of gases (g-moles),
R = Universal gas constant (8.314 J/g-mol-K)),
T = Gas temperature (K),
V = Gas volume (m^3), and
P = Internal pressure (Pa).

The TN44B DSC cavity free volume is calculated as DSC cavity volume minus basket and fuel assemblies' volume. The DSC cavity volume is calculated as

$$V_{DSC\ cavity} = \frac{\pi \cdot ID^2_{can\ shell} \cdot L_{can\ cavity}}{4}$$

Where:
$ID_{can\ shell}$ = DSC shell inside diameter = 64.75",
$L_{can\ cavity}$ = DSC cavity length (min.) = 178.38".

TN44B basket and fuel assemblies' volumes are based on the basket components' weight data provided in Chapter B.2. The TN44B DSC free helium volume is summarized below.

Number of FAs		44
DSC cavity volume	in^3	590,668
Basket volume	in^3	188,564
Fuel assemblies' volume	in^3	102,408
Free helium volume in the DSC	in^3	299,696
Free helium volume used (98%)	in^3	293,702

For conservatism, only 98% of DSC free cavity volume is used for the pressure calculation.

The DSC free volume is filled with a maximum 3.5 psig of helium after vacuum drying operation. The average helium backfill temperature after vacuum drying is determined using the TN44B DSC model with the conditions described in Section B.3.3.4. Based on this analysis an average helium backfill temperature of 385°F (845°R) is used for the calculation of the initial helium fill gas quantity. Using the ideal gas law, the initial quantity of helium in the cavity for the TN44B DSC is:

$$n_{he_Backfill} = \frac{(18.2\,psia)(6894.8\,Pa/psi)(293702\,in^3)(1.6387\cdot 10^{-5}\,m^3/in^3)}{(8.314\,J/(mol\cdot K))(845\,°R)(5/9\,K/°R)},$$

$$n_{he_Backfill} = 154.74\ g-moles.$$

The volume of the helium fill gas in a SVEA-100 fuel assembly, at cold unirradiated conditions is 2.136 in^3, and there are a maximum of 100 fuel pins in a fuel assembly. The SVEA-100 fuel assembly has bounding (highest) number of fuel rods per assembly, which results in the highest quantity of helium fill gas in fuel rods per DSC.

The maximum fill pressure is 145.3 psig (160 psia) and the fill gas is assumed to be at room temperature (70°F or 530°R). Per the ideal gas law, the quantity of fuel rod fill gas in 44 fuel assemblies is:

$$n_{he} = \frac{(160\,psia)(6894.8\,Pa/psi)(44\cdot 100\cdot 2.136\,in^3)(1.6387\cdot 10^{-5}\,m^3/in^3)}{(8.314\,J/(mol\cdot K))(530\,°R)(5/9\,K/°R)},$$

$$n_{he} = 69.45\,g-moles.$$

The quantity of fill gas rods (n_{he_FA}) and quantity of gases released as a result of 3% ruptured rods is calculated as follows:

$$n_{he_FA} = n_{he} * 0.03 = 69.45 * 0.03 = 2.08\,g-moles$$

The fuel assembly used in the pressure calculations is assumed to have a maximum burnup of up to 62 GWd/MTU, which is the highest burnup proposed for the NUHOMS® TAD System. The maximum burnup creates a bounding case for the amount of fission gas produced in a fuel rod during reactor operation. Based on the inventory of the released irradiation gases for a generic BWR fuel assembly, the amount of irradiation gases at STP for each fuel assembly is 20.2 g-moles.

The number of moles of gas released into the DSC cavity from one fuel assembly because of irradiation is given by:

$n_{ig\,1\,FA}$ = 20.2 g-moles * 0.3 = 6.06 g-moles.

The quantity of gases released as a result of irradiation (n_{ig}) due to 3% ruptured rods are calculated as follows:

$$n_{ig} = n_{ig\,1\,FA} * 44 * 0.03 = 6.06 * 44 * 0.03 = 8\,g - moles$$

The maximum pressure in TN44B DSC for NCT is calculated below. The total amount of gas in the DSC cavity is therefore:

$$n_{DSC-NC} = n_{he_Backfill} + n_{he_FA} + n_{ig}$$

$$n_{DSC-NC} = 154.74 + 2.08 + 8 = 164.82\,g - moles\,.$$

Ruptured rods will vent plenum gas until it comes into equilibrium with the DSC pressure. The plenum volume (V_{Rod_Plenum}) for a 3% rod rupture is calculated as follows:

$$V_{Rod_Plenum} = 100\,rods/assy * 2.136\,in^3/rod * 44\,assy/basket * 0.03 = 282\ in^3$$

The maximum internal pressure in the TN44B DSC with 3% ruptured rods during NCT in the TAD TO, with an average helium temperature of 560 °F (1020 °R) is calculated as follows and is shown in Table B.3- 19.

$$P_{NCT,TN44B} = \frac{\left(1.4504 \cdot 10^{-4}\,\frac{psia}{Pa}\right)(164.82\,g - moles)(8.314\,J/(mol \cdot K))(1020°R)(5/9\,K/°R)}{(293702\,in^3 + 282\,in^3)(1.6387 \cdot 10^{-5}\,m^3/in^3)}$$

$$P_{NCT,TN44B} = 23.4\,psia\ (8.7\,psig).$$

As seen from Table B.3- 20, the maximum internal pressures for TN44B DSC during NCT are within the design limits.

B.3.3.4 Thermal Evaluation for Loading/Unloading Operations

Normal operational procedures will not require submergence of the MP197TAD TO into a pool at the ISFSI or repository site; however the MP197TAD TO loaded with TN44B DSC is analyzed to determine the effects during loading and unloading operations in a spent fuel pool as described in Chapter B.7.

All fuel transfer operations occur when the TN44B DSC and MP197TAD TO are in the spent fuel pool. The fuel is always submerged in free-flowing pool water permitting heat dissipation. After completion of fuel loading, the TN44B DSC and MP197TAD TO are removed from the pool and the DSC is drained, dried, sealed and backfilled with helium.

Based on the operations described in Chapter B.7, water in the TN44B DSC cavity is forced out (blowdown operation) before the start of the vacuum drying. Helium is used as the medium to remove water and subsequent vacuum drying occurs with a helium environment in the DSC cavity.

A thermal analysis is performed using the TN44B DSC model to determine the maximum fuel cladding temperature and the average helium temperature within the DSC cavity for the steady-state conditions at the end of vacuum drying operation. Since the water in the DSC/TC annulus remains in place during the vacuum drying, a bounding conservative temperature of 225°F is considered at the outer surface of the DSC shell for this evaluation. This temperature is determined based on the saturation boiling temperature of the annulus water at the mid-length of the DSC shell. At the end of the vacuum drying operation, the maximum fuel cladding temperature and the average helium temperature in the DSC cavity are 528°F and 385°F, respectively.

The maximum fuel cladding temperature during vacuum drying is 528°F and the limit of 400°C (752°F) in ISG-11 [6] is satisfied for the TN44B DSC during vacuum drying operations.

The bounding unloading operation considered is the reflood of the TN44B DSC with water. For unloading operations, the TN44B DSC is filled with the spent fuel pool water through its siphon port. During this filling operation, the DSC vent port is maintained open with effluents routed to the plant's off-gas monitoring system. The NUHOMS® TAD operating procedures recommend that the DSC cavity atmosphere be sampled prior to introducing any reflood water in the DSC cavity.

The maximum fuel cladding temperature during the reflooding event is significantly less than the vacuum drying condition owing to the presence of water/steam in the DSC cavity. Based on the above discussion, the maximum cladding temperature during vacuum drying is bounded by 528°F. Hence, the peak cladding temperature during the reflooding operation will be less than 528°F.

B.3.4 Thermal Evaluation under Hypothetical Accident Conditions

The thermal performance of the MP197TAD TO loaded with TN44B DSC with a heat load of 22 kW is evaluated in this section under the HAC described in 10 CFR 71.73 [5]. This evaluation is performed primarily to demonstrate the containment integrity of the MP197TAD TO for HAC. This is assured as long as the O-rings seals in the cask lid and cask bottom plate remain below the maximum short-term seal temperature limits of 482°F (250°C) and the cask cavity pressure is less than the design pressure as specified in Section B.3.1.

The finite element model of the MP197TAD TO developed in Section B.3.3.1.1 is modified in this evaluation to determine the maximum component temperatures for HAC. For the transient runs considering HAC conditions, the basket is homogenized using SOLID70 elements. Thermal properties for the homogenized basket are discussed in Section B.3.3.1.5. The elements for other components are the same as those described in Section B.3.3.1.1.

Ambient conditions for HAC are based on 10 CFR 71 [5] requirements and are applied on the boundaries of the cask model. These conditions are listed below.

Hypothetical Accident Conditions for MP197TAD TO

Period	Ambient temperature (°F)	Insolance	Duration (hr)
Initial Conditions	100	Yes	N/A
Fire	1475	No	0.5
Wood Smoldering	100	Yes	0.5
Cool-Down	100	Yes	N/A

The assumptions and conservatism considered in evaluation for HAC are described in Sections B.3.4.1 and B.3.4.2.

B.3.4.1 Initial Conditions

The initial temperatures for the MP197TAD TO transient model before the fire accident are determined using the boundary conditions for NCT (100°F ambient with insolation) described in Section B.3.3.1.1 except that the decay heat load is applied as a uniform heat generation rate over the homogenized basket.

$$q''' = \frac{Q}{(\pi/4)\, D_i^{\,2}\, L_b} = 0.129 \text{ Btu/hr-in}^3$$

where

q''' = decay heat generation rate (Btu/hr-in^3),
Q = decay heat load = 22 kW = 75,071 (Btu/hr),
D_i = canister body inner diameter = 64.75 (in),
L_b = basket length = 176.5 (in).

All the assumptions and conservatism described in Section B.3.3.1.1 for the MP197TAD TO model are valid for determination of initial conditions.

B.3.4.2 Fire Test Conditions

No fire test is performed. Instead, the fire conditions are simulated using the finite element model of the MP197TAD TO.

Based on the requirements in 10 CFR 71, part 73 [5], a fire temperature of 1475 °F, a conservative fire emissivity of 1.0 and a period of 30 minutes are considered for the fire conditions. A bounding forced convection coefficient of 4.5 Btu/hr-ft^2-°F is considered during burning period based on data from reference [10]. Surface emissivity of 0.8 is considered for the packaging surfaces exposed to fire based on 10 CFR 71, part 73 [5].

The total heat transfer coefficient during fire is determined using the following equations.

$$h_{t,fire} = h_{r,fire} + h_{c,fire}$$

where,

$h_{r,fire}$ = fire radiation heat transfer coefficient (Btu/hr-in^2-°F),
$h_{c,fire}$ = forced convection heat transfer coefficient during fire = 4.5 Btu/hr-in^2-°F.

The radiation heat transfer coefficient, $h_{r,fire}$, is given by the equation:

$$h_{r,fire} = \varepsilon_w F_{wf} \left[\frac{\sigma(\varepsilon_f T_f^4 - T_w^4)}{T_f - T_w} \right] \quad \text{Btu/hr-in}^2\text{-°F}$$

where,

ε_w = MP197TAD TO outer surface emissivity = 0.8 [5],
ε_f = fire emissivity = 1.0,
F_{wf} = view factor from MP197TAD TO surface to fire = 1.0,
σ = Stefan-Boltzmann Constant = 0.1714×10^{-8} Btu/hr-ft^2-°R^4,
T_w = surface temperature (°R),
T_f = fire temperature = 1475°F = 1,935°R.

The following gaps are reduced from 0.25" under NCT to 0.01" under HAC to maximize the heat input from the fire toward the cask after free drop.

- axial gap between the impact limiter spacers and the cask top or bottom end surfaces,
- axial gap between the cask spacers and the inner surfaces of impact limiter cover plate.

The sizes of these gaps are maintained at 0.01" for the cool down period.

The following modifications are performed to maximize the heat input from the fire toward the cask during fire period and bound the maximum temperatures during the cool-down period.

a) The thermal properties of the gaps considered for initial conditions are changed to the properties for one of the adjacent components. The thermal properties of these gaps are restored after the fire during cool-down period. These gaps are listed in Table B.3-13.

b) Based on the MP197TAD TO slide rail thickness and orientation shown in Figure B.3– 1, the gap between the highest point of the TN44B DSC body and the cask inner shell is maximized when the canister centerlines is shifted downwards by 0.26" calculated in Section B.3.3.1.1. For the HAC analysis, the canister centerline is shifted

by the same amount to maximize the initial and the cool-down temperatures for MP197TAD TO and TN44B DSC components.

c) The MP197 TAD TO slide rails are assumed to be in contact with canister body during the fire period. The properties of the cask slide rail are changed to helium for cool-down period.

d) The neutron shield resin remains intact during the fire period and disintegrates completely after the fire. Air with conduction only properties replaces these resins during the cool-down period.

e) Based on structural evaluation in Chapter B.2, the aluminum blocks of impact limiter spacers will not be deformed significantly. The un-deformed shapes of the spacers are considered in this evaluation to maximize the heat input from fire toward the cask.

f) No heat dissipation is considered for the impact limiter outer surfaces to evaluate the maximum canister body temperatures under steady state cool-down conditions.

The trunnion plugs are modeled using polypropylene thermal properties for the pre-fire and hypothetical fire conditions. The properties of the trunnion plugs are changed to air after the fire for the cool-down period in the model. Stainless steel is considered as the material of the trunnion plugs in the final design of TAD TO. Since these plugs are covered by the impact limiters, they do not provide a major conduction path. Therefore, change of their material properties does not affect any maximum temperatures.

In order to maximize the heat input from the fire toward the MP197 TAD TO content, the impact limiters of the MP197TAD TO model are modified to reflect deformation due to drop accidents. The crush depths of impact limiters are determined in Chapter B.2 based on end, side, corner, and slap down accident drops. The minimum distances between the cask and the surface of the damaged impact limiters are recalculated based on the crush depths given in Chapter B.2 and depicted in Figure B.3– 20 and Figure B.3– 21. For conservatism, the maximum crush depth experienced by the impact limiter in a given direction is assumed to occur everywhere on the impact limiter.

Comparison between Figure B.3– 20 and Figure B.3– 21 shows that the maximum deformation is caused by the slap down and corner drop accidents. The shortest distances between the cask and the surface of the damaged impact limiter are 10.9" and 13.0" in the radial and axial directions, respectively.

To bound the impact limiter deformations conservatively in the model, the deformations caused by normal drops are subtracted from the deformed dimensions and the resultant values are rounded down. The outer diameter (OD_{Model}) and height (h_{Model}) of the deformed of the impact limiters considered in the model are 98" and 12", respectively.

Since the impact limiter deformations are considered uniformly in all directions, the thermal model bounds conservatively the deformations determined in Chapter B.2.

Although the impact limiters are locally deformed during the drop accident, they remain attached to the cask. Since the welds of the impact limiter shell do not break, the wood within the impact limiter shell cannot access air and would char but not burn during the hypothetical fire accident.

Hence, the steel encased wood impact limiters still protect the bottom plate and the lid of the cask from the external heat input caused by the fire.

Although unlikely, the worst-case damage due to a hypothetical puncture condition based on 10 CFR71, part 73 [5] may result in tearing off the outer steel skin of the impact limiter, crushing the wood out of the damaged area, and exposing the partially contained wood to the hypothetical fire conditions.

A study of fire performance of wood at elevated temperatures and heat fluxes [11] shows that the surface temperature for the rapid spontaneous ignition of wood is between 330 °C and 600 °C (626 °F and 1,112 °F). Based on standard fire test (ASTM E119, 1988) reported in [11], if a thick piece of wood is exposed to fire temperatures between 815 °C and 1,038 °C (1,500 °F and 1,900 °F), the outermost layer of wood is charred. At a depth of 13 mm (~0.5") from the active char zone, the wood is only 105 °C (220 °F). This behavior is due to the low conductivity of wood and fire retardant characteristics of char.

It is also shown that the char forming rate under high temperature fire conditions is between 37 mm/hr for soft woods and 55 mm/hr for hard woods. Redwood has a char rate of 46 mm/hr [11].

Based on the shortest distance considered between the cask and impact limiter in the axial direction, the thickness of Redwood at the central segment of the impact limiter is approximately 5" (127 mm) in the model. Assuming the Redwood is compressed after drop accident, a char rate of 55 mm/hr can be considered for the wood in the central segment of the impact limiter. The time interval for the charring until the active char zone reaches 13 mm above the inner surface of the center cover plate can be calculated as follows.

$$\text{(Redwood thickness -13) / char rate} = \frac{(127-13)}{55} = 2.1 \text{ hr.}$$

After this moment, the temperature of active char would be gradually imposed at the impact limiter inner surface. It takes another 14 minutes until the last 13 mm of Redwood is charred as shown below:

$$\text{(Thickness of last portion of hot Redwood) / char rate} = \frac{13}{55} = 0.24 \text{ hr} = 14.2 \text{ min.}$$

During the last 14 minutes the inner surface of the impact limiter is exposed to the high temperature of the charring wood. The impact of charring wood on the cask is maximized if the inner surface of the impact limiter is exposed to active char immediately after fire for 14 minutes.

To bound the problem and remain conservative, it is considered in the finite element model that the inner surface of the impact limiter inner cover is exposed to the char wood temperature for 30 minutes immediately after the end of fire. A char wood temperature of 900°F is considered for these conditions, which is approximately the average of the maximum and minimum char wood temperatures given in [11].

No heat dissipation is considered for the open surface of the torn segment after this period, assuming conservatively that this surface is entirely covered with a thin layer of low conductivity wood char.

The puncture damages to the rear and front impact limiters are considered in two separate transient runs to bound the maximum seal temperatures at the top and bottom of the MP197TAD TO under HAC.

Transient runs are performed for 20 hours after the fire. The results discussed in Section B.3.4.3 show that the maximum temperatures of cask components are declining so that the maximum cask component temperatures at 20 hours after the fire accident bound the maximum temperatures for the steady state conditions.

Due to large thermal mass of the TN44B basket, the maximum basket component temperatures will be achieved under steady state conditions after the fire accident. The results of transient runs discussed in Section B.3.4.3 and shown in Table B.3- 14 in comparision to steady state results verify this conclusion. A steady state run is performed with cool-down boundary conditions to bound the maximum TN44B basket component temperatures.

For the post fire conditions, it is assumed that all external surfaces are covered with soot. The solar absorptivity of soot is 0.95 [18]. To bound the problem, the thermal analysis uses a solar absorptivity of 1.0 and an emissivity of 0.9 for the packaging outer surfaces during the cool-down period.

Insolance during the post fire, cool-down conditions is applied as a heat flux over the MP197TAD TO outer surfaces using average insolence values from 10 CFR 71 [5]. The insolance values are averaged over 24 hours and multiplied by the surface absorptivity factor to calculate the solar heat flux. The solar heat flux values used in MP197TAD TO models for cool-down conditions are summarized below.

Solar Heat Flux for Cool-Down Period

Surface Material	Shape	Insolance over 12 hrs [5] (gcal/cm^2)	Solar Absorptivity	Total solar heat flux averaged over 24 hrs (Btu/hr-in^2)
All materials	Curved	400	1.0	0.4267
	Flat vertical	200	1.0	0.2133

For cool-down conditions, convection and radiation heat transfer from the MP197TAD TO outer surfaces are combined together as total heat transfer coefficients using the same methodology described in Section B.3.3.1.1 with an emissivity of 0.9 representing the soot covered external surfaces.

The finite element models described in Section B.3.3.1.1 are used for the steady state runs considering cool-down conditions. These models are modified to consider the deformed shape of the impact limiters. In addition, the material property of neutron shield resin is changed to air (conduction only) to to indicate that the resin is decomposed completely after fire.

The following modifications are considered for the steady state runs to maximize the canister body temperatures, conservatively.

1) Homogenized baskets are not considered for the steady state cool-down conditions. Instead decay heat fluxes are applied on the inner surface of the canister body using the same methodology and values described in Section B.3.3.1.1 for NCT.

2) Adiabatic boundary conditions are imposed on the impact limiter outer surfaces for steady state runs under cool-down conditions.

The other boundary conditions, the material properties, and the surface properties for steady state runs are the same as those considered for cool-down period in the transient runs.

The material properties used in the MP197TAD TO model are listed in Section B.3.2.1.

The geometry of the MP197TAD TO model with deformed impact limiters is shown in Figure B.3– 22.

Typical boundary conditions for HAC are shown in Figure B.3– 23 and Figure B.3– 24.

The TN44B DSC shell temperatures for cool down conditions described above are retrieved from the MP197TAD TO model analyzed with 22 kW. However, the TN44B DSC model used in determining the maximum fuel cladding and basket component temperartures are based on a heat load of 24 kW. Also, the DSC shell temperature profiles used for the TN44B DSC model is based on a 24 kW heat load. This is conservative since it increases the maximum fuel cladding and basket component temperatures.

B.3.4.3 Maximum Temperatures and Pressure

The maximum component temperatures for HAC are listed in Table B.3- 14.

The seal O-rings are not explicitly considered in the models. The maximum seal temperatures are retrieved from the models by selecting the nodes at the locations of the corresponding seal O-rings.

The time temperature histories for the MP197TAD TO components, TN44B DSC body, and homogenized basket are shown in Figure B.3– 25 and Figure B.3– 26. The time temperature histories show that the basket temperature increases steadily during cool-down period. It indicates that the maximum basket component temperatures will be reached for steady state conditions after fire. This behavior was expected due to large thermal mass of the basket and the relative large gap between the canister body and the cask inner shell, which damps the effect of the local maximum temperatures on the cask inner shell.

The maximum TN44B DSC body temperature is determined using a steady state run of the MP197TAD TO model with cool-down boundary conditions described in Section B.3.4.2. The maximum DSC shell temperature for steady state runs is 424°F as listed in Table B.3- 14.

However, the maximum fuel cladding and basket component temperatures within the TN44B DSC for cool-down conditions are analyzed with a heat load of 24 kW. A conservative DSC shell temperature profile with a maximum canister shell temperature of 538° is used in this evaluation. This bounds the DSC shell temperature of 424°F obtained with TN44B DSC in MP197TAD TO with cool-down conditions and 22kW heat load.

Based on the above conservatism, the thermal analysis results for TN44B DSC with 24kW heat load and higher DSC shell temperatures represent the bounding fuel cladding and basket component temperatures for cool-down conditions with 22kW and lower DSC shell

temperatures. The estimated maximum component temperatures for the TN44B DSC under HAC are summarized in Table B.3- 16.

The maximum MP197TAD TO and TN44B DSC component temperatures for HAC are summarized in Table B.3- 17. It shows that the maximum temperatures of the MP197TAD TO and TN44B DSC components calculated for HAC are lower than the allowable limits.

The maximum long-term temperature for the Viton fluorocarbon seals is 356°F belonging to drain port seal under steady state cool-down conditions. This temperature is well below the long-term limit of 400°F specified for continued seal function shown in Section B.3.1.

The maximum short-term temperature for the Viton fluorocarbon seals is 454°F belonging to ram closure plate seal. This short-term temperature is below the short-term limit of 482°F as listed in Section B.3.1. The maximum exposure time to high temperatures for this seal is only 2 hours as shown in Table B.3- 15.

As shown in Section B.3.1, the Viton seal remains leak tight at 470°F for 10 hours. Since the maximum short-term seal temperature and the duration of short-term exposure are lower than those studied in [15], the integrity of seal during HAC is assured.

The maximum temperature of gamma shield (lead) is 580°F, which is well below the lead melting point of 621°F as listed in Section B.3.1.

The maximum fuel cladding temperature is <765°F with 22 kW heat load remains below the allowable limit of 1,058°F (570°C) [6].

The resins and wood are assumed to be decomposed or charred after fire accident. Therefore, the maximum temperatures for these components are irrelevant for HAC.

Typical temperature distributions for the MP197TAD TO under HAC are shown in Figure B.3–27.

The temperature distributions of TN44B DSC with 24 kW and bounding DSC shell temperature profile used in for HAC are shown in Figure B.3– 28.

1) MP197TAD TO Cask Cavity HAC Pressure

The maximum cask cavity pressure in the MP197TAD TO for HAC is calculated using the same methodology and assumptions as described for NCT in Section B.3.3.3. The nomenclature used is defined in Section B.3.3.3.

The maximum pressure in the cask cavity for HAC is calculated as:

$$P_{HAC} = \frac{\left(1.4504*10^{-4}\frac{psia}{Pa}\right)*(n_{he,initial})*R*T_{avg,he,HAC}*(5/9K/^{o}R)}{0.98*V_{free,cc}*(1.6387*10^{-5}m^{3}/in^{3})}$$

Based on $T_{avg,he,HAC}$ of 367°F for TN44B DSC with 22 kW heat load shown in Table B.3- 18, the maximum pressure in the cask cavity of MP197TAD TO for HAC is 14.3 psig.

2) Internal Pressure for TN44B DSC under HAC

Based on methodology presented in Section B.3.3.3.2, the maximum internal pressures for TN44B DSC analyzed for HAC conditions with a 100% ruptured fuel rods. The evaluated internal pressure for TN44B DSC to be transported within MP197TAD TO is 58.3 psig is shown in Table B.3- 19. As seen from Table B.3- 20, the maximum internal pressures under HAC remains below the corresponding design limits for TN44B DSC.

B.3.4.4 Maximum Thermal Stresses

Thermal stresses for the MP197TAD TO loaded with TN44B DSC are discussed in Chapter B.2.

B.3.4.5 Accident Conditions for Fissile Material Packages for Air Transport

The MP197TAD TO is not designed for air transportation. Therefore, the accident conditions for air transport are irrelevant.

B.3.5 References

1. Updated Final Safety Analysis Report for the Standardized NUHOMS® Horizontal Modular Storage System for Irradiated Nuclear Fuel, NUH-003, Rev. 10.
2. NOT USED
3. NOT USED
4. Perry, Chilton, Chemical Engineers' Handbook, 5th Edition, 1973.
5. U.S. Code of Federal Regulations, Part 71, Title 10, "Packaging and Transportation of Radioactive Material."
6. U.S. NRC, Spent Fuel Project Office, Interim Staff Guidance, ISG-11, Rev. 3, Cladding Considerations for the Transportation and Storage of Spent Fuel.
7. U.S. Code of Federal Regulations, Part 72, Title 10, Licensing Requirements for the Independent Storage of Spent Nuclear Fuel and High-Level Radioactive Waste.
8. U.S. Nuclear Regulatory Commission, Standard Review Plan for Transportation Packages for Spent Nuclear Fuel, Final Report, NUREG-1617, January 2000.
9. ASME Boiler and Pressure Vessel Code, Section II, Part D, Material Properties, 2004.
10. Gregory, et al., Thermal Measurements in a Series of Long Pool Fires, SANDIA Report, SAND 85-0196, TTC-0659, 1987.
11. Mitchell S. Sweet, Fire Performance of Wood: Test Methods and Fire Retardant Treatments, Fire Safety of Wood Products, USDA Forest Service, http://www.fpl.fs.fed.us/documnts/pdf1993/sweet93a.pdf
12. Bucholz, J. A., Scoping Design Analysis for Optimized Shipping Casks Containing 1-, 2-, 3-, 5-, 7-, or 10-Year old PWR Spent Fuel, Oak Ridge National Laboratory, January, 1983, ORNL/CSD/TM-149.
13. Test Report, Properties to be Considered for Safety for Resin Vyal B, Transnuclear International, Report No. DI/RI-A-1-5-02, Rev. 1, 2006.
14. Parker Hannifin Corporation, O-Ring Division, "Parker O-ring Handbook", ORD 5700, http://www.parker.com/literature/ORD%205700%20Parker_O-Ring_Handbook.pdf.
15. T. Eric Skidmore, "Performance Evaluation of O-Ring Seals in Model 9975 Packaging Assemblies (U)," Westinghouse Savannah River Company, Document No. WSRC-TR-98-00439, December 1998, http://sti.srs.gov/fulltext/1998/tr98439.pdf.
16. U.S. Department of Agriculture, Forest Service, Wood Handbook: Wood as an Engineering Material, March 1999.
17. Rohsenow, Hartnett, Cho, Handbook of Heat Transfer, 3rd Edition, 1998.
18. Siegel, Howell, Thermal Radiation Heat Transfer, 4th Edition, 2002.

19. Rohsenow, Hartnett, Handbook of Heat Transfer Fundamentals, 2nd Edition, 1985.

20. NOT USED

21. ANSYS computer code and On-Line User's Manuals, Version 8.1 and 10.0.

22. NOT USED

23. NOT USED

24. Henninger, J. H., "Solar Absorptance and Thermal Emittance of Some Common Spacecraft Thermal-Control Coatings," NASA Scientific and Technical Information Branch, NASA Reference Publication 1121, 1984.

25. Safety Analysis Report for the NUHOMS® - MP187 Multi-Purpose Cask", Docket 71-9255, TN Document Number NUH-05-151, Revision 17, July 2003

26. NUREG/CR-0497, *MATPRO-Version 11 (Revision 2): A Handbook of Materials Properties for Use in the Analysis of Light Water Reactor, Fuel Rod Behavior*, EG&G, Inc. TREE-1280, August 1981.

27. Test Report TPRL 1275, *Thermophysical Properties of Neutrosorb Plus - A Report to Carpenter Technology Corp*, University of Purdue, West Lafayette, Indiana, May 1993.

28. NOT USED

29. Moore, R. S., Notz, K. J., *Physical Characteristics of GE BWR Fuel Assemblies*, Oak Ridge National Laboratory, Report No. ORNL/TM-10902, June 1989.

30. Updated Final Safety Analysis Report for the Standardized NUHOMS® Horizontal Modular Storage System for Irradiated Nuclear Fuel, NUH-003, Appendix T.

31. Kreith, Frank, *Principles of Heat Transfer*, 3rd Edition, 1973.

32. Transnuclear Letter to U.S. NRC, *Revision 1 to Transnuclear, Inc. (TN) Application for Amendment 1 to the NUHOMS® HD System, Response to Request for Additional Information (Docket No. 72-1030; TAC NO. L24153)*, Transnuclear Letter No. E-27377, December 15, 2008.

33. U.S. NRC NUREG-1536, *Standard Review Plan for Dry Cask Storage Systems,* January 1997.

34. SAND90-2806, Sanders, T. L., et al., *A Method for Determining the Spent-Fuel Contribution to Transport Cask Containment Requirements*, TTC-1019, UC-820, November 1992.

35. Report, *Topical Report on Actinide-Only Burnup Credit for PWR Spent Nuclear Fuel Packages*, Office of Civilian Radioactive Waste Management, DOE/RW-0472, Revision 2, September 1998.

B.3.6 Appendices

B.3.6.1 Macros for Heat Transfer Coefficient

The information on pages
B.3-57 through B.3-60 is
Proprietary Information Withheld
Pursuant to 10 CFR 2.390

B.3.6.2 Mesh Sensitivity

B.3.6.2.1 MP197TAD TO Model Mesh Sensitivity

A slice of the MP197TAD TO model containing TN44B DSC shell is recreated for mesh sensitivity analysis. The length of the MP197TAD TO slice model is 69.44" and includes the canister shell and cask shells. The mesh density of this model is the same as the mesh density of the geometry model used in Section B.3.3.1.1 from z=67.00" to z=136.44". The slice model contains 30,534 elements and 32,655 nodes. The number of nodes and elements in the slice model are identical to the model used in Section B.3.3.1.1 from z=67.00" to z=136.44".

For fine mesh, the mesh density of the slice model is increased to approximately nine times of its original value so that the number of elements and nodes are increased to 271,046 elements and 273,470 nodes, respectively.

Ambient temperature of 100°F with insolation and a decay heat of 22 kW are considered as boundary conditions for both MP197TAD TO slice models with coarse and fine meshes. The boundary conditions are applied using the same methodology as described in Section B.3.3.1.1.

The major component temperatures for fine mesh model decrease by 3 to 6°F. Therefore, the mesh density of the MP197TAD TO model is conservative for evaluation of the thermal performance. The maximum temperature of the shield shell increases by less than 2°F for the fine mesh model. Since the shield shell does not have any structural or thermal function, this temperature increase is insignificant. In conclusion, the results reported in Sections B.3.3.2 and Section B.3.4.3 based on the coarse mesh of the MP197TAD TO model are conservative to evaluate the thermal performance.

B.3.6.3 Acceptance Criteria for Coating Damages for MP197TAD TO

During handling and operation of MP197TAD TO, the painted surfaces of the shield shell can be scratched, peeled off, or physically damaged. The emissivity and solar absorptivity of the painted surfaces are considered as inputs for the thermal evaluation. Physical damages on the coating change the emissivity and absorptivity values of the surface, which affect the thermal performance of the MP197TAD TO.

The acceptance criterion for coating damages is the surface area of the damaged coating below which the effects on the thermal performance of the MP197TAD TO are insignificant.

The criteria is based on the maximum damaged coating areas, which will have minimum effects (less than 1°F) on the maximum temperatures of the MP197TAD TO. The maximum acceptable damaged surface area for the paint on the neutron shield shell of MP197TAD TO is 500 sq. in.

The analysis concludes that the effects of the neutron shield paint damages on the maximum component temperatures of MP197TAD TO are insignificant (less than 1°F), if the accumulated paint damages are limited to 500 square inches.

B.3.6.4 Justification of Hot Gaps

The following hot gap is assumed in the MP197TAD TO and justified in this section.

a) A radial gap of 0.015" is assumed between the gamma shield and the cask outer shell in MP197TAD TO model.

B.3.6.4.1 Gap between Gamma Shield and Cask Outer Shell

A 0.015" radial air gap is assumed between the gamma shield (lead) and the MP197TAD TO outer shell within the finite element model described in Section B.3.3.1.1. This air gap is due to the differential thermal expansion of the cask body and the gamma shield during the lead pour.

The following assumptions are made for the verification of the gap:

- The cask body has nominal dimension at 70°F.
- During the lead pour the overpack body and lead are at 620°F.
- The inner diameter of the gamma shell (lead) is equal to the outer diameter of the cask inner shell at thermal equilibrium.

The average coefficients of thermal expansion for SA-240, Type 304 and lead are listed in the following table.

Thermal Expansion Coefficients

Temperature (°F)	SA-240, Type 304 α (in/in-°F) [9]
70	8.50E-06
200	8.90E-06
300	9.20E-06
400	9.50E-06
500	9.70E-06
600	9.80E-06
700	10.00E-06

Temperature (°F)	Lead α (in/in-°F) [Table 2.3.4-2 of Ref. 25]
70	16.07 E-6
100	16.21 E-6
175	16.58 E-6
250	16.95 E-6
325	17.54 E-6
440	18.50 E-6
620	20.39 E-6

The density of lead as a function of temperature is listed in the Section B.3.2.1, material # 5.

The volume within the "lead cavity" is found by determining the cask body dimensions at 620°F. As no gaps will be present between the molten lead and the cask body, this volume is also equal to the volume of lead at 620°F. The mass of the lead that fills the lead cavity at 620°F is then determined.

The dimensions of the "lead cavity" are calculated based on the cask body temperature. A temperature of 300°F is considered for the cask body. This temperature is lower than the maximum cask inner shell temperature shown in Table B.3- 10 for 22 kW heat load. Since the gap size increases at lower temperatures, the above chosen value is conservative. From the mass of the lead and its density at 300°F, the lead volume is determined.

The length of the gamma shield at the overpack body temperature is calculated based on thermal expansion coefficients listed in the above table. The lead volume is used to determine the maximum size of the air gap adjacent to the lead.

<u>Determination of Lead Mass</u>

$\alpha_{SS,\,620}$ = 9.84 x 10^{-6} in/in-°F at 620°F (via linear interpolation from expansion coefficients table, above),
$\rho_{lead,\,620}$ = 0.3978 lbm/in^3 at 620°F (from Section B.3.2.1, material # 5),

R_{in} = inner radius of lead cavity at 70°F= 34.75",
R_{out} = outer radius of lead cavity at 70°F = 37.00",
L_{cavity} = length of lead cavity at 70°F = 202.50",

$R_{in,\,620} = (R_{in})(1+(\alpha_{SS,\,620})(\Delta T)) = (34.75)[1+(9.84E\text{-}6)(550)] = 34.9381$",

$R_{out,\,620} = (R_{out})(1+(\alpha_{SS,\,620})(\Delta T)) = (37.00)[1+(9.84E\text{-}6)(550)] = 37.2002$",

$L_{cavity,\,620} = (L_{cavity})(1+(\alpha_{SS,\,620})(\Delta T)) = (202.50)[1+(9.84E\text{-}6)(550)] = 203.5959$",

$V_{cavity} = V_{lead,\,620} = (\pi)(R_{out,620}^2 - R_{in,620}^2)(L_{cavity,\,620}) = 104{,}378.6\ in^3$,

$M_{lead} = (V_{lead,\,620})(\rho_{lead,\,620}) = (154{,}274.9\ in^3)(0.3978\ lbm/in^3) = 41{,}517.1$ lbm.

Determination of Lead Gap

$\alpha_{SS,\,300}$ = 9.20 x 10^{-6} in/in-°F at 300°F (from expansion coefficients table, above),
$\alpha_{lead,\,620}$ = 20.39 x 10^{-6} in/in-°F at 620°F (from expansion coefficients table, above),
$\alpha_{lead,\,300}$ = 17.34 x 10^{-6} in/in-°F at 300°F (via linear interpolation from expansion coefficients table, above),
$\rho_{lead,300}$ = 0.4049 lbm/in^3 at 300°F (via linear interpolation from Section B.3.2.1, material # 5),

$R_{in,\,SS,\,300} = (R_{in})(1+(\alpha_{SS,\,300})(\Delta T)) = (34.75)[1+(9.20E\text{-}6)(230)] = 34.8235$",

$R_{out,\,SS,\,300} = (R_{out})(1+(\alpha_{SS,\,300})(\Delta T)) = (37.00)[1+(9.20E\text{-}6)(230)] = 37.0783$",

$L_{lead,\,300} = (L_{cavity,\,620})/(1+(\alpha_{lead,620})(620-70))*(1+(\alpha_{lead,300})(300-70)) =$,
$(203.5959) / [1+(20.39E\text{-}6)(550)] * [1+(17.34E\text{-}6)(230)] = 202.1412$",

$V_{lead,\,300} = M_{lead} / \rho_{lead,\,300} = 41{,}517.1 / 0.4049 = 102{,}536.7\ in^3$.

Since $R_{in,SS,\,300} = R_{in,\,lead,\,300}$, then :

$V_{lead,300} = (\pi)(R_{out,\,lead,300}^2 - R_{in,\,ss,\,300}^2)(L_{lead,\,300})$.

It gives:

$R_{out,\,lead,\,300}$ = 37.0694",

Air gap = $R_{out,\,SS,\,300} - R_{out,\,lead,\,300}$ = 37.0783 – 37.0694 = 0.0089".

The assumed air gap of 0.015" is larger than the above calculated gap. Therefore, using a gap of 0.015" is conservative to maximize the TN44B DSC shell temperature.

Table B.3- 1
TN44B DSC Shell Nominal Dimensions

Parameter	Top Recess	Outer Top Cover	Inner Top Cover	Top Shield Plug	Inner Bottom Cover	Bottom Shield Plug	Outer Bottom Cover	Cavity Length	Canister Length (w/o grapple)(1)	Minimum Basket Length
Dimension (in)	0.12	2.50	2.00	5.75	1.75	2.75	2.00	179.38	196.25	176.5

Note:
(1) The canister length in the model is the sum of the top recess, total top end (cover plates and shield plug), total bottom end (cover plates and shield plug), and the cavity length.

Table B.3- 2
Peaking Factors for TN44B Fuel

Region #	Fuel Model Z-Coordination (in) from	to	Average Height from Bottom (in)	Peaking Factor	Area under Curve
1	14.125	24.225	5.050	0.394	3.981
2	24.225	34.325	15.150	0.957	9.664
3	34.325	44.425	25.250	1.126	11.374
4	44.425	54.525	35.350	1.181	11.929
5	54.525	64.625	45.450	1.194	12.057
6	64.625	64.750	50.563	1.199	0.150
7	64.750	74.708	55.604	1.200	11.950
8	74.708	84.667	65.563	1.200	11.951
9	84.667	94.625	75.521	1.198	11.931
10	94.625	104.580	85.478	1.181	11.756
11	104.580	114.540	95.435	1.147	11.421
12	114.540	124.500	105.395	1.093	10.886
13	124.500	124.625	110.438	1.066	0.133
14	124.625	133.000	114.688	1.035	8.672
15	133.000	141.380	123.065	0.891	7.467
16	141.380	149.750	131.440	0.660	5.525
17	149.750	158.125	139.813	0.274	2.295
				Sum	143.143
				Normalized	0.99405
				Corr. Factor	1.006

Table B.3- 3
List of Homogenized Multiple Plates in TN44B DSC Model

Location [1]	Plate List	Thickness	ANSYS Material No.
Center Plates in Nine-Comp. Assembly	Total Thickness	1.645"	3, 13
	Borated SS Plate Thickness	7/16"	
	Wrap Thickness	0.21"	
	Al Plate Thickness	15/16"	
	Helium Gap thickness	0.06"	
	Total Thickness	0.655"	
Middle Plates in Nine-Comp. Assembly	Borated SS Plate Thickness	7/16"	4, 14
	Wrap Thickness	0	
	Al Plate Thickness	3/16"	
	Helium Gap thickness	0.03"	
Corner Plates in Nine-Comp. Assembly	Total Thickness	0.5625"	5, 15
	Borated SS Plate Thickness	7/16"	
	Wrap Thickness	0.105"	
	Al Plate Thickness	0	
	Helium Gap thickness	0.02"	
Center Plates in Two-Comp. Assembly	Total Thickness	1.6025"	6, 16
	Borated SS Plate Thickness	7/16"	
	Wrap Thickness	0"	
	Al Plate Thickness	9/8"	
	Helium Gap thickness	0.04"	
Corner Plates in Two-Comp. Assembly	Total Thickness	0.5725"	7, 17
	Borated SS Plate Thickness	7/16"	
	Wrap Thickness	0.105"	
	Al Plate Thickness	0	
	Helium Gap thickness	0.03"	
Fuel Comp. with Comp. Assembly Wrap Plates	Total Thickness	0.3025"	2, 12
	Borated SS Plate Thickness	0	
	Fuel Comp. /Wrap Thickness	0.2925"	
	Al Plate Thickness	0	
	Helium Gap thickness	0.01"	
Long Al Thermal Plate w/gap	Total Thickness	0.52"	8, 18
	Borated SS Plate Thickness	0	
	Fuel Comp. /Wrap Thickness	0	
	Al Plate Thickness	0.5"	
	Helium Gap thickness	0.02"	
Short Al Thermal w/ R45 Rail Plate	Total Thickness	0.77"	9, 19
	Borated SS Plate Thickness	0	
	Rail SS Plate Thickness	0.25"	
	Al Plate Thickness	0.5"	
	Helium Gap thickness	0.02"	

Notes:
(1) Figure B.3– 12 illustrates the location of homogenized plates in TN44B DSC model.

Table B.3- 4
Effective Density for TN44B Basket

Components	Material	Total Weight (lbm)
Fuel Assembly	---	31020
Fuel Compartment	SS304	10874
Poison Plate	Borated SS	16573
Sub-Assy Wrap+Insert	SS304	3054
Aluminum Plates	Aluminum	4994
Rail 90	Aluminum	1711
Rail 45	SS405	4342
Total		72568
D_{basket}	64.75	in
L_{basket}	176.5	in
V_{basket}	581185	in^3
$\rho_{eff\ basket}$	0.125	lbm/in^3

Table B.3- 5
Effective Specific Heat for the TN44B Basket

Components	Fuel Assembly	Fuel compartments	Poison Plates	Wrap/Insert Plates	Aluminum Plates	Rail 90	Rail 45	Total	Calculated	
Material	---	Stainless Steel	Borated SS	St. Steel	Al	Al	Al	---		
Weight (lbm)	31020	10874	16573	3054	4994	1711	4342	72568		
Temperature	$m.c_P$	$m.c_P$	$m.c_P$	$m.c_P$	$m.c_P$	$m.c_P$	$m.c_P$	$\Sigma m.c_P$	c_{Peff}	c_{Peff} (2)
(°F)	(Btu/°F)	(Btu/°F)	(Btu/°F)	(Btu/°F)	(Btu/°F)	(Btu/°F)	(Btu/°F)	(Btu/°F)	(Btu/lbm-°F)	(Btu/lbm-°F)
70	1,784	1,262	1922	354	1064	364	504	7,255	0.100	0.099
100	1,784	1,268	1922	356	1074	368	506	7,279	0.100	0.099
200	1,784	1,321	1922	371	1104	378	527	7,407	0.102	0.101
300	1,784	1,357	1922	381	1129	387	542	7,502	0.103	0.102
400	1,784	1,397	1922	392	1149	394	558	7,595	0.105	0.104
500	1,784	1,429	1922	401	1149	394	571	7,649	0.105	0.104
600	1,784	1,439	1922	404	1149	394	575	7,666	0.106	0.105
700	1,784	1,461	1922	410	1149	394	583	7,702	0.106	0.105
800	1,784	1,481	1922	416	1149	394	591	7,737	0.107	0.106
900	1,784	1,489	1922	418	1149	394	595	7,750	0.107	0.106
1000	1,784	1,496	1922	420	1149	394	597	7,762	0.107	0.106
1100	1,784	1,522	1922	428	1149	394	608	7,806	0.108	0.107

Notes:
(1) Not Used.
(2) The conservative values are assumed according to the calculated values.

Table B.3- 6
Effective Axial Conductivity for TN44B Basket

T_2 (T_{top}) (°F)	T_1 (T_{bottom}) (°F)	Q_{axl} (Btu/hr)	T_{avg} (°F)	$k_{basket, axl}$ (Btu/hr-in-°F)
50	0	3051.2	25	1.184
150	100	3060.8	125	1.188
250	200	3071.8	225	1.192
350	300	3065	325	1.189
450	400	3064.3	425	1.189
550	500	3056.5	525	1.186
650	600	3040.3	625	1.180
750	700	3024.9	725	1.174
850	800	3009.2	825	1.167
950	900	2992.2	925	1.160
1050	1000	2979.3	1025	1.156
1150	1100	2988.6	1125	1.160

Table B.3- 7
Effective Radial Conductivity for TN44B Basket

T_{max} (°F)	T_o (°F)	Q_{rad} (Btu/hr)	T_{avg} (°F)	k_{basket_rad} (Btu/hr-in-°F)
402	0	11543	201	0.129
477	100	11543	289	0.138
554	200	11543	377	0.147
633	300	11543	467	0.156
715	400	11543	557	0.165
799	500	11543	650	0.173
889	600	11543	744	0.180
981	700	11543	841	0.184
1075	800	11543	937	0.189
1169	900	11543	1034	0.193
1264	1000	11543	1132	0.197
1359	1100	11543	1230	0.200

Table B.3- 8
Maximum Temperatures of MP197TAD TO Components/TN44B DSC Shell for NCT (100°F and Insolation)

Ambient	100°F	
Insolance	Yes	
Component	T_{max} (°F)	Limit (°F)
Canister shell	422	---
Canister shell at mid-length (1)	419	---
Inner shell	337	---
Gamma shield	333	621 [4]
Outer shell	327	---
Shield shell	271	---
Cask lid	265	---
Ram closure plate	321	
Cask bottom plate	326	---
Neutron Shield Resin (2)	281	320 [13]
Lid seal	267	400 [14]
Ram plate seal	322	400 [14]
Vent seal at top	264	400 [14]
Test seal at top	264	400 [14]
Drain port seal at bottom	324	400 [14]
Test seal at bottom	322	400 [14]
Wood in Impact limiter	305	320 [16]

Notes
(1) This value is the maximum canister shell temperature in the region where the fuel assemblies have the maximum peaking factor.
(2) This temperature is the volumetric, average temperature of the elements located at hottest cross section of the neutron shield resin.

Table B.3- 9
Maximum Fuel Cladding and Basket Component Temperatures for NCT

Component	T_{max} (1) (°F)	Limit (°F)
Fuel cladding	< 701	752 [6]
Fuel compartment	< 667	---
Al/ poison plates	< 667	---
Basket Rails	< 605	---

Note: (1) Based on Bounding DSC shell profile and 24 kW heat load.

Table B.3- 10
Maximum/Minimum MP197TAD TO and TN44B DSC Component Temperatures for NCT

Conditions	100°F with Insolation	-40°F and no Insolation (2)	
Component	T_{max} (°F)	T_{min} (°F)	Limit (°F)
Fuel cladding	< 701	-40	752 [6]
Fuel compartment	< 667	-40	
Al/ poison plates	< 667	-40	
Basket Rails	< 605	-40	
Canister shell	422	-40	---
Inner shell	337	-40	---
Gamma shield	333	-40	621 [4]
Outer shell	327	-40	---
Shield shell	271	-40	---
Cask lid	265	-40	---
Cask bottom plate	326	-40	---
Neutron Shield Resin (1)	281	-40	320 [13]
Seals	324	-40	400 [14]
Wood in Impact limiter	305	-40	320 [16]

Notes:
(1) The resin temperature is the volumetric, average temperature at the hottest cross section.
(2) These temperatures are based on assuming no credit for decay heat and a daily average ambient temperature of -40°F

Table B.3- 11
Maximum Temperatures of MP197TAD TO Components and TN44B DSC Shell for Cold NCT

Ambient Temperature	-20°F	-40°F
Component	T_{max} (°F)	T_{max} (°F)
Canister shell	339	326
Inner shell	243	227
Gamma shield	239	223
Outer shell	231	215
Shield shell	178	162
Cask lid	164	147
Cask bottom plate	230	214
Wood in Impact limiter	204	187

Table B.3- 12
Average Component Temperatures for NCT

Ambient Condition	Component	T_{avg} Overall (°F)	T_{avg} at Hottest X-Section of Canister Shell (°F)
100°F with Insolation	Canister Shell	363	384
	Cask Inner Shell	308	325
	Lifting Device Spacers	264	---
	Helium in MP197TAD TO cavity	308	---
-20°F without Insolation	Canister Shell	276	297
	Cask Inner Shell	213	229
	Lifting Device Spacers	163	---
-40°F without Insolation	Canister Shell	261	283
	Cask Inner Shell	196	212
	Lifting Device Spacers	146	---

Table B.3- 13
List of the Gaps and Thermal Properties for HAC Analysis

Gap Size (in)	Location	Initial / Cool-down Properties	Properties during Fire
0.01 (1)	Axial gap between the aluminum spacers and the impact limiter case	Air	Al 6063 (Spacers)
0.01 (1)	Axial gap between the aluminum spacers and the cask top or bottom end surfaces	Air	Al 6063 (Spacers)
0.06	Axial gap between the cask lid and the cask flange	Helium	SA-240, type 304 (Cask lid)
0.06	Axial gap between the ram closure plate and the cask bottom plate	Helium	SA-240, type 304 (Ram Closure Plate)
0.01	Radial gaps between the neutron shield boxes and the surrounding shells	Air	Al 6063 (Neutron shield boxes)
0.015	Radial gap between the gamma shield and the cask outer shell	Air	ASTM B-29 (Lead) (Gamma shield)
0.06	Axial gaps between the canister bottom shield plug and bottom cover plates	Air	SA-240, type 304 (Canister bottom shield plug)
0.06	Axial gaps between the canister top inner cover and the adjacent plates	Air	SA-240, type 304 (Canister top inner cover plate)

Notes:
(1) The size of this axial gap is 0.25" for initial conditions.

Table B.3- 14
Maximum Temperatures of MP197TAD TO Components / TN44B DSC Shell for HAC

Conditions	Rear Impact Limiter Punctured			Front Impact Limiter Punctured			
Component	Time (hr)	T_{max} (°F)	T_{∞} (°F) (2)	Time (hr)	T_{max} (°F)	T_{∞} (°F) (2)	Limit (°F)
Canister body	1.9	466	424 (4)	1.8	466	424 (4)	---
Canister body @ mid-length (1)	1.9	466	420	1.8	466	419	---
Cask inner shell	0.5	505	359	0.5	505	348	---
Gamma shield	0.5	580	358	0.5	580	345	621 [4]
Outer shell	0.5	849	356	0.5	849	341	---
Shield shell	0.5	1217	320	0.5	1217	312	---
Cask lid	9.5	301	291	1.0	533	310	---
Cask bottom plate	1.0	553	356	6.4	350	340	---
Ram closure plate	1.0	511	350	1.1	342	332	---
Cask lid seal	9.5	306	294	1.1	437	311	400 [14] / 482 [14] (3)
Vent & test seal @ top	9.5	300	290	1.1	444	310	400 [14] / 482 [14] (3)
Ram plate seal	1.1	454	351	1.8	340	333	400 [14] / 482 [14] (3)
Test seal @ bottom	1.0	446	352	9.4	340	333	400 [14] / 482 [14] (3)
Drain port seal @ bottom	1.1	451	356	6.4	349	338	400 [14] / 482 [14] (3)
Helium in MP197TAD TO Cavity	3.5	343	329	3.5	351	333	---

Notes:

(1) This value is the maximum canister body temperature in the region where the fuel assemblies have the maximum peaking factor.
(2) These values are retrieved from the transient model at 20 hrs after fire accident. Based on the time-temperature histories shown in Figure B.3– 25 and Figure B.3– 26, the steady state temperatures are bounded by the temperatures at 20 hr transient.
(3) For the Viton O-rings, the temperature limit of 400°F is for long-term exposure and the temperature limit of 482°F is for short-term exposure as shown in Section B.3.1.
(4) This temperature is calculated based on the steady state run discussed in Section B.3.4.2.

Table B.3- 15
Time Intervals for Short Term Exposure of Seals to High Temperatures

	Ram Plate Seal		Test Seal at Bottom Plate		Drain Port Seal at Bottom	
Conditions	Time (hr)	Temp (°F)	Time (hr)	Temp (°F)	Time (hr)	Temp (°F)
HAC, Rear Impact Limiter Punctured	0.67	369	0.67	377	0.67	368
	0.78	400	0.76	400	0.79	400
	0.83	415	0.83	417	0.83	411
	1.00	451	1.00	446	1.00	443
	1.14	454	1.14	439	1.14	451
	1.9	413	1.9	409	1.9	418
	2.8	400	2.7	400	3.2	400
	3.5	390	3.5	391	3.5	395
Approximate Short-term Exposure Time (hr)	2		2		2	

	Lid Seal		Vent and Test Seal at Top	
Conditions	Time (hr)	Temp (°F)	Time (hr)	Temp (°F)
HAC, Front Impact Limiter Punctured	0.83	373	0.67	346
	0.93	400	0.83	400
	1.00	419	0.83	401
	1.14	437	1.00	442
	1.8	402	1.14	444
	1.9	400	1.8	400
	3.5	361		
Approximate Short-term Exposure Time (hr)	1		1	

Notes:
(1) The shaded cells are calculated based on linear interpolation from transient data.

Table B.3- 16
Maximum Fuel Cladding and Basket Component Temperatures for HAC

Component	T_{max} (1) (°F)	Limit (°F)
Fuel cladding	< 765	1,058 [6]
Fuel compartment	< 733	---
Al/ Neutron absorber plates	< 733	---
Basket Rails	< 671	---

Note: (1) Based on Bounding DSC shell profile and 24 kW heat load.

Table B.3- 17
Summary of the MP197TAD TO/TN44B DSC Maximum Temperatures for HAC

Component	Time (hr)	T_{max} (°F)	T_{∞} (°F)	Limit (°F)
Fuel cladding	∞	< 765	< 765	1,058 [6]
Fuel compartment	∞	< 733	< 733	---
Al/ Neutron absorber plates	∞	< 733	< 733	---
Basket Rails	∞	< 671	< 671	---
Canister body	1.8	466	424 (3)	---
Cask inner shell	0.5	505	359(1)	---
Gamma shield	0.5	580	358(1)	621 [4]
Outer shell	0.5	849	356(1)	---
Shield shell	0.5	1217	320(1)	---
Cask lid	1.0	533	310(1)	---
Cask bottom plate	1.0	553	356(1)	---
Ram closure plate	1.0	511	350(1)	---
Seal at cask lid	1.1	444	311(1)	400 [14] / 482 [14] (2)
Seal at bottom plate	1.1	454	356(1)	400 [14] / 482 [14] (2)
Helium in MP197TAD TO Cavity	3.5	351	333(1)	---

Notes:

(1) These values are retrieved from the transient model at 20 hrs after fire accident. Based on the time-temperature histories shown in Figure B.3– 25 and Figure B.3– 26, the steady state temperatures are bounded by the temperatures at 20 hr transient.

(2) For the Viton O-rings, the temperature limit of 400°F is for long-term exposure and the temperature limit of 482°F is for short-term exposure as shown in Section B.3.1.

(3) This temperature is calculated based on the cool down steady state run discussed in Section B.3.4.2.

Table B.3- 18
MP197TAD TO Cavity Pressure for NCT and HAC

$V_{free,cc}$ [(1)]	$n_{he\text{-}initial}$	$T_{avg,\ he,NCT}$	P_{NCT}	$T_{avg,\ he,HAC}$	P_{HAC}
in^3	g-moles	°F	psig	°F	psig
27189	23.3	324	12.8	367	14.3

Note: [(1)] 98% of the MP197TAD TO cavity free volume is conservatively used in calculating the maximum pressures.

Table B.3- 19
Maximum Internal Pressures of TN44B DSC in MP197TAD TO for NCT and HAC

Operating Condition	Canister Cavity Free Volume	Plenum volume	Helium fill amount	Plenum helium amount	Fission products amount	Total gas amount	$T_{avg,He}$	Cavity Pressure	Design Pressure
	in^3	in^3	g-moles	g-moles	g-moles	g-moles	°F	psig	psig
NCT	293,702	282	154.74	2.08	8.00	164.82	560	8.7	15.0
HAC	293,702	9398	154.7	69.5	266.6	490.8	642	58.3	100.0

Table B.3- 20
Maximum Internal Pressures of TN44B DSC in MP197TAD TO for NCT and HAC

Operating conditions	Pressure (Transport)	Pressure Limit
	psig	psig
NCT	8.7	15
HAC	58.3	100

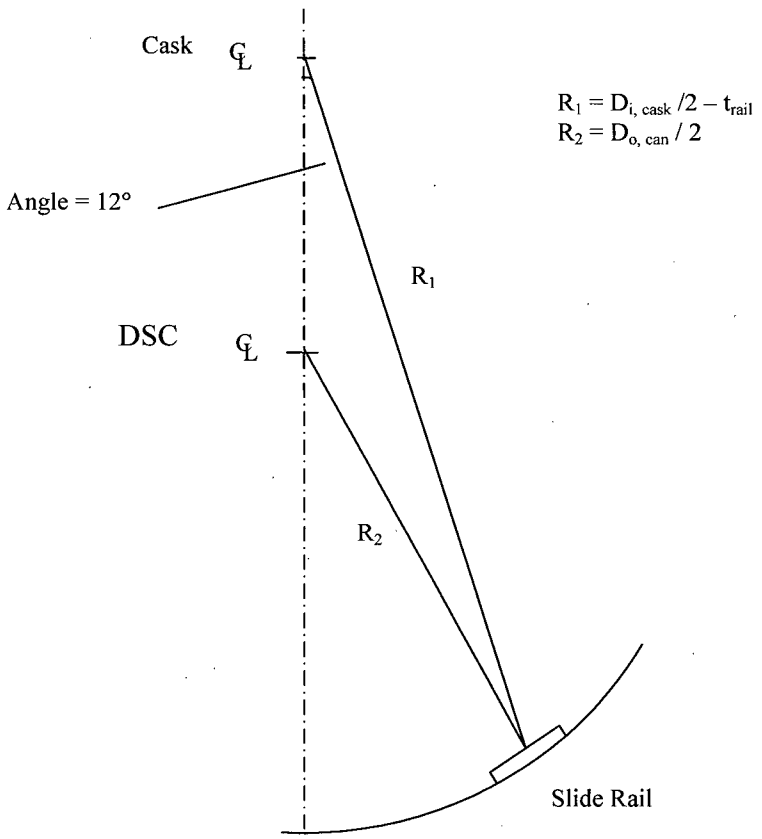

Figure B.3– 1
Location of TN44B DSC within TAD Transport Overpack

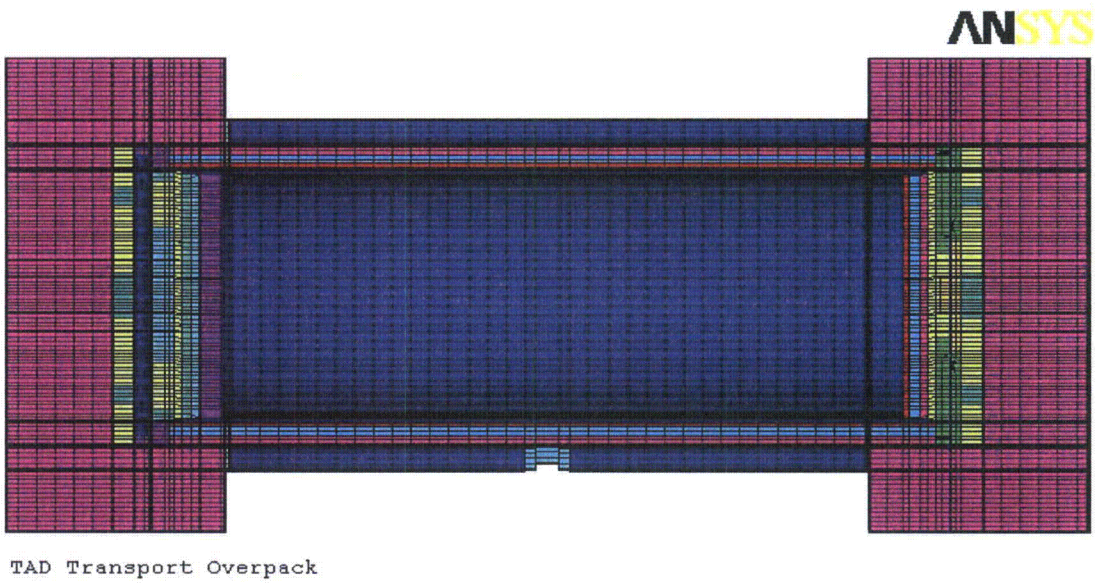

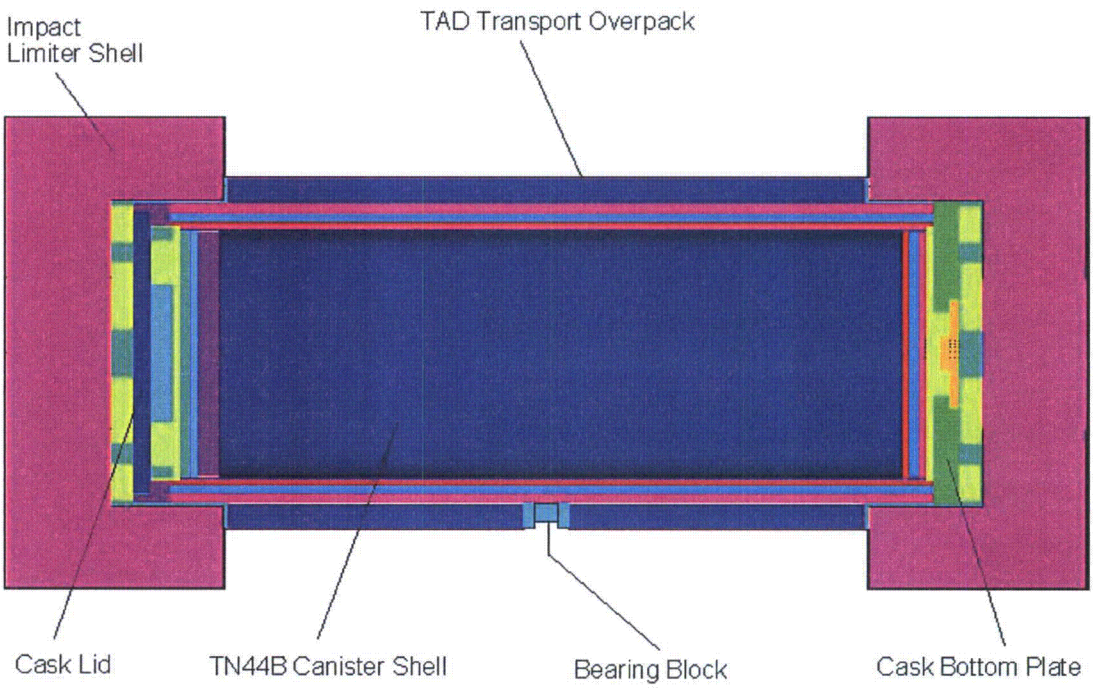

Figure B.3– 2
Finite Element Model of MP197TAD TO with TN44B DSC, Longitudinal Section

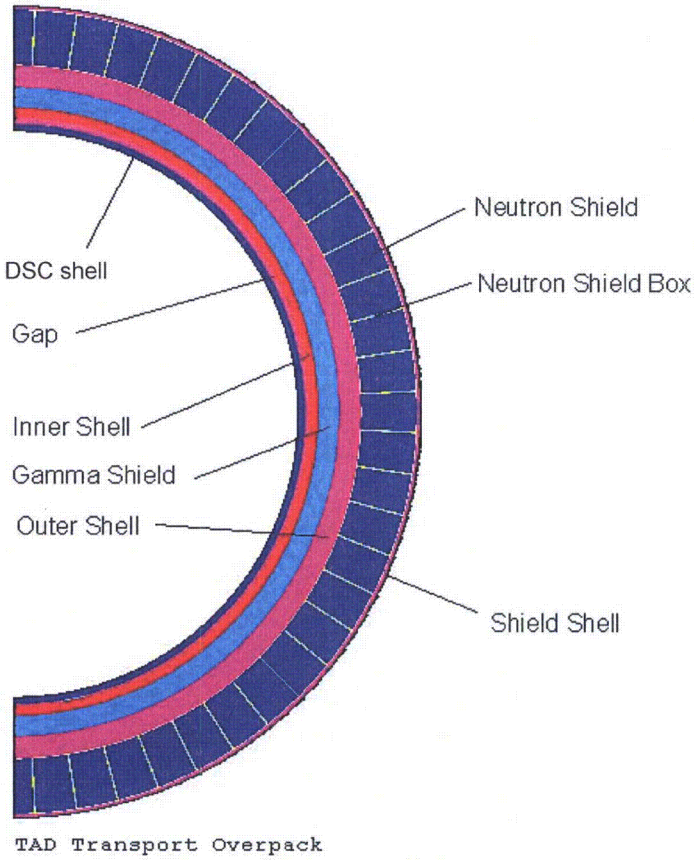

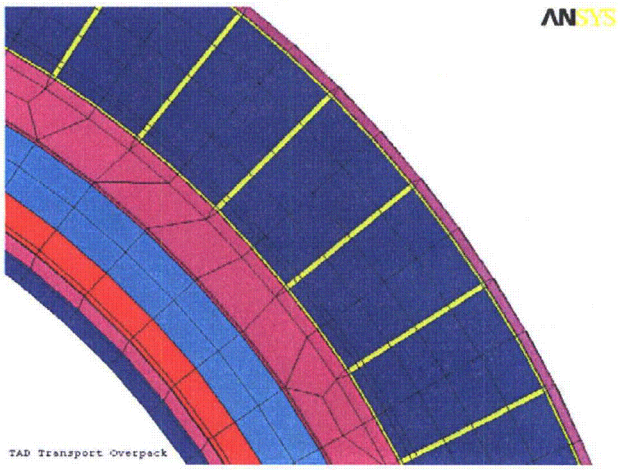

Figure B.3– 3
Finite Element Model of TAD TO with TN44B DSC, Cross Section

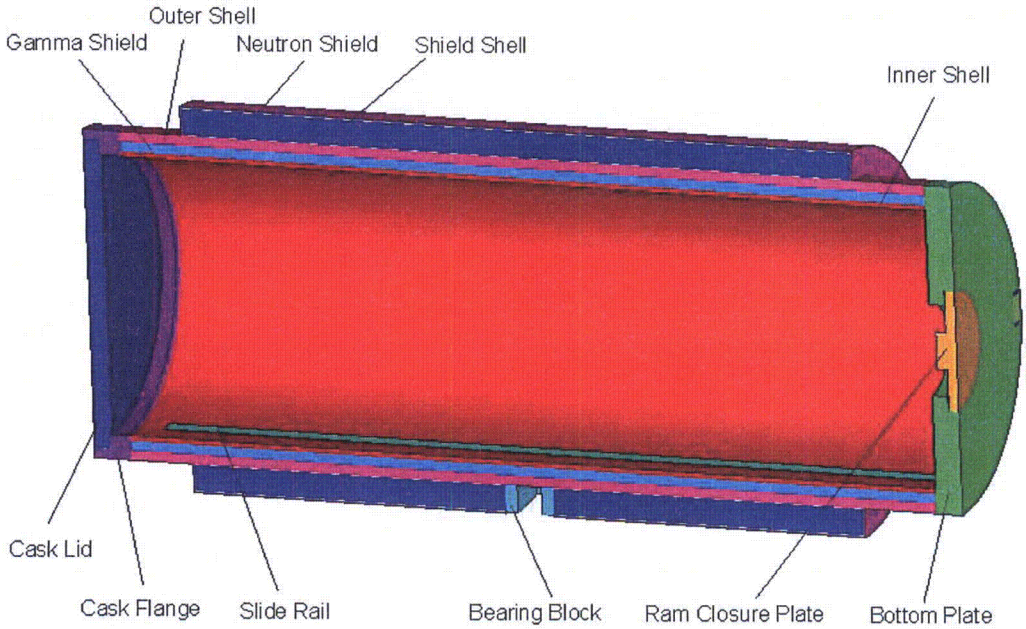

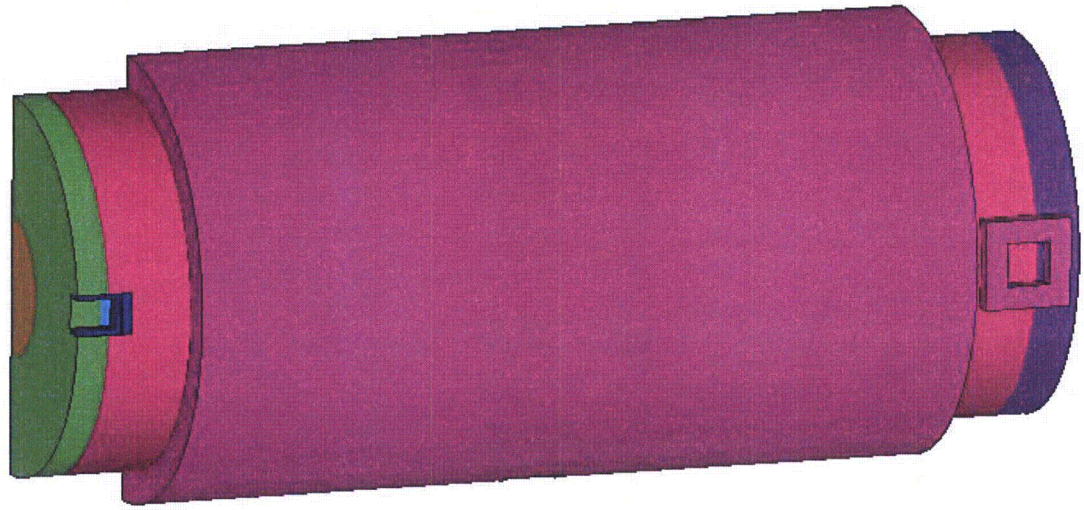

Trunnion Plugs are removed for clarity

Figure B.3– 4
MP197TAD TO Finite Element Model, Cask Components

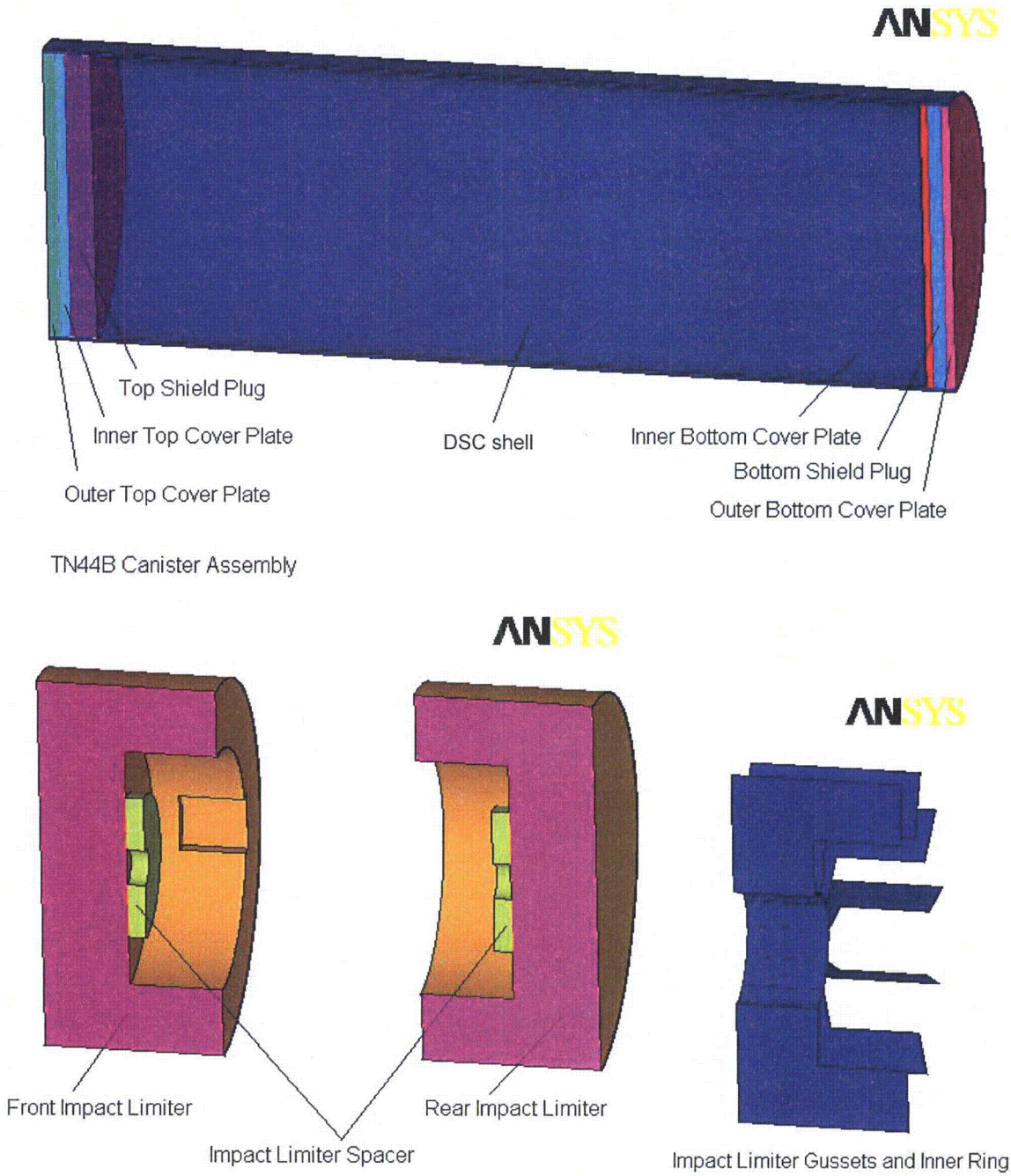

Figure B.3– 5
MP197TAD TO Finite Element Model, TN44B DSC Shell and Impact Limiter Components

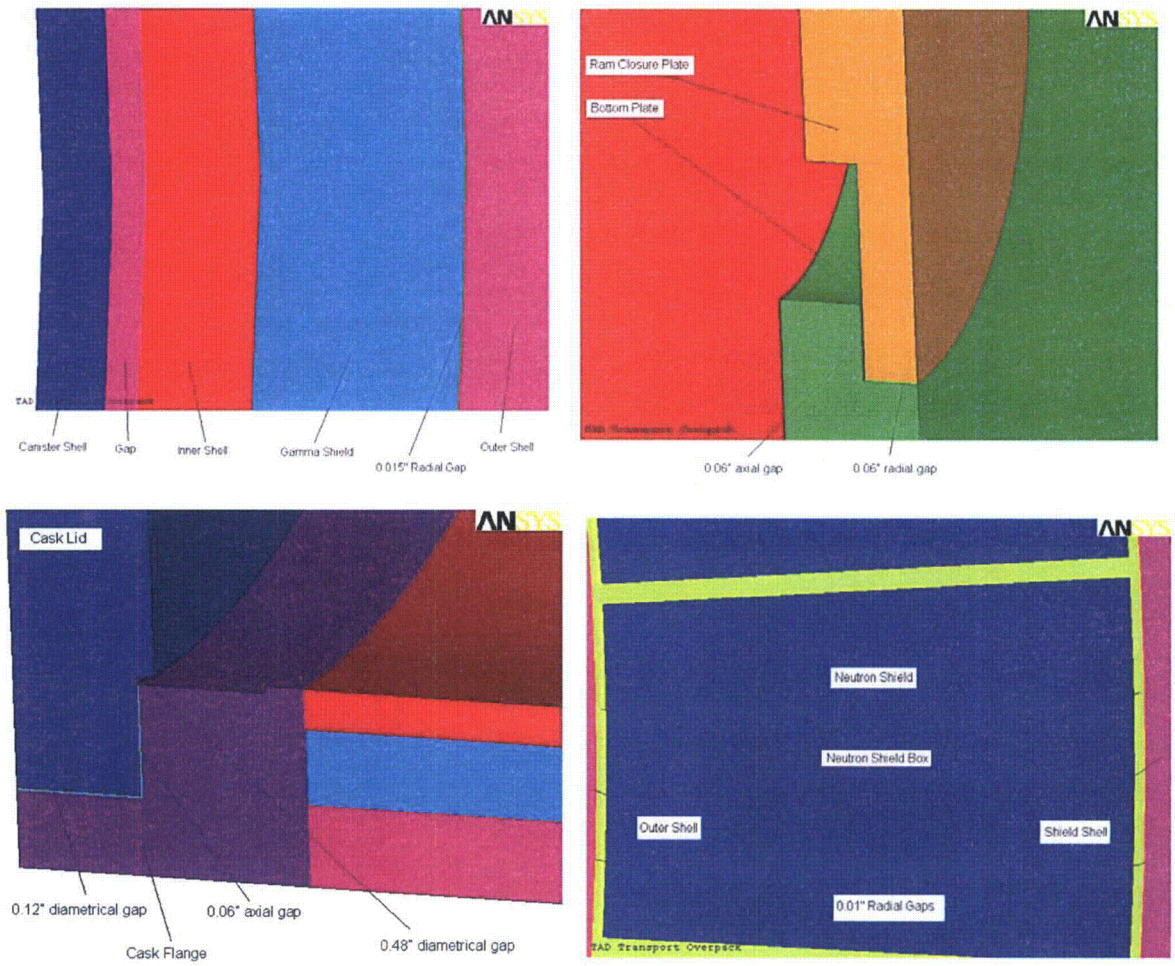

Figure B.3– 6
Gaps in MP197TAD TO Model

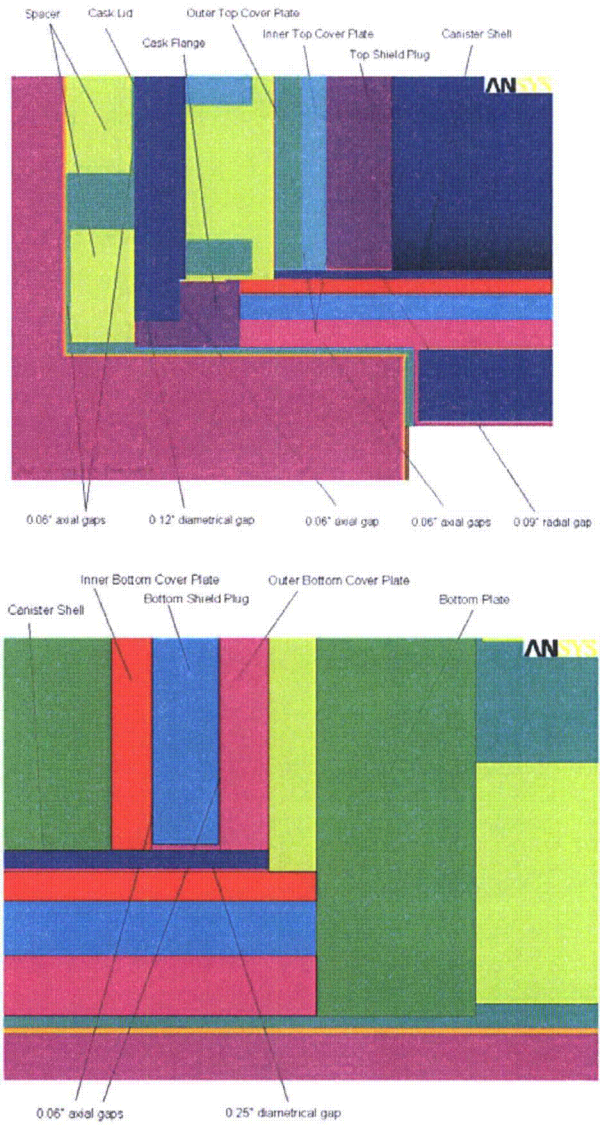

Figure B.3– 7
Gaps in MP197TAD TO and TN44B DSC Assembly Model

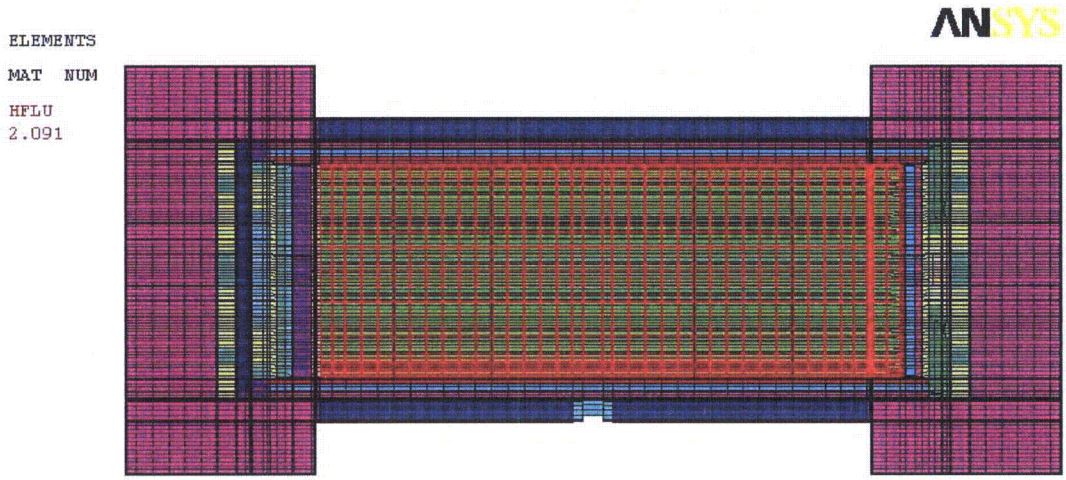

Decay Heat Load

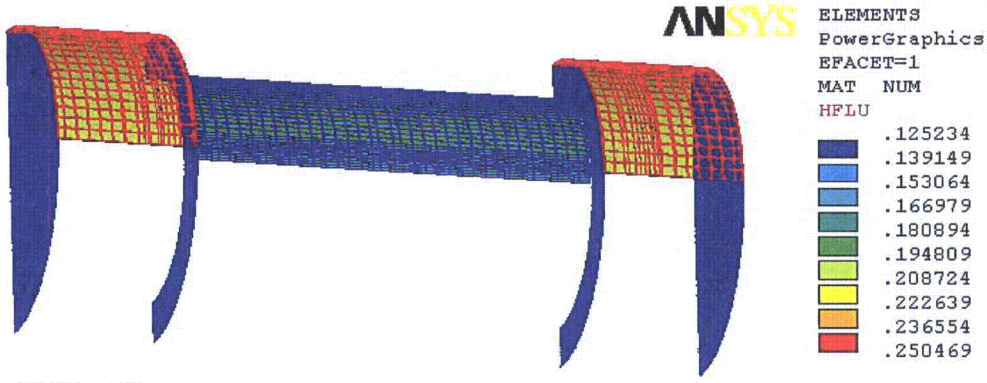

Solar Heat Flux

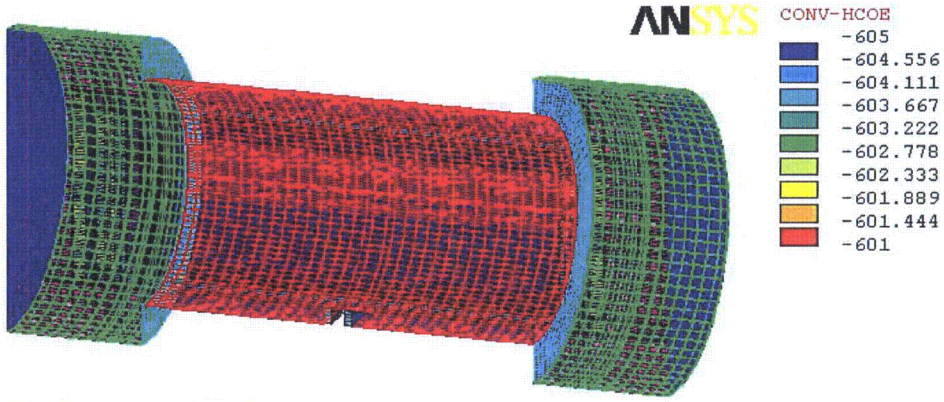

Free Convection and Radiation to Ambient

Figure B.3– 8
Typical Boundary Conditions for MP197TAD TO Model

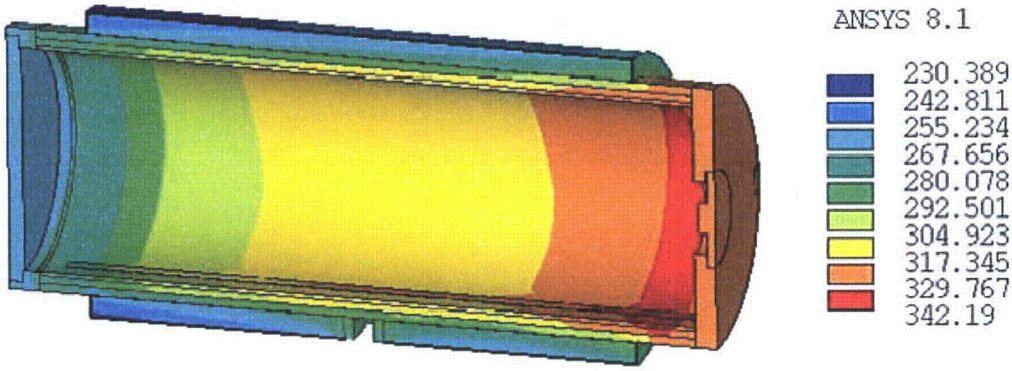

MP197TAD TO temperature profile, NCT

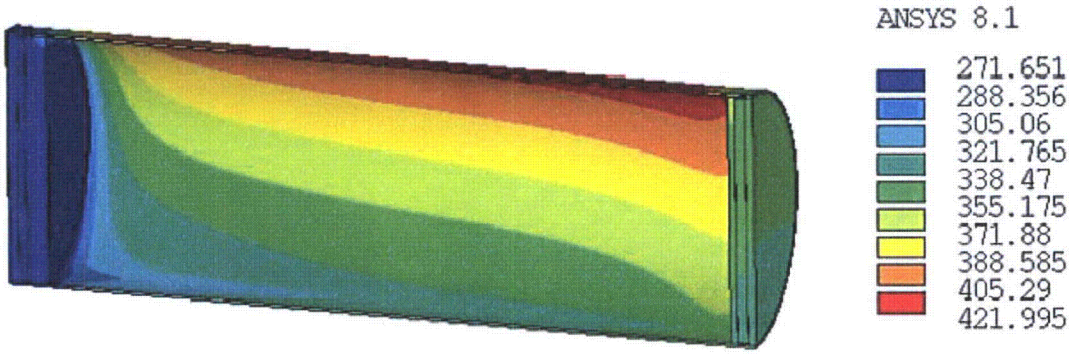

TN44B DSC temperature profile, NCT

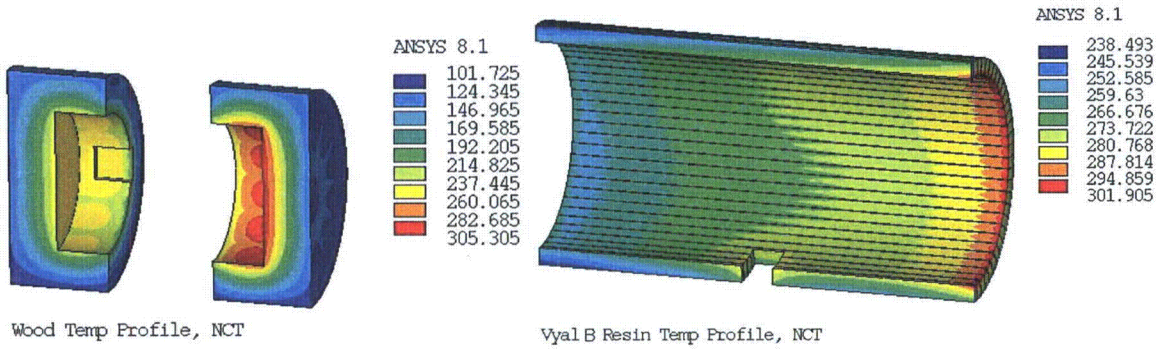

Figure B.3– 9
Temperature Profiles for MP197TAD TO with TN44B DSC NCT, 100°F, Insolation, 22 kW

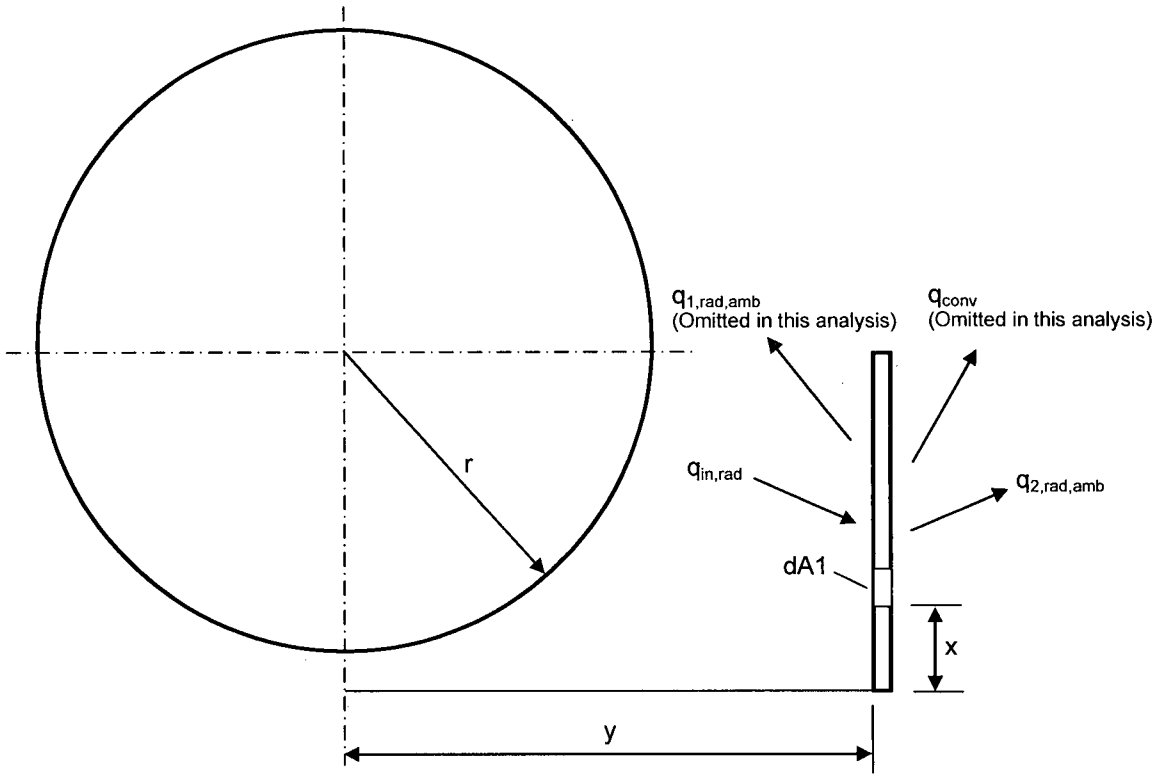

Figure B.3– 10
Schematic View of Cask and Personnel Barrier

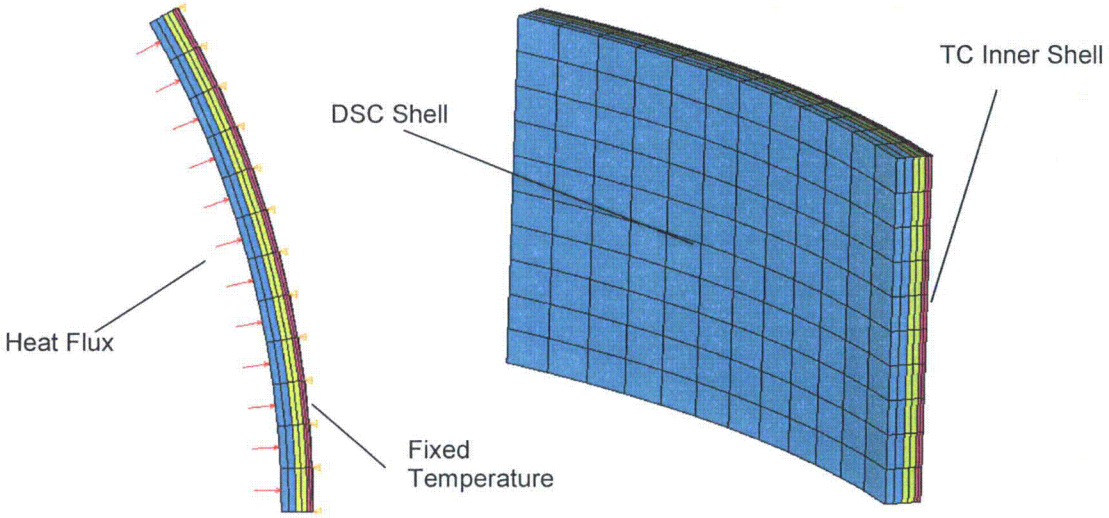

Figure B.3– 11
Sub-Model for Helium Gap Effective Conductivity Calculation

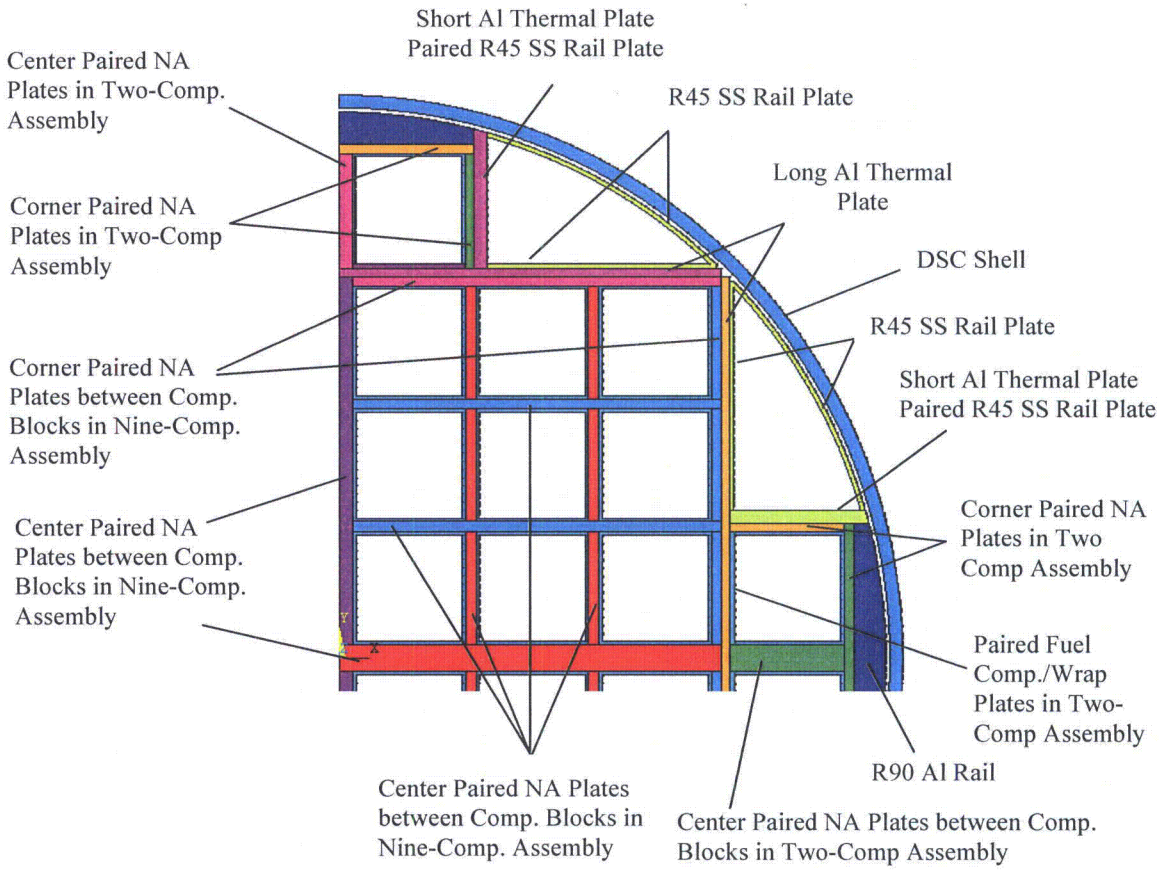

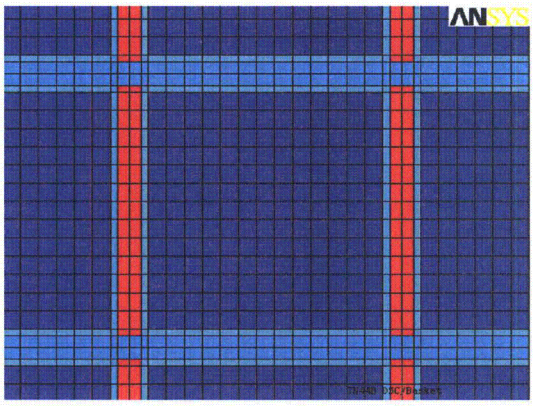

Mesh Density

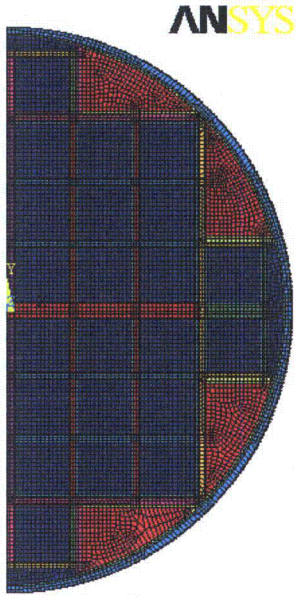

TN44B DSC/Basket

Figure B.3– 12
Thermal Model of TN44B DSC, Cross Sectional View

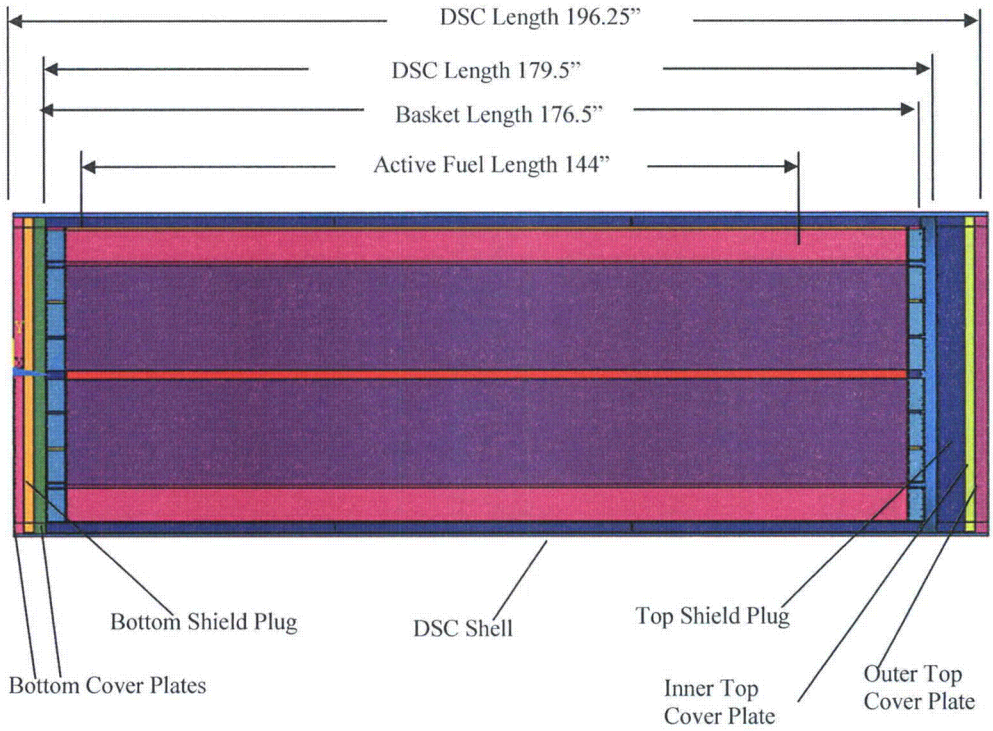

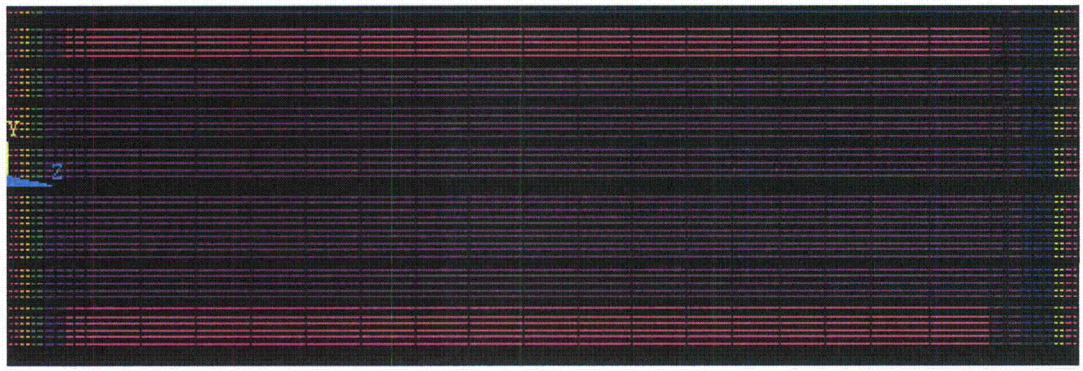

TN44B DSC 3D Model

Mesh Density

Figure B.3– 13
Thermal Model of TN44B DSC, Longitudinal View

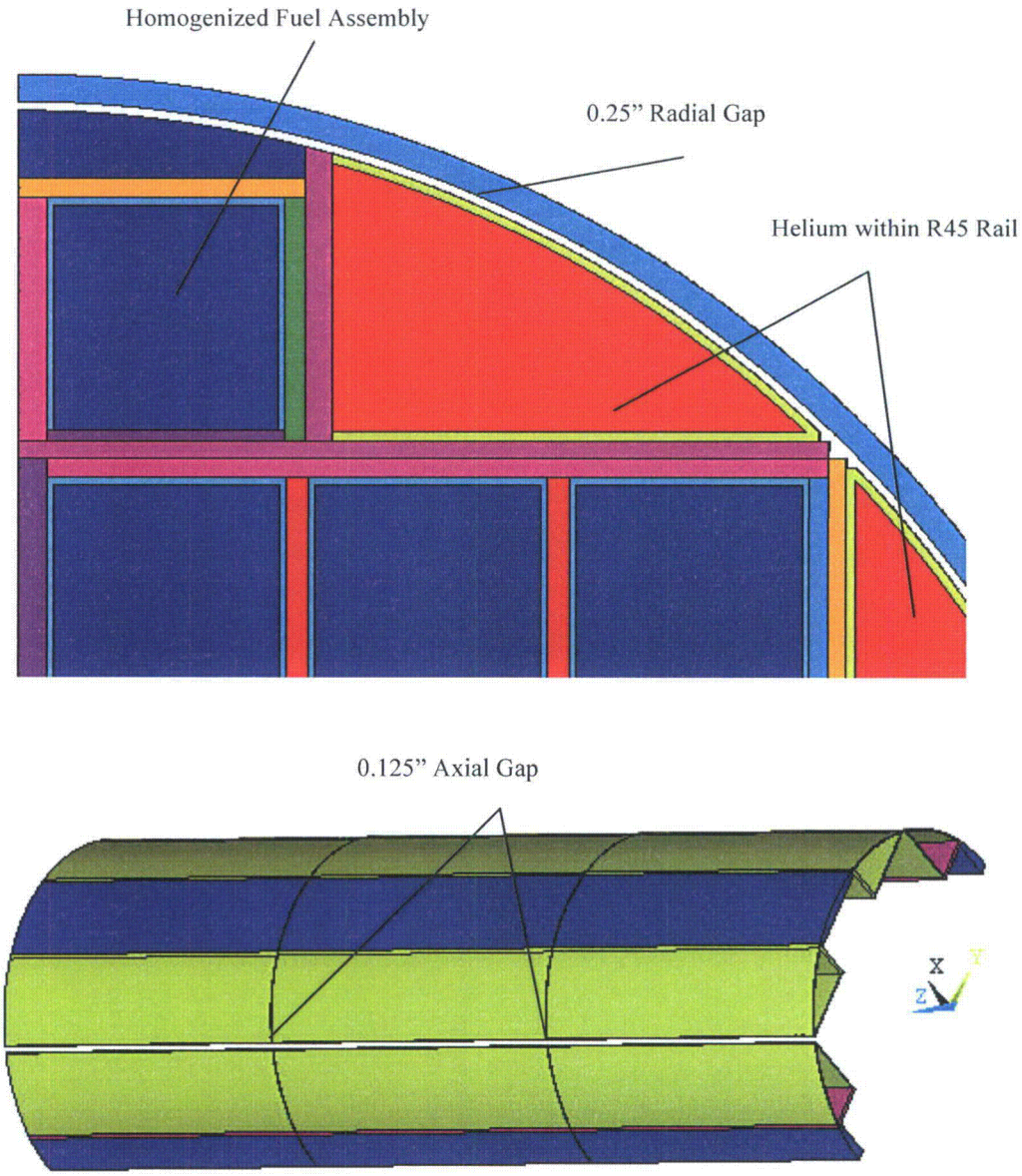

Figure B.3– 14
TN44B DSC Model – Gaps between Rail Sections

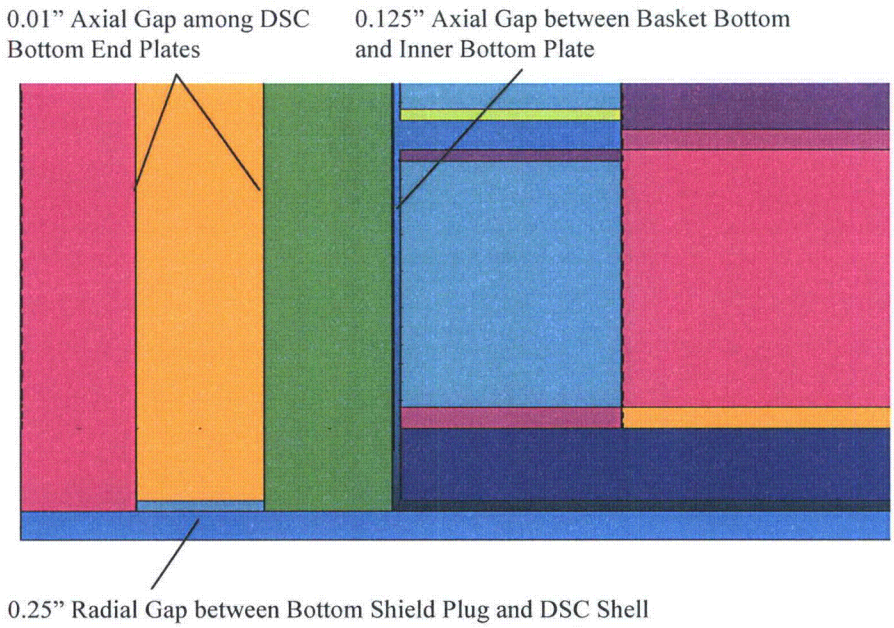

DSC Bottom End Plates

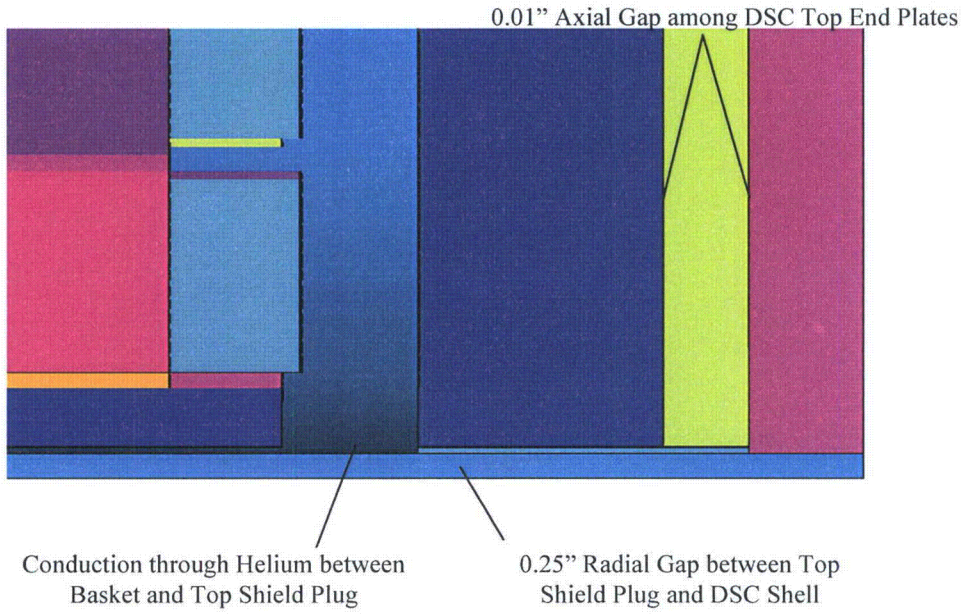

DSC Top End Plates

Figure B.3– 15
TN44B DSC Model – Axial Gaps at DSC End Plates

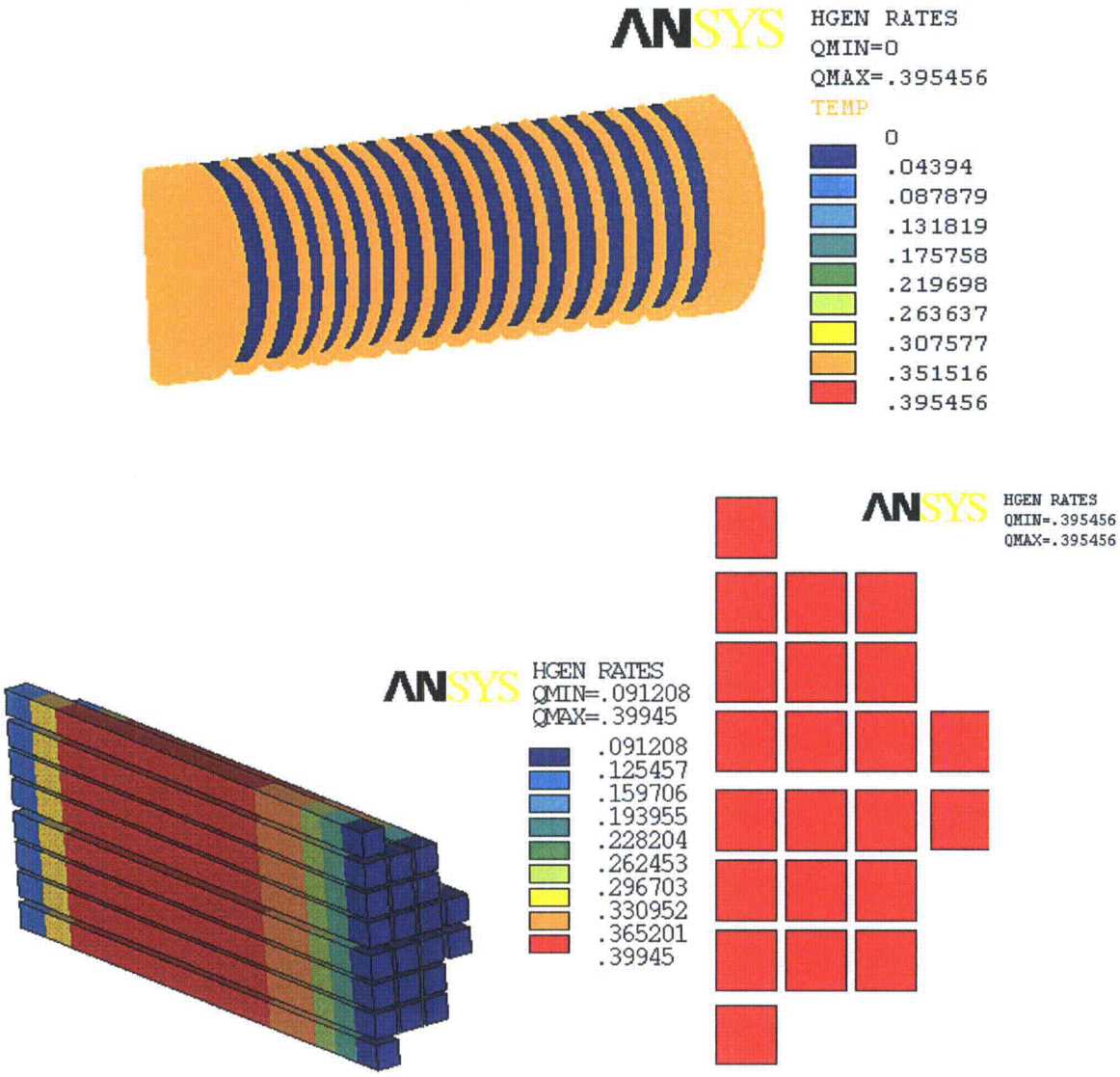

Figure B.3– 16
Typical Boundary Conditions for TN44B DSC Model

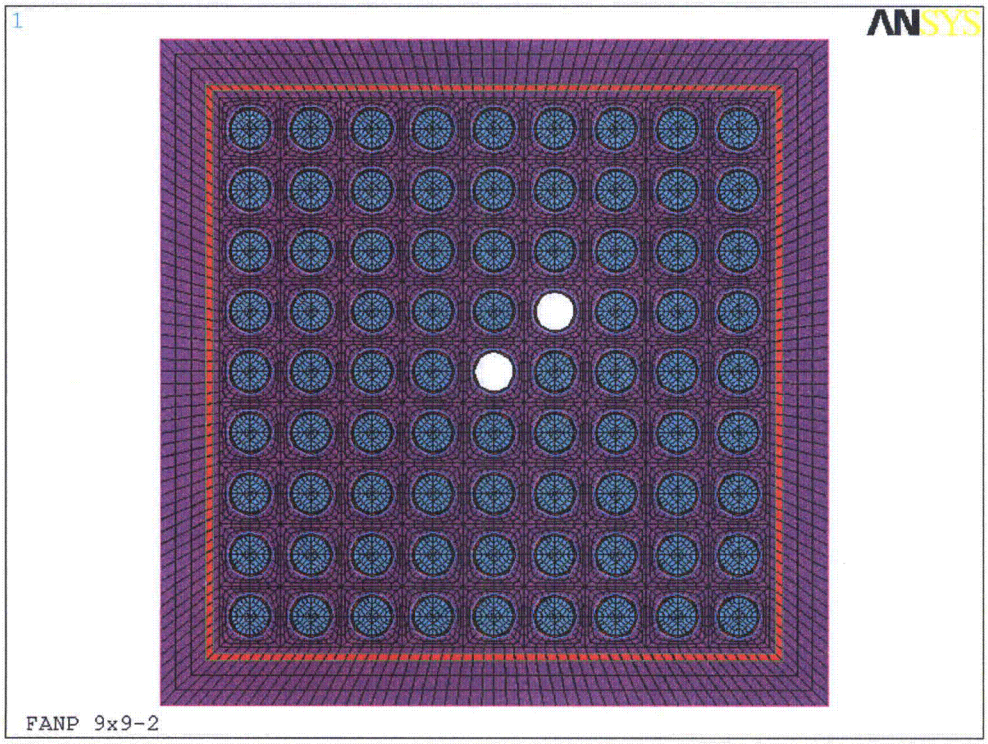

Figure B.3– 17
Finite Element Model of FANP 9x9-2 Fuel Assembly

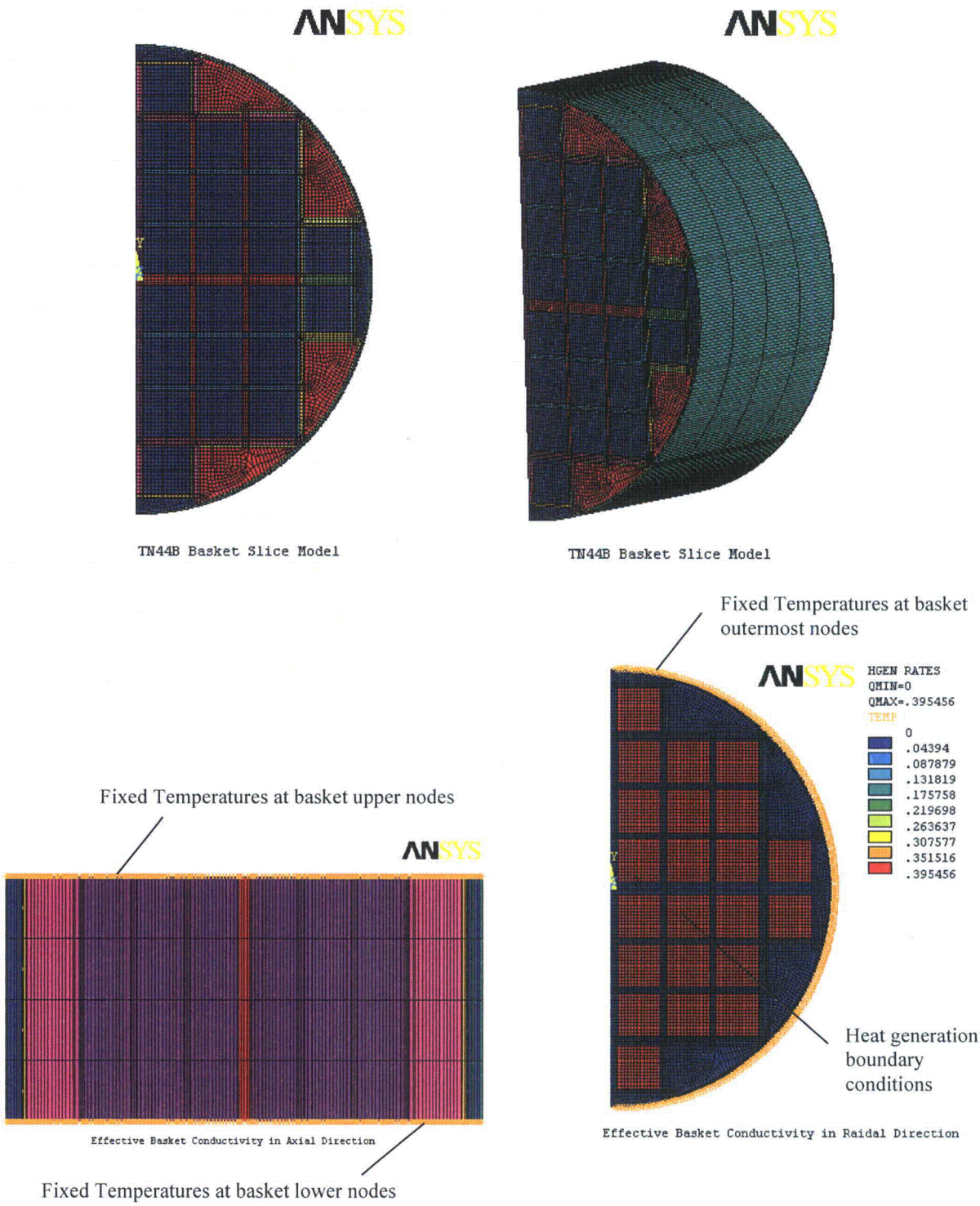

Figure B.3– 18
Basket Slice Models and Boundary Conditions

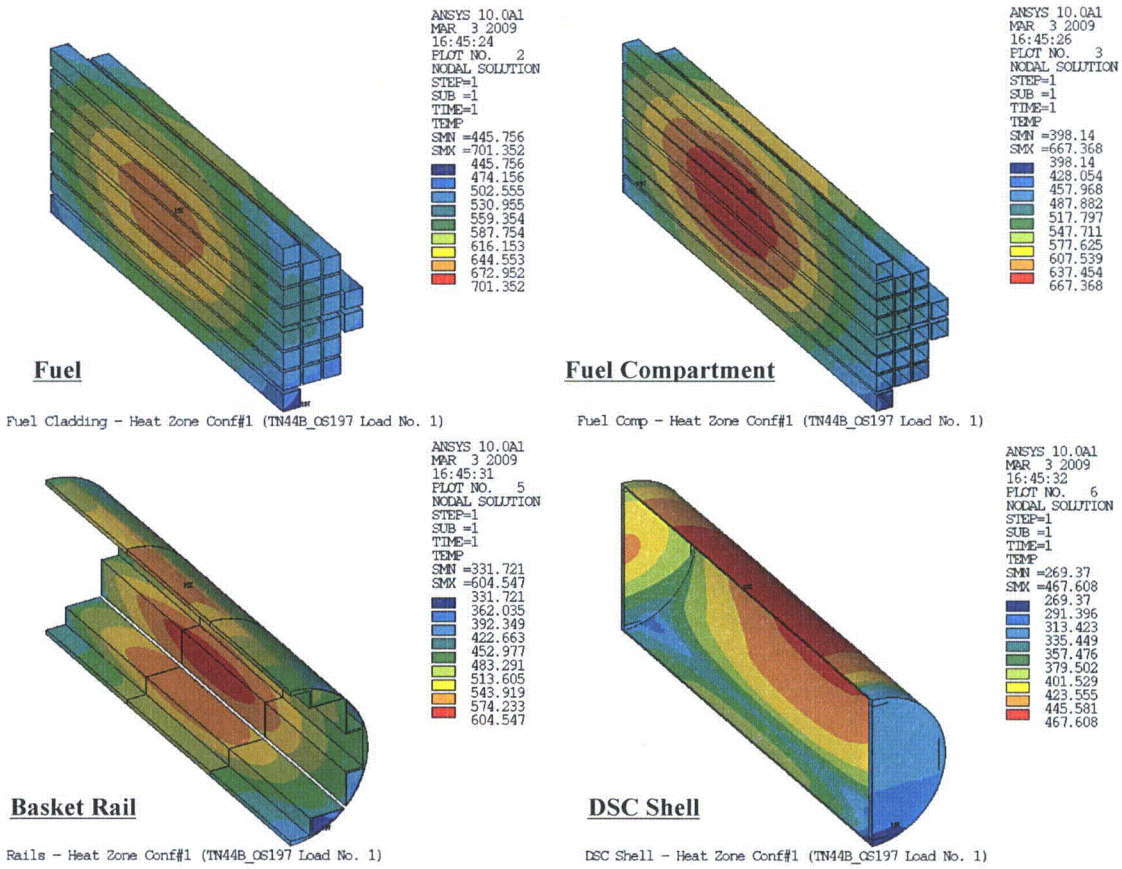

Figure B.3– 19
Bounding Temperature Profiles for TN44B DSC under NCT

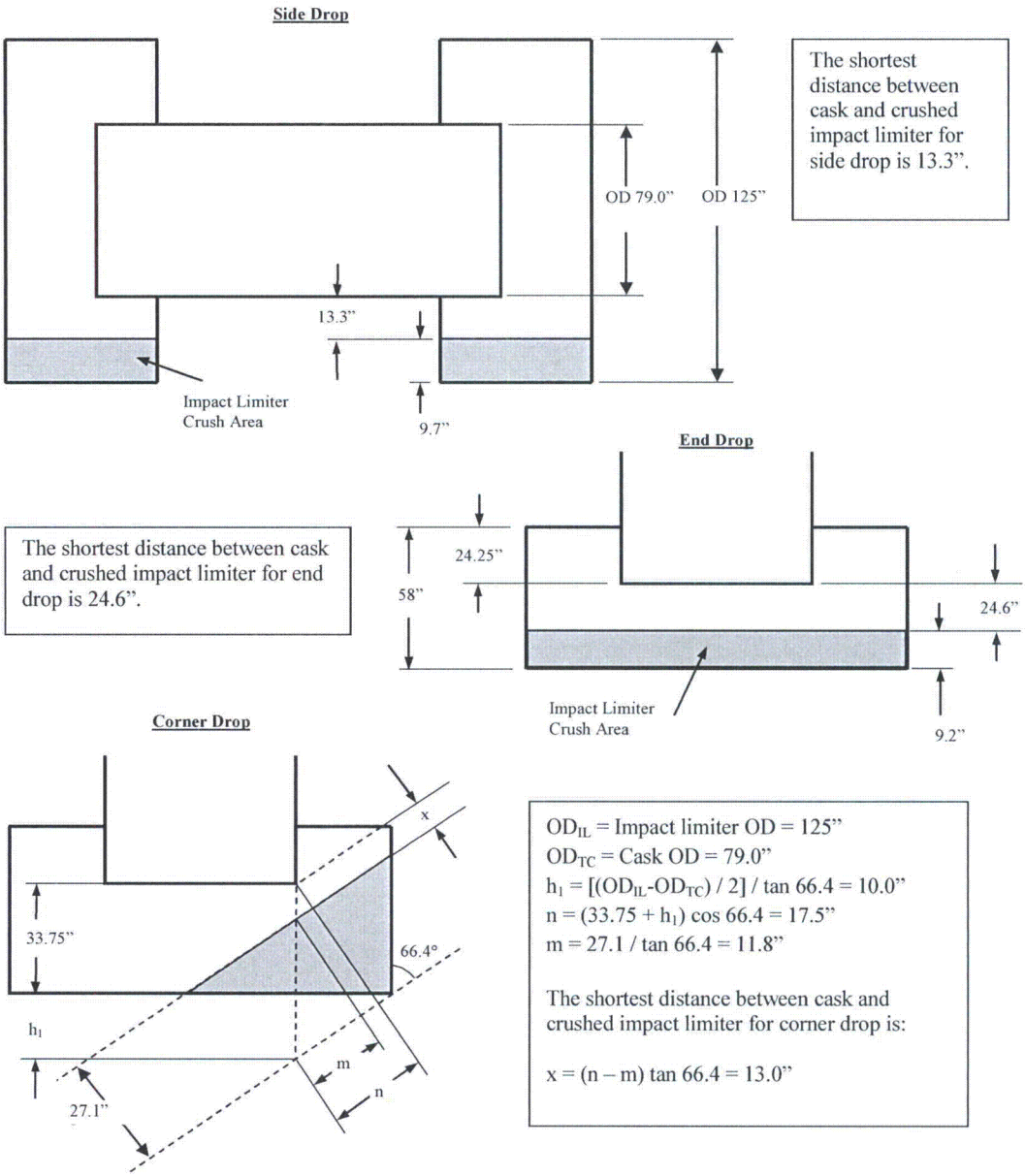

Figure B.3– 20
Impact Limiter Crush Areas for MP197TAD TO (Side, End and Corner Drop)

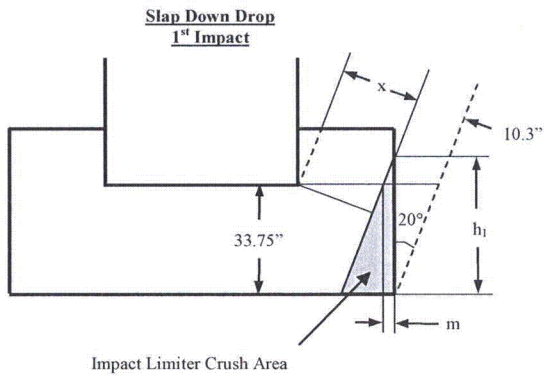

OD_{IL} = Impact limiter OD = 125"
OD_{TC} = Cask OD = 79.0"
h_1 = 13.7 / sin 20 = 40.1"
m = (h_1 – 33.75) tan 20 = 2.3"
The shortest distance between cask and crushed impact limiter for slap down drop, 1st impact is:

x = [(OD_{IL} – OD_{TC}) /2 – m] cos 20 = 19.5"

The shortest distance between cask and crushed impact limiter for slap down drop, 2nd impact is 10.9"

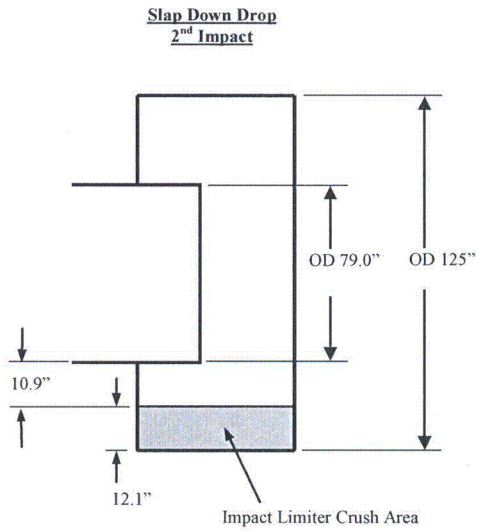

Figure B.3– 21
Impact Limiter Crush Areas for MP197TAD TO (Slap Down Drop)

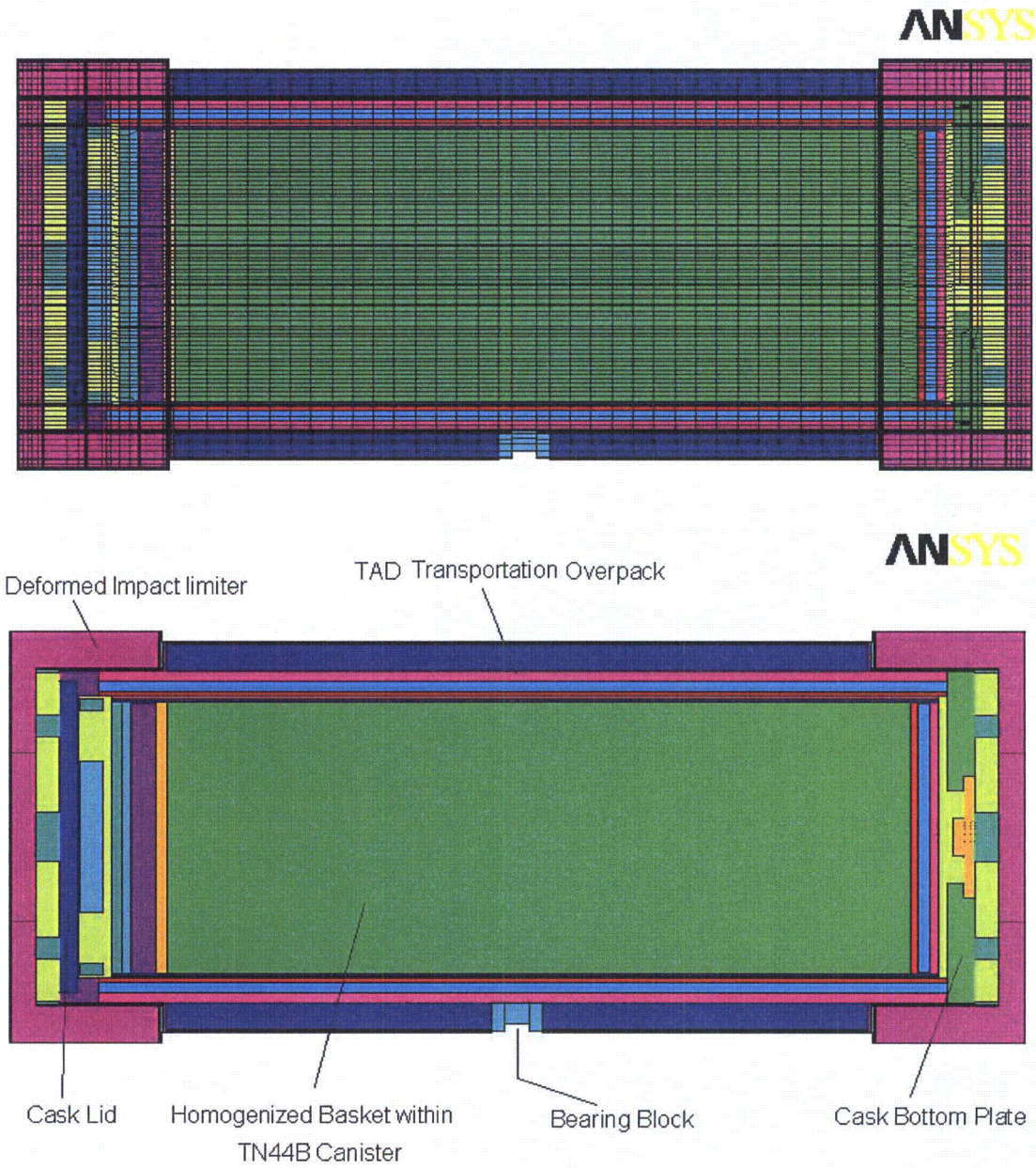

Figure B.3– 22
Finite Element Model of MP197TAD TO with Deformed Impact Limiters

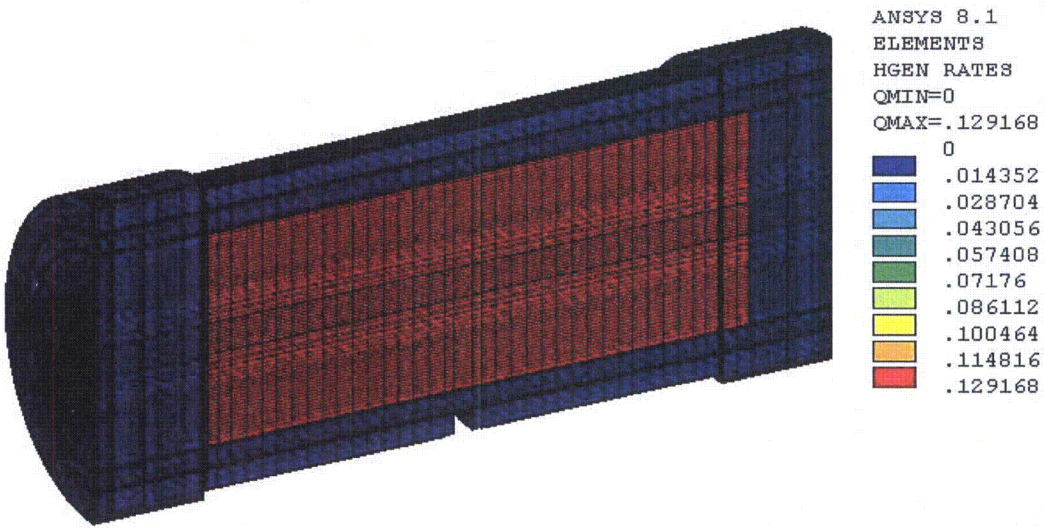

Heat Generation Boundary Conditions for TAD TO with TN44B under HAC

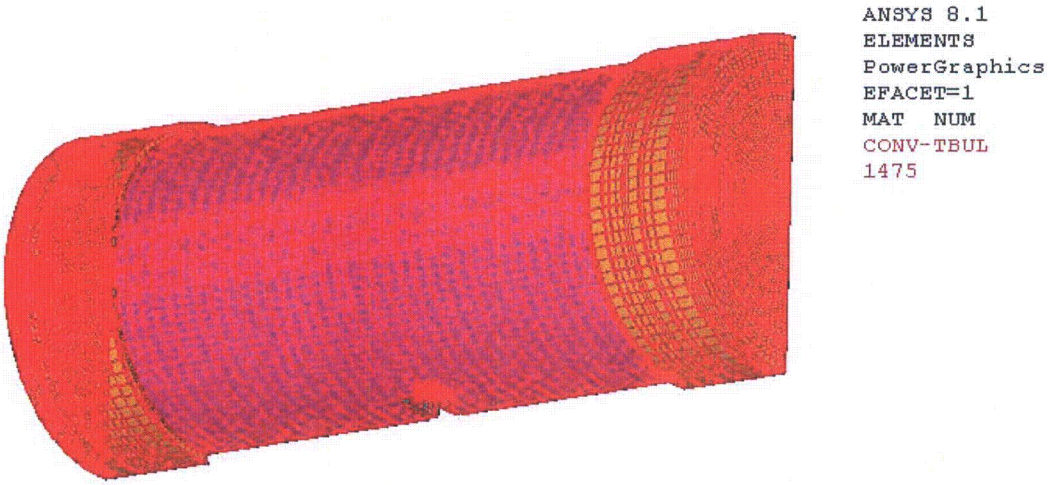

Convection and Radiation from Fire to TAD TO with TN44B Canister

Figure B.3– 23
Typical Boundary Conditions for MP197TAD TO during Fire Conditions

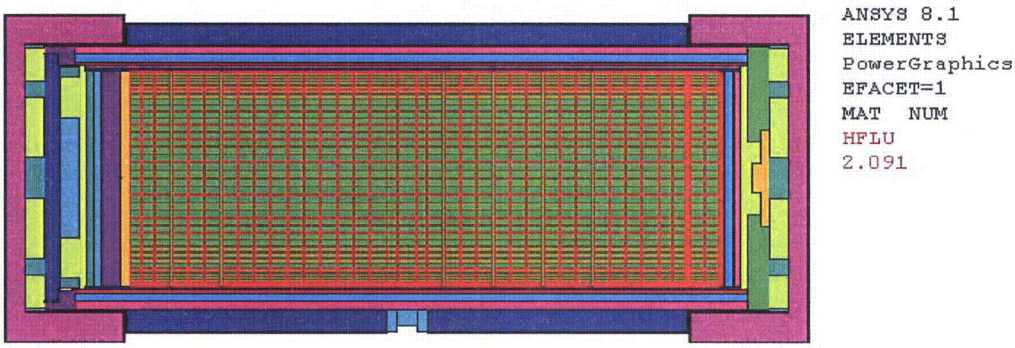

Heat Flux on TN44B Body, TAD TO Model during Cool-Down

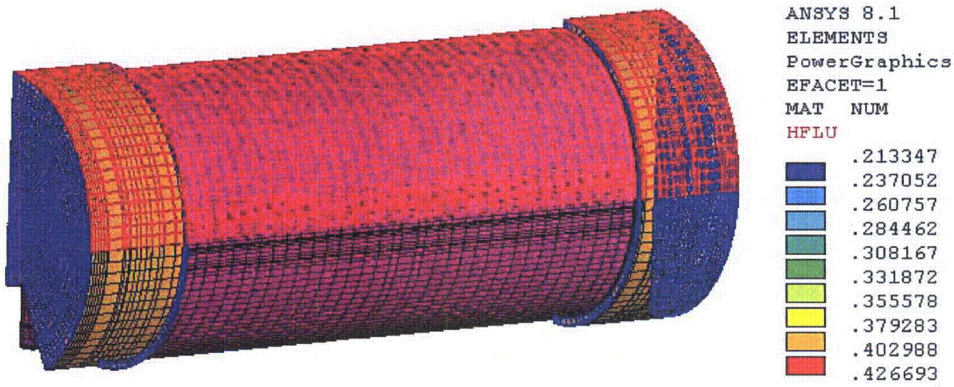

Solar Heat Flux, TAD TO with TN44B Canister, Smoldering/Cool-Down

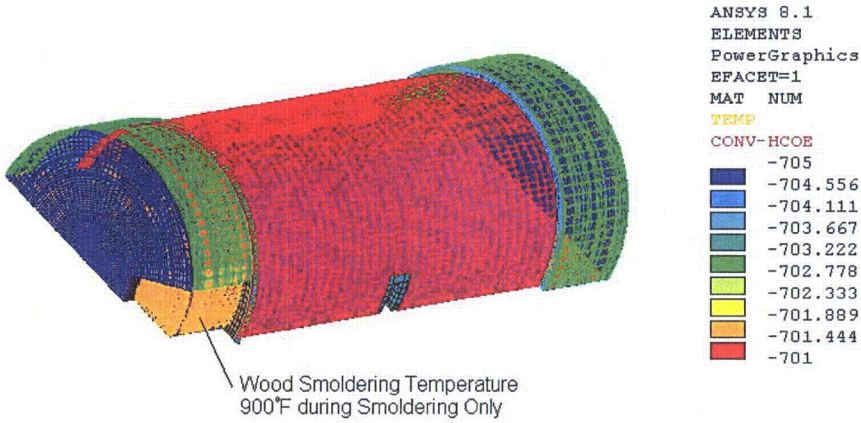

Convection and Radiation to Ambient, TAD TO with TN44B, Wood Smoldering/Cool-Down

Figure B.3– 24
Typical Boundary Conditions for MP197TAD TO during Smoldering/Cool-Down Periods

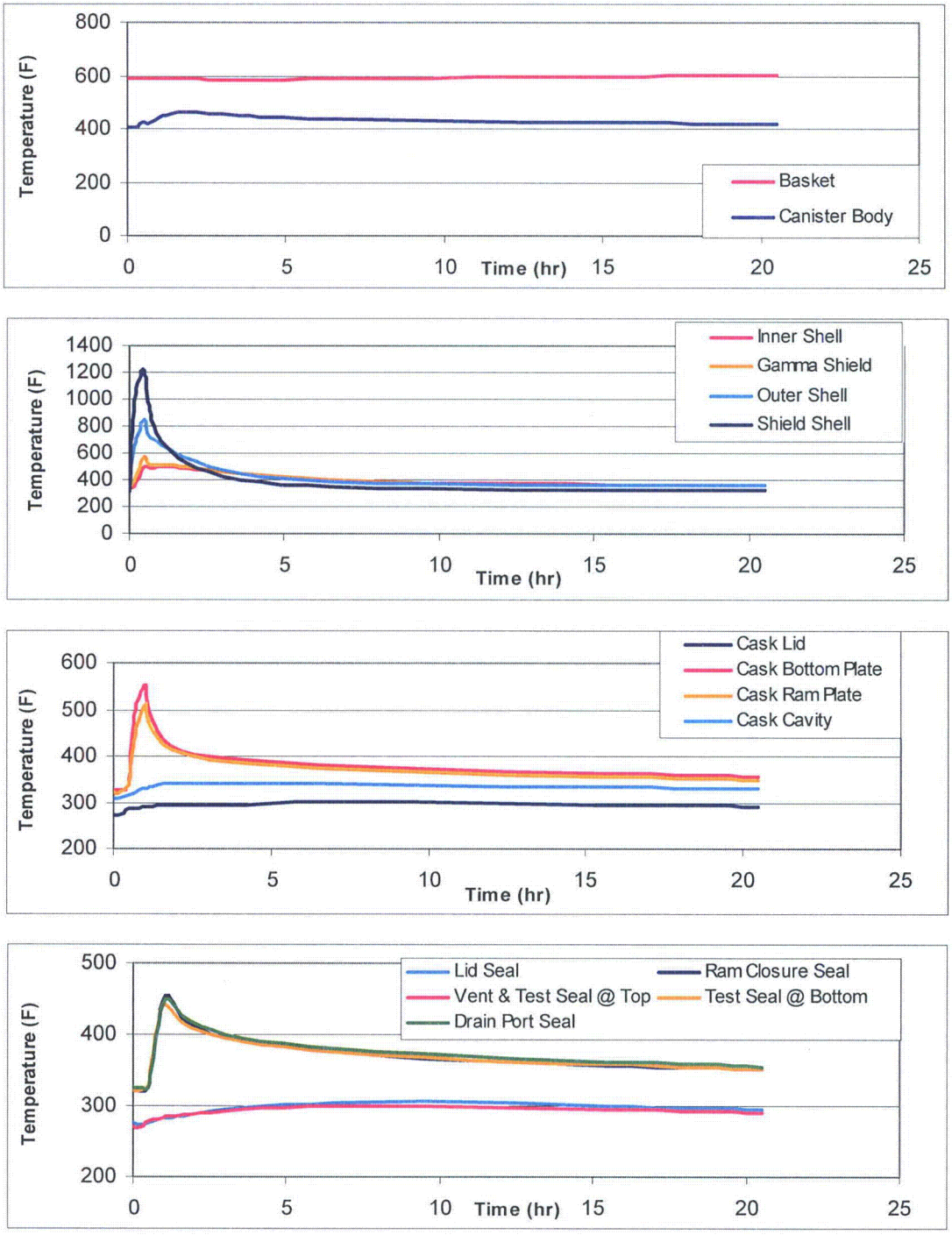

Figure B.3– 25
Time-Temperature Histories for MP197TAD TO / TN44B, HAC Rear Impact Limiter Punctured

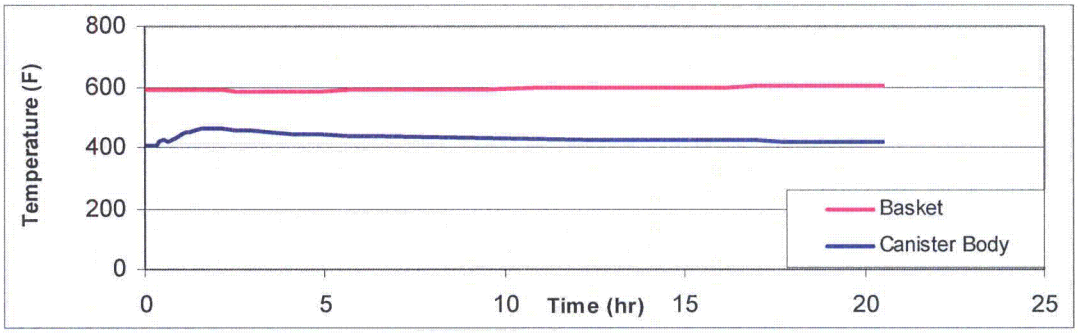

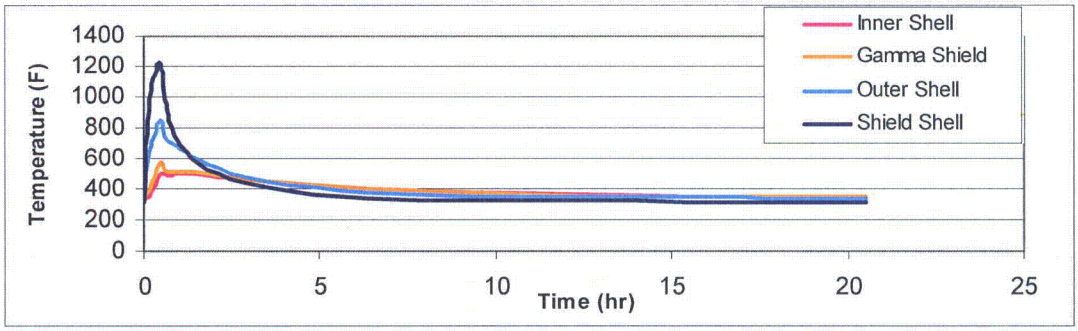

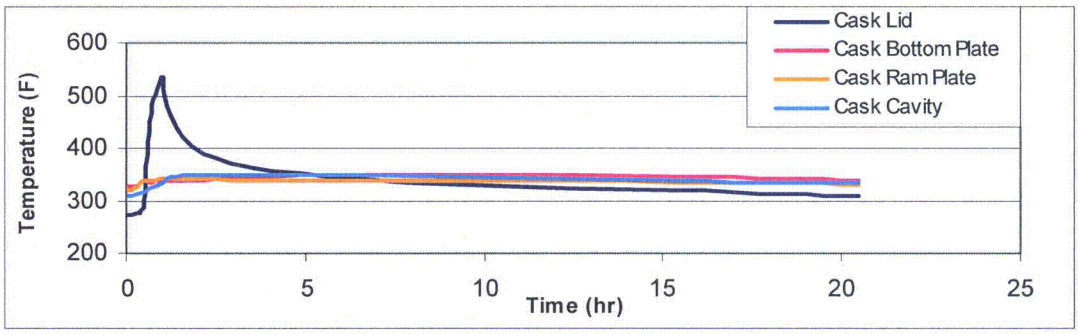

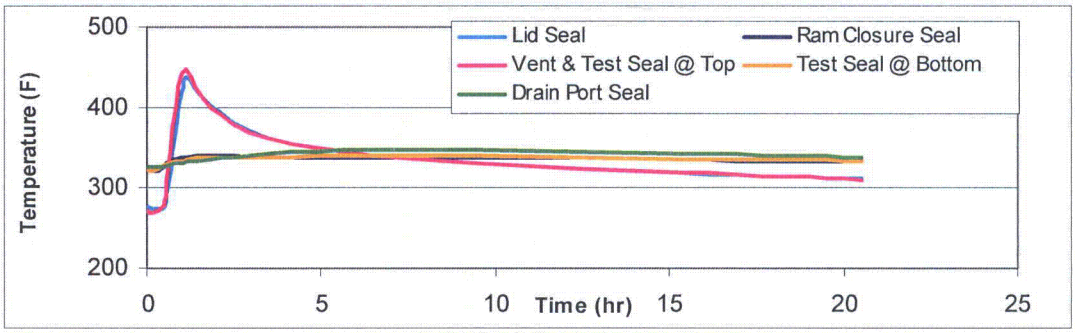

Figure B.3– 26
Time-Temperature Histories for MP197TAD TO / TN44B, HAC Front Impact Limiter Punctured

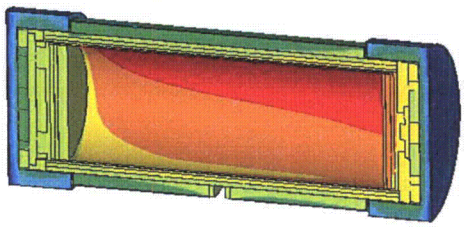

TO TAD, TN44B 22 kW, HAC Initial Temperatures

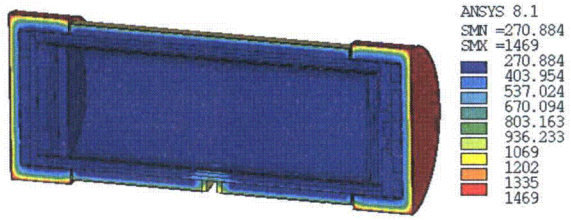

TO TAD, TN44B 22 kW, End of Fire

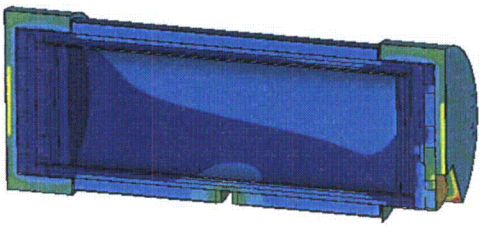

TO TAD, TN44B 22 kW, Smoldering Wood after Fire

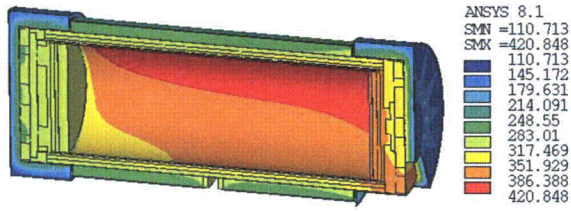

TO TAD, TN44B 22 kW, Puncture Rear IL, 20 hrs after Fire

Rear Impact Limiter Punctured

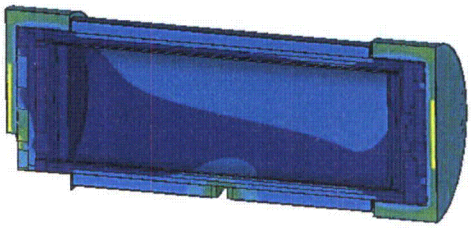

TO TAD, TN44B 22 kW, Smoldering Wood after Fire

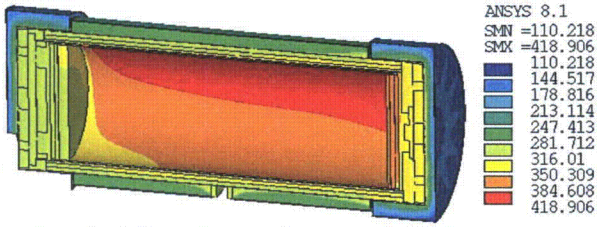

TO TAD, TN44B 22 kW, Puncture Front IL, 20 hrs after Fire

Front Impact Limiter Punctured

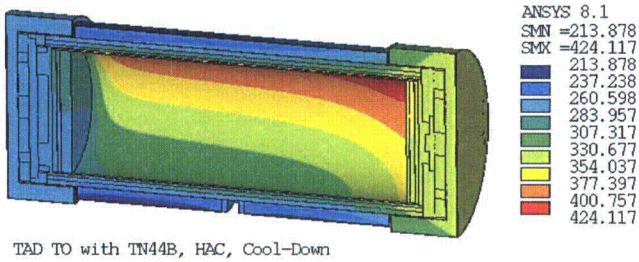

TAD TO with TN44B, HAC, Cool-Down

Figure B.3– 27
Temperature Profiles for MP197TAD TO with TN44B DSC under HAC

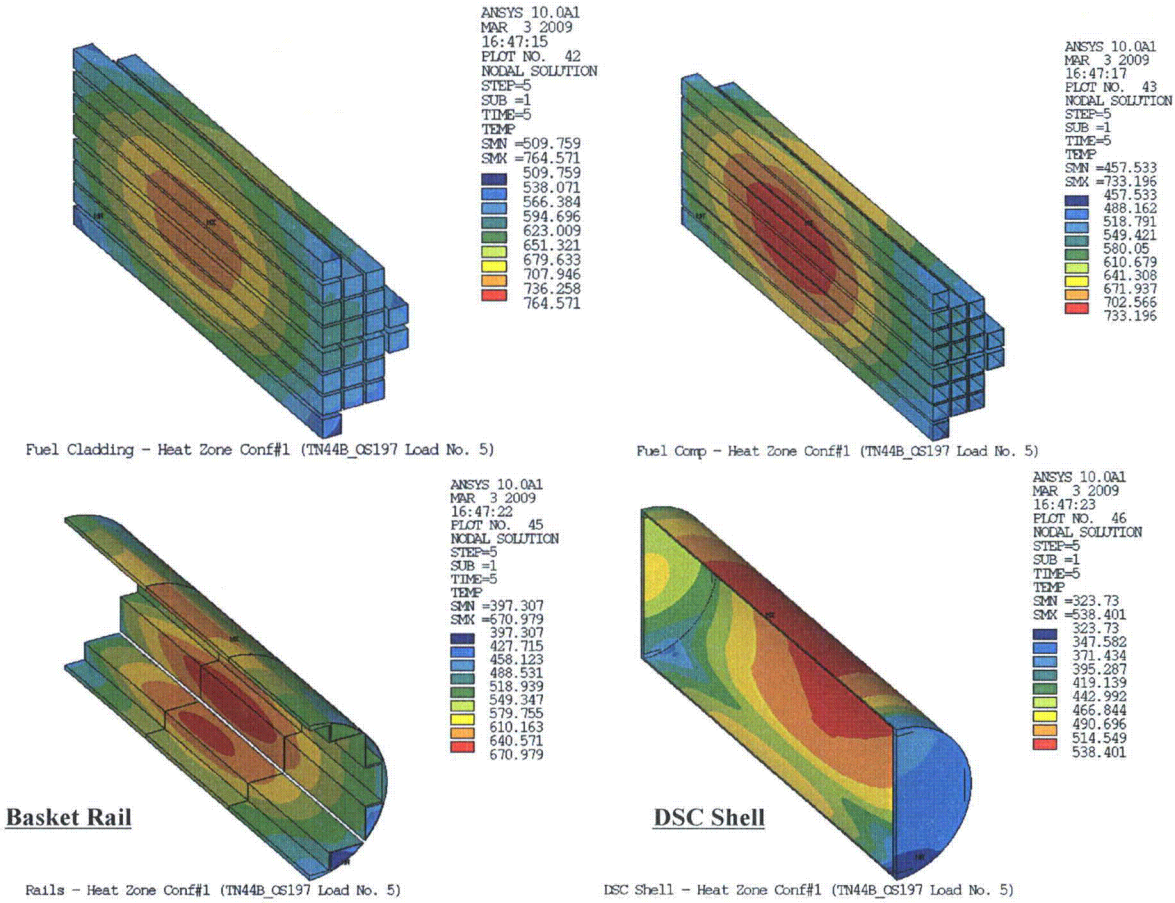

Figure B.3– 28
Bounding Temperature Profiles for TN44B DSC under HAC

CHAPTER B.5
SHIELDING EVALUATION

CONTENTS

B.5.1 Description of Shielding Design B.5-1
B.5.1.1 Design Features B.5-1
B.5.1.2 Summary Table of Maximum Radiation Levels B.5-2
B.5.2 Source Specification B.5-2
B.5.2.1 Gamma Source B.5-5
B.5.2.2 Neutron Source B.5-6
B.5.2.3 Source Conversion Factors B.5-6
B.5.2.4 Fuel Qualification B.5-7
B.5.2.5 Response Functions for Transportation and Transportation FQTs B.5-8
B.5.2.6 BWR Decay Heat Equation B.5-13
B.5.3 Shielding Model B.5-13
B.5.3.1 Configuration of Sources and Shielding B.5-13
B.5.3.2 Material Properties B.5-16
B.5.4 Shielding Evaluation B.5-16
B.5.4.1 Methods B.5-17
B.5.4.2 Input Data B.5-19
B.5.4.3 Flux-to-Dose-Rate Conversion B.5-19
B.5.4.4 External Radiation Levels B.5-19
B.5.5 References B.5-20
B.5.6 Appendices B.5-21
B.5.6.1 SAS2H/ORIGEN-S Input File B.5-21
B.5.6.2 MCNP Neutron Model Input File B.5-24

LIST OF TABLES

Table B.5-1 MP197TAD TO Cask Shield Materials B.5-53
Table B.5-2 Summary of MP197TAD TO Dose Rates B.5-54
Table B.5-3 BWR Fuel Assembly Material Mass B.5-55
Table B.5-4 Elemental Composition of LWR Fuel-Assembly Structural Materials B.5-56
Table B.5-5 Flux Scaling Factors By Fuel Assembly Region B.5-57
Table B.5-6 Source Term Peaking Summary B.5-58
Table B.5-7 Design Basis Source Terms for the NCT (44 Locations) B.5-59
Table B.5-8 Design Basis Source Terms for the HAC (44 Locations) B.5-60
Table B.5-9 Three Zone Response Function for the TN44B B.5-61
Table B.5-10 VYAL B Chemical Composition B.5-62
Table B.5-11 Fuel Assembly Materials Input For MCNP B.5-63
Table B.5-12 Package Materials Input for MCNP B.5-64
Table B.5-13 Flux-to-Dose Rate Conversion Factors for Gamma B.5-65
Table B.5-14 Flux-Dose-Rate Conversion Factors for Neutron B.5-66
Table B.5-15 Maximum Dose Rate Values at Various Radial Distances from Side of Cask and Impact Limiter – Normal Conditions B.5-67

LIST OF FIGURES

Figure B.5-1 MP197TAD TO Cask Shielding Configuration B.5-68
Figure B.5-2 Sketch of MP197TAD TO Transport Cask with TN44B DSC – Top and Bottom Views B.5-69
Figure B.5-3 Wide View of MP197TAD TO Transport Cask with TN44B DSC: MCNP Model Cut-through YZ Plane, Normal Condition B.5-70
Figure B.5-4 MP197TAD TO Transport Cask with TN 44B DSC: MCNP Model Cut-through XY Plane (Z=0.0 cm), Normal Condition B.5-71
Figure B.5-5 Radial, 1/4 View of MP197TAD TO Transport Cask within TN 44B DSC: MCNP Model Cut-through XY Plane, Normal Condition B.5-72
Figure B.5-6 TN44B DSC and MP197TAD TO Bottom Plugs with Grapple Ring Cut-Out (Not to Scale) B.5-73
Figure B.5-7 MP197TAD TO Shear Key ZY and XY View at Z=36) (Not to Scale) B.5-74
Figure B.5-8 TN 44 DSC Fuel Compartments Zone Matrix Indices B.5-75
Figure B.5-9 Normal Condition –Radial Dose Rates at Axial Locations B.5-76

CHAPTER B.5
SHIELDING EVALUATION

B.5.1 Description of Shielding Design

B.5.1.1 Design Features

Shielding for the MP197TAD TO package is provided by the TN44B DSC and basket and the cask body. The cask body is made up of the containment vessel, the gamma shielding and the lid. For the neutron shielding, a borated polyester resin compound surrounds the TO structural outer shell in the radial direction. Additional shielding is provided by the steel outer shell surrounding the neutron shield resin layer and by the aluminum boxes containing the neutron shielding.

For transport, wood filled impact limiters are installed on either end of the cask and provide additional shielding for the ends and some radial shielding for the areas at either end of the radial neutron shield. Figure B.5-1 shows the shielding configuration of the package (without impact limiters). Table B.5-1 lists the compositions of the shielding materials.

The BWR fuel assemblies acceptable for transport in the MP197TAD TO are listed in Chapter B.1, Section B.1.2.3. The radiation source terms are calculated using the SAS2H/ORIGEN-S modules of SCALE [1]. From a decay heat load perspective, fuel assemblies with a maximum fuel assembly decay heat load of 0.54 kW and a total canister heat load of 22 kW are authorized for transport in the MP197TAD TO. However, in order to meet the 10CFR71 transport dose rate requirments, fuel assemblies with burnup, enrichment and cooling time (BECT) combinations that result in lower decay heat loads must be loaded. The design basis shielding configuration evaluated is based on a single zone loading of 44 BWR fuel assemblies within the TN44B DSC. The bounding design basis fuel utilized in the dose rate calculations for the normal conditions of transport (NCT) has an initial enrichment of 1.90 wt. % U-235, a burnup of 26 GWD/MTU and a cooling time of 6.5 years (0.262 kW per fuel assembly). The bounding design basis fuel utilized in the dose rate calculations for the hypothetical accident condition (HAC) has an initial enrichment of 2.60 wt. % U-235, a burnup of 62 GWD/MTU and a cooling time of 31.5 years (0.316 kW per fuel assembly). The fuel qualification tables (FQTs) that determine the acceptable BECT combinations for loading, shown in Chapter B.1, Section B.1.2.3 are developed such that the resulting NCT dose rates are approximately the same.

The GE 7x7 BWR fuel assembly contains the maximum heavy metal loading of 0.198 MTU (Chapter B.1, Table B.1-3) which results in bounding neutron and gamma source terms and is therefore identified as the design basis fuel assembly. Section B.5.2 describes the source specification and Section B.5.4 describes the shielding analysis performed for the MP197TAD TO. The shielding analysis models are described in Section B.5.3.

Normal conditions of transport are modeled with the neutron shielding and impact limiters on MP197TAD TO intact. This shielding calculation is performed using the Monte Carlo computer code MCNP[5]. Dose rates on the side, top and bottom of the MP197TAD TO package are calculated for the various sources described in Section B.5.2 and combined to give a total gamma and neutron dose rate.

Hypothetical accident conditions assume a partial credit for the neutron shield (75% of the neutron shielding is lost) and that no wood is left inside the impact limiters and that the steel shell remains attached to the cask. Tests have shown that the neutron shielding material retains more than 60% of its principal contents (hydrogen, boron etc) following a design basis fire accident and a 25% credit employed in the shielding calculations is conservative. This evaluation bounds the accident conditions since it is shown in Chapter B.2 that the neutron shielding is not lost and the impact limiters remain on the cask during HAC. These calculations are also performed by considering a lead slump of 0.465" at the axial ends of the cask consistent with the results in Chapter B.2, Appendix B.2.13.3. Shielding calculations for the HAC are also performed using the MCNP Code.

The results of the shielding analyses show that the MP197TAD TO complies with dose rates restrictions of 10 CFR 71 during NCT and HAC.

Dose rates restriction criteria for the transportation are the following:

- External dose rate at any point on the outer accessible surface of the vehicle under normal conditions: 200 mrem/hr (max).
- External dose rate at any point 2 m from the outer lateral surfaces of the vehicle under normal conditions: 10 mrem/hr (max).
- External dose rate at any point 1 m from the outer lateral surfaces of the vehicle under hypothetical accident conditions: 1000 mrem/hr (max).
- The transportation package must not result in dose rates greater than 2.0 mrem/hr at occupied locations near the package during the transportation. Ends of the conveyance are considered the occupied locations.

B.5.1.2 Summary Table of Maximum Radiation Levels

The expected maximum dose rates (for NCT and HAC) from the MP197TAD TO package are provided in Table B.5-2. These evaluations were performed to determine the fuel assembly parameters of burnup, percent initial enrichment and cooling time that would result in decay heat and radiological sources that would meet the decay heat requirements (Chapter B.3), source terms for containment (Chapter B.4) and radiological sources that provide dose rates less than the current design basis fuel mentioned above and thus would be acceptable for transport in the MP197TAD TO package. Section B.5.2 describes these evaluations in more detail. The dose rate results shown in Table B.5-2 for NCT and HAC demonstrate that the MP197TAD TO package meets the relevant criteria for transportation.

B.5.2 Source Specification

There are five principal sources of radiation associated with transport of spent nuclear fuel that are of concern for radiation protection:

- Primary gamma radiation from spent fuel,
- Primary neutron radiation from spent fuel (both alpha-n reactions and spontaneous fission),
- Gamma radiation from activated fuel structural materials,

- Capture gamma radiation produced by attenuation of neutrons by shielding material of the cask, and
- Neutrons produced by sub-critical multiplication in fuel.

The MP197TAD TO package is designed to transport irradiated BWR fuel assemblies. The fuel assemblies acceptable for transport in the MP197TAD TO are described in Chapter B.1, Section B.1.2.2. The various fuel assembly designs were separated according to fuel assembly array, the maximum metric tons of uranium, and the number of fuel pins. These parameters are the significant contributors to the SAS2H/ORIGEN-S model. The largest uranium loading results in the largest source term at the design basis enrichment and burnup, thus the GE 7x7 is the bounding assembly type.

Assembly hardware information for all the various fuel assembly designs is not included in the SAR, (except for the design basis fuel assembly as shown in Table B.5-3) however, the MTU loading is the most important parameter from a source term calculation standpoint. The fuel assembly hardware for the GE 7x7 fuel assembly is bounding as it contains the maximum amount of steel and inconel than any other BWR fuel design.

Characteristics of the design basis BWR fuel assembly used in the source term analyses is described in Chapter B.1, Section B.1.2.3. The SAS2H/ORIGEN-S modules of the SCALE code are used to generate gamma and neutron source terms for the bounding GE 7x7 fuel assembly. Source terms were generated for initial enrichments ranging from 0.70 wt% to 5.00 wt% U235 and the fuel is irradiated using multiple cycles to achieve the desired burnup. Burnup values range from 6 GWD/MTU to 62 GWD/MTU using a specific radiation power between 7.0 MW/assembly and 14 MW/assembly. A conservative operating cycle history is utilized with a 73 day down time between cycles. Details of the analyses are given in Section B.5.2.5.

The source terms are generated for the fuel assembly (with channel) active fuel region, the plenum region, and the end fitting regions. The fuel assembly hardware materials and masses on a per assembly basis are listed in Table B.5-3. Table B.5-4 provides the material composition of fuel assembly hardware materials. Cobalt impurities are included in the SAS2H model.

The spent fuel payload consists of the TN44B DSC with BWR fuel assemblies with or without channels and is specified in Chapter B.1, Section B.1.2.3. The source term calculations for the DSC with the BWR fuel payload include the contribution from the channel while the shielding calculations do not take credit for them. This represents conservatism in the gamma dose rate calculations of approximately 15% (estimated based on the use of a 0.100″ zirconium alloy channel with a density of 6.50 g/cm^3) for fuel assemblies with channels (typically the most representative of all loaded BWR fuel assemblies).

The masses for the materials in the top end fitting, the plenum, and the bottom fitting regions are multiplied by 0.1, 0.2 and 0.15, respectively [4]. These factors are used to correct for the spatial and spectral changes of the neutron flux outside of the active fuel zone and are also shown in Table B.5-5. The material compositions of the fuel assembly hardware are included in the SAS2H/ORIGEN-S model on a per assembly basis.

Axial Source Distribution

Axial variation in the moderator density along the BWR fuel assembly was considered by including a volume averaged density for the moderator around the fuel pins. Axial variation of temperatures and moderator densities from reference [1] were used to calculate the volume average moderator density for use in the BWR source term models. The fuel assembly water temperature and volume averaged density used are 558 K and 0.4323 g/cm^3, respectively. The fuel channel water temperature and density are 552 K and 0.669 g/cm^3, respectively. Because temperature of moderator varies significantly in BWR fuel assembly along axial direction, different moderator densities are used in SAS2H\ORIGEN-S models when calculating radiological sources due to different axial exposure regions. The water is coolest near bottom of the fuel assembly and its temperature rises until it reaches the top of the fuel assembly. One can assume that water density is nearly the same inside and outside of the fuel channel at the bottom region of the fuel assembly. A water density of 0.743 g/cm^3 is used for the bottom region and a density of 0.264 g/cm^3 is used inside of the fuel channel near the plenum/top nozzle area. Channel water temperature at the bottom and top regions is 552 K and 558 K, respectively.

The *44GROUPNDF5* cross section library was used for the SAS2H/ORIGEN-S depletion calculations. This library contains data on approximately 300 nuclides from the ENDF/B-V data. It was designed to accommodate two windows in oxygen cross section spectrum, a window in the iron cross section, the Maxwellian peak in the thermal range and the 0.3-eV resonance in ^{239}Pu.

The peaking factors for both neutron and gamma sources as a function of active fuel height are also listed in Table B.5-6. These factors are directly applied to MCNP source input for the fuel region.

These factors are determined based on typical axial burnup distributions for BWR assemblies and based on typical axial water density distribution that occurs during core operation.

Using the base SAS2H/ORIGEN-S input for the 7x7 BWR, selected as the design basis assembly for this application, neutron and gamma source terms are generated for axial zones as a function of burnup and moderator density. This estimates both the non-linear behavior of the neutron source with burnup and the core operating moderator density effects on the actinide isotopic concentrations (neutron source). This axial distribution is conservative at high burnup because the burnup distribution will flatten out with increased burnup resulting in a reduction in the overall peaking factor.

The average values of the axial peaking distributions are also provided in Table B.5-6. For the gamma distribution, the average value is 1.0. However, for the neutron distribution, the average value of the distribution is 1.326. The average value of the axial neutron distribution may be interpreted as the ratio of the true total neutron source in an assembly to the neutron source calculated by SAS2H/ORIGEN-S for the same assembly average burnup. Therefore, to properly correct the magnitude of the neutron source, the neutron source per fuel assembly as reported in Table B.5-7 and Table B.5-8, is multiplied by 1.326.

Radial Source Distribution

As discussed in Section B.5.1.1, the dose rate calculation is performed using a single zone radial source distribution (fuel loading configuration). However, the radial source distribution can be described as an arrangement of three concentric rings of spent fuel assemblies comprising of 4, 20 and 20 assemblies in each of these rings. The position of the fuel assemblies within the TN44B basket is shown in Figure B.5-8 for Zones 1, 2 and 3. For the design basis shielding analysis, all 44 positions are occupied with fuel assemblies having the design basis shielding source. The methodology described for the fuel qualification, Section B.5.2.4, ensures that the shielding calculations performed with a uniform zone loading are bounding.

Normal and Accident Conditions

Normal condition calculations are performed with no degradation in the cask geometry or materials. The conservatisms include the reduction in the density of lead and the use of the neutron shielding material properties at their minimum tolerance band. Because the FQTs presented in Chapter B.2, Table B.1-4 and Table B.1-5, ensure that the most limiting NCT dose rates are below the acceptance limits with a 5% margin, it is expected that any set of acceptable BECT combination is sufficient for shielding evaluation.

It is expected that neutron shielding will be degraded at HAC. Therefore in order to determine the bounding source terms at HAC, it is desirable to utilize a bounding BECT combination where the contribution from the neutron sources to the total dose rates are maximized. Response functions developed to determine the BECT combinations for NCT are utilized to determine the above mentioned combinations. When the neutron shielding is lost or degraded, this bounding BECT combination will result in bounding HAC dose rate at one meter from the package.

For the NCT evaluations, the source that results in bounding gamma source is due to fuel assemblies with a burnup of 26 GWD/MTU, an enrichment of 1.9 wt. % U-235, and 6.5 years cooling time. Alternatively, the the source that results in bounding neutron source is due to fuel assemblies with a burnup of 62 GWD/MTU, an enrichment of 2.6 wt. % U-235, and 31.5 years cooling time. Evaluations with such sources result in similar maximum dose rate at two meters from side of impact limiters at NCT. The evaluation shows that 87 % of the total dose rate from the first source (26 GWD/MTU) is due to primary gamma radiation source. Also, the evaluation shows that for the second radiological source, 93% of the total dose rate is due to neutron radiation. Therefore, the second source (neutron) will be utilized for the MP197TAD TO bounding shielding evaluation at HAC. Further, to determine the surface dose rates for NCT, the maximum calculated gamma dose rate using the first source term and the maximum calculated neutron dose rate using the second source term will be employed for conservatism.

B.5.2.1 Gamma Source

The gamma source terms for the design basis spent fuel assemblies for NCT and HAC are provided in Table B.5-7 and Table B.5-8 respectively. Table B.5-7 presents the source terms for a GE 7x7 fuel assembly with an initial enrichment of 1.90 wt. % U-235, a burnup of 26 GWD/MTU, a cooling time of 6.5 years with a 0.100-inch zircalloy channel included in the source term calculation. Table B.5-8 presents the HAC source terms for a GE 7x7 fuel assembly

with an initial enrichment of 2.60 wt. % U-235, a burnup of 62 GWD/MTU, a cooling time of 31.5 years with a 0.100-inch zircalloy channel included in the source term calculation.

The gamma source spectra are presented in the 18-group structure consistent with the SCALE 27n-18γ cross section library. The conversion of the source spectra from the default ORIGEN-S energy grouping to the SCALE 27n-18γ energy grouping is performed directly through the ORIGEN-S code. The SAS2H/ORIGEN-S input file for this fuel assembly is provided in Section B.5.6.1.

The gamma source for the fuel assembly hardware is primarily from the activation of cobalt. This activation contributes primarily to SCALE Energy Groups 36 and 37. The gamma source for the plenum region, the top fitting region and the bottom fitting regions for fuel from the inner and outer zones is also provided in Table B.5-7 and Table B.5-8, respectively.

The spent fuel assemblies may contain irradiated fuel channels which also provide a gamma source. This gamma source contribution is already included in the fuel assembly source terms for conservatism.

An axial burnup profile has been developed as discussed in Section B.5.2. above. Table B.5-6 provides the axial gamma peaking factors that were utilized in the MCNP shielding model.

B.5.2.2 Neutron Source

The total neutron source for the design basis fuel assemblies under the irradiation/decay history described above in Section B.5.2 for the NCT and HAC are also shown in Table B.5-7 and Table B.5-8 respectively. To determine the NCT dose rate at 2m the neutron source term based on a cooling time of 5.4 years was conservatively employed instead of 6.5 years. Further, the HAC neutron source shown in Table B.5-8 was employed to determine the package surface dose rate to maximize the total dose rate for conservatism. The neutron source for the MCNP analyses was specified using the default Cm-244 energy spectrum.

The neutron source is not linearly dependent with burnup, and therefore calculations were performed to determine the axial neutron source distribution (Section 5.2.). The axial neutron peaking factors are also shown in Table B.5-6.

To conservatively account for subcritical multiplication inside the TN44B, the neutron source terms and the (n,γ) sources are multiplied by $1/(1-k_{eff})$. k_{eff} is the effective neutron multiplication factor determined using criticality codes that involved more detailed analysis and treatment of fuel region during criticality calculations. A $k_{eff} = 0.42$ is used for the bounding shielding evaluation.

B.5.2.3 Source Conversion Factors

The following equation defines how the absolute tallies are calculated:

$$\dot{D} = T \cdot S \cdot C_{BU}$$

Where,

$\dot{D}$ is the absolute dose rate in mrem/hr,
T is the MCNP tally result in mrem/hr per particle/sec,
S is the source strength in source particle/sec, and
C_{BU} is the axial burnup normalization constant.

In the above relationship the constants multiplied against the tally result, T, define the tally multiplier. Therefore, the tally conversion factor, C_T, is defined below.

$$C_T = S \cdot C_{BU}$$

The source strength must be scaled appropriately by the axial burnup normalization constant. For the axial profile the cumulative density of the burnup profile is 1.000 (Table B.5-6). This corresponds to the C_{BU} for the gamma source. The corresponding neutron C_{BU} is 1.326 (Section B.5.2, above).

Neutron Source Term

NCT:
C_T = 5.25E+07 neutron/sec/assy x 44 x 1.326 x 1/(1-0.42)
= 5.281E+9 neutron/sec

HAC:
C_T = 3.32E+08 neutron/sec/assy x 44 x 1.326 x 1/(1-0.42)
= 3.339E+10 neutron/sec

Gamma Source Term

NCT: (Note: source is 1.9% U-235, 26 GWD/MTU, 6.5 yrs cooled)
C_T = 1.320E+15 gamma/sec/assy x 44 x 1.0
= 5.809E+16 gamma/sec

HAC: (Note: conservatively used gamma source from Table B.5-7)
C_T = 1.595E+15 gamma/sec/assy x 44 x 1.0
= 7.018E+16 gamma/sec

B.5.2.4 Fuel Qualification

An evaluation was performed for fuel assembly BECT combinations that would result in normal conditions of transport dose rate at 2.0 meters from the transportation vehicle side not exceeding the applicable regulatory limit of 10.0 mrem/hr. The results are expressed in tabular format showing the minimum required cooling times as a function of enrichment and burnup. These tables are referred to as the FQTs for shielding evaluation or transportation FQTs. Note, that after the cooling times to meet 10.0 mrem/hr dose rate requirement were determined, they were rounded up to the nearest 1/2-year in the final transportation FQTs. For example 6.1 is rounded up to 6.5, 8.8 is rounded up to 9.0, etc. At the end, the cooling times in the final transportation FQTs actually stand for minimum required cooling time not to exceed 9.5 mrem/hr NCT dose rate at 2 meters from the package.

Due to shielding properties of the MP197TAD TO cask and concentration of the most of the radiological source strength in the in-core region, dose rate values along the cask side between ends of impact limiters are larger than dose rates at the same distances from ends of impact limiters, regardless of the fuel assembly types loaded, conditions of transport (NCT or HAC) and the orientation of the TN44B DSC. The results from the bounding shielding evaluation verify this assumption. Therefore, if dose rates along the side of the package at two meters from impact limiters comply with NCT dose rate restrictions specified at the end of Section B.5.1, dose rates at the same distance from the cask ends will also be compliant.

The transportation FQTs are, therefore, a set of acceptable combinations of burnup, enrichment, and cooling times such that the calculated NCT dose rates at two meters from the transport vehicle will not exceed the 10 mrem/hr regulatory limit within an adequate margin.

The TN44B DSC thermal heat load is 22.0 kW for transport. However, the cask/canister with this total heat load may produce dose rates around the MP197TAD TO cask that are unacceptable for transport. Therefore, the transportation FQT tables that have been generated are based only on transport dose rate requirements. Acceptable assemblies from the transport FQT tables will meet the decay heat requirements for transport. The decay heat equation (DHE) specified in Section B.5.2.6 can be utilized to determine the decay heat of the fuel assembly as a function of enrichment, burnup and cooling time. Further, this equation is employed to determine whether the fuel assembly with a given BECT combination is acceptable for loading from a decay heat standpoint.

B.5.2.5 Response Functions for Transportation and Transportation FQTs

The analyses for determination of parameters for radiological sources (and decay heat) were carried out using the SAS2H\ORIGEN-S depletion modules from the SCALE computer software. SAS2H\ORIGEN-S computer simulations were performed for various BECT combinations. Radiological sources from SAS2H\ORIGEN-S models of GE 7x7 assembly are bounding for radiological sources relative to other BWR assemblies. These sources along with response functions were employed for generating transportation FQTs.

For all the SAS2H calculations the 44 group ENDF/B-V (44groupndf5 for source term calculations) and the 27 group burnuplib (for FQT and decay heat calculations) cross-section library from SCALE4.4 was used. MCNP calculations used the default cross section libraries.

A response function is created by utilizing the basic MCNP cask/canister model with a known source term and spectra. The primary gamma response function is energy group specific and is based on a reduced set of gamma energy groups (the groups that contribute the majority of the dose) while the neutron and secondary gamma response function is scalar. Since a default spectrum is employed to calculate the neutron dose rates in the shielding analysis models, the response function calculations for neutron and secondary gamma radiation are also performed with the same spectrum thereby eliminating the need for multi-group calculations. Utilizing a unit particle (gamma or neutron), the dose rate at the axial center of the cask, at two meters from the transport vechicle is calculated by MCNP for each energy group utilized. Thus, a response function (the dose rate per unit source – mrem/hour per particle/sec, a source-to-dose scaling factor) is created for each gamma and neutron energy group evaluated. The source terms created by SAS2H can then be multiplied by the response function to estimate the 2 meter dose rate. The

main difference in the response function evaluation (model) and the regulatory MCNP shielding evaluation is the reduced number of energy groups used in the response function model.

The basic MCNP models (gamma and neutron) for NCT were utilized to calculate response functions at 2 meters from the transportation vehicle. The MCNP model specification regarding axial burn-up profile variation along the in-core axial region of fuel, corrections to source strengths due to the burn-up profile variation, and treatment of neutron subcritical multiplication are described in Section B.5.3.1 below.

Considerations and a specification of cylindrical (with "angular-axial" segmentation) mesh tallies set up along side of the cask between ends of impact limiters at 2 meters radial distance from surface of impact limiters provided in Section B.5.3.1.2 is applicable. Fine axial and angular segmentation segments are used. Size (*axial length* × *arc length*) of the cylindrical mesh tally grid segments is approximately 21x21 cm over the cask side between impact limiters and over impact limiters.

Although the design basis dose rate evaluation for transport assumes only a single zone containing 44 assemblies, in the response function MCNP model the fuel assemblies are grouped by three concentric radial zones in a description of the radiological sources. These zones are shown in Figure B.5-8. The inner zone encompasses fuel assemblies in the 4 central compartments of the TN44B DSC. The intermediate zone and the outer or peripheral zone each contain 20 fuel assemblies. Such a definition of response functions provides flexibility in increasing the overall radiation and thermal capacity of the system. Results indicate that more than 80% of the radial dose rates around the cask are due to fuel assemblies in outer radial zone. Therefore, it would be possible to increase the source terms for the fuel assemblies located in the inner and intermediate zones and still not significantly increase the overall dose rate distribution around the cask due to self-shielding provided by the surrounding assemblies.

The source terms for primary gamma, response functions are generated for the following energy groups:

- Group 32: 1.00E+00 – 1.33E00 MeV,
- Group 31: 1.33E+00 – 1.66E00 MeV,
- Group 29: 2.00E+00 – 2.50E00 MeV,
- Group 28: 2.50E+00 – 3.00E00 MeV.

This is done because these four energy groups account for a majority of the dose (greater than 90%) associated with the gamma radiation from the spent fuel.

Response functions are calculated with MCNP for the TN44B DSC/ cask shielding configuration. The response functions are essentially source to dose conversion factors as a function of energy, (for gamma). The "conversion factors" corresponding to neutron radiation source are multiplied by "adjustment" factors to account for the axial burn-up profile of the fuel and neutrons subcritical multiplication to obtain the response functions that are used for the fuel

qualification evaluation. The axial burn-up profile utilized in the fuel qualification analysis is the same as in the bounding shielding evaluation (Table B.5-6). For neutrons and associated (n,γ) radiation, since a bounding energy spectrum is used, the response function calculated is just a total source to dose factor. A verification calculation was performed with an MCNP to determine the fidelity of the dose rate distribution calculated by the response functions. This verification calculation utilized the same demonstration sources. The demonstration sources are treated in the explicit MCNP calculations in the same manner as in the models used for the bounding shielding evaluation described in Section B.5.3. The dose rates predicted with response functions and those calculated with the explicit MCNP calculations at the location of interest are in agreement within an acceptable ±10% uncertainty, consistent with MCNP methodology for MCNP calculations uncertainty, 10%.

After verification of the response functions, qualification of assemblies for the transportation purpose was performed. Multiple SAS2H analyses were performed to determine gamma and neutron radiation source terms as a function of burn-up, enrichment and cooling time. The gamma source was obtained as a function of energy for the four important energy groups. The radiological sources are determined using SAS2H\ORIGEN-S models of design basis BWR assemblies described in the previous sections of this chapter. Two meter radial primary gamma dose rates were estimated/calculated by multiplying the individual energy group MCNP generated response function and the appropriate SAS2H gamma energy source and performing a summation over all the energy groups. Since a bounding energy spectrum was used for the neutrons, the neutron and secondary gamma dose rates were calculated by multiplying the neutron response function and the total SAS2H neutron source and the secondary gamma response function and the neutron source. Moreover, the response function as a function of azimuthal angle was employed to determine a dose rate "map" around the cask containing the TN44B DSC. Therefore, for each set of source terms (one BECT combination), a dose rate map is estimated at a distance of 2 meters from the radial surface of the MP197TAD TO transportation package. The dose rates at the axial ends were not estimated using this approach since the bounding dose rates are not expected in the vicinity of the axial ends of the package. An iterative approach is used for finding suitable cooling times for every FQT burn-up and enrichment. Calculation of radiological sources using SAS2H\ORIGEN-S is repeated until cooling time corresponding to radiological source resulting in dose rate less than 9.5 mrem/hr at two meters radial distance from side of impact limiters is identified. This ensures that differences between the dose rates predicted by the response function and explicitly calculated by MCNP are minimized.

There are multiple options for an arrangement of assemblies in the TN44B DSC fuel compartments to satisfy decay heat load restriction per assembly or canister and 10CFR71 dose rate requirements. There are unlimited variations on how to achieve this. The same additional cooling time can be imposed to all the assemblies in all zones or different cooling times can be added to assemblies in different or the same zones.

Because there are radiological sources at some burnup, enrichment and cooling times (BECTs) that result in dose rates at the location of interest less than 9.5 mrem/hr, it is reasonable to consider zoning options for an arrangement of radiological sources. A three-zone configuration depicted on Figure B.5-8, consistent with the response function calculations was utilized. The simplest arrangement would be to consider a uniform source in the two inner zones with a higher

heat load (maximum fuel assembly heat load of 0.48 kW or 0.54 kW) and determine the minimum required cooling time as a function of burnup and enrichment for the outer zone. The response function results shown in Table B.5-9 are utilized to determine the FQT for the outer zone and to ensure that the resulting total dose rate remains below 9.5 mrem/hour.

The fuel qualification for Zone 3 (the outer zone) is shown in Table B.1-4, which shows the minimum required cooling time as a function of initial enrichment and burnup. The fuel qualification for Zones 1 and 2 is straightforward – in most cases, fuel assemblies with a burnup, enrichment and cooling time that result in a decay heat less than or equal to 0.54 kW per assembly are qualified. The decay heat is calculated using the decay heat equation shown in Section 5.2.6 below. However, if the enrichment and burnup combinations for Zones 1 and 2 fall within the shaded region of the FQT (Table B.1-4, Part 2), the maximum decay heat for Zone 1 and Zone 2 fuel assemblies is restricted to 0.48 kW per fuel assembly. This qualification of fuel assemblies for Zones 1 and 2 is summarized in Table B.1-5. Further, the minimum cooling time in all the three zones is restricted to 6 years in these FQTs for conservatism.

As described above, the TN44B DSC will be loaded using a three zone loading configuration with the hotter source in the inner zones (24 fuel assemblies) and a colder source in the outer zone (20 fuel assemblies). The design basis radiological source terms for shielding and the shielding calculations are performed using an equivalent (if not bounding) source uniformly in all the 44 fuel assembly locations. The following reasoning is employed to provide a comparison of the allowable NCT and HAC BECT combinations (radioactive source terms) for the three-zone loading configuration and the actual BECT combinations employed in the source term and shielding calculations.

The NCT design basis calculations are performed using a uniform single zone loading configuration as shown below:

- a burnup of 26 GWD/MTU, an initial enrichment of 1.9 wt. % U-235 and a cooling time of 6.5 years for design basis calculations
- a burnup of 62 GWD/MTU, an initial enrichment of 2.6 wt. % U-235 and a cooling time of 31.5 years for package surface dose rate calculations for neutron radiation

For a configuration with three radial zones for NCT, the following are the allowable BECT combinations that are essentially equivalent to the uniform source used in the calculation.

- a burnup of 26 GWD/MTU, an initial enrichment of 1.9 wt. % U-235 and a cooling time of 6 years in the two inner zones
- a burnup of 26 GWD/MTU, an initial enrichment of 1.9 wt. % U-235 and a cooling time of 8 years for the outer zone

The cooling time in the peripheral zone employed in the design basis shielding calculations is 6.5 years, while the allowable cooling time in the peripheral zone is 8.0 years. Therefore, the gamma dose rates from the design basis shielding calculations will be bounding. Moreover, a

larger neutron source term is employed to determine the package surface dose rates. Therefore, for NCT, the use of an equivalent (if not bounding), single zone radial source distribution is reasonable.

The HAC design basis calculations are performed using an equivalent uniform single zone loading configuration as shown below:

- a burnup of 62 GWD/MTU, an initial enrichment of 2.6 wt. % U-235 and a cooling time of 31.5 years for design basis calculations

For a configuration with three radial zones for HAC, the following are the allowable BECT combinations that are essentially equivalent to the uniform source used in the calculation:

- a burnup of 62 GWD/MTU, an initial enrichment of 2.6 wt. % U-235 and a cooling time of 14.5 years (using the decay heat equation) in the two inner zones
- a burnup of 62 GWD/MTU, an initial enrichment of 2.6 wt. % U-235 and a cooling time of 44.5 years for the outer zone

The cooling time in the peripheral zone employed in the design basis shielding calculations is 31.5 years, while the allowable cooling time in the peripheral zone is 44.5 years. Even though the neutron source terms are not very sensitive to cooling time at cooling times greater than 25 years, the source term employed in the design basis HAC calculations are comparable to those that are allowable for the TN44B DSC. Sensitivity calculations performed to compare these source terms also demonstrate that these sources result in similar dose rates (within 1%).

In summary, the response function methodology was employed to determine the FQT for a three zone loading configuration for shielding (actually two distinct zones). The design basis source terms employed to determine the dose rates on and around the MP197TAD TO transportation package result in bounding dose rates.

B.5.2.6 BWR Decay Heat Equation

From the numerous SAS2H evaluations performed for the FQTs discussed above, a non linear regression analysis was performed to obtain a fit of the BWR decay heat data as a function of burnup, enrichment and cooling time. A very good fit was obtained based on an iterative evaluation using a 9-parameter model. The functional form is expressed below:

The decay heat (DH) in watts is expressed as:

$$\mathbf{F1 = A + B*X1 + C*X2 + D*X1^2 + E*X1*X2 + F*X2^2}$$
$$\mathbf{DH = F1*Exp(\{[1-(1.2/X3)]*G\}*[(X3-4.5)^H]*[(X2/X1)^I]) + 16}$$

where,

F1	Intermediate function
X1	Assembly burnup in GWD/MTU
X2	Initial enrichment in wt. % U-235
X3	Cooling time in years

A	-59.1
B	23.4
C	-21.1
D	0.280
E	-3.52
F	12.4
G	-0.720
H	0.157
I	-0.132

The calculation uncertainty is 16 watts. It is added to the equation above as the last term. The actual calculational uncertainty is approximately 10 watts. An additional uncertainty of 6 watts is added for conservatism. The minimum cooling time for decay heat calculation is 5 years.

B.5.3 Shielding Model

The design basis shielding calculations are performed using the 3-D Monte Carlo transport code, MCNP. As explained earlier, the determination of the FQT ensures that the dose rate obtained using any set of source terms (due to use of acceptable combinations of burnup, enrichment and cooling time) is within acceptable limits. This section provides details of the geometry, material and source term configurations employed in the calculational shielding models to determine the dose rates.

B.5.3.1 Configuration of Sources and Shielding

B.5.3.1.1. Source Configuration

A detailed description of the source term calculations and the fuel qualification methodology employed to determine the design basis source terms for shielding is provided in Section B.5.2.

The source terms – shown in Table B.5-7 and Table B.5-8 for the NCT and HAC are utilized in the shielding calculations. For dose rate calculations around the MP197TAD TO, the source is divided into four separate regions: fuel, plenum, top end fitting, and bottom end fitting. The model is utilized in two separate computer runs consisting of contributions from the following sources:

- Primary gamma radiation from the active fuel and from activated hardware within the top end fitting, plenum region and bottom end fitting (axial and radial directions).
- Neutron radiation from the active fuel region and secondary gamma radiation from neutron interactions.

The sources in the active fuel region (gamma and neutron) are modeled as uniform radially but vary axially. The sources in the structural hardware regions (plenum, top end fitting, and bottom end fitting) are modeled as uniform both radially and axially. The results from the individual runs are combined to provide the total gamma, neutron and total dose for the package.

B.5.3.1.2. Shielding Configuration

Normal Condition of Transport

Two base models were constructed. The first model corresponds to the neutron transport problem and the second is the gamma. Variance reduction was accomplished by means of importance zoning. The importance function was created to balance the particles (per volume) throughout the problem geometry.

One shielding configuration is used for the NCT configuration. The model is a complete three dimensional representation of the MP197TAD TO transportation package. The MP197TAD TO, the TN44B DSC and its contents are modeled with a discrete representation of the basket and fuel structure. Each fuel assembly is divided into four axial zones. The bottom zone represents the lower end fittings, the middle zone the active fuel region and the upper zones represent the plenum and upper end fittings, respectively. The axial locations of the plenum and the end fittings of the fuel assembly are similar to those provided in Reference [8]. The modeled active fuel length is 144 inches and the plenum length is 12.93 inches. The modeled bottom end fitting and top end fitting lengths are 6.65 inches and 12.62 inches, respectively. The fuel, end fittings and plenum are homogenized within the each assembly envelope and the axial length of their respective zones.

The basket structure is modeled as a grid of steel, aluminum and neutron poison panels. The neutron poison material is modeled as borated stainless steel. There are solid aluminum transition rails at the 0°, 90°, 180° and 270° peripheral locations of the basket. Therefore, the cells outside of the fuel cells at these locations are modeled as solid aluminum. All other cells outside the fuel cells have some aluminum components. However, for conservative reasons these cells are modeled as air.

Screenshots of the MCNP models generated by MCNP geometry plotter are shown on Figures B.5-2 through B.5-7. Origin of MCNP coordinate system is on canister axis and positioned at the center of the fuel assemblies' active, in-core region. "Z" axis coincides with the canister/TO axis

and is directed from DSC bottom to top (from front to rear of the cask). "ZX" and "ZY" plane passes through the axis of the transport cask trunnions and shear key, respectively.

The borated neutron shielding material (VYAL-B) is a vinylester resin mixed with aluminum hydrate and zinc borate which are added for their fire retardant properties. Minimal VYAL-B elemental weight fractions after manufacturing as well as composition after continuous exposure to heat at different temperatures and durations of exposure are given in Table B.5-10. Conservatively, shielding properties of the mixture, aged under high temperature VYAL-B chemical composition are used. The VYAL-B used, after 1 year exposure at 134 degrees Celsius, has a hydrogen concentration of 4.54% and density of 1.743 g/cc. The neutron shielding material is embedded into 0.12" thick aluminum boxes. There are 60 such boxes around the side of the cask perimeter between impact limiters. Sides of the boxes adjacent to 2.50" thick cask Outer Shell and 0.375" Shield Shell are modeled as 0.125" thick aluminum cylindrical shells. The other two sides of the aluminum boxes are homogenized with the neutron shielding material. Mass of the homogenized aluminum is 0.753 kg.

Steel trunnion plugs are utilized to replace the top (lifting) trunnions which are removed for transport. However, the NCT and HAC MCNP models conservatively assume that the trunnion plugs are not attached to the cask.

Conservatism is also extended to the modeling of lead gamma shielding under NCT. The lead gamma shield is modeled with a density equal to 98.5% of theoretical density to account for uncertainties in the uniformity of lead pouring and fabrication. The lead slump as a result of HAC is calculated to be 0.465″ in Chapter B.2, Appendix B.2.13.3. Therefore, for both NCT and HAC, the lead gamma shell is modeled with a 0.465″ slumped region (modeled as air) at the axial ends of the cask.

Geometry of the grapple ring cut-out on the cask bottom and shear key cut out on the side in MCNP models are shown on sketches of Figure B.5-6 and Figure B.5-7. The shear key cut-out is closed with a steel shear key plug when the cask is on a transportation platform. However, before the cask is placed on a horizontal position and secured on the platform, the shear key cut-out is closed with a plug made with the same neutron shielding material as that on the cask side.

The cask is secured in a horizontal position on a skid attached to a railcar or other trailer with a deck or floor during transportation. However the cask and its content are modeled as a stand alone entity, without any surroundings in computational models for bounding shielding evaluation. Therefore, the effect of transportation equipment on dose rate distributions below the cask (which can be especially important for the close, less than 2 meters distances) is conservatively not accounted for in the current analysis.

The impact limiters are modeled as wood surrounded by a 0.25 in. thick steel shell. The interior steel gussets are conservatively neglected. The wood is modeled using both balsa and redwood, as shown in drawings (Chapter B.1, Section B.1.3.1). All other geometry features of the MP197TAD TO are modeled using the appropriate materials and dimensions shown in the drawings in Chapter B.1, Section B1.3.1.

Voids are neglected within the fuel assembly. The voids within the cask cavity are modeled.

Hypothetical Accident Conditions

For the HAC models, the wood inside the impact limiters are assumed to be absent. The neutron shielding resin is modeled with a density of 25% of the original 1.743 g/cm^3 utilized in the NCT models. The HAC models utilize the HAC neutron and gamma source terms in place of the NCT source terms in all other aspects the HAC models are identical to the NCT models. Other modeling features like trunnion plugs and lead slump that are specifically applicable for HAC have been described and conservatively applied to NCT models.

B.5.3.2 Material Properties

For the MCNP model, four source areas, shown in Figure B.5-3, are utilized: fuel zone, plenum, top and bottom end fitting. The sources are uniformly homogenized over the cross section and the appropriate zone length. The fuel basket is discreetly represented by the stainless steel, borated stainless steel and aluminum plates that bound the fuel assemblies.

The radial resin and aluminum boxes are homogenized into a single composition based on the mass of each component. Measured dose rates around the TN-24P [7], the TN-40, and the TN-32 casks have shown no streaming effects because of the aluminum boxes. This is because the neutrons will not generally travel in a direct path, but scatter, such that the majority of the neutrons will not be able to travel through the aluminum box wall for the full 6.25 inches of resin box thickness. The materials input for the MCNP model is listed in Table B.5-11 and Table B.5-12.

For the HAC models, the wood inside the impact limiters is assumed to be absent. The neutron shielding resin is modeled with a density of 25% of the original 1.743 g/cm^3 utilized in the NCT models. The structural evaluations documented in Chapter B.2 demonstrate that the neutron shielding shell remains intact and the cask geometry is maintained during hypothetical accidents. In order to bound (conservatively) the consequences of a design basis fire, 75% of the neutron shielding capability is assumed to be lost. Apart from these two modeling considerations, there is no difference between NCTand HAC models from a material property standpoint. The lead gamma shield for both NCT and HAC is modeled with a density that is 98.5 % of theoretical density.

B.5.4 Shielding Evaluation

Dose rates around the MP197TAD TO package are determined by choosing the most conservative (all allowable source terms are expected to result in equivalent source strength) source and using it within a three dimensional MCNP model. Dose rates were calculated both axially and radially outside the cask. Further, dose rates were also calculated at several angular intervals around the cask to ensure that the location of maximum dose rates is determined accurately. Several mesh tallies were used to accomplish this. All tallies are volume flux (F4) tallies and are converted into dose rates using energy dependent dose conversion factors listed in Tables B.5-13 [6] for gamma and Table B.5-14 [6] for neutron radiation. The tallies are further scaled by the source conversion factors described in Section B.5.2.4. The tally locations were chosen to best evaluate the external dose rate requirements of 10 CFR 71.47(b). Tally segmentation was used to analyze the surface dose rates for any spatial peaking. This was done axially, radially and azimuthally. The segment dimensions were typically 30 cm. Note that dose

rates were calculated at several locations from the ends of the cask to assess hypothetical occupational exposure at all locations as a function of railcar length. The MCNP shielding evaluation does not account for subcritical neutron multiplication. A conservative k_{eff} value of 0.42 was employed to calculate the subcritical neutron multiplication. Therefore, a factor of 1.72 (1/(1-0.42)) was utilized to further scale the neutron and secondary gamma tallies to account for subcritical neutron multiplication.

B.5.4.1 Methods

The source term and decay heat calculations are performed using the SAS2H/ORIGEN-S modules with the 44-group ENDF/B-V cross section library from the SCALE [1] computer code system. These modules are based on a one-dimensional representation of the fuel assembly/lattice and are generally accurate for the purpose of calculation of decay heat and source terms. These methods have been utilized extensively in the calculation of source terms.

The shielding calculations are performed using the three dimensional Monte Carlo code, MCNP5 [5] (with the continuous energy cross section based on ENDF/B-VI) is a general-purpose Monte Carlo N-Particle code that can be used for neutron, photon, electron, or coupled neutron/photon/electron transport. The code treats an arbitrary three-dimensional configuration of materials in geometric cells bounded by first- and second-degree surfaces and some special fourth-degree surfaces. Pointwise (continuous energy) cross-section data are used. For neutrons, all reactions given in a particular cross-section evaluation are accounted for in the cross section set. For photons, the code takes account of incoherent and coherent scattering, the possibility of fluorescent emission after photoelectric absorption, absorption in pair production with local emission of annihilation radiation, and bremsstrahlung. Important standard features that make MCNP5 very versatile and easy to use include a powerful general source; an extensive collection of cross-section data; and an extensive collection of variance reduction techniques that can be employed to track particles through very complex deep penetration problems. MCNP5 was employed to take advantage of its mesh tallies capabilities in calculating dose rates distributed over the surface of the MP197TAD TO package.

Upper energy limit for detailed photon physics treatment during MCNP calculation is set to 20.0 MeV. Photons with energy less than 0.001 MeV are cut off. This covers energy spectrum from the fuel assemblies in storage or qualified for transportation. Physics photon treatment accounts for coherent scattering and Doppler energy broadening. It does not account for bremmstrahlung and photonuclear collisions photons because dose rates are negligible from gamma radiation sources at energy less than 0.8 MeV and greater than 5.0 MeV, respectively.

MCNP default parameters for neutron transport physics are used: no lower cut off or upper limit for the neutron source energy; neutrons are treated with implicit capture, no delayed neutrons since the fission is turned off by using ***nonu*** card in MCNP input decks for neutron transport and the subcritical multiplication factor discussed in Section B.5.2.2.

Geometry splitting is used as a variance reduction technique to the extent practical. The idea behind using a variance reduction technique is to keep population of radiation particles constant while they are spreading away from the source region and\or disappear throughout absorption in shielding materials surrounding the source. The normal technique for geometry splitting variance reduction is to set the thickness of the splitting regions to about (or less than) a mean free path of

radiation particles when they reach that region. Splitting rate is set to 2 in MCNP models which means each particle is split by 2 when moving from lower to higher "importance" splitting region. The splitting occurs when crossing an interface between the adjacent regions.

Bounding dose rates are computed at various distances from MP197TAD TO transportation package. Mesh tallies calculate neutron, primary and secondary gamma radiation dose rate distributions at various distances from side and ends of the impact limiters (ILs). Cylindrical and rectangular mesh types are used.

Locations of mesh nodes are defined either in cylindrical or rectangular Cartesian coordinate systems. Z-axis of the rectangular coordinate system is along the cask axis. X-axis is on an imaginary plane through the cask axis and trunnions. It is perpendicular to the cask axis. XZ plane is a horizontal plane and Y axis runs in vertical elevation when the cask is on a transportation position. Rectangular (X-Y) mesh tallies are used to calculate spatial distributions at distances less than or equal to two meters from the cask ends. Size of the mesh unit segment is 30x30 cm. The central node of the grid is symmetric around the cask axis. The mesh grid extends up to 12 feet from the cask axis in X and Y directions.

The cylindrical (angular-axial) mesh is used for determining dose rate distribution along the cask side between ends of impact limiters, at various radial distances from the cask side. Because the dose rate around the cask is the highest along the cask side, the cylindrical (angular-axial) mesh tally along the side of the cask between ends of impact limiters was also employed for determining response functions used for fuel assemblies qualification for transportation purpose. The Z axis of the cylindrical coordinate system coincides with the cask axis. The axial coordinates of the mesh nodes are measured from end of the bottom impact limiter. Angular coordinate is measured in counter-clockwise rotations from an imaginary plane through the cask axis and the shear key, which is YZ plane in the rectangular coordinate system. For the dose rates at less than or equal to two meters from the cask side, segmentation of the angular coordinate is performed to keep an arc length a cylindrical grid constant, about 30 cm.

Because of the shear key cut-out on the cask side, the shielding properties on the cask against gamma and neutron radiation vary significantly. The transport cask shear key is oriented towards the ground when in the transport configuration and has a steel insert in place. The radiation streaming through the shear key cut-out of the neutron shielding on side of the cask will be within a solid angle not encompassing the accessible area near the transportation package. Therefore, the maximum dose rates determined with cylindrical mesh tallies around the cask side and reported in this chapter are at angular coordinates not encompassing the shear key. The maximum dose rates for HAC are determined regardless of orientation and includes the shear key location, which was not considered for the NCT models.

Mesh tallies are also used for calculating dose rates distributions at "large" distances. The large distances are 2.7, 4.3, 5.8, 7.3, 8.8, 10.4 and 11.9 meters measured from side and ends of the impact limiters at NCT. Note that "long distances" from ends of impact limiters correspond to edges of 40, 50, 60, 70, 80, 90 and 100 feet long "platform" for transportation of the cask. Dose rates at these distances are calculated to assure that the applicable regulatory limit for the normall occupied space of 2 mrem/hr is met. The axial dose rates at 2m from surface of the package are

below the regulatory limits and therefore, the results obtained from these calculations and distances greater than 2m are not reported.

The statistical uncertainties associated with the MCNP calculations are generally less than 5% for the majority of tallies except for some accident calculation tallies. For the accident the gamma dose rates have the highest relative error of approximately 10%. The statistical uncertainties associated with the neutron and gamma dose rates on the top and bottom impact limiter surfaces are high, but since the dose rates are very low (less than 0.1 mrem/hr) this is judged acceptable.

B.5.4.2 Input Data

The source terms input to the MCNP models are provided in Table B.5-7 and Table B.5-8. The material densities input to the MCNP models are provided in Table B.5-11 and Table B.5-12.

An example MCNP input file employed in the primary gamma dose rate calculation is listed in Section B.5.6.2.

B.5.4.3 Flux-to-Dose-Rate Conversion

The flux distribution calculated by the MCNP code is converted to dose rates using flux-to-dose rate conversion factors from ANSI/ANS-6.1.1-1977 [6] given in Table B.5-13 for gammas and Table B.5-14 for neutrons.

B.5.4.4 External Radiation Levels

The dose rate results from the shielding calculation are shown in Table B.5-2 and Table B.5-15 through B.5-17 for NCT models. The side (radial) dose rates (Table B.5-15) are shown as a function of distance from the cask body, and from the impact limiter OD. Axial dose rates are shown as a function of the distance from the top and bottom impact limiter surfaces in Table B.5-2. These results demonstrate that the maximum side surface dose rate ("the" maximum dose rate) under normal conditions is below 200 mrem/hour. The results of the dose rate calculations along the side surface, 1 m, and at 2 m from the side surface are shown in Figure B.5-9. These curves represent the maximum dose rate distribution on and around the MP197TAD TO. As discussed earlier, mesh tallies were employed to determine the three-dimensional dose rate distribution. The limiting NCT dose rates for comparison to applicable limits are shown in Table B.5-2.

The typical limiting dose rate requirement is 10 mrem/hr at 2 meters from the edge, (vertical plane), of the transport vehicle. A typical transport vehicle is approximately 10 ft in width which is approximately the OD of the MP197TAD TO impact limiter. Therefore, the calculated MCNP dose rate at 2 meters from the impact limiter OD is required to be less than the 10CFR71 regulatory limit of 10 mrem/hr. The results of the NCT calculations demonstrates that the maximum calculated dose rate for the most limiting configuration is less than the regulatory limit of 10 mrem/hour with sufficient margin – at least 5%.

Dose rate calculations for the normally occupied position at 2m from the axial ends of the MP197TAD TO package demonstrate that the maximum dose rate will be below the limit of 2 mrem/hour at 2m from the surface of the package.

The results from the HAC model calculations indicate that the maximum dose rate at a distance of 1m from the package surface is 380 mrem/hour. The limiting accident condition dose rates for comparison to applicable limits are shown in Table B.5-2.

In general, the NCT dose rates are dominated by the gamma source term. The results indicate that typically the total dose rates are comprised of 88% gamma. As expected, the accident dose rates are produced mostly from the neutron (≈85%) source due to loss of neutron shielding material and impact limiter.

B.5.5 References

1. SCALE 4.4, "Modular Code System for Performing Standardized Computer Analyses for Licensing Evaluation for Workstations and Personal Computers," CCC-545, ORNL.
2. ORNL/TM-11018, "Standard- and Extended-Burnup PWR and BWR Reactor Models for the ORIGEN2 Computer Code," Oak Ridge National Laboratory, December 1989.
3. NUREG/CR-6801 (ORNL/TM-2001/273), March 2003, "Recommendations for Addressing Axial Burnup in PWR Burnup Credit Analyses."
4. Luksic, "Spent Fuel Assembly Hardware: Characterization and 10 CFR 61 Classification for Waste Disposal," PNL-6906, UC-85, June 1989.
5. MCNP – A General Monte Carlo N-Particle Transport Code, Version 5, Volume I: Overview and Theory, LA-UR-03-0245, 2003, Volume II: User's Guide, LA-CP-03-0245, 2003.
6. "American National Standard for Calculation and Measurement of Direct and Scattered Gamma Radiation from LWR Nuclear Power Plants," ANSI/ANS-6.1.1-1977, American Nuclear Society, Illinois, 1977.
7. EPRI-NP-5128, "The TN-24P PWR Spent-Fuel Storage Cask: Testing and Analyses," prepared by Pacific Northwest Laboratory, Virginia Power Company and EG&G Idaho National Engineering Laboratory, April 1987.
8. DOE/ET/47912-3 Vol. III, "Domestic Light Water Reactor Fuel Design Evolution," Prepared for U. S. Department of Energy Savannah River Operations Office, September 1981.

B.5.6 Appendices

The information on pages
B.5-21 through B.5-52 is
Proprietary Information Withheld
Pursuant to 10 CFR 2.390

Table B.5-1
MP197TAD TO Cask Shield Materials

Component	Material	Density (g/cm^3)	Thickness (inches)
Canister Shell	Stainless Steel	7.92	0.75
Cask Inner Shell	Stainless Steel	7.92	1.25
Cask Gamma Shield	Lead	11.34[2]	2.25
Cask Outer Shell	Stainless Steel	7.92	2.50
Canister Top	Stainless Steel	7.92	10.25
Cask Lid (Top)	Stainless Steel	7.92	4.50
Canister Bottom	Stainless Steel	7.92	6.50
Cask Bottom	Stainless Steel	7.92	6.50
Resin [1]	Polyester Resin	1.75	6.25
	Styrene		
	Aluminum Hydrate		
	Zinc Borate		
Aluminum Box	Aluminum	2.7	0.12
Outer Shell	Stainless Steel	7.92	0.375
Basket	Stainless Steel (fuel compartment)	7.92	0.45
	Aluminum	2.70	0.45
	Neutron Poison – Borated Stainless Steel	7.90	0.45
Impact Limiter	Stainless Steel	7.92	0.25
	Redwood	0.387	16.0[3]
	Balsa Wood	0.125	16.0[3]

Notes:

[1] The neutron shielding is borated polyester resin compound with a density of 1.75 g/cc. The four major constituents are listed in the table.

[2] A density of 11.17 (98.5 % of theoretical density) was employed in the shielding calculation models.

[3] Thickness of wood is variable.

Table B.5-2
Summary of MP197TAD TO Dose Rates
(Exclusive Use Package for Transportation)

Normal Conditions Of Transport	Vehicle Edge[1] mSv/h (mrem/h)			2 Meter from Vehicle mSv/h (mrem/h)		
Radiation	**Top**	**Side[2]**	**Bottom**	**Top**	**Side**	**Bottom**
Gamma	0.006 (0.6)	0.34 (34)	0.073 (7.3)	0.002 (0.20)	0.077 (7.7)	0.011 (1.1)
Neutron	0.001 (0.1)	0.64 (64)[3]	0.0073 (0.73)	0.0004 (0.04)	0.011 (1.1)	0.0017 (0.17)
Total	0.007 (0.7)	0.98 (98)	0.081 (8.1)	0.0024 (0.24)	0.088 (8.8)	0.013 (1.3)
Limit	10 (1000)	10 (1000)	10 (1000)	0.1 (10)	0.1 (10)	0.1 (10)

(1) Conservatively assumed to be coincident with the impact limiter outer surface, except for the region between the impact limiters, where it is assumed to be coincident with the cask body.
(2) Maximum gamma and neutron dose rate.
(3) Maximum neutron dose rate calculated using the HAC source term.

Hypothetical Accident Conditions[4]	1 Meter from Package Surface mSv/h (mrem/h)		
Radiation	**Top**	**Side**	**Bottom**
Gamma	0.008 (0.80)	0.68 (68)	0.038 (3.8)
Neutron	0.049 (4.9)	3.13 (313)	0.20 (20)
Total	0.057 (5.7)	3.8 (380)	0.24 (24)
Limit	10 (1000)	10 (1000)	10 (1000)

(4) The neutron shield is partially credited and the impact limiters are removed.

Table B.5-3
BWR Fuel Assembly Material Mass

Hardware Item	Material	Average Mass, (kg/FA)	Comments
In-core Zone, (144.00 inch long, **4.73** g/FA total cobalt content)			
Cladding	Zircaloy-2	49.2	
Fuel channel sleeve	Zircaloy-4	37.1	
Grid spacers	Zircaloy-4	1.95	7 spacers*~0.28 kg/spacer
Spacer springs	Inconel X-750	0.36	7 springs*0.051 kg/spring
Channel spring & bolt	Inconel X-750	0.13	
Channel fastener guard	Stainless Steel	0.46	
Channel spacer & rivet	Stainless Steel	0.13	
Fuel	Uranium	198	wt. of UO_2=224.643 kg.=0.198 mtu/0.8814
Gas Plenum Zone, (12.93 inch long, **0.89** g/FA total cobalt content)			
Cladding	Zircaloy-2	4.89	
Fuel channel	Zircaloy-4	0.00	
Plenum springs	Stainless Steel	1.05	
Top End Fitting Zone, (12.62 inch long, **4.51** g/FA total cobalt content)			
Upper tie plate	Stainless Steel	2.08	
Lock tab washers & nuts	Stainless Steel	0.05	
Expansion springs	Inconel X-750	0.43	
End plugs	Zircaloy	1.26	
Bottom End Fitting Zone, (6.65 inch long, **4.10** g/FA total cobalt content)			
Finger springs	Inconel	0.05	
End plugs	Zircaloy	1.26	
Lower tie plate	Stainless Steel	4.7	
Total, kgs.(1)		329.7	
Total, lbs.(1)		726.3	

(1) This mass is very conservative for the source term calculation because the maximum weight of fuel assembly with or without channel is limited to 705 lbs per Chapter B.1, Table B.1-2.

Table B.5-4
Elemental Composition of LWR Fuel-Assembly Structural Materials

Element	Atomic Number	Material Composition, grams per kg of material				$U0_2$ Fuel, Grams/1.345 kgs
		Zircaloy-4	Inconel-718	Inconel X-750	Stainless Steel 304	
H	1	1.30E-02	-	-	-	-
Li	3	-	-	-	-	1.00E-03
B	5	3.30E-04	-	-	-	1.00E-03
C	6	1.20E-01	4.00E-01	3.99E-01	8.00E-01	8.94E-02
N	7	8.00E-02	1.30E+00	1.30E+00	1.30E+00	2.50E-02
O	8	9.50E-01	-	-	-	1.34E+02
F	9	-	-	-	-	1.07E-02
Na	11	-	-	-	-	1.50E-02
Mg	12	-	-	-	-	2.00E-03
Al	13	2.40E-02	5.99E+00	7.98E+00	-	1.67E-02
Si	14	-	2.00E+00	2.99E+00	1.00E+01	1.21E-02
P	15	-	-	-	4.50E-01	3.50E-02
S	16	3.50E-02	7.00E-02	7.00E-02	3.00E-01	-
Cl	17	-	-	-	-	5.30E-03
Ca	20	-	-	-	-	2.00E-03
Ti	22	2.00E-02	7.99E+00	2.49E+01	-	1.00E-03
V	23	2.00E-02	-	-	-	3.00E-03
Cr	24	1.25E+00	1.90E+02	1.50E+02	1.90E+02	4.00E-03
Mn	25	2.00E-02	2.00E+00	6.98E+00	2.00E+01	1.70E-03
Fe	26	2.25E+00	1.80E+02	6.78E+01	6.88E+02	1.80E-02
Co	27	1.00E-02	4.69E+00	6.49E+00	8.00E-01	1.00E-03
Ni	28	2.00E-02	5.20E+02	7.22E+02	8.92E+01	2.40E-02
Cu	29	2.00E-02	9.99E-01	4.99E-01	-	1.00E-03
Zn	30	-	-	-	-	4.03E-02
Zr	40	9.79E+02	-	-	-	-
Nb	41	-	5.55E+01	8.98E+00	-	-
Mo	42	-	3.00E+01	-	-	1.00E-02
Ag	47	-	-	-	-	1.00E-04
Cd	48	2.50E-04	-	-	-	2.50E-02
In	49	-	-	-	-	2.00E-03
Sn	50	1.60E+01	-	-	-	4.00E-03
Gd	64	-	-	-	-	2.50E-03
Hf	72	7.80E-02	-	-	-	-
W	74	2.00E-02	-	-	-	2.00E-03
Pb	82	-	-	-	-	1.00E-03
U	92	2.00E-04	-	-	-	1.00E-03

Table B.5-5
Flux Scaling Factors By Fuel Assembly Region

Fuel Assembly Region	Flux Factor
Bottom	0.15
In-Core	1.00
Plenum	0.20
Top	0.10

Table B.5-6
Source Term Peaking Summary

Fraction of Core Height	Neutron Peaking Factor	Gamma Peaking Factor
0.05	0.0018	0.2256
0.1	0.1683	0.7674
0.2	0.8447	1.0854
0.3	1.3859	1.2027
0.4	1.5288	1.2223
0.5	1.5775	1.2244
0.6	1.5624	1.2164
0.7	1.3842	1.1227
0.8	1.0707	1.0964
0.9	0.5047	0.9053
0.95	0.1093	0.6255
1	0.0028	0.2303
Average (Ratio to Non-Uniform Case)	1.326	0.989 (1.0)[1]

(1) 1.0 is used as a correction factor in MCNP models for the total primary gamma radiation source terms strength to account for an axial burn-up profile variation.

Table B.5-7
Design Basis Source Terms for the NCT (44 Locations)
(26 GWD/MTU, 1.9 wt.%, after 6.5 years of cooling)

E_{min}, (MeV)	to	E_{max}, (MeV)	Bottom Nozzle (gammas/sec*FA)	In-core (gammas/sec*FA)	Plenum (gammas/sec*FA)	Top Nozzle (gammas/sec*FA)
0.00E+00	to	5.00E-02	7.5142E+10	4.1180E+14	6.0328E+10	5.9913E+10
5.00E-02	to	1.00E-01	8.9316E+09	8.1644E+13	2.9982E+09	7.0127E+09
1.00E-01	to	2.00E-01	2.5421E+09	6.1700E+13	3.7968E+09	2.0857E+09
2.00E-01	to	3.00E-01	1.3021E+08	1.7848E+13	2.2010E+08	1.0762E+08
3.00E-01	to	4.00E-01	2.3303E+08	1.2240E+13	7.8214E+08	2.0441E+08
4.00E-01	to	6.00E-01	2.0808E+09	1.0495E+14	1.6438E+10	2.1131E+09
6.00E-01	to	8.00E-01	1.0819E+09	5.3394E+14	8.5102E+09	1.1252E+09
8.00E-01	to	1.00E+00	6.7960E+09	4.5773E+13	2.9949E+09	3.1401E+09
1.00E+00	to	1.33E+00	2.6003E+12	3.3988E+13	8.1716E+11	2.0400E+12
1.33E+00	to	1.66E+00	7.3432E+11	8.9371E+12	2.3077E+11	5.7609E+11
1.66E+00	to	2.00E+00	2.4874E+00	1.3817E+11	1.5071E+01	2.7162E+00
2.00E+00	to	2.50E+00	1.7427E+07	2.2819E+11	5.4764E+06	1.3671E+07
2.50E+00	to	3.00E+00	2.7022E+04	9.8359E+09	8.4917E+03	2.1199E+04
3.00E+00	to	4.00E+00	7.9455E-13	1.2345E+09	2.5392E-16	6.1668E-12
4.00E+00	to	5.00E+00	0.0	1.7332E+06	0.0	0.0
5.00E+00	to	6.50E+00	0.0	6.9555E+05	0.0	0.0
6.50E+00	to	8.00E+00	0.0	1.3643E+05	0.0	0.0
8.00E+00	to	1.00E+01	0.0	2.8966E+04	0.0	0.0
Total Gamma:			3.4316E+12	1.3132E+15	1.1440E+12	2.6918E+12
Total Neutrons[1], n/(sec*FA)			5.04E+07			

[1] The total neutron source term of 5.25E+07 n/(sec*FA) corresponding to a cooling time of 5.4 years was utilized in the design basis shielding calculations to determine the neutron dose rate as a function of distance.

Table B.5-8
Design Basis Source Terms for the HAC (44 Locations)
(62 GWD/MTU, 2.6 wt.%, after 31.5 years of cooling)

E_{min}, (MeV)	to	E_{max}, (MeV)	Bottom Nozzle (gammas/sec*FA)	In-core (gammas/sec*FA)	Plenum (gammas/sec*FA)	Top Nozzle (gammas/sec*FA)
0.00E+00	to	5.00E-02	7.148E+09	3.816E+14	2.144E+09	5.080E+09
5.00E-02	to	1.00E-01	7.691E+08	7.682E+13	2.269E+08	5.642E+08
1.00E-01	to	2.00E-01	1.868E+08	4.747E+13	6.776E+07	1.378E+08
2.00E-01	to	3.00E-01	9.300E+06	1.466E+13	3.519E+06	6.884E+06
3.00E-01	to	4.00E-01	1.247E+07	9.803E+12	6.708E+06	9.255E+06
4.00E-01	to	6.00E-01	1.017E+07	7.234E+12	7.036E+07	9.550E+06
6.00E-01	to	8.00E-01	1.939E+07	5.789E+14	3.639E+07	7.5561+07
8.00E-01	to	1.00E+00	2.372E+07	3.569E+12	2.933E+06	7.5504+07
1.00E+00	to	1.33E+00	2.238E+11	6.441E+12	6.578E+10	1.643E+11
1.33E+00	to	1.66E+00	6.321E+10	7.880E+11	1.858E+10	4.639E+10
1.66E+00	to	2.00E+00	5.757E+00	2.500E+10	4.562E+01	5.880E+00
2.00E+00	to	2.50E+00	1.500E+06	1.331E+09	4.408E+05	1.101E+06
2.50E+00	to	3.00E+00	2.326E+03	1.667E+08	6.836E+02	1.707E+03
3.00E+00	to	4.00E+00	9.323E-12	3.382E+07	5.352E-15	5.244E-11
4.00E+00	to	5.00E+00	0.0	1.142E+07	0.0	0.0
5.00E+00	to	6.50E+00	0.0	4.582E+06	0.0	0.0
6.50E+00	to	8.00E+00	0.0	8.989E+05	0.0	0.0
8.00E+00	to	1.00E+01	0.0	1.909E+05	0.0	0.0
Total Gamma:			2.952E+11	1.127E+15	8.692E+10	2.166E+11
Total Neutrons, n/(sec*FA)			3.32E+08			

Table B.5-9
Three Zone Response Function for the TN44B

	Response Function Parameter for	Lower Boundary of Energy Group, MeV	Upper Boundary of Energy Group, MeV	Middle of MP197TAD TO - 2m		
				neutron (mrem/hr)	gamma (mrem/hr)	Total (mrem/hr)
Zone 1 4 assy.	Neutrons	0.00E+00	2.0E+01	3.462E-10	2.404E-10	5.866E-10
	Group 32	1.00E+00	1.33E+00	-	0.000E+00	0.000E+00
	Group 31	1.33E+00	1.66E+00	-	3.062E-17	3.062E-17
	Group 29	2.00E+00	2.50E+00	-	5.298E-16	5.858E-16
	Group 28	2.50E+00	3.00E+00	-	1.336E-15	1.336E-15
Zone 2 20 assy.	Neutrons	0.00E+00	2.0E+01	5.250E-09	1.924E-09	7.174E-09
	Group 32	1.00E+00	1.33E+00	-	1.518E-15	1.518E-15
	Group 31	1.33E+00	1.66E+00	-	1.293E-14	1.293E-14
	Group 29	2.00E+00	2.50E+00	-	1.425E-13	1.425E-13
	Group 28	2.50E+00	3.00E+00	-	3.294E-13	3.294E-13
Zone 3 20 assy.	Neutrons	0.00E+00	2.0E+01	1.303E-08	3.302E-09	1.633E-08
	Group 32	1.00E+00	1.33E+00	-	5.412E-14	5.412E-14
	Group 31	1.33E+00	1.66E+00	-	3.238E-13	3.238E-13
	Group 29	2.00E+00	2.50E+00	-	2.494E-12	2.494E-12
	Group 28	2.50E+00	3.00E+00	-	4.943E-12	4.943E-12

Table B.5-10
VYAL B Chemical Composition

Mass Ratios, wt %	Elemental Composition						Density, g/cm^3
	H	B	C	Al	Zn	O	
Nominal at Room Temperature	4.59	0.82	23.35	19.5	1.40	50.34	1.750
134 °C Exposure for 1 year.	4.54	0.82	23.35	19.5	1.40	50.39	1.743
150 °C Exposure for 1 year.	4.49	0.82	23.35	19.5	1.40	50.44	1.735
130 °C Exposure for 40 year.	4.38	0.82	23.35	19.5	1.40	50.55	1.720

Table B.5-11
Fuel Assembly Materials Input For MCNP

BWR Assembly[1] Region Material Densities					
Element/Isotope	Atomic Number	Density (g/cm^3)			
		Bottom Fitting	Fuel	Plenum	Top Fitting
C	6	1.166E-3	6.759E-6	1.340E-4	2.784E-4
O	8	-	3.806E-1	-	-
Si	14	1.496E-2	2.599E-4	1.675E-3	5.237E-3
P	15	6.558E-4	3.802E-6	7.535E-5	1.566E-4
Ti	22	3.876E-4	1.754E-4	-	1.757E-3
Cr	24	2.796E-1	3.390E-3	3.260E-2	7.687E-2
Mn	25	2.915E-2	1.690E-4	3.349E-3	6.961E-3
Fe	26	9.984E-1	7.806E-3	1.161E-1	2.433E-1
Ni	28	1.498E-1	5.925E-3	1.591E-2	8.435E-2
Zr	40	3.838E-1	7.195E-1	7.660E-1	2.022E-1
Sn	50	5.665E-3	1.062E-2	1.131E-2	2.985E-3
Hf	72	3.907E-5	7.325E-5	7.799E-5	2.059E-5
U-234	92	-	1.008E-3	-	-
U-235	92	-	1.132E-1	-	-
U-236	92	-	5.209E-4	-	-
U-238	92	-	2.716E+0	-	-
Total		1.864	3.960	0.947	0.624

(1) Densities calculated ignoring the fuel channel zircaloy and channel hardware.

Table B.5-12
Package Materials Input for MCNP

Element	Atomic Number, Z	Weight fraction, (%)						
		VYAL-B/Al	Air	Lead	Carbon Steel	Stainless Steel	Aluminum	Wood
H	1	4.17						6.218
B-10	5	0.139						
B-11	5	0.615						
C	6	23.46	0.01		1	2		44.450
N	7		75.52					
O	8	46.32	23.18					49.333
Al	13	26.00					100	
Si	14							
P	15							
Ar	18		1.29					
Ca	20							
Cr	24					19		
Mn	25							
Fe	26				99	69.5		
Ni	28					9.5		
Zn	30	1.29(1)						
Pb	82			100				
Density, g/cm^3		1.794(2)	1.127E-3	11.17(4)	7.82	7.92	2.72(3)	0.125

(1) Cu was used for Zn in MCNP input decks. Since weight fraction of Zn is not significant and Z-s of Cu and Zn are close this will not have any significant effect on the calculated dose rates.

(2) The density corresponds to homogenized mixture of 1 years aged at 134 °C VYAL-B (1.743 g/cc) and aluminum from 60 Al boxes surrounding neutron shielding material, where VYAL-B and Al from the boxes account for 91.92% and 8.08% of the mixture weight, respectively. Used composition and the density of the neutron shielding material results in bounding dose rates if a mixture of the normal condition VYAL-B and 0.753 kg. Al from the encompassing 60 aluminum boxes were used instead.

(3) Reference model value is 2.702 g/cc. This discrepancy does not affect dose rates significantly.

(4) Theoretical lead density is 11.34 g/cm^3. 98.5% of theoretical is used for conservatism, 11.17 g/m^3.

Table B.5-13
Flux-to-Dose Rate Conversion Factors for Gamma

Photon Energy (MeV)	Conversion Factor (mrem/hr) / (γ/cm^2-s)
0.01	3.96E-03
0.03	5.82E-04
0.05	2.90E-04
0.07	2.58E-04
0.1	2.83E-04
0.15	3.79E-04
0.2	5.01E-04
0.25	6.31E-04
0.3	7.59E-04
0.35	8.78E-04
0.4	9.85E-04
0.45	1.08E-03
0.5	1.17E-03
0.55	1.27E-03
0.6	1.36E-03
0.65	1.44E-03
0.7	1.52E-03
0.8	1.68E-03
1	1.98E-03
1.4	2.51E-03
1.8	2.99E-03
2.2	3.42E-03
2.6	3.82E-03
2.8	4.01E-03
3.25	4.41E-03
3.75	4.83E-03
4.25	5.23E-03
4.75	5.60E-03
5	5.80E-03
5.25	6.01E-03
5.75	6.37E-03
6.25	6.74E-03
6.75	7.11E-03
7.5	7.66E-03
9	8.77E-03
11	1.03E-02
13	1.18E-02
15	1.33E-02

Table B.5-14
Flux-Dose-Rate Conversion Factors for Neutron

Neutron Energy (MeV)	Conversion Factor (mrem/hr) / (n/cm^2-s)
2.50E-08	3.67E-03
1.00E-07	3.67E-03
1.00E-06	4.46E-03
1.00E-05	4.54E-03
1.00E-04	4.18E-03
1.00E-03	3.76E-03
1.00E-02	3.56E-03
1.00E-01	2.17E-02
5.00E-01	9.26E-02
1	1.32E-01
2.5	1.25E-01
5	1.56E-01
7	1.47E-01
10	1.47E-01
14	2.08E-01
20	2.27E-01

Table B.5-15
Maximum Dose Rate Values at Various Radial Distances from Side of Cask and Impact Limiter – Normal Conditions of Transport

Radial Distance from Side of ILs, m	Primary Gamma		Secondary Gamma		Total Gamma		Neutron		Total	
	Dose Rate, mrem/hr	Relative Error	Dose Rate, mrem/hr	Relative Error	Dose Rate, mrem/hr	Relative Error	Dose Rate, mrem/hr	Relative Error	Dose Rate, mrem/hr	Relative Error
Cask Body	31.5	0.04	2.1	0.020	33.6	0.04	30.0	0.03	44.5	0.03
1	11.7	0.03	0.6	0.018	12.3	0.03	2.2	0.03	14.2	0.02
2	7.4	0.03	0.3	0.022	7.7	0.03	1.1	0.03	8.8	0.03
2.7	5.7	0.03	0.2	0.023	5.9	0.03	0.1	0.01	6.0	0.03
4.3	3.4	0.04	0.1	0.026	3.5	0.04	0.0	0.01	3.5	0.04
5.8	2.3	0.04	0.1	0.03	2.3	0.04	0.0	0.01	2.4	0.04
7.3	1.7	0.04	0.0	0.03	1.8	0.04	0.0	0.02	1.8	0.04
8.8	1.2	0.04	0.0	0.03	1.3	0.04	0.0	0.02	1.3	0.04
10.4	0.9	0.05	0.0	0.03	1.0	0.05	0.0	0.02	1.0	0.05
11.9	0.8	0.06	0.02	0.03	0.8	0.06	0.01	0.02	0.8	0.06

Note: Dose rates are considered only above an imaginary plane through the cask trunnions. Maximum gamma and neutron dose rates may not occur at the same axial location. The neutron and secondary gamma dose rates at the cask body location, as reported in Table B.5-2 are calculated by conservatively employing the HAC source term and is equal to 64 mrem/hour.

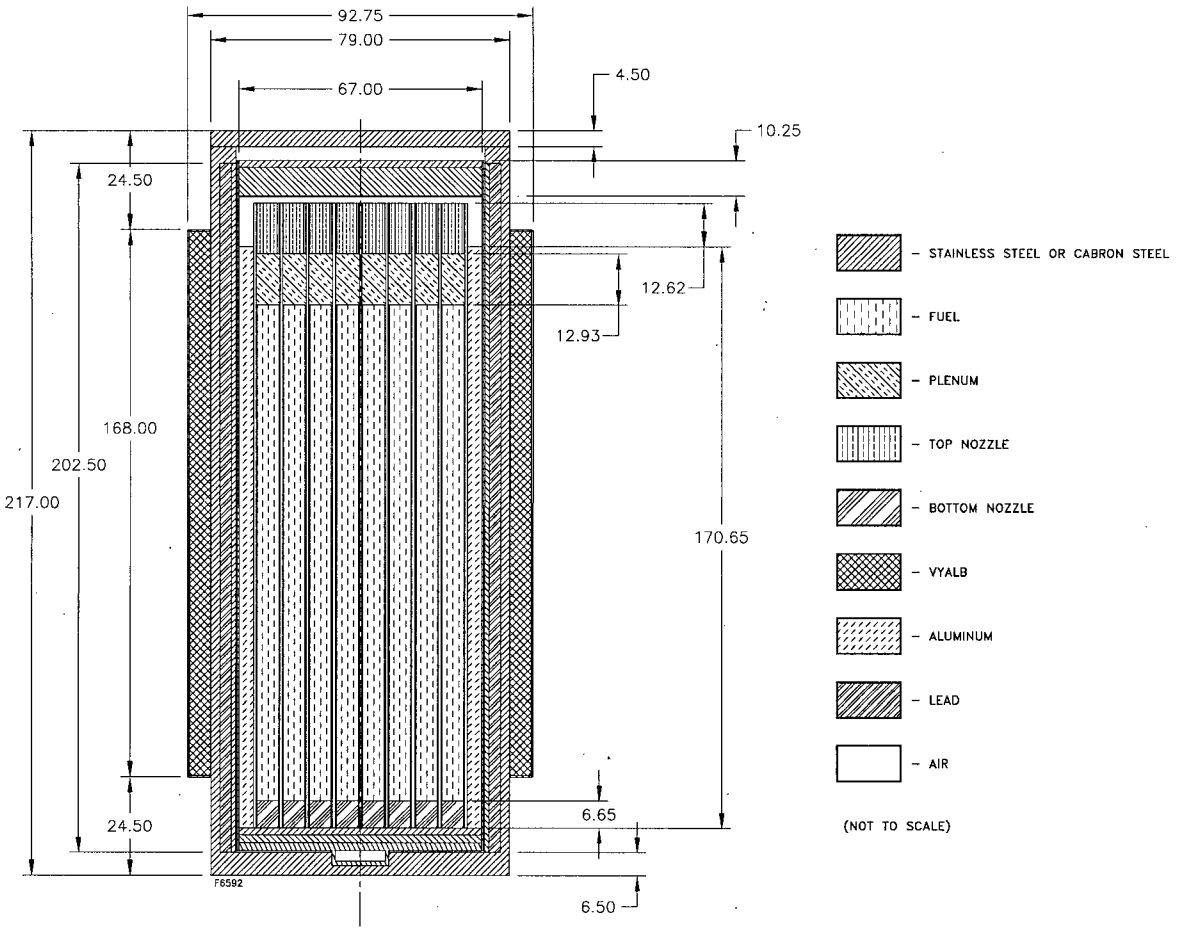

Figure B.5-1
MP197TAD TO Cask Shielding Configuration

Note: All dimensions are in inches. Impact limiters are not shown.

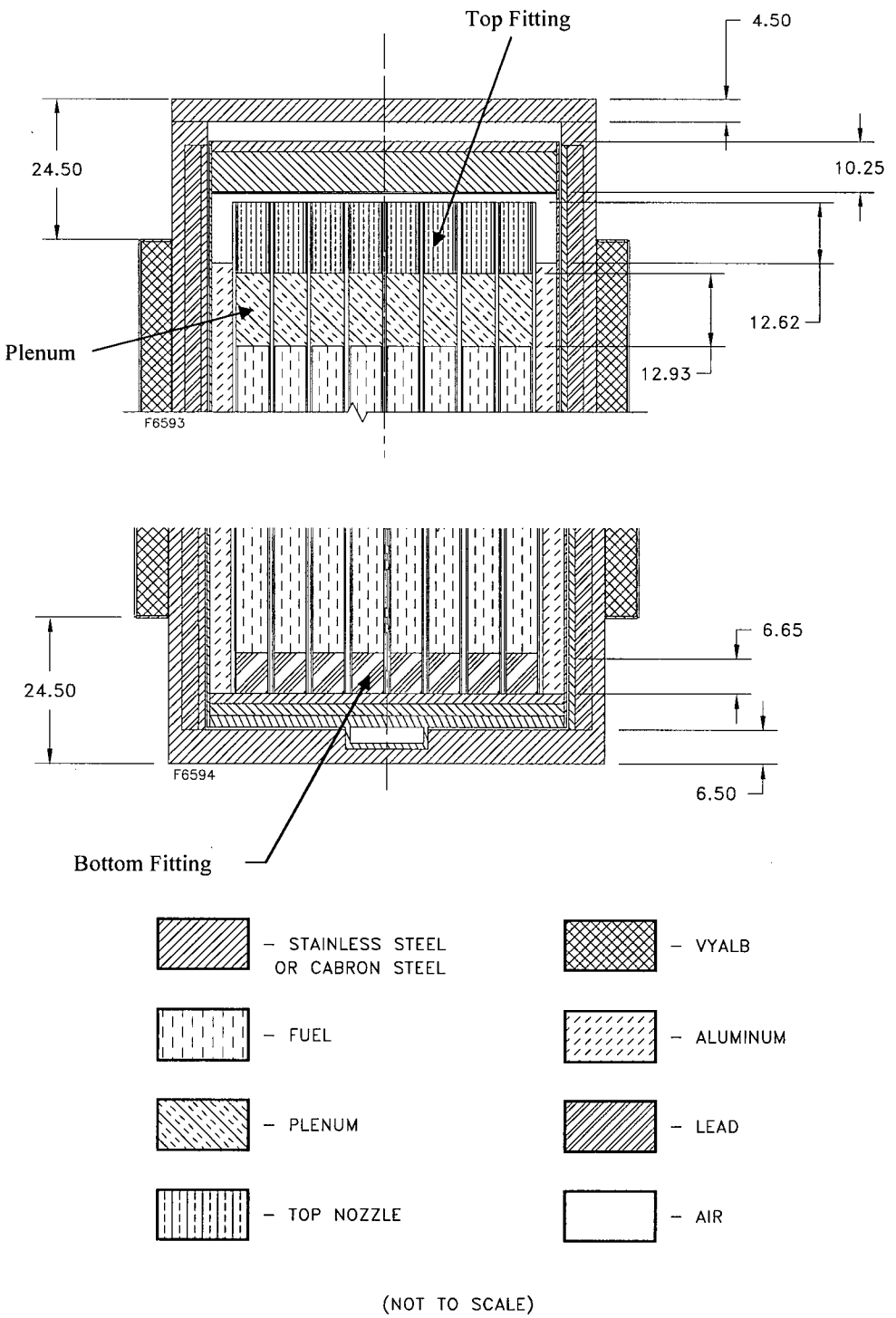

Figure B.5-2
Sketch of MP197TAD TO Transport Cask with TN44B DSC – Top and Bottom Views

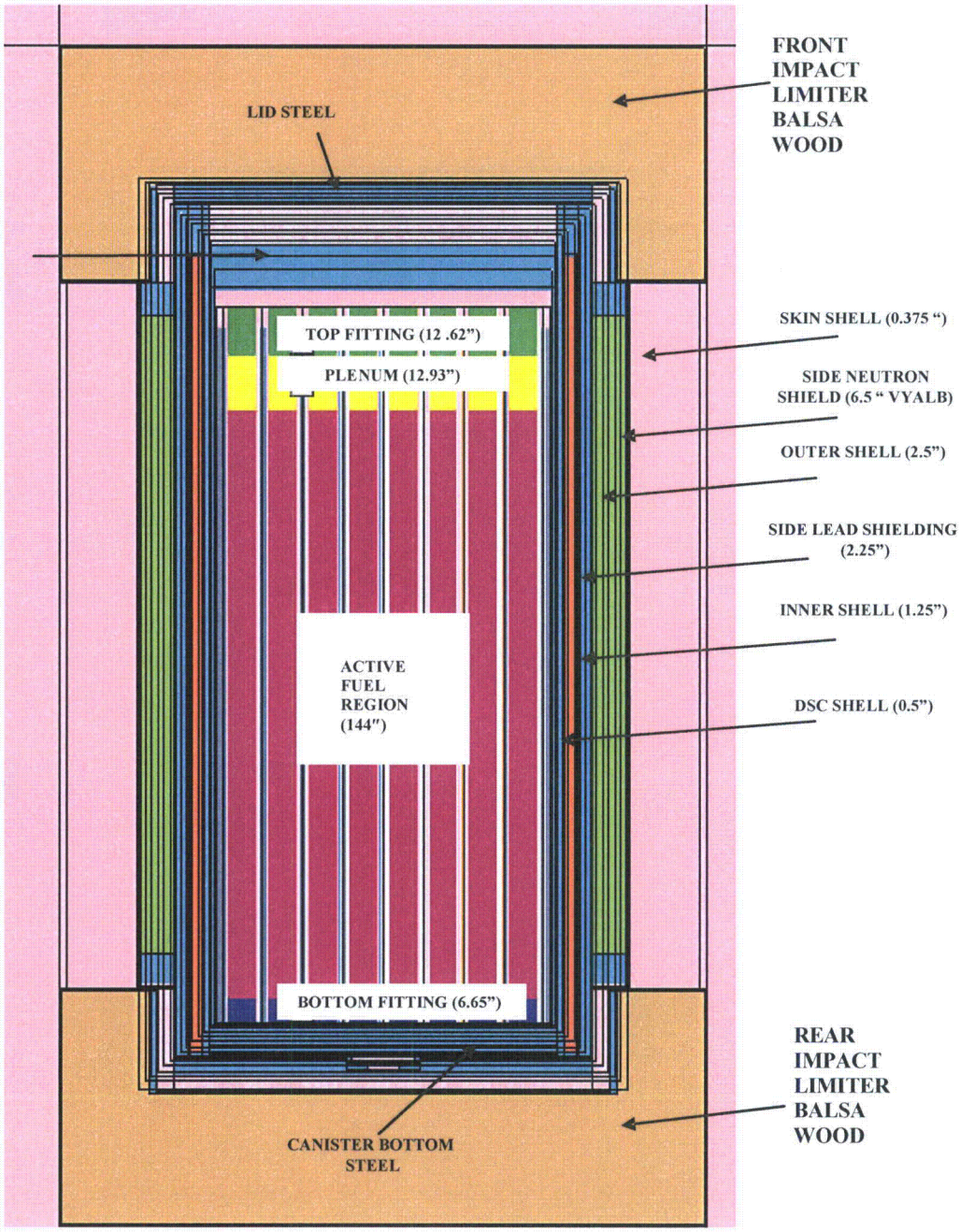

Figure B.5-3
Wide View of MP197TAD TO Transport Cask with TN44B DSC:
MCNP Model Cut-through YZ Plane, Normal Condition

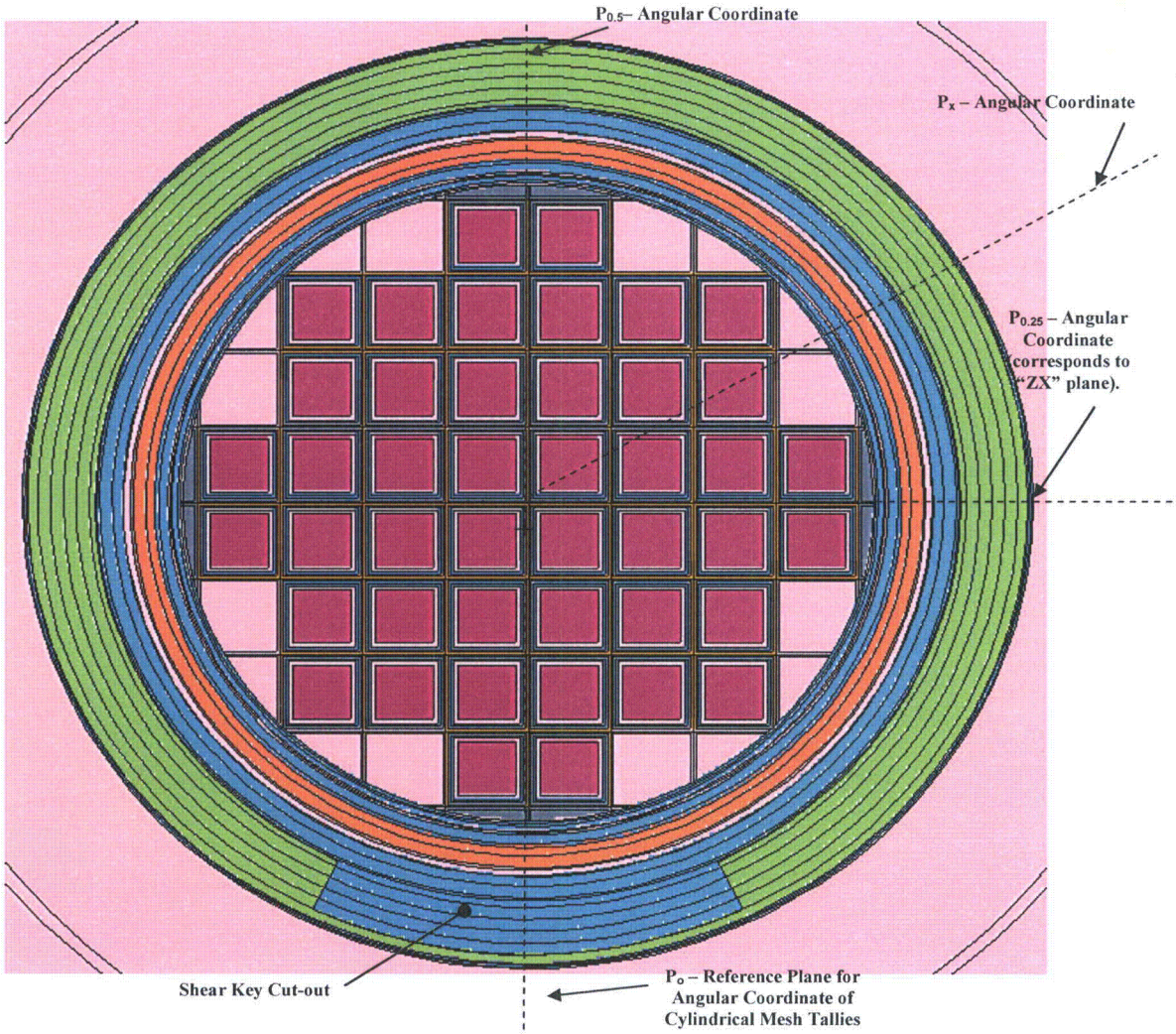

Figure B.5-4
MP197TAD TO Transport Cask with TN 44B DSC:
MCNP Model Cut-through XY Plane (Z=0.0 cm), Normal Condition

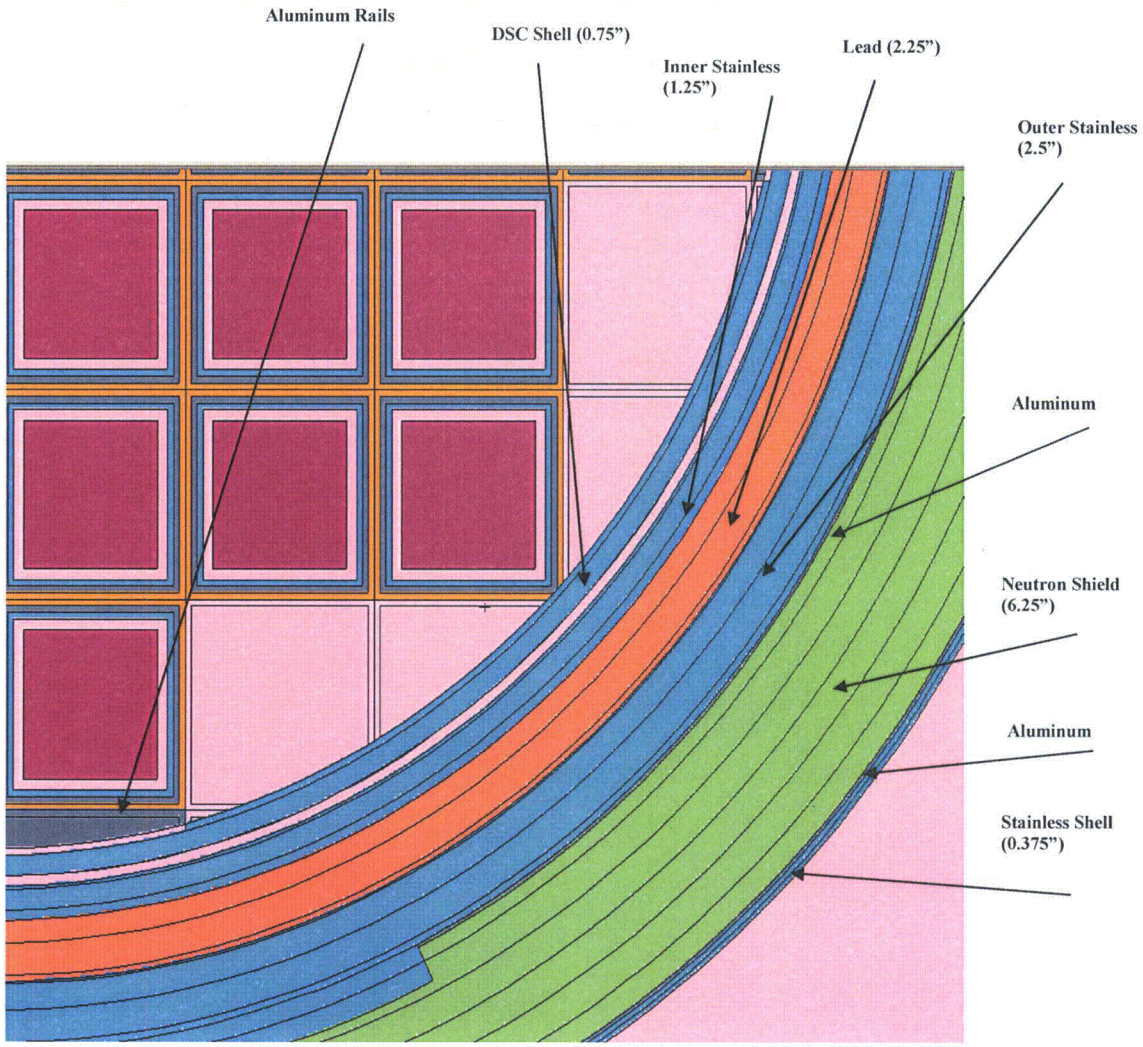

Figure B.5-5
Radial, 1/4 View of MP197TAD TO Transport Cask within TN 44B DSC: MCNP Model Cut-through XY Plane, Normal Condition

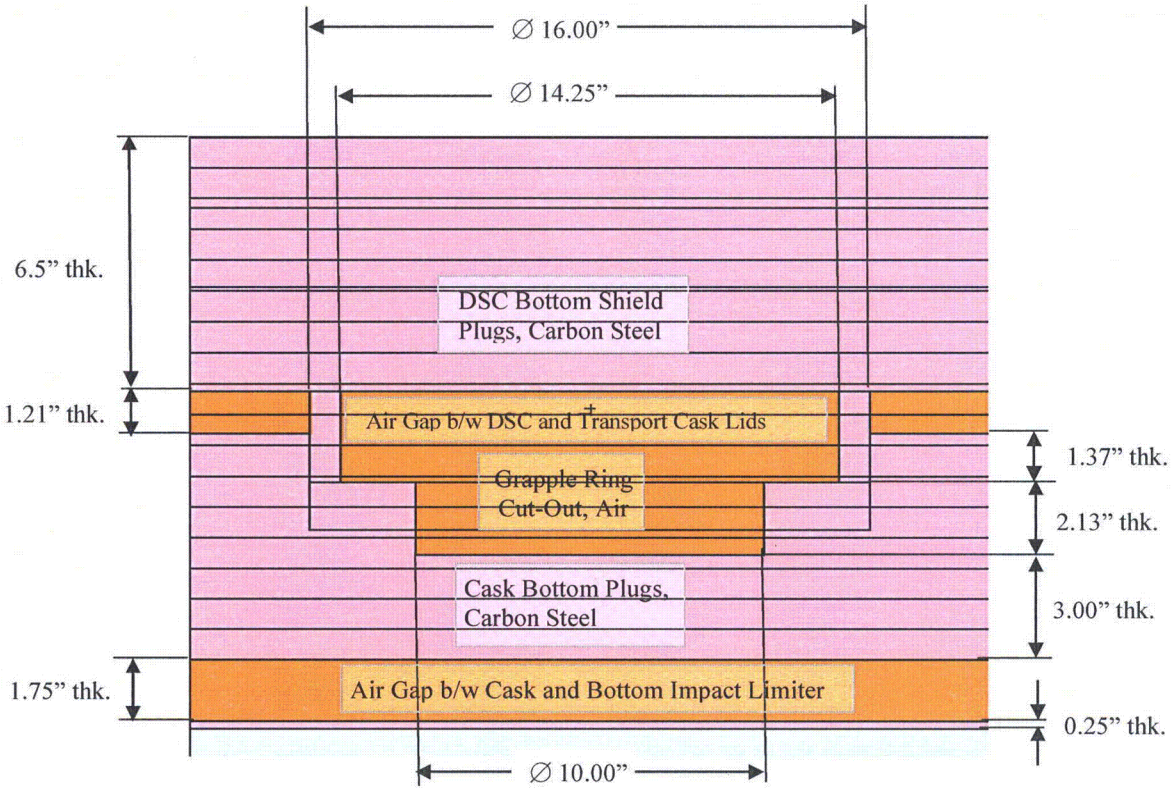

Figure B.5-6
TN44B DSC and MP197TAD TO Bottom Plugs with Grapple Ring Cut-Out (Not to Scale)

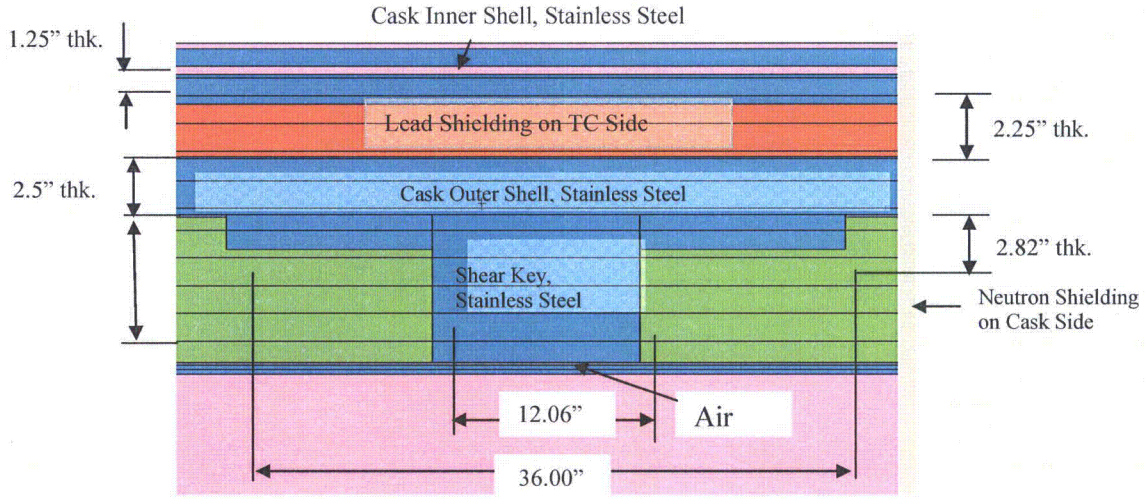

a) ZY View

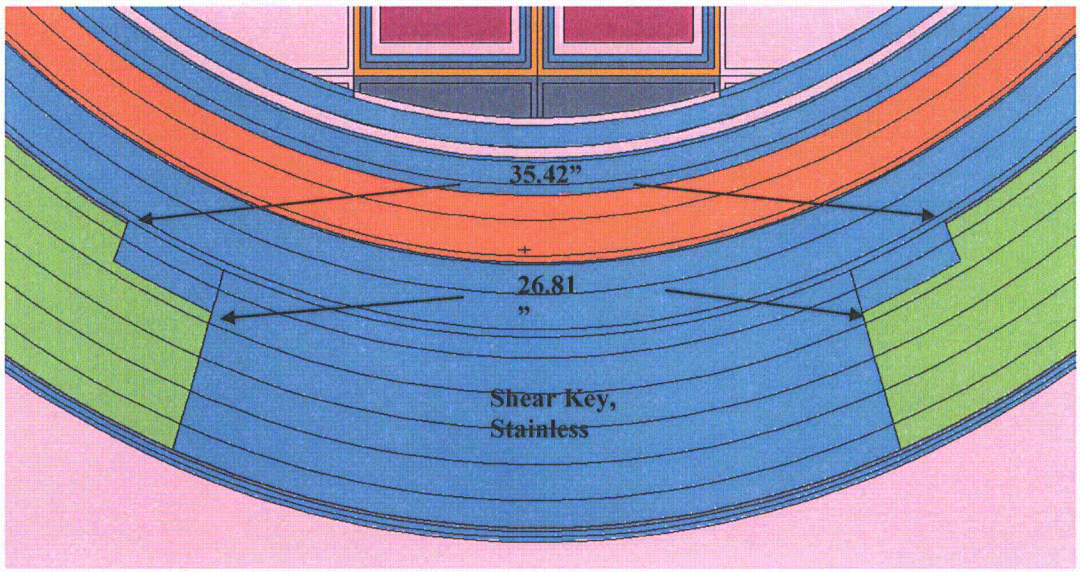

b) XY View

Figure B.5-7
MP197TAD TO Shear Key ZY and XY View at Z=36) (Not to Scale)

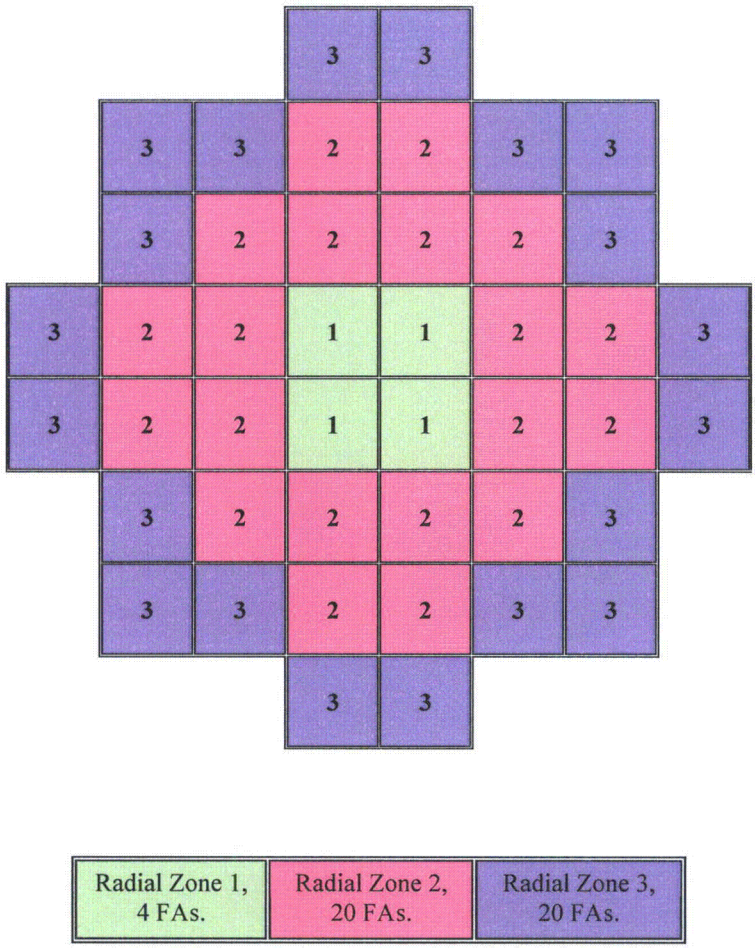

Figure B.5-8
TN 44 DSC Fuel Compartments Zone Matrix Indices

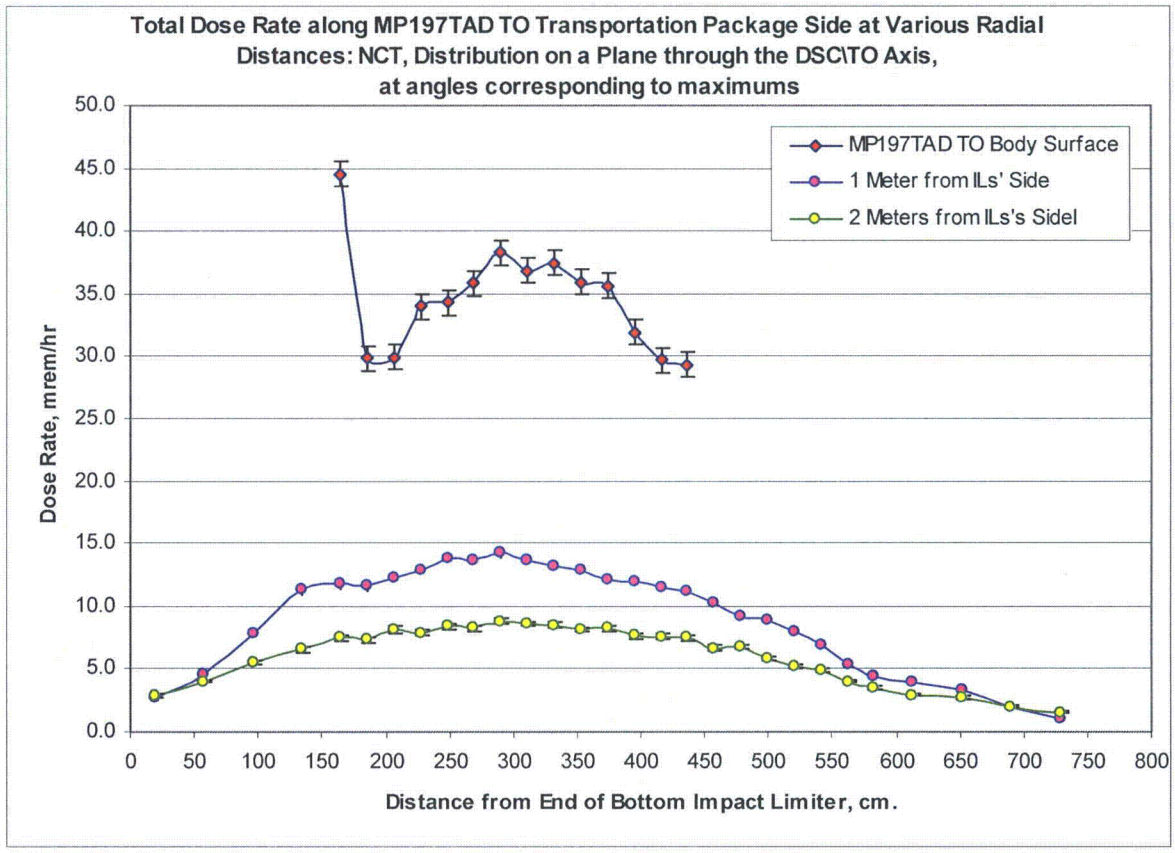

Figure B.5-9
Normal Condition –Radial Dose Rates at Axial Locations

CHAPTER B.6
CRITICALITY EVALUATION

CONTENTS

B.6.1 Description of Criticality Design B.6-1
B.6.1.1 Design Features B.6-1
B.6.1.2 Summary Table of Criticality Evaluation B.6-2
B.6.1.3 Criticality Safety Index B.6-3
B.6.2 Fissile Material Contents B.6-3
B.6.3 General Considerations B.6-3
B.6.3.1 Model Configuration B.6-3
B.6.3.2 Material Properties B.6-4
B.6.3.3 Computer Codes and Cross-Section Libraries B.6-4
B.6.3.4 Demonstration of Maximum Reactivity B.6-5
B.6.4 Single Package Evaluation B.6-10
B.6.4.1 Configuration B.6-11
B.6.4.2 Results B.6-11
B.6.5 Evaluation of Package Arrays under Normal Conditions of Transport B.6-11
B.6.5.1 Configuration B.6-11
B.6.5.2 Results B.6-11
B.6.6 Package Arrays under Hypothetical Accident Conditions B.6-11
B.6.6.1 Configuration B.6-11
B.6.6.2 Results B.6-12
B.6.7 Fissile Material Packages for Air Transport B.6-12
B.6.7.1 Configuration B.6-12
B.6.7.2 Results B.6-12
B.6.8 Benchmark Evaluations B.6-12
B.6.8.1 Applicability of Benchmark Experiments B.6-13
B.6.8.2 Bias Determination B.6-13
B.6.9 References B.6-13
B.6.10 Appendices B.6-14

LIST OF TABLES

Table B.6-1 Minimum B-10 Enrichment by Basket Type B.6-25
Table B.6-2 Criticality Results B.6-26
Table B.6-3 Authorized Contents for TN44B DSC/MP197HB TO Package B.6-27
Table B.6-4 Parameters for BWR Assemblies[1] B.6-28
Table B.6-5 Material Property Data B.6-31
Table B.6-6 Most Reactive Fuel Type B.6-32
Table B.6-7 Most Reactive Configuration B.6-37
Table B.6-8 Effect of External Moderator Density on Reactivity B.6-38
Table B.6-9 Effect of Basket Thickness on Reactivity B.6-39
Table B.6-10 Criticality Results for Basket/Poison Types B.6-40
Table B.6-11 Benchmarking Results B.6-41
Table B.6-12 USL-1 Results B.6-44
Table B.6-13 USL Determination for Criticality Analysis B.6-45

LIST OF FIGURES

Figure B.6-1 TN44B DSC Radial Cross Section B.6-46
Figure B.6-2 KENO V.a units and Radial Cross Sections of the Model B.6-47
Figure B.6-3 Representative KENO V.a Model Cross Section – Most Reactive Fuel B.6-67
Figure B.6-4 Fuel Assembly Layouts B.6-68
Figure B.6-5 Variable Enrichment Fuel Assembly Layouts B.6-71

CHAPTER B.6
CRITICALITY EVALUATION

B.6 Criticality Evaluation

The TN44B DSC as transported in the MP197TAD TO provides criticality control to meet the criticality performance requirements specified in Section 71.55 and 71.59 of 10 CFR Part 71. The criticality control design ensures that the effective multiplication factor (k_{eff}) of the contained fuel is no greater than an Upper Subcritical Limit (USL) for the most reactive configuration. The USL includes a confidence band with an administrative safety margin of 0.05. The design has a Criticality Safety Index (CSI, given in 10 CFR 71.59(b) as CSI = 50/"N") of 0 because "N" is infinity (∞). The number "N" is based on all of the following conditions being satisfied:

1. Five times "N" undamaged packages with nothing between the packages are subcritical.
2. Two times "N" damaged packages, if each package is subjected to the tests specified in 10 CFR 71.73 ("Hypothetical accident conditions"), are subcritical with optimum interspersed hydrogenous moderation; and
3. The value of "N" cannot be less than 0.5.

B.6.1 Description of Criticality Design

The design criteria for the TN44B DSC to be transported in the TN TAD TO require that the package remain subcritical under normal conditions of transport (NCT) and hypothetical accident conditions (HAC) as defined 10 CFR Part 71.

B.6.1.1 Design Features

The MP197TAD TO is a modified version of the NUHOMS®-MP197 Cask. The MP197TAD TO provides impact protection, containment, and shielding during off-site transportation.

The cask is designed without any form of internal basket structure. Its payload is one DSC. The DSC provides full containment and moderator exclusion for the fuel under any credible accident scenario; however, no credit is taken for moderator exclusion by the DSC in the criticality analysis.

The TN44B DSC consists of a stainless steel cylindrical shell, top and bottom shield plugs, inner and outer bottom closure plates, inner and outer top cover plates, and the internal basket. The TN44B DSC is designed to store and transport 44 BWR fuel assemblies with or without channels.

The TN44B DSC stainless steel basket consists of tubular fuel compartments grouped together and wrapped by over-sleeves to form 9 and 2 compartment assemblies. The compartment assemblies are connected to perimeter rail assemblies. The rail assemblies provide the circular perimeter geometry that fits the basket inside the DSC shell.

By incorporating the bundled tube and tube-in-tube geometry features, the basket compartment assemblies of this TN44B DSC achieves superior structural rigidity, while minimizing welding. The perimeter rail assemblies provide a wide footprint for distributing the mechanical loads applied by the basket onto the shell, and increase the area of thermal conduction from the basket to the shell.

The basket utilizes borated stainless steel as its neutron poison material. This material is ideal for long-term use in radiation and thermal environments of a dry cask storage DSC.

The TN44B DSC and MP197TAD TO system's criticality safety is ensured by both fixed neutron absorbers and favorable geometry. The neutron absorber is present in the form of borated metallic (borated stainless steel) plates with three B-10 enrichments. The required B-10 enrichment in the borated stainless steel is a function of assembly lattice average enrichment. Table B.6-1 lists the minimum B-10 poison loading required for each basket/poison type. The presence of absorbers can be verified visually at the time of DSC fabrication or any time before DSC closure. The materials description is included in Chapter B.8. Based on the testing requirements specified in Chapter B.8, 90% credit is taken for the B-10 content in the poison plates in the criticality analysis.

No credit is taken for moderator exclusion from the DSC or the burnup of the fuel.

B.6.1.2 Summary Table of Criticality Evaluation

Figure B.6-1 shows the radial cross section of the TN44B DSC. The cask consists of an inner stainless steel shell, a lead gamma shield, a stainless steel structural shell and a hydrogenous neutron shield with a thin stainless steel skin. TN44B DSC/Cask configuration is shown to be subcritical under normal and accident conditions of transport.

As required by 10 CFR Part 71.55(b), the MP197TAD TO containing the TN44B DSC is shown to be subcritical for the most reactive credible configuration and moderation by water to the most reactive credible extent. The cask is shown to be subcritical for five times "N" or an infinite number of packages with void between packages and no inleakage of water, as required by 10 CFR Part 71.59(a)(1). In addition, as required by 10 CFR Part 71.59(a)(2), two times "N" or an infinite array of packages is shown to be subcritical with the fissile material in its most reactive configuration, optimum water moderation and close full water reflection consistent with its damaged condition.

The criticality calculations utilize the General Electric (GE) 10x10-fuel assembly because for the maximum enrichments allowed for each assembly type, it is the most reactive authorized fuel assembly/initial enrichment combination. The calculations determine k_{eff} with the CSAS25 control module of SCALE-4.4 [1] for various configurations and initial enrichments, including all uncertainties to assure criticality safety under all credible conditions.

The results of the evaluation demonstrate that the maximum expected k_{eff}, including statistical uncertainty, will be less than the USL determined from a statistical analysis of benchmark criticality experiments. The statistical analysis procedure includes a confidence band with an administrative safety margin of 0.05.

Table B.6-2 lists the bounding results for all conditions of transport. The highest calculated k_{eff}, including 2σ uncertainty, is for the GE 10x10 assembly with 0.120 in. fuel channel in the Type A basket configuration with an initial U-235 enrichment of 4.35 wt. %, full internal moderator density and 70% external moderator density. The maximum allowed initial enrichment for each assembly type and basket/poison configuration is listed in Table B.6-1.

These criticality calculations were performed with CSAS25 of SCALE-4.4. For each case, the result includes (1) the KENO-calculated k_{KENO}, (2) the one sigma uncertainty σ_{KENO}, and (3) the final k_{eff}, which is equal to $k_{KENO} + 2\sigma_{KENO}$.

The criterion for subcriticality is that

$$k_{KENO} + 2\sigma_{KENO} \leq USL,$$

where USL is the upper subcritical limit established by an analysis of benchmark criticality experiments. From Section B.6.8, the minimum USL over the parameter range is 0.9414. From Table B.6-2 for the most reactive case,

$$k_{KENO} + 2\sigma_{KENO} = 0.9361 + 2\ (0.0009) = 0.9379 \leq 0.9414.$$

B.6.1.3 Criticality Safety Index

The design has a Criticality Safety Index (CSI, given in 10 CFR 71.59(b) as CSI = 50/"N") of 0 because "N" is infinity (∞).

B.6.2 Fissile Material Contents

The TN44B DSC is capable of transferring; storing; and transporting intact BWR fuel assemblies (including reconstituted fuel) with or without fuel channels. The fuel assemblies considered as authorized contents are listed in Table B.6-3.

Table B.6-4 lists the fuel parameters for the BWR fuel. Reload fuel from other manufactures with the same parameters are also considered as authorized contents. The design basis fuel chosen for the TN44B DSC/ MP197TAD TO is the GE 10x10 fuel assembly. The GE 10x10 assembly is used because, as demonstrated in Section B.6.3.4.1, it is the most reactive assembly/initial enrichment combination authorized for the TN44B DSC.

B.6.3 General Considerations

The following subsections describe the physical models and materials of the TN44B DSC/ MP197TAD TO used for input to the CSAS25 module of SCALE-4.4 [1] to perform the criticality evaluation. The final model developed is for an infinite array of damaged casks. This model bounds the single package evaluation. Therefore, a separate model is not developed for a single cask.

B.6.3.1 Model Configuration

The cask and DSC are explicitly modeled using the appropriate geometry options in KENO V.a of the CSAS25 module in SCALE-4.4.

Two basic models are developed. The first model is a full-active fuel height model and full-radial cross section of the DSC alone with water boundary conditions on the ends and reflective boundary conditions on the sides. This model does not include gaps between the poison plates and is described in more detail in Section B.6.10.1. This model is only used to determine the most reactive fuel assembly/channel/initial enrichment combination and to justify use of the maximum planar average initial enrichment for the intact fuel analysis.

The second model is a full-active fuel height model and full radial cross section of the cask and DSC with reflective boundary conditions on the sides and water boundary conditions on the axial ends. This model includes the worst case gaps between the poison plates and the basket internals modeled to maximize reactivity of the system. This model includes the GE12 10x10 fuel assembly with the 0.12" thick fuel channel because this assembly type/channel configuration is determined to be the most reactive fuel assembly type for the given allowed initial enrichments of the authorized contents. The GE12 10x10 fuel assembly is modeled as a 10x10 array comprising 92 fuel rods, including fuel gap and cladding and two large water holes. The fuel cladding OD is also reduced by 0.010 inches in the models to conservatively bound fuel manufacturing tolerances. The cask neutron shield and outer steel skin are modeled as water.

Figure B.6-2 is a sketch of each KENO V.a unit showing all materials and "final" dimensions for each unit and an annotated cross section map showing the assembled geometry units in the radial direction of the model. The fuel assembly-to-fuel assembly pitch is a variable in the model, with the fuel assemblies modeled in the center of the fuel cells (compartments) and pushed toward the outside of the DSC or pushed towards the center of the DSC. The poison plates are modeled with the minimum allowed B-10 enrichment and with only 90% credit for the boron in the stainless steel. Section B.6.10.2 is an example input deck for the design basis case.

B.6.3.2 Material Properties

The Oak Ridge National Laboratory (ORNL) SCALE code package [1] contains a standard material data library for common elements, compounds, and mixtures. All the materials used for the cask and DSC analysis are available in this data library.

Table B.6-5 provides a complete list of all the relevant materials used for the criticality evaluation. The cask neutron shield is conservatively modeled as water. The hydrogen atom density of the solid neutron shield is lower than that of water; however, the external moderator density calculations demonstrate the exterior moderator density has a statistically insignificant impact on reactivity. Finally, the material density for the boron in the stainless steel poison plates includes a 10% reduction for the criticality models.

B.6.3.3 Computer Codes and Cross-Section Libraries

The CSAS25 control module of SCALE-4.4 [1] is used to calculate the effective multiplication factor (k_{eff}) of the fuel in the cask. The CSAS25 control module allows simplified data input to the functional modules BONAMI-S, NITAWL-S, and KENO V.a. These modules process the required cross sections and calculate the k_{eff} of the system. BONAMI-S performs resonance self-shielding calculations for nuclides that have Bondarenko data associated with their cross sections. NITAWL-S applies a Nordheim resonance self-shielding correction to nuclides having resonance parameters. Finally, KENO V.a calculates the k_{eff} of a three-dimensional system. A

sufficiently large number of neutron histories are run so that the standard deviation is below 0.0015 for all calculations.

The Monte Carlo calculations performed with CSAS25 (KENO V.a) use a flat neutron starting distribution. The total number of histories traced for each calculation is over 800,000. This number of histories is sufficient to converge the source and produce standard deviations of less than 0.15% in k_{eff}. The maximum k_{eff} for the calculation is determined with the following formula:

$$k_{eff} = k_{KENO} + 2\sigma_{KENO}.$$

The physical and nuclear data required for the criticality analysis include the fuel assembly data and cross-section data as described below.

Table B.6-4 lists the pertinent data for criticality analysis for each fuel assembly evaluated in the TN44B DSC loaded in a generic cask described in Section B.6.1.2.

The criticality analysis uses the 44-group cross-section library built into the SCALE system. ORNL used ENDF/B-V data to develop this broad-group library specifically for criticality analysis of a wide variety of thermal systems.

B.6.3.4 Demonstration of Maximum Reactivity

This section describes the criticality analysis. The analyses are performed with the CSAS25 module of the SCALE system. A series of calculations are performed to determine the relative reactivity of the various fuel assembly designs evaluated and to determine the most reactive fuel and configuration. The most reactive fuel/enrichment combination, as demonstrated by the analyses, is the GE10x10 assembly. The most reactive credible configuration is an infinite array of flooded casks with void in the gaps between the basket plates, minimum assembly-to-assembly pitch, minimum shell thickness, and minimum fuel compartment inner diameter with maximum moderator density.

B.6.3.4.1 Bases and Assumptions

The analytical results reported in Chapter B.2 demonstrate that the cask containment boundary and DSC basket structure do not experience any significant distortion under hypothetical accident conditions. Therefore, for both normal and hypothetical accident conditions, the cask geometry is identical except for the neutron shield and skin. As discussed above, the neutron shield and skin are conservatively removed and the interstitial space modeled as water in both the normal and accident condition models.

The cask is modeled with KENO V.a using the available geometry input. This option allows a model to be constructed that uses regular geometric shapes to define the material boundaries. No cases have been made to model the fuel assemblies with fission products or burnable absorbers; rather the fuel is modeled using the Maximum Planar Average Initial Enrichment for the fuel assembly. This results in a very large margin of conservatism in the calculated k_{eff}.

The following conservative assumptions are also incorporated into the criticality calculations:

1. Omission of grid plates, spacers, and hardware in the fuel assembly.

2. Unirradiated fuel – no credit taken for fissile depletion, fission product poisoning or burnable absorbers.

3. Use of maximum planar average initial enrichment everywhere in the lattice. Natural Uranium blankets, Gadolinia, Integral Fuel Burnable Absorber (IFBA), Erbia or any other burnable absorber rods and axial or radial enrichment zones are modeled as enriched uranium, uniform everywhere.

4. All fuel rods are assumed to be filled with 100% pure water in the fuel/cladding gap to account for the possibility of water being entrained in the fuel pin and because it has a slight positive effect on reactivity.

5. The fuel pellet stack is conservatively modeled at 97% of theoretical density with no allowance for dishing or chamfer.

6. Water density is at optimum internal and external moderator density.

7. Only the active fuel length of each assembly type is explicitly modeled. The presence of plenum, end fittings, and channels above and below the active fuel reduce the k_{eff} of the system; therefore, these regions are modeled as water. This results in a model that effectively models the poison only over the active fuel region with water above and below even though the fixed poison and remaining basket materials span the entire length of the basket.

8. For the transport accident condition case, the neutron shield and stainless steel skin of the cask are assumed to be replaced with external moderator.

9. The maximum allowed gap between the poison plates in the worst case position is explicitly modeled to maximize k_{eff}.

10. Only 90% credit is taken for the B-10 in the poison plates.

11. Temperature at 20°C (293K).

12. All zirconium based materials in the fuel are modeled as Zircalloy-2. The small differences in the composition of the various clad / tube/ channel materials have no effect on the results of the calculations.

13. The cask containment boundary does not experience any significant distortion under accident conditions.

B.6.3.4.2 Fuel Loading Optimization

All fuel lattices with and without channels, listed in Table B.6-3 are qualified to be stored in the TN44B DSC as intact fuel with the maximum planar average initial enrichment limit provided as

a function of basket/poison type and fuel assembly design (if applicable). In addition, lattices containing reconstituted rods (lower enriched fuel rods, stainless steel / zircaloy / aluminum rods) or non-fuel rods that displace the same amount of water in the active fuel region of the fuel assembly are conservatively considered intact assemblies. Short loading of the DSC is permitted (empty locations or locations containing dummy fuel assemblies) and is not explicitly analyzed here since that configuration will result in a reduction in the system reactivity.

Determination of the Most Reactive Fuel Type

All fuel lattices, with and without channels, listed in Table B.6-4 are evaluated to determine the most reactive fuel assembly type. The lattices are analyzed with water in the fuel pellet cladding annulus and are centered in the fuel compartments. Each lattice (except Allis Chalmers and Exxon/ANF) is analyzed with a 0.065, 0.080 and 0.120 inch thick channel to determine the most reactive configuration. Finally, this model is used to demonstrate that the use of maximum planar average initial enrichment is conservative. Several cases are run to demonstrate that the use of maximum planar average initial enrichment is conservative for intact fuel. Section B.6.10.1 includes a more detailed description of these models.

Many of the fuel assembly types listed in Table B.6-4 are modeled with a water hole rather than a water rod. FANP 9x9 cases are run with both a water rod and water hole, and it is determined that modeling a water hole is more reactive due to increased moderation, although the effect is small. This result is assumed to be applicable to the other fuel assembly types.

For this analysis, only the DSC is modeled. The DSC is modeled over the active fuel height with water reflectors on the top and bottom ends and reflective boundary conditions outside the DSC (infinite array in the x-y directions). The DSC model for this evaluation differs from the actual design in the following ways:

- Type A basket/poison the B-10 content in the poison plates is 10% lower than the minimum required,
- no gaps between poison plates are modeled, and
- the stainless steel and aluminum transition rails that provide support to the fuel compartment grid are modeled as water.

In all other respects, the model is the same as that described in Sections B.6.3.1. The sole purpose of this model is to determine the relative reactivity of different fuel lattices in a configuration similar to the actual DSC. A representative KENO plot of these models is included in Section B.6.10.1.

These calculations are carried out with use of a planar average initial enrichment used for most cases of 4.6 wt. % U-235. For two assembly types, Allis Chalmers 10x10 (Lacrosse) and SVEA-92 (ABB-10-2, Table B.6-3), the planar average initial enrichment of 4.5 wt. % U-235 is used. The ABB SVEA 10x10 bundles (the last six assembly types in Table B.6-3) consist of multiple lattices with varying design parameters such as rod pitch, clad OD, clad thickness, and pellet OD. In order to perform encompassing analyses, these lattices are designated as different types (ABB-10-1 through ABB-10-6). For criticality analysis, the maximum pitch, the minimum clad

OD, and the maximum pellet OD will be employed. These bundles are also assembled using four sub-assemblies. Note that these assemblies are in actuality six different representations of the same fuel assembly, although only SVEA-92 (ABB-10-2) is run with a lower enrichment. The minimum enrichment utilized is used as the limiting value. For conservatism, results from the most limiting ABB 10x10 fuel assembly analysis will be applied to all the ABB 10x10 evaluations.

A typical input file is included in Section B.6.10.1. The results of these calculations are listed in Table B.6-6. The most reactive lattice/enrichment combination for the DSC design is the GE 10x10 with a 0.120 inch fuel channel. This case also bounds the configuration in which there is no fuel channel and the fuel assemblies are pushed toward the center of the basket. The results show that the Allis Chalmers 10x10 (Lacrosse) and SVEA-92 (ABB-10-2) assemblies require a maximum reduction of 0.1 wt. % in initial enrichment of U-235. This conclusion is also verified for each basket/Poison type allowed for the TN44B DSC.

Determination of the Most Reactive Configuration

The fuel-loading configuration of the DSC/cask affects the reactivity of the package. Several series of analyses determine the most reactive configuration for the DSC/cask.

For this analysis, the DSC/cask is modeled over the active fuel height of the fuel assembly with water reflection on the top and bottom and reflective boundary conditions on the sides of the model. This represents an infinite array of DSC/casks. The DSC/cask model for this evaluation differs from the actual design in the following ways:

- the B-10 content in the poison plates is 10% lower than the minimum required,
- maximum gaps between poison and aluminum plates/sheets are modeled in their worst cask configuration,
- the stainless steel and aluminum transition rails that provide support to the fuel compartment grid are modeled as water, and
- the neutron shield and the skin of the cask are conservatively replaced with water between the infinite array of casks.

The models are fully described in Section B.6.3.1. When determining the most reactive configuration of the DSC/cask, an enrichment of 4.4 wt. % U-235 is utilized. However, in the final cases, the enrichment is determined as a function of basket and fuel assembly type.

The first series of analyses examines the effect of void versus water in the gaps between the basket materials. The GE10x10 with the 0.120 in. fuel channel (determined in the previous section to be the most reactive fuel/enrichment combination) centered in a Type A basket/poison loading are used as the basis for the model. The results in Table B.6-7 demonstrate that modeling all these gaps as void results in higher reactivity as compared to the models with all gaps modeled with water and some gaps modeled with water and some with void.

The second series of analyses examines the effect of assembly-to-assembly pitch on reactivity. The model begins with all gaps modeled as void shown to be most reactive above. The most

reactive configurations occur at the minimum assembly-to-assembly pitch, therefore; the minimum assembly-to-assembly pitch is used for the balance of this analysis. The results of the three runs (assemblies centered in fuel compartments, assemblies all pushed to center of DSC and all assemblies pushed to outside of DSC are shown in Table B.6-7.

The third series of analyses evaluates the effect of DSC shell thickness on the system reactivity. The model starts with the most reactive assembly-to-assembly pitch (minimum pitch) case above and the DSC shell thickness is varied from 0.74 in to 0.85 in. The results are provided in Table B.6-7 and demonstrate that the effect of shell thickness are statistically insignificant, however the minimum shell thickness is used for the balance of the analysis as it resulted in a slightly higher calculated k_{eff}.

The fourth series of analyses evaluates the impact of fuel compartment internal dimension (cell width) on the system reactivity. The model starts with minimum shell thickness model above and the DSC fuel cell width is varied from 6.2 in. to 6.35 in. The results are provided in Table B.6-7 and demonstrate that as expected the minimum cell width results in the most reactive configuration because it results in the fuel assemblies being closer together in the DSC.

The fifth series of analyses verifies that the most reactive configuration is when the internal moderator density is maximized. The model starts with the minimum cell width case from above and the internal moderator density is varied from full to 0% water. The case with 0% internal water is also run with a reduced enrichment of 4.35 wt. % U-235, and void between the casks. This case is the NCT array case. The results are provided in Table B.6-7.

The sixth series of analyses to determine the most reactive configuration is to evaluate the effect of external moderator density on the reactivity of the system. The model begins with the full moderator density case from above and varies the external moderator density from full to 0% water between the casks. The results are provided in Table B.6-8 and demonstrate that the effect of external moderator density in statistically insignificant, although the maximum reactivity is obtained with an external moderator density of 70%. This demonstrates that each cask even without its neutron shield and outer steel neutron shield skin is effectively isolated from its neighbor. The 70% external moderator case is also rerun with a reduced enrichment of 4.35 wt. % U-235.

The seventh series of analyses to determine the most reactive configuration is to evaluate the effect of basket tolerances on the reactivity of the system. The results are provided in Table B.6-9. Three configurations are evaluated, taking into account tolerances of the fuel compartment and/or wrapper thickness (see #1 or #2 on Figure B.6-1), the borated stainless steel and aluminum thickness (see #3 and #4 on Figure B.6-1) and the aluminum thickness between compartments (see #6 and #7 on Figure B.6-1). The evaluations utilize a tolerance of -0.01" for steel plates and -0.075" for aluminum plates. Only the minimum tolerance configurations are performed because thicker basket materials would increase parasitic neutron absorption. The external moderator density is modeled at 70% in the basket tolerance analysis.

The first four cases of Table B.6-9 evaluate the tolerances on the fuel compartment and wrapper. In the first case, the minimum tolerance is equally divided (-0.01"/2) on the fuel compartment and wrapper thicknesses. In the second case, the fuel compartment is modeled at the minimum thickness, while the wrapper is modeled at the nominal thickness. In the third case, the wrapper

is modeled at the minimum thickness, and the fuel compartment is modeled at the nominal thickness. In the fourth case, both the fuel compartment and wrapper are modeled at the minimum thickness. The first case is the most reactive, although the k_{eff} values for several cases are within the statistical uncertainties.

The fifth case of Table B.6-9 takes the previous most reactive configuration, and evaluates the impact of the minimum tolerance on the combined borated stainless steel and aluminum thicknesses. The evaluation takes into account the minimum aluminum tolerance on the combined borated stainless steel and aluminum thicknesses (0.63″), and is applied to the aluminum member. The results are within the statistical uncertainty of the first case.

The last case of Table B.6-9 takes the previous most reactive configuration (the first case), and evaluates the impact of the minimum tolerance on aluminum thicknesses between the 9-compartment-assembly (0.5″, #7 on Figure B.6-1) and between the fuel assemblies in the 2-compartment-assembly (0.63″, #6 on Figure B.6-1). The results are again within the statistical uncertainty of the method.

The results demonstrate that the effect on k_{eff} considering minimum tolerances on the basket thicknesses are relatively low. The difference in k_{eff} between the most reactive minimum tolerance configuration (the first case of Table B.6-9) and the nominal basket configuration (70% external moderator density case from Table B.6-8) is limited to 0.0008 in Δk_{eff}. This result shows that considering minimum tolerances on the basket thicknesses has limited impact on the reactivity comparing to the nominal basket, and the difference is less than the statistical uncertainties in KENO V.a. Therefore, the nominal basket configuration is used in the remaining cases.

Finally, the maximum planar average initial enrichment as a function of basket/poison type is calculated for the most reactive configuration. The model starts with the full external moderator density case from above and the B-10 enrichment is varied for the three basket/poison cases, A, B and C. The results are provided in Table B.6-10. Also included in Table B.6-10 are explicit evaluations of the AC Lacrosse and ABB-10-2 assembly types with their initial enrichment reduced as appropriate (≤0.1 wt. % U-235) to verify that the system loaded with these assemblies with their reduced enrichment (if necessary) is less reactive than the other fuels loaded with their maximum allowed initial enrichments. As shown in Table B.6-10 the most reactive configuration allowed by the authorized contents is for the GE 10x10 assembly with a 0.120 in. fuel channel, and initial enrichment of 4.35 wt. % U-235 in a Type A basket/poison (natural boron) configuration.

The results in Table B.6-10 are computed for full-density water between the packages in the array. Because Table B.6-8 indicates that an external water density at 70% of full is the most reactive, the 70% external water density case is the limiting HAC array case reported in Table B.6-2, with $k_{eff} = 0.9379$.

B.6.4 Single Package Evaluation

As stated above, the evaluations for an infinite array of casks bounds the single package evaluation, therefore a single package is not explicitly evaluated.

B.6.4.1 Configuration

See Sections B.6.3.1 and B.6.3.2 for models of bounding infinite array of casks, which bounds the single package.

B.6.4.2 Results

As stated above, the evaluations for an infinite array of casks bounds the single package evaluation, therefore a single package is not explicitly evaluated.

B.6.5 Evaluation of Package Arrays under Normal Conditions of Transport

For the MP197TAD TO, "N" is infinity (∞), therefore 5N is also infinity. As discussed in Section B.6.3.1 the cask neutron shield and outer steel skin are conservatively removed, and void is modeled between the casks. This is conservative, because it allows the casks to be moved closer together, which tends to increase reactivity.

B.6.5.1 Configuration

The models, assumptions and analysis performed to determine the most reactive configuration is provided in Section B.6.3.4. Because the cask is designed and tested to be leak-tight (10^{-7} ref/cm^3-s) as demonstrated in Chapter B.4, for normal conditions, the DSC and cask are dry. Therefore, the most reactive configuration with the internal moderator set to zero is used for the infinite array of casks under NCT. The model used for this evaluation is conservative, because the cask neutron shield and skin are assumed removed, allowing the casks in the infinite array to be pushed closer together.

B.6.5.2 Results

The bounding k_{eff}, including 2σ uncertainty, for an infinite array of casks under NCT is 0.4104 from Table B.6-2.

B.6.6 Package Arrays under Hypothetical Accident Conditions

For Hypothetical Accident Conditions the DSC and cask are both assumed to allow water in-leakage. The models, assumptions and analysis performed to determine the most reactive configuration is provided in Section B.6.3.4.

B.6.6.1 Configuration

The models, assumptions and analysis performed to determine the most reactive configuration is provided in Section B.6.3.4. The highest calculated k_{eff}, including 2σ uncertainty, is for the GE 10x10 assembly with 0.120 in. fuel channel in the Type A poison configuration with an initial U-235 enrichment of 4.35 wt. %, full internal moderator density and 70% external moderator density.

B.6.6.2 Results

The maximum calculated k_{eff}, including 2σ uncertainty, for an infinite array of casks under hypothetical accident conditions of transport is 0.9379 from Table B.6-2.

B.6.7 Fissile Material Packages for Air Transport

Not Applicable to this DSC and cask system.

B.6.7.1 Configuration

Not Applicable to this DSC and cask system.

B.6.7.2 Results

Not Applicable to this DSC and cask system.

B.6.8 Benchmark Evaluations

The criticality safety analysis of the MP197TAD TO containing the TN44B DSC uses the CSAS25 module of the SCALE system of codes. The CSAS25 control module allows simplified data input to the functional modules BONAMI-S, NITAWL-S, and KENO V.a. These modules process the required cross-section data and calculate the k_{eff} of the system. BONAMI-S performs resonance self-shielding calculations for nuclides that have Bondarenko data associated with their cross sections. NITAWL-S applies a Nordheim resonance self-shielding correction to nuclides having resonance parameters. Finally, KENO V.a calculates the effective neutron multiplication (k_{eff}) of a 3-D system.

The analysis presented herein uses the fresh fuel assumption for criticality analysis. The analysis employs the 44-group ENDF/B-V cross-section library because it has a small bias, as determined by 125 benchmark calculations. The upper subcritical limit (USL-1) is determined using the results of these 125 benchmark calculations.

The benchmark problems used to perform this verification are representative of benchmark arrays of commercial light water reactor (LWR) fuels with the following characteristics:

(1) water moderation,
(2) boron neutron absorbers,
(3) unirradiated light water reactor type fuel (no fission products or "burnup credit") near room temperature (vs. reactor operating temperature),
(4) close reflection, and
(5) Uranium Oxide.

The 125 uranium oxide experiments were chosen to model a wide range of uranium enrichments, fuel pin pitches, assembly separation, and fixed neutron absorbers in order to test the codes ability to accurately calculate k_{eff}.

B.6.8.1 Applicability of Benchmark Experiments

A summary of all of the pertinent parameters for each experiment is included in Table B.6-11 along with the results of each run. The best correlation is observed for fuel assembly separation distance with a correlation of 0.65. All other parameters show much lower correlation ratios indicating no real correlation. All parameters were evaluated for trends and to determine the most conservative USL.

The Upper Subcritical Limit (USL) is calculated in accordance to NUREG/CR-6361 [2]. USL Method 1 (USL-1) applies a statistical calculation of the bias and its uncertainty plus an administrative margin (0.05) to the linear fit of results of the experimental benchmark data. The basis for the administrative margin is from Reference [3]. Results from the USL evaluation are presented in Table B.6-12.

The criticality evaluation used the same cross section set, fuel materials and similar material/geometry options that were used in the 125 benchmark calculations as shown in Table B.6-11. The modeling techniques and the applicable parameters listed in Table B.6-13 for the actual criticality evaluations fall within or very close the range of those addressed by the benchmarks in Table B.6-11.

B.6.8.2 Bias Determination

The results from the comparisons of physical parameters of each of the fuel assembly types to the applicable USL value are presented in Table B.6-13. The minimum value of the USL is determined to be 0.9414 based on comparisons to the limiting assembly parameters as shown in Table B.6-13.

B.6.9 References

1. Oak Ridge National Laboratory, RSIC Computer Code Collection, "SCALE: A Modular Code System for Performing Standardized Computer Analysis for Licensing Evaluations for Workstations and Personal Computers," NUREG/CR-0200, Revision 6, ORNL/NUREG/CSD-2/V2/R6.
2. U.S. Nuclear Regulatory Commission, "Criticality Benchmark Guide for Light-Water-Reactor fuel in Transportation and Storage Packages," NUREG/CR-6361, Published March 1997, ORNL/TM-13211.
3. U.S. Nuclear Regulatory Commission, "Recommendations for Preparing the Criticality Safety Evaluation of Transportation Packages," NUREG/CR-5661, Published April 1997, ORNL/TM-11936.

B.6.10 Appendices

The information on pages
B.6-14 through B.6-24 is
Proprietary Information Withheld
Pursuant to 10 CFR 2.390

Table B.6-1
Minimum B-10 Enrichment by Basket Type

Basket Type	Minimum B-10 Enrichment (wt. % B-10 in Boron)	Minimum B-10 Content (mg/cm^2)	
		Utilized in Analysis	Specified for 90% Credit
A	Natural (18.4)	15.6	17.4
B	25	21.3	23.7
C	35	29.8	33.1

Table B.6-2
Criticality Results

Model Description	k_{KENO}	1σ	k_{eff}
NCT and HAC Single Package (Bounded by HAC infinite array of casks) [10 CFR 71.55(b) (d) (e)]	0.9361	0.0009	0.9379
NCT Infinite Array [10 CFR 71.59(a) (1)]	0.4096	0.0004	0.4104
HAC Infinite Array [10 CFR 71.59(a) (2)]	0.9361	0.0009	0.9379

Table B.6-3
Authorized Contents for TN44B DSC / MP197HB TO Package

Assembly Designation	Array	Maximum Lattice Average Initial Enrichment (wt. % U-235)		
		Basket A	Basket B	Basket C
General Electric 7x7 /GE1	7x7	4.35	4.6	5.0
General Electric 7x7 /GE2	7x7	4.35	4.6	5.0
General Electric 7x7 /GE3	7x7	4.35	4.6	5.0
Exxon/ANF 7x7 /ENC IIIA	7x7	4.35	4.6	5.0
Exxon/ANF 7x7 /ENC III	7x7	4.35	4.6	5.0
General Electric 8x8 /GE4	8x8	4.35	4.6	5.0
General Electric 8x8 /GE5	8x8	4.35	4.6	5.0
General Electric 8x8 /GE-Pres	8x8	4.35	4.6	5.0
General Electric 8x8 /GE-Barrier	8x8	4.35	4.6	5.0
General Electric 8x8 /GE8 Type I	8x8	4.35	4.6	5.0
General Electric 8x8 /GE8 Type II	8x8	4.35	4.6	5.0
General Electric 8x8 /GE9	8x8	4.35	4.6	5.0
General Electric 8x8 /GE10	8x8	4.35	4.6	5.0
Exxon/ANF 8x8 /ENC Va and Vb	8x8	4.35	4.6	5.0
Framatome ANP 8x8-62/2	8x8	4.35	4.6	5.0
XXX-RCN	8x8	4.35	4.6	5.0
General Electric 9x9 /GE11	9x9	4.35	4.6	5.0
General Electric 9x9 / GE13	9x9	4.35	4.6	5.0
Siemens QFA	9x9	4.35	4.6	5.0
Framatome ANP 9x9-79/2 [FANP9]	9x9	4.35	4.6	5.0
General Electric 10x10/GE12	10x10	4.35	4.6	5.0
General Electric 10x10/GE14	10x10	4.35	4.6	5.0
Framatome ANP ATRIUM-10	10x10	4.35	4.6	5.0
Allis Chalmers - LaCrosse	10x10	4.30	4.6	4.9
Exxon/ANF - LaCrosse	10x10	4.35	4.6	5.0
SVEA-64 (ABB-8-1)	4x(4x4)	4.35	4.6	5.0
SVEA-64 (ABB-8-2)	4x(4x4)	4.35	4.6	5.0
SVEA-92 (ABB-10-1)	4x(5x5-2)	4.30	4.6	4.9
SVEA-92 (ABB-10-2)	4x(5x5-2)	4.30	4.6	4.9
SVEA-96 (ABB-10-3)	4x(5x5-1)	4.30	4.6	4.9
SVEA-96 (ABB-10-4)	4x(5x5-1)	4.30	4.6	4.9
SVEA-100 (ABB-10-5)	4x(5x5)	4.30	4.6	4.9
SVEA-100 (ABB-10-6)	4x(5x5)	4.30	4.6	4.9

(1) Or Equivalent Reload Fuels

Table B.6-4
Parameters for BWR Assemblies[1]

Manufacturer[1]	Array	Version	Active Fuel Length (in)	Number Fuel Rods per Assembly	Pitch (in)	Fuel Pellet OD (in)
GE	7x7	GE1, GE2, GE3	144	49	0.738	Note 2
Exxon/ANF	7x7	ENC IIIA	144	49	0.738	Note 3
Exxon/ANF	7x7	ENC III[9]	144	48	0.738	Note 4
GE	8x8	GE4	146	63	0.640	0.416
GE	8x8	GE5	150	62	0.640	0.411[5]
GE	8x8	GE-Pres	150	62	0.640	0.411[5]
GE	8x8	GE-Barrier	150	62	0.640	0.411[5]
GE	8x8	GE8 Type I	150	62	0.640	0.411[5]
GE	8x8	GE8 Type II	150	60	0.640	0.411[5]
GE	8x8	GE9, GE10	150	60	0.640	0.411
Exxon/ANF	8x8	ENC Va and Vb	144	60	0.642	0.4195
Framatome ANP	8x8	8x8-62/2	150	62	0.641	Note 6
XXX-RCN	8x8	8x8 -59/5	150	59 - 64	0.640	0.416
GE	9x9	GE11, GE13	146[7]	74[7]	0.566	0.376
Siemens	9x9	QFA	145.24	72	0.569	0.3737
Framatome ANP	9x9	9x9-79/2	150	79	0.572	0.3565
GE	10x10	GE12, GE14	150[7]	92[7]	0.510	0.345
Framatome-ANP	10x10	ATRIUM-10	149.54[7]	91[7]	0.510	0.3413
Allis Chalmers	10x10	LaCrosse	83	100	0.565	0.350
Exxon/ANF	10x10	LaCrosse	83	96	0.557	0.343
ABB	4x(4x4)	SVEA-64 (ABB-8-1)	150.59	64	0.610	0.3940
ABB	4x(4x4)	SVEA-64 (ABB-8-2)	150.59	64	0.622	0.4110
ABB	4x(5x5-2)	SVEA-92 (ABB-10-1)	150.59	92-96	0.500	0.3350
ABB	4x(5x5-2)	SVEA-92 (ABB-10-2)	150.59	92-96	0.500	0.3224
ABB	4x(5x5-1)	SVEA-96 (ABB-10-3)	150.59	96	0.496	0.3350
ABB	4x(5x5-1)	SVEA-96 (ABB-10-4)	150.59	96	0.488	0.3224
ABB	4x(5x5)	SVEA-100 (ABB-10-5)	151	100	0.500	0.3745
ABB	4x(5x5)	SVEA-100 (ABB-10-6)	151	100	0.496	0.3350

Table B.6-4
Paramaters for BWR Assemblies[1]
(continued)

Manufacturer[1]	Array	Version	Clad Thickness (in)	Clad OD (in)	Water Rod OD (in)	Water Rod ID (in)
GE	7x7	GE1, GE2, GE3	0.032[8]	0.563	NA	NA
Exxon/ANF	7x7	ENC IIIA	0.0355[8]	0.570	NA	NA
Exxon/ANF	7x7	ENC III[9]	0.0355[8]	0.570	0.572[10]	Note 10
GE	8x8	GE4	0.034	0.493	0.493	0.425
GE	8x8	GE5	0.032	0.483	0.591	0.531
GE	8x8	GE-Pres	0.032	0.483	0.591	0.531
GE	8x8	GE-Barrier	0.032	0.483	0.591	0.531
GE	8x8	GE8 Type I	0.032	0.483	0.591	0.531
GE	8x8	GE8 Type II	0.032	0.483	2@0.591 2@0.483	2@0.531 2@0.419
GE	8x8	GE9, GE10	0.032	0.483	1.34[14]	1.26[14]
Exxon/ANF	8x8	ENC Va and Vb	0.036	0.5015	0.5015[10]	Note 10
Framatome ANP	8x8	8x8-62/2	0.035	0.484	0.484	0.414
XXX-RCN	8x8	8x8 -59/5	0.034	0.493	0.493[12]	0.425
GE	9x9	GE11, GE13	0.028	0.440	0.980[14]	0.920[14]
Siemens	9x9	QFA	0.0262	0.433	1.516 sq[14]	1.458 sq[14]
Framatome ANP	9x9	9x9-79/2	0.030	0.424	0.425/0.424[13]	0.364
GE	10x10	GE12, GE14	0.026[15]	0.404[15]	0.980[14]	0.920[14]
Framatome-ANP	10x10	ATRIUM-10	0.0239	0.3957	1.378 sq[14]	1.321 sq[14]
Allis Chalmers	10x10	LaCrosse	0.020	0.396	NA	NA
Exxon/ANF	10x10	LaCrosse	0.022	0.394	0.394[10]	Note 10
ABB	4x(4x4)	SVEA-64 (ABB-8-1)	0.027	0.461	Note 11	Note 11
ABB	4x(4x4)	SVEA-64 (ABB-8-2)	0.031	0.483	Note 11	Note 11
ABB	4x(5x5-2)	SVEA-92 (ABB-10-1)[16]	0.0243	0.387	Note 11	Note 11
ABB	4x(5x5-2)	SVEA-92 (ABB-10-2)[16]	0.0243	0.378	Note 11	Note 11
ABB	4x(5x5-1)	SVEA-96 (ABB-10-3)[16]	0.0243	0.387	Note 11	Note 11
ABB	4x(5x5-1)	SVEA-96 (ABB-10-4)[16]	0.0243	0.378	Note 11	Note 11
ABB	4x(5x5)	SVEA-100 (ABB-10-5)[16]	0.0280	0.443	Note 11	Note 11
ABB	4x(5x5)	SVEA-100 (ABB-10-6)[16]	0.0243	0.387	Note 11	Note 11

Table B.6-4
Paramaters for BWR Assemblies[1]
(concluded)

Notes:

1. Maximum fuel assembly weight with channel is 705 lb.
2. Variable fuel pellet OD – 0.477 to 0.487 in. (maximum OD modeled)
3. Variable fuel pellet OD – 0.468 to 0.488 in. (maximum OD modeled)
4. Variable fuel pellet OD – 0.468 to 0.491 in. (maximum OD modeled)
5. Variable fuel pellet OD – 0.410 to 0.411 in. (maximum OD modeled)
6. Variable fuel pellet OD – 0.4045 to 0.4055 in. (maximum OD modeled)
7. Includes Partial Length Rods (partial length rods are conservatively modeled as full length)
8. Variable clad thickness – Thinnest clad thickness shown and conservatively modeled)
9. Includes ENC III-E and ENC III-F
10. Solid Zirc Rod(s)
11. Fuel assembled from four sub-assemblies with cruciform center. Most Reactive distance between four sub-assemblies is modeled.
12. Some locations may contain solid Zirc rod
13. Modeled with 0.424 OD waterhole
14. Water rods are not modeled and replaced by water holes. Replacing water rods by water holes increases moderation and is more conservative.
15. Cladding thickness and cladding OD are modeled at 0.021 in and 0.394 in, respectively.
16. The ABB SVEA 10x10 bundles consist of multiple lattices with varying design parameters such as rod pitch, clad OD, clad thickness, and pellet OD. In order to perform encompassing analyses, these lattices are designated as different types (ABB-10-1 through ABB-10-6). For criticality analysis, the maximum pitch, the minimum clad OD, and the maximum pellet OD will be employed. These bundles are also assembled using four sub-assemblies.

Table B.6-5
Material Property Data

Material	Density g/cm^3	Element	Weight %	Atom Density (atoms/b-cm)
UO_2 (Enrichment - 4.35 wt%)	10.63	U-235	3.83	1.0445E-03
		U-238	84.32	2.2676E-02
		O	11.85	4.7442E-02
UO_2 (Enrichment - 5.0 wt%)	10.63	U-235	4.41	1.2001E-03
		U-238	83.74	2.2522E-02
		O	11.85	4.7445E-02
Zircaloy-2	6.56	Zr	98.250	4.2550E-02
		Sn	1.450	4.8254E-04
		Fe	0.135	9.5501E-05
		Cr	0.100	7.5978E-05
		Ni	0.055	3.7023E-05
		Hf	0.010	2.2133E-06
Water	0.9982	H	11.2	6.6769E-02
		O	88.8	3.3385E-02
Stainless Steel (SS304)	7.94	C	0.080	3.1877E-04
		Si	1.000	1.7025E-03
		P	0.045	6.9468E-05
		Cr	19.000	1.7473E-02
		Mn	2.000	1.7407E-03
		Fe	68.375	5.8545E-02
		Ni	9.500	7.7402E-03
Aluminum	2.702	Al	100.0	6.0307E-02
Lead	11.344	Pb	100.0	3.2969E-02
Borated Stainless Steel (Natural B-10 18.4%)	7.106	C	0.08	2.8220E-04
		Si	0.99	1.5072E-03
		P	0.04	6.1498E-05
		Cr	18.80	1.5468E-02
		Mn	1.98	1.5410E-03
		Fe	67.64	5.1827E-02
		Ni	9.40	6.8521E-03
		B-10	0.20	8.4700E-04
		B-11	0.88	3.4163E-03
Boron Content for 25% Enriched in B-10 Borated SS	7.106(1)	B-10	0.27	1.1508E-03
		B-11	0.81	3.1400E-03
Boron Content for 35% Enriched in B-10 Borated SS	7.106(1)	B-10	0.38	1.6112E-03
		B-11	0.70	2.7213E-03

(1) Stainless Steel portion of the model identical to that of that of the Borated Stainless Steel with Natural Boron.

Table B.6-6
Most Reactive Fuel Type

Manufacturer	Array	Version	k_{KENO}	1σ	k_{eff}	Enrichment wt% U-235
GE	7x7	GE1, GE2, GE3	0.9214	0.0011	0.9237	4.6
GE	7x7 0.120 channel	GE1, GE2, GE3	0.9218	0.0010	0.9239	4.6
GE	7x7 0.080 channel	GE1, GE2, GE3	0.9225	0.0010	0.9245	4.6
GE	7x7 0.065 channel	GE1, GE2, GE3	0.9204	0.0009	0.9222	4.6
GE	7x7 variable enrich.	GE1, GE2, GE3	0.9079	0.0009	0.9098	4.6
Exxon/ANF	7x7	ENC III-A	0.9166	0.0009	0.9184	4.6
Exxon/ANF	7x7 0.120 channel	ENC III-A	0.9176	0.0010	0.9195	4.6
Exxon/ANF	7x7 0.080 channel	ENC III-A	0.9186	0.0010	0.9206	4.6
Exxon/ANF	7x7 0.065 channel	ENC III-A	0.9188	0.0009	0.9206	4.6
Exxon/ANF	7x7	ENC-III	0.9117	0.0010	0.9137	4.6
Exxon/ANF	7x7 0.120 channel	ENC-III	0.9173	0.0012	0.9196	4.6
Exxon/ANF	7x7 0.080 channel	ENC-III	0.9160	0.0010	0.9179	4.6
Exxon/ANF	7x7 0.065 channel	ENC-III	0.9138	0.0010	0.9158	4.6
GE	8x8	GE4	0.9129	0.0010	0.9149	4.6
GE	8x8 0.120 channel	GE4	0.9156	0.0009	0.9173	4.6
GE	8x8 0.080 channel	GE4	0.9125	0.0011	0.9146	4.6
GE	8x8 0.065 channel	GE4	0.9147	0.0008	0.9163	4.6
GE	8x8	GE5, GE8 Type I, GE-Pres, GE-Barrier	0.9203	0.0010	0.9222	4.6
GE	8x8 0.120 channel	GE5, GE8 Type I, GE-Pres, GE-Barrier	0.9218	0.0010	0.9237	4.6
GE	8x8 0.080 channel	GE5, GE8 Type I, GE-Pres, GE-Barrier	0.9209	0.0010	0.9229	4.6
GE	8x8 0.065 channel	GE5, GE8 Type I, GE-Pres, GE-Barrier	0.9196	0.0010	0.9216	4.6
GE	8x8 variable enrich	GE5, GE8 Type I, GE-Pres, GE-Barrier	0.9111	0.0011	0.9132	4.6

Table B.6-6
Most Reactive Fuel Type
(continued)

Manufacturer	Array	Version	k_{KENO}	1σ	k_{eff}	Enrichment wt% U-235
GE	8x8	GE8, Type II	0.9200	0.0010	0.9219	4.6
GE	8x8 0.120 channel	GE8, Type II	0.9212	0.0009	0.9230	4.6
GE	8x8 0.080 channel	GE8, Type II	0.9205	0.0011	0.9227	4.6
GE	8x8 0.065 channel	GE8, Type II	0.9215	0.0009	0.9234	4.6
GE	8x8	GE9, GE10	0.9200	0.0010	0.9221	4.6
GE	8x8 0.120 channel	GE9, GE10	0.9241	0.0009	0.9259	4.6
GE	8x8 0.080 channel	GE9, GE10	0.9237	0.0009	0.9255	4.6
GE	8x8 0.065 channel	GE9, GE10	0.9233	0.0012	0.9256	4.6
GE	8x8	ENC Va and Vb	0.9032	0.0011	0.9053	4.6
GE	8x8 0.120 channel	ENC Va and Vb	0.9036	0.0011	0.9059	4.6
GE	8x8 0.080 channel	ENC Va and Vb	0.9044	0.0009	0.9063	4.6
GE	8x8 0.065 channel	ENC Va and Vb	0.9035	0.0009	0.9053	4.6
FANP	8x8	FANP 8x8-2	0.9170	0.0013	0.9195	4.6
FANP	8x8 0.120 channel	FANP 8x8-2	0.9185	0.0010	0.9204	4.6
FANP	8x8 0.080 channel	FANP 8x8-2	0.9189	0.0009	0.9207	4.6
FANP	8x8 0.065 channel	FANP 8x8-2	0.9168	0.0011	0.9189	4.6
GE	9x9	GE11, GE13	0.9227	0.0011	0.9249	4.6
GE	9x9 0.120 channel	GE11, GE13	0.9264	0.0009	0.9281	4.6
GE	9x9 0.080 channel	GE11, GE13	0.9242	0.0010	0.9262	4.6
GE	9x9 0.065 channel	GE11, GE13	0.9230	0.0010	0.9251	4.6
FANP	9x9	FANP 9x9-2	0.9240	0.0010	0.9260	4.6
FANP	9x9 with water hole	FANP 9x9-2	0.9266	0.0008	0.9282	4.6
FANP	9x9 0.120 channel	FANP 9x9-2	0.9268	0.0010	0.9288	4.6
FANP	9x9 0.080 channel	FANP 9x9-2	0.9262	0.0009	0.9281	4.6
FANP	9x9 0.065 channel	FANP 9x9-2	0.9247	0.0010	0.9268	4.6
Siemens	9x9	QFA	0.9262	0.0009	0.9280	4.6
Siemens	9x9 0.120 channel	QFA	0.9290	0.0010	0.9310	4.6
Siemens	9x9 0.080 channel	QFA	0.9278	0.0010	0.9298	4.6
Siemens	9x9 0.065 channel	QFA	0.9267	0.0010	0.9286	4.6

Table B.6-6
Most Reactive Fuel Type
(continued)

Manufacturer	Array	Version	k_{KENO}	1σ	k_{eff}	Enrichment wt% U-235
GE	10x10	GE12, GE14	0.9340	0.0009	0.9357	4.6
GE	10x10 pushed in	GE12, GE14	0.9368	0.0010	0.9387	4.6
GE	**10x10 0.120 channel**	**GE12, GE14**	**0.9375**	**0.0011**	**0.9396**	**4.6**
GE	10x10 0.080 channel	GE12, GE14	0.9365	0.0010	0.9384	4.6
GE	10x10 0.065 channel	GE12, GE14	0.9364	0.0011	0.9386	4.6
FANP	10x10	ATRIUM-10	0.9262	0.0009	0.9280	4.6
FANP	10x10 0.120 channel	ATRIUM-10	0.9290	0.0010	0.9309	4.6
FANP	10x10 0.080 channel	ATRIUM-10	0.9282	0.0010	0.9302	4.6
FANP	10x10 0.065 channel	ATRIUM-10	0.9273	0.0011	0.9294	4.6
Allis Chalmers	10x10	Lacrosse	0.9336	0.0009	0.9354	4.5
Exxon/ANF	10x10	Lacrosse	0.9130	0.0010	0.9150	4.6
RCN	8x8	RCN -5 rods, config. 1	0.9181	0.0009	0.9199	4.6
RCN	8x8	RCN -5 rods, config. 2	0.9193	0.0009	0.9211	4.6
RCN	8x8 0.120 channel	RCN -5 rods, config. 2	0.9234	0.0010	0.9254	4.6
RCN	8x8 0.080 channel	RCN -5 rods, config. 2	0.9233	0.0010	0.9253	4.6
RCN	8x8 0.065 channel	RCN -5 rods, config. 2	0.9219	0.0010	0.9239	4.6
RCN	8x8	RCN -5 rods, config. 3	0.9181	0.0010	0.9202	4.6
RCN	8x8	RCN -5 rods, config. 4	0.9148	0.0011	0.9171	4.6
RCN	8x8	RCN -4 rods	0.9162	0.0011	0.9184	4.6
RCN	8x8	RCN -3 rods	0.9149	0.0010	0.9170	4.6
RCN	8x8	RCN -2 rods	0.9164	0.0011	0.9186	4.6
RCN	8x8	RCN -1 rods	0.9155	0.0009	0.9173	4.6
RCN	8x8	RCN -0 rods	0.9119	0.0010	0.9138	4.6
ABB	4x(4x4)	SVEA-64 ABB-8-1	0.9031	0.0009	0.9048	4.6
ABB	4x(4x4) 0.120 channel	SVEA-64 ABB-8-1	0.9074	0.0009	0.9092	4.6
ABB	4x(4x4) 0.080 channel	SVEA-64 ABB-8-1	0.9051	0.0011	0.9072	4.6
ABB	4x(4x4) 0.065 channel	SVEA-64 ABB-8-1	0.9047	0.0010	0.9066	4.6
ABB	4x(4x4)	SVEA-64 ABB-8-2	0.9116	0.0011	0.9138	4.6
ABB	4x(4x4) 0.120 channel	SVEA-64 ABB-8-2	0.9128	0.0010	0.9148	4.6

Table B.6-6
Most Reactive Fuel Type
(continued)

Manufacturer	Array	Version	k_{KENO}	1σ	k_{eff}	Enrichment wt% U-235
ABB	4x(4x4) 0.080 channel	SVEA-64 ABB-8-2	0.9143	0.0011	0.9165	4.6
ABB	4x(4x4) 0.065 channel	SVEA-64 ABB-8-2	0.9123	0.0010	0.9143	4.6
ABB	4x(5x5-2) (*)	SVEA-92 ABB-10-1	0.9189	0.0010	0.9208	4.6
ABB	4x(5x5-2) 0.120 channel (*)	SVEA-92 ABB-10-1	0.9221	0.0010	0.9241	4.6
ABB	4x(5x5-2) 0.080 channel (*)	SVEA-92 ABB-10-1	0.9201	0.0010	0.9221	4.6
ABB	4x(5x5-2) 0.065 channel (*)	SVEA-92 ABB-10-1	0.9214	0.0011	0.9236	4.6
ABB	4x(5x5-2) (*)	SVEA-92 ABB-10-2	0.9152	0.0009	0.9170	4.5
ABB	4x(5x5-2) 0.120 channel (*)	SVEA-92 ABB-10-2	0.9170	0.0009	0.9188	4.5
ABB	4x(5x5-2) 0.080 channel (*)	SVEA-92 ABB-10-2	0.9172	0.0009	0.9190	4.5
ABB	4x(5x5-2) 0.065 channel (*)	SVEA-92 ABB-10-2	0.9170	0.0009	0.9188	4.5
ABB	4x(5x5-2) (**)	SVEA-92 ABB-10-1	0.9359	0.0011	0.9381	4.6
ABB	4x(5x5-2) 0.120 channel (**)	SVEA-92 ABB-10-1	0.9380	0.0009	0.9398	4.6
ABB	4x(5x5-2) 0.080 channel (**)	SVEA-92 ABB-10-1	0.9371	0.0009	0.9390	4.6
ABB	4x(5x5-2) 0.065 channel (**)	SVEA-92 ABB-10-1	0.9386	0.0011	0.9408	4.6
ABB	4x(5x5-2) (**)	SVEA-92 ABB-10-2	0.9324	0.0009	0.9342	4.5
ABB	4x(5x5-2) 0.120 channel (**)	SVEA-92 ABB-10-2	0.9328	0.0010	0.9347	4.5
ABB	4x(5x5-2) 0.080 channel (**)	SVEA-92 ABB-10-2	0.9320	0.0011	0.9341	4.5
ABB	4x(5x5-2) 0.065 channel (**)	SVEA-92 ABB-10-2	0.9328	0.0010	0.9348	4.5
ABB	4x(5x5-1)	SVEA-96 ABB-10-3	0.9321	0.0010	0.9342	4.6
ABB	4x(5x5-1) 0.120 channel	SVEA-96 ABB-10-3	0.9313	0.0010	0.9334	4.6
ABB	4x(5x5-1) 0.080 channel	SVEA-96 ABB-10-3	0.9320	0.0010	0.9340	4.6
ABB	4x(5x5-1) 0.065 channel	SVEA-96 ABB-10-3	0.9306	0.0010	0.9327	4.6
ABB	4x(5x5-1)	SVEA-96 ABB-10-4	0.9194	0.0009	0.9212	4.6
ABB	4x(5x5-1) 0.120 channel	SVEA-96 ABB-10-4	0.9217	0.0010	0.9237	4.6
ABB	4x(5x5-1) 0.080 channel	SVEA-96 ABB-10-4	0.9218	0.0010	0.9238	4.6
ABB	4x(5x5-1) 0.065 channel	SVEA-96 ABB-10-4	0.9207	0.0010	0.9227	4.6

(*) modeled with 92 fuel rods
(**) modeled with 96 fuel rods

Table B.6-6
Most Reactive Fuel Type
(concluded)

Manufacturer	Array	Version	k_{KENO}	1σ	k_{eff}	Enrichment wt% U-235
ABB	4x(5x5)	SVEA-100 ABB-10-5	0.9043	0.0011	0.9065	4.6
ABB	4x(5x5) 0.120 channel	SVEA-100 ABB-10-5	0.8990	0.0010	0.9008	4.6
ABB	4x(5x5) 0.080 channel	SVEA-100 ABB-10-5	0.9018	0.0011	0.9040	4.6
ABB	4x(5x5) 0.065 channel	SVEA-100 ABB-10-5	0.9005	0.0009	0.9023	4.6
ABB	4x(5x5)	SVEA-100 ABB-10-6	0.9247	0.0010	0.9266	4.6
ABB	4x(5x5) 0.120 channel	SVEA-100 ABB-10-6	0.9268	0.0010	0.9288	4.6
ABB	4x(5x5) 0.080 channel	SVEA-100 ABB-10-6	0.9269	0.0010	0.9289	4.6
ABB	4x(5x5) 0.065 channel	SVEA-100 ABB-10-6	0.9261	0.0010	0.9281	4.6

Table B.6-7
Most Reactive Configuration

Model Description	k_{KENO}	1σ	k_{eff}
Analysis Set 1: Gaps			
Corner gaps water/internal gaps void	0.9287	0.0009	0.9305
All gaps water	0.9261	0.0010	0.9282
All gaps void	**0.9325**	**0.0009**	**0.9343**
Analysis Set 2: Assembly-to-Assembly Pitch			
Maximum Assembly-to-Assembly Pitch	0.8760	0.0012	0.8784
Assemblies Centered in Sleeves	0.9325	0.0009	0.9343
Minimum Assembly-to-Assembly Pitch	**0.9344**	**0.0009**	**0.9361**
Analysis Set 3: Shell Thickness Study			
Minimum Shell Thickness (0.74")	**0.9342**	**0.0012**	**0.9365**
Nominal Shell Thickness (0.75")	0.9344	0.0009	0.9362
Maximum Shell Thickness (0.85")	0.9331	0.0011	0.9353
Analysis Set 4: Cell Width			
Minimum Cell width (6.2")	**0.9370**	**0.0011**	**0.9393**
Nominal Cell width (6.25")	0.9342	0.0012	0.9365
Larger Cell width (6.35")	0.9265	0.0009	0.9283
Analysis Set 5: Internal Moderator Density			
Internal Moderator Density at Full	**0.9370**	**0.0011**	**0.9393**
Internal Moderator Density at 90%	0.9157	0.0011	0.9179
Internal Moderator Density at 80%	0.8882	0.0009	0.8900
Internal Moderator Density at 70%	0.8552	0.0009	0.8570
Internal Moderator Density at 60%	0.8179	0.0008	0.8195
Internal Moderator Density at 50%	0.7671	0.0009	0.7688
Internal Moderator Density at 40%	0.7104	0.0009	0.7122
Internal Moderator Density at 30%	0.6375	0.0008	0.6391
Internal Moderator Density at 20%	0.5552	0.0006	0.5564
Internal Moderator Density at 10%	0.4655	0.0005	0.4665
Internal Moderator Density at 0%	0.3692	0.0004	0.3700
Internal Moderator Density at 0% - Air around/4.35% enrichment	0.4096	0.0004	0.4104

Note: U-235 Enrichment = 4.4%, except for the last case in the table.

Table B.6-8
Effect of External Moderator Density on Reactivity

Model Description	k_{KENO}	1σ	k_{eff}
External Moderator Density at Full	0.9370	0.0011	0.9393
External Moderator Density at 90%	0.9374	0.0010	0.9393
External Moderator Density at 80%	0.9374	0.0011	0.9396
External Moderator Density at 70%	0.9384	0.0008	0.9400
External Moderator Density at 60%	0.9375	0.0009	0.9393
External Moderator Density at 50%	0.9379	0.0010	0.9399
External Moderator Density at 40%	0.9369	0.0011	0.9391
External Moderator Density at 30%	0.9378	0.0010	0.9397
External Moderator Density at 20%	0.9371	0.0010	0.9392
External Moderator Density at 10%	0.9361	0.0010	0.9381
External Moderator Density at 0%	0.9364	0.0009	0.9382
External Moderator Density at 70% - 4.35% enrichment	0.9361	0.0009	0.9379

Note: U-235 Enrichment = 4.4% except for the last case in the table.

Table B.6-9
Effect of Basket Thickness on Reactivity

Model Description	k_{KENO}	1σ	k_{eff}
Minimum combined fuel compartment-wrapper thickness	0.9388	0.0010	0.9408
Minimum fuel compartment thickness	0.9371	0.0010	0.9391
Minimum wrapper thickness	0.9353	0.0009	0.9371
Minimum fuel compartment and minimum wrapper thicknesses	0.9380	0.0011	0.9402
Minimum aluminum in combined borated stainless steel-aluminum thickness and minimum combined fuel compartment-wrapper thickness	0.9386	0.0009	0.9404
Minimum aluminum and minimum fuel compartment-wrapper thicknesses	0.9383	0.0009	0.9402

Note: U-235 Enrichment = 4.4%

Table B.6-10
Criticality Results for Basket/Poison Types

Model Description	k_{KENO}	1σ	k_{eff}
All fuel assembly types (except Allis Chalmers and SVEA-96)			
4.35 wt. % U-235; Natural Boron (Type A)	**0.9343**	**0.0007**	**0.9357**
4.6 wt. % U-235; 25% Enriched Boron (Type B)	0.9320	0.0010	0.9339
5.0 wt. % U-235; 35% Enriched Boron (Type C)	0.9336	0.0010	0.9357
Allis Chalmers			
AC - 4.3 wt. % U-235; Natural Boron (Type A)	0.9321	0.0009	0.9340
AC - 4.6 wt. % U-235; 25% Enriched Boron (Type B)	0.9340	0.0007	0.9355
AC - 4.9 wt. % U-235; 35% Enriched Boron (Type C)	0.9335	0.0007	0.9349
SVEA-96 (ABB-10-2)			
ABB-10-2 4.3 wt. % U-235; Natural Boron (Type A)	0.9332	0.0008	0.9348
ABB-10-2 4.6 wt. % U-235; 25% Enriched Boron (Type B)	0.9335	0.0011	0.9356
ABB-10-2 4.9 wt. % U-235; 35% Enriched Boron (Type C)	0.9303	0.0009	0.9321

Table B.6-11
Benchmarking Results

Run ID	U Enrich. Wt%	Pu Enrich. Wt%	Pitch (cm)	H_2O/fuel volume	Separation of assemblies (cm)	AEG	k_{eff}	1σ
B1645SO1	2.46		1.41	1.015		32.8194	0.9967	0.0009
B1645SO2	2.46		1.41	1.015		32.7584	1.0002	0.0011
BW1231B1	4.02		1.511	1.139		31.1427	0.9966	0.0012
BW1231B2	4.02		1.511	1.139		29.8854	0.9972	0.0009
BW1273M	2.46		1.511	1.376		32.2106	0.9965	0.0009
BW1484A1	2.46		1.636	1.841	1.636	34.5304	0.9962	0.0010
BW1484A2	2.46		1.636	1.841	4.908	35.1629	0.9931	0.0010
BW1484B1	2.46		1.636	1.841		33.9421	0.9979	0.0010
BW1484B2	2.46		1.636	1.841	1.636	34.5820	0.9955	0.0012
BW1484B3	2.46		1.636	1.841	4.908	35.2609	0.9969	0.0011
BW1484C1	2.46		1.636	1.841	1.636	34.6463	0.9931	0.0011
BW1484C2	2.46		1.636	1.841	4.908	35.2422	0.9939	0.0012
BW1484S1	2.46		1.636	1.841	1.636	34.5105	1.0001	0.0010
BW1484S2	2.46		1.636	1.841	1.636	34.5569	0.9992	0.0010
BW1484SL	2.46		1.636	1.841	6.544	35.4151	0.9935	0.0011
BW1645S1	2.46		1.209	0.383	1.778	30.1040	0.9990	0.0010
BW1645S2	2.46		1.209	0.383	1.778	29.9961	1.0037	0.0011
BW1810A	2.46		1.636	1.841		33.9465	0.9984	0.0008
BW1810B	2.46		1.636	1.841		33.9631	0.9984	0.0009
BW1810C	2.46		1.636	1.841		33.1569	0.9992	0.0010
BW1810D	2.46		1.636	1.841		33.0821	0.9985	0.0013
BW1810E	2.46		1.636	1.841		33.1600	0.9988	0.0009
BW1810F	2.46		1.636	1.841		33.9556	1.0031	0.0011
BW1810G	2.46		1.636	1.841		32.9409	0.9973	0.0011
BW1810H	2.46		1.636	1.841		32.9420	0.9972	0.0011
BW1810I	2.46		1.636	1.841		33.9655	1.0037	0.0009
BW1810J	2.46		1.636	1.841		33.1403	0.9983	0.0011
DSN399-1	4.74		1.6	3.807	1.8	33.9520	1.0036	0.0015
DSN399-2	4.74		1.6	3.807	5.8	34.4207	0.9989	0.0016
DSN399-3	4.74		1.6	3.807		35.3140	1.0024	0.0015
DSN399-4	4.74		1.6	3.807		35.3784	0.9977	0.0013
EPRU65	2.35		1.562	1.196		33.9106	0.9960	0.0011
EPRU65B	2.35		1.562	1.196		33.4013	0.9993	0.0012
EPRU75	2.35		1.905	2.408		35.8671	0.9958	0.0010
EPRU75B	2.35		1.905	2.408		35.3043	0.9996	0.0010
EPRU87	2.35		2.21	3.687		36.6129	1.0007	0.0011
EPRU87B	2.35		2.21	3.687		36.3499	1.0007	0.0011
NSE71SQ	4.74		1.26	1.823		33.7610	0.9979	0.0012
NSE71W1	4.74		1.26	1.823		34.0129	0.9988	0.0013
NSE71W2	4.74		1.26	1.823		36.3037	0.9957	0.0010
P2438BA	2.35		2.032	2.918	5.05	36.2277	0.9979	0.0013
P2438SLG	2.35		2.032	2.918	8.39	36.2889	0.9986	0.0012
P2438SS	2.35		2.032	2.918	6.88	36.2705	0.9974	0.0011
P2438ZR	2.35		2.032	2.918	8.79	36.2840	0.9987	0.0010
P2615BA	4.31		2.54	3.883	6.72	35.7286	1.0019	0.0014
P2615SS	4.31		2.54	3.883	8.58	35.7495	0.9952	0.0015
P2615ZR	4.31		2.54	3.883	10.92	35.7700	0.9977	0.0014
P2827L1	2.35		2.032	2.918	13.27	36.2526	1.0057	0.0011
P2827L2	2.35		2.032	2.918	11.25	36.2908	0.9999	0.0012

Table B.6-11
Benchmarking Results
(Continued)

Run ID	U Enrich. Wt%	Pu Enrich. Wt%	Pitch (cm)	H_2O/fuel volume	Separation of assemblies (cm)	AEG	k_{eff}	1σ
P2827L3	4.31		2.54	3.883	20.78	35.6766	1.0092	0.0012
P2827L4	4.31		2.54	3.883	19.04	35.7131	1.0073	0.0012
P2827SLG	2.35		2.032	2.918	8.31	36.3037	0.9957	0.0010
P3314BA	4.31		1.892	1.6	2.83	33.1881	0.9988	0.0012
P3314BC	4.31		1.892	1.6	2.83	33.2284	0.9992	0.0012
P3314BF1	4.31		1.892	1.6	2.83	33.2505	1.0037	0.0013
P3314BF2	4.31		1.892	1.6	2.83	33.2184	1.0009	0.0013
P3314BS1	2.35		1.684	1.6	3.86	34.8594	0.9956	0.0013
P3314BS2	2.35		1.684	1.6	3.46	34.8356	0.9949	0.0010
P3314BS3	4.31		1.892	1.6	7.23	33.4247	0.9970	0.0013
P3314BS4	4.31		1.892	1.6	6.63	33.4162	0.9998	0.0012
P3314SLG	4.31		1.892	1.6	2.83	34.0198	0.9974	0.0012
P3314SS1	4.31		1.892	1.6	2.83	33.9601	0.9999	0.0012
P3314SS2	4.31		1.892	1.6	2.83	33.7755	1.0022	0.0012
P3314SS3	4.31		1.892	1.6	2.83	33.8904	0.9992	0.0013
P3314SS4	4.31		1.892	1.6	2.83	33.7625	0.9958	0.0011
P3314SS5	2.35		1.684	1.6	7.8	34.9531	0.9949	0.0013
P3314SS6	4.31		1.892	1.6	10.52	33.5333	1.0020	0.0011
P3314W1	4.31		1.892	1.6		34.3994	1.0024	0.0013
P3314W2	2.35		1.684	1.6		35.2167	0.9969	0.0011
P3314ZR	4.31		1.892	1.6	2.83	33.9954	0.9971	0.0013
P3602BB	4.31		1.892	1.6	8.3	33.3221	1.0029	0.0013
P3602BS1	2.35		1.684	1.6	4.8	34.7750	1.0027	0.0012
P3602BS2	4.31		1.892	1.6	9.83	33.3679	1.0039	0.0012
P3602N11	2.35		1.684	1.6	8.98	34.7438	1.0023	0.0012
P3602N12	2.35		1.684	1.6	9.58	34.8391	1.0030	0.0012
P3602N13	2.35		1.684	1.6	9.66	34.9337	1.0013	0.0012
P3602N14	2.35		1.684	1.6	8.54	35.0282	0.9974	0.0013
P3602N21	2.35		2.032	2.918	11.2	36.2821	0.9987	0.0011
P3602N22	2.35		2.032	2.918	10.36	36.1896	1.0025	0.0011
P3602N31	4.31		1.892	1.6	14.87	33.2094	1.0057	0.0013
P3602N32	4.31		1.892	1.6	15.74	33.3067	1.0093	0.0012
P3602N33	4.31		1.892	1.6	15.87	33.4174	1.0107	0.0012
P3602N34	4.31		1.892	1.6	15.84	33.4683	1.0045	0.0013
P3602N35	4.31		1.892	1.6	15.45	33.5185	1.0013	0.0012
P3602N36	4.31		1.892	1.6	13.82	33.5855	1.0004	0.0014
P3602N41	4.31		2.54	3.883	12.89	35.5276	1.0109	0.0013
P3602N42	4.31		2.54	3.883	14.12	35.6695	1.0071	0.0014
P3602N43	4.31		2.54	3.883	12.44	35.7542	1.0053	0.0015
P3602SS1	2.35		1.684	1.6	8.28	34.8701	1.0025	0.0013
P3602SS2	4.31		1.892	1.6	13.75	33.4202	1.0035	0.0012
P3926L1	2.35		1.684	1.6	10.06	34.8519	1.0000	0.0011
P3926L2	2.35		1.684	1.6	10.11	34.9324	1.0017	0.0011
P3926L3	2.35		1.684	1.6	8.5	35.0641	0.9949	0.0012
P3926L4	4.31		1.892	1.6	17.74	33.3243	1.0074	0.0014
P3926L5	4.31		1.892	1.6	18.18	33.4074	1.0057	0.0013
P3926L6	4.31		1.892	1.6	17.43	33.5246	1.0046	0.0013
P3926SL1	2.35		1.684	1.6	6.59	33.4737	0.9995	0.0012
P3926SL2	4.31		1.892	1.6	12.79	33.5776	1.0007	0.0012

Table B.6-11
Benchmarking Results
(concluded)

Run ID	U Enrich. Wt%	Pu Enrich. Wt%	Pitch (cm)	H_2O/fuel volume	Separation of assemblies (cm)	AEG	k_{eff}	1σ
P4267B1	4.31		1.8901	1.59		31.8075	0.9990	0.0010
P4267B2	4.31		0.89	1.59		31.5323	1.0033	0.0010
P4267B3	4.31		1.715	1.09		30.9905	1.0050	0.0011
P4267B4	4.31		1.715	1.09		30.5061	0.9996	0.0011
P4267B5	4.31		1.715	1.09		30.1011	1.0004	0.0011
P4267SL1	4.31		1.89	1.59		33.4737	0.9995	0.0012
P4267SL2	4.31		1.715	1.09		31.9460	0.9988	0.0016
P62FT231	4.31		1.891	1.6	5.19	32.9196	1.0012	0.0013
P71F14F3	4.31		1.891	1.6	5.19	32.8237	1.0009	0.0014
P71F14V3	4.31		1.891	1.6	5.19	32.8597	0.9972	0.0014
P71F14V5	4.31		1.891	1.6	5.19	32.8609	0.9993	0.0013
P71F214R	4.31		1.891	1.6	5.19	32.8778	0.9969	0.0012
PAT80L1	4.74		1.6	3.807	4.9	35.0253	1.0012	0.0012
PAT80L2	4.74		1.6	3.807	4.9	35.1136	0.9993	0.0015
PAT80SS1	4.74		1.6	3.807	4.9	35.0045	0.9988	0.0013
PAT80SS2	4.74		1.6	3.807	4.9	35.1072	0.9960	0.0013
W3269A	5.7		1.422	1.93		33.1480	0.9988	0.0012
W3269B1	3.7		1.105	1.432		32.4055	0.9961	0.0011
W3269B2	3.7		1.105	1.432		32.3921	0.9963	0.0011
W3269B3	3.7		1.105	1.432		32.2363	0.9944	0.0011
W3269C	2.72		1.524	1.494		33.7727	0.9989	0.0012
W3269SL1	2.72		1.524	1.494		33.3850	0.9981	0.0014
W3269SL2	5.7		1.422	1.93		33.0910	1.0005	0.0013
W3269W1	2.72		1.524	1.494		33.5114	0.9966	0.0014
W3269W2	5.7		1.422	1.93		33.1680	1.0014	0.0014
W3385SL1	5.74		1.422	1.932		33.2387	1.0009	0.0012
W3385SL2	5.74		2.012	5.067		35.8818	0.9997	0.0013
EPRI70UN	0.71	2	1.778	1.2		31.6775	0.9983	0.0012
EPRI70B	0.71	2	1.778	1.2		30.9021	1.0009	0.0012
EPRI87UN	0.71	2	2.2098	2.53		33.3230	1.0096	0.0011
EPRI87B	0.71	2	2.2098	2.53		31.6775	0.9983	0.0012
EPRI99UN	0.71	2	2.5146	3.64		35.1817	1.0063	0.0011
EPRI99B	0.71	2	2.5146	3.64		34.4098	1.0095	0.0011
SAXTON52	0.71	6.6	1.3208	1.68		30.2980	1.0020	0.0014
SAXTON56	0.71	6.6	1.4224	2.16		31.4724	1.0010	0.0014
SAXTON56B	0.71	6.6	1.4224	2.16		31.0038	0.9994	0.0013
SAXTN735	0.71	6.6	1.8669	4.7		34.1848	1.0007	0.0016
SATN792	0.71	6.6	2.01168	5.67		34.6401	1.0026	0.0013
SAXTN104	0.71	6.6	2.6416	10.75		35.8333	1.0054	0.0014
Correlation	0.31	-0.26	0.43	0.25	0.65	-0.01	N/A	N/A

Table B.6-12
USL-1 Results

Parameter	Range of Applicability	USL-1
U Enrichment (wt. % U-235)	2.4	0.9424
	2.8	0.9430
	3.3	0.9435
	3.8 – 5.7	0.9438
Fuel Rod Pitch (cm)	0.89	0.9396
	1.1	0.9408
	1.4	0.9421
	1.6	0.9433
	1.9 – 2.6	0.9439
Water/Fuel Volume Ratio	0.38	0.9414
	1.9	0.9425
	3.3 – 11	0.9426
Assembly Separation (cm)	1.6	0.9410
	4.4	0.9425
	7.1	0.9440
	9.8 – 21	0.9441
Average Energy Group Causing Fission (AEG)	30 – 37	0.9433

Table B.6-13
USL Determination for Criticality Analysis

Parameter	Value from Limiting GE 10x10 Analysis	Bounding USL-1
U Enrichment (wt. % U-235)	4.3 – 5.0	0.9438
Fuel Rod Pitch (cm)	1.2954	**0.9414**
Water/Fuel Ratio	1.44	0.9420
Assembly Separation (cm)	4.63	0.9425
Average Energy Group Causing Fission (AEG)	~33	0.9433

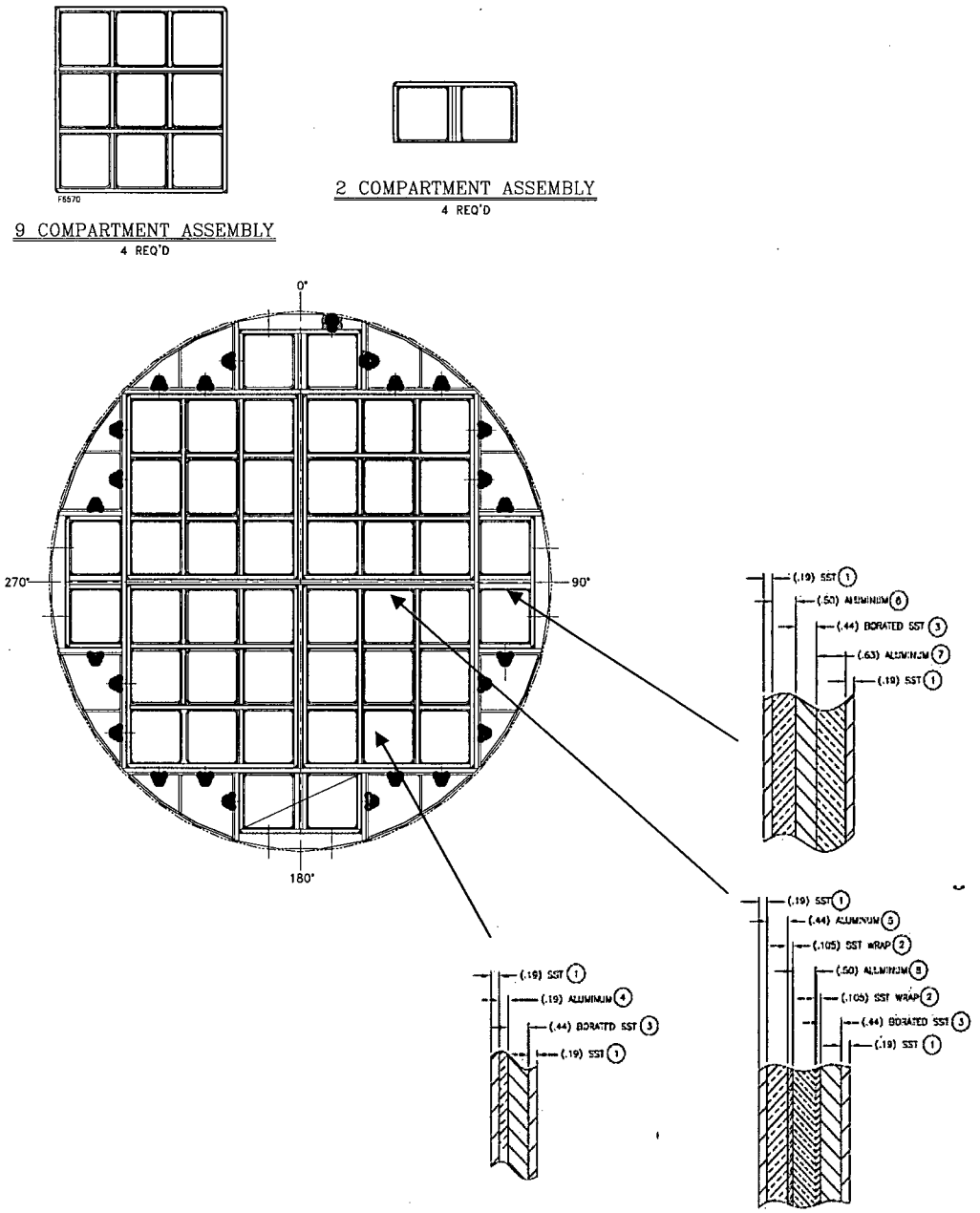

Figure B.6-1
TN44B DSC Radial Cross Section

Unit 1 GE10x10 Fuel Rod (fuel)

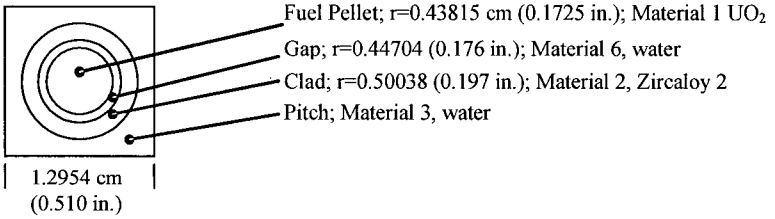

Unit 88 Water Hole (water hole)

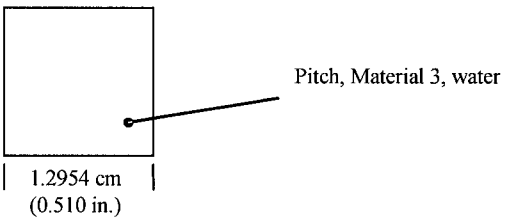

Array 1 GE 10x10 Fuel Assembly made up of a 10x10 array of Unit 1 (fuel) and Unit 88 (water hole)

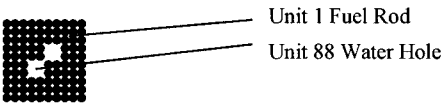

Unit 2 GE 10x10 Fuel Assembly shifted to lower left corner of fuel compartment

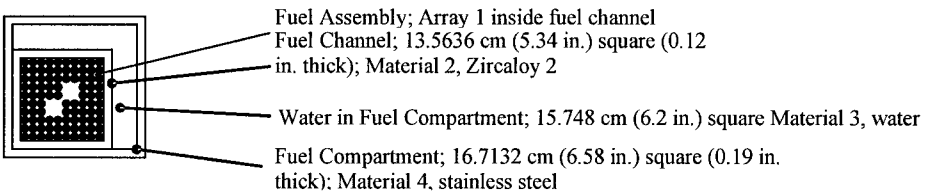

Figure B.6-2
KENO V.a units and Radial Cross Sections of the Model
Part 1 of 20 - (all units 381.00 cm (150 inches) long)

Unit 20 GE 10x10 Fuel Assembly shifted to lower right corner of fuel compartment

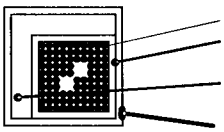

Fuel Assembly; Array 1 inside fuel channel
Fuel Channel; 13.5636 cm (5.34 in.) square (0.12 in. thick); Material 2, Zircaloy 2
Water in Fuel Compartment; 15.748 cm (6.2 in.) square; Material 3, water
Fuel Compartment; 16.7132 cm (6.58 in.) square (0.19 in. thick); Material 4, stainless steel

Unit 30 GE 10x10 Fuel Assembly shifted to upper right corner of fuel compartment

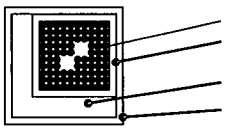

Fuel Assembly; Array 1 inside fuel channel
Fuel Channel; 13.5636 cm (5.34 in.) square (0.12 in. thick); Material 2, Zircaloy 2
Water in Fuel Compartment; 15.748 cm (6.2 in.) square; Material 3, water
Fuel Compartment; 16.7132 cm (6.58 in.) square (0.19 in. thick); Material 4, stainless steel

Unit 40 GE 10x10 Fuel Assembly shifted to upper left corner of fuel compartment

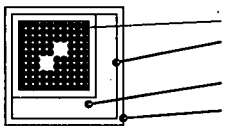

Fuel Assembly; Array 1 inside fuel channel
Fuel Channel; 13.5636 cm (5.34 in.) square (0.12 in. thick); Material 2, Zircaloy 2
Water in Fuel Compartment 15.748 cm (6.2 in.) square
Material 3, water
Fuel Compartment; 16.7132 cm (6.58 in.) square (0.19 in. thick); Material 4, stainless steel

Unit 3 Aluminum Sheet

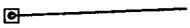

Thermal Shunt; 1.1112 cm (0.4375 in.) square; Material 8, aluminum

Unit 4 Aluminum Sheet

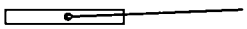

Thermal Shunt; 16.7132 x 1.1112 cm (6.58 x 0.4375 in.); Material 8, aluminum

Figure B.6-2
KENO V.a units and Radial Cross Sections of the Model
Part 2 of 20 - (all units 381.00 cm (150 inches) long)

Unit 5 Poison Plate

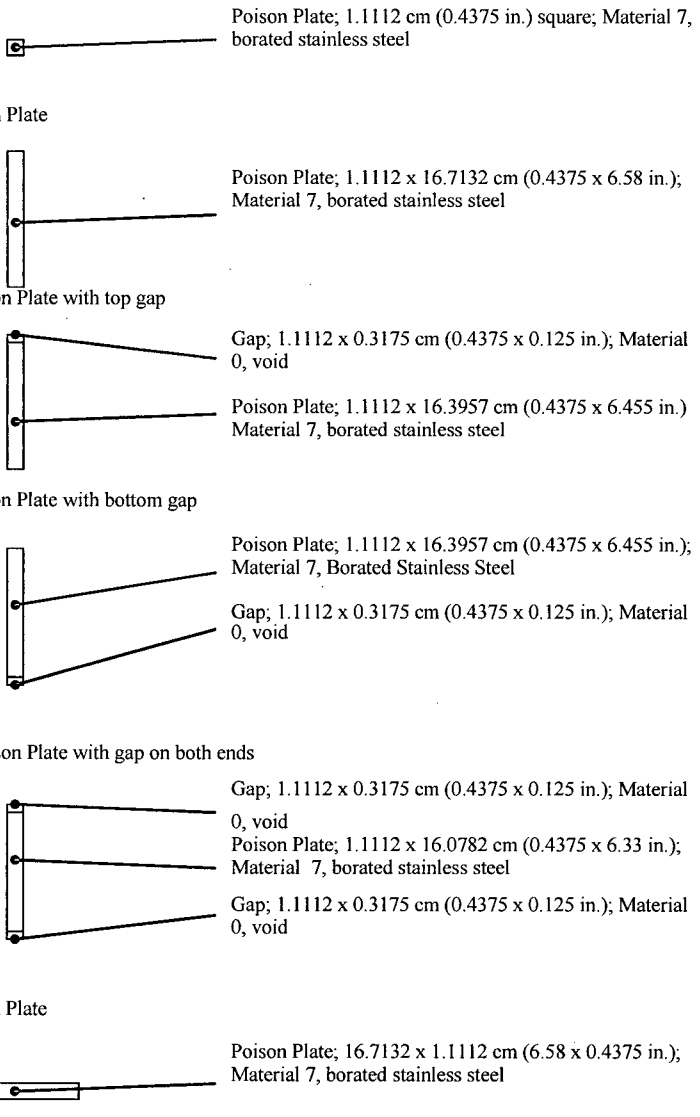

Figure B.6-2
KENO V.a units and Radial Cross Sections of the Model
Part 3 of 20 - (all units 381.00 cm (150 inches) long)

Unit 67 Poison Plate with gap on both ends

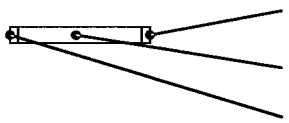

Unit 107 Poison Plate with left gap

Unit 117 Poison Plate with right gap

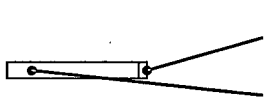

Unit 8 Aluminum Sheet

Unit 58 Aluminum Sheet with top gap

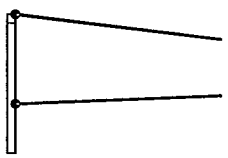

Figure B.6-2
KENO V.a units and Radial Cross Sections of the Model
Part 4 of 20 - (all units 381.00 cm (150 inches) long)

Unit 68 Aluminum Sheet with bottom gap

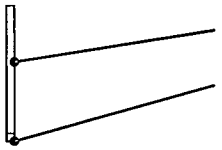

Thermal Shunt; 0.4826 x 16.3957 cm (0.19 x 6.455 in.); Material 8 aluminum

Gap; 0.4826 x 0.3175 cm (0.19 x 0.125 in.); Material 0, void

Unit 108 Aluminum Sheet with gap on both ends

Gap; 0.4826 x 0.3175 cm (0.19 x 0.125 in.); Material 0, void

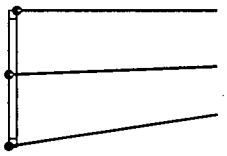

Plate; 0.4826 x 16.0782 cm (0.19 x 6.33 in.); Material 8, aluminum

Gap; 0.4826 x 0.3175 cm (0.19 x 0.125 in.); Material 0, void

Unit 9, 13 Aluminum Sheet

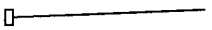

Thermal Shunt; 0.4826 x 1.1112 cm (0.19 x 0.4375 in.); Material 8, aluminum

Unit 10 Aluminum Sheet

Thermal Shunt; 16.7132 x 0.4826 cm (6.58 x 0.19 in.); Material 8, aluminum

Unit 60 Aluminum Sheet with gap on both ends

Gap; 0.3175 x 0.4826 cm (0.125 x 0.19 in.); Material 0, void

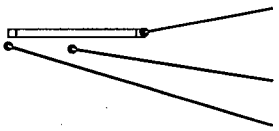

Poison Plate; 16.0782 x 0.4826 cm (6.33 x 0.19 in.); Material 8, aluminum

Gap; 0.3175 x 0.4826 cm (0.125 x 0.19 in.); Material 0, void

Figure B.6-2
KENO V.a units and Radial Cross Sections of the Model
Part 5 of 20 - (all units 381.00 cm (150 inches) long)

Unit 100 Aluminum Sheet with left gap

Gap; 0.3175 x 0.4626 cm (0.125 x 0.19 in.); Material 0, void

Plate; 16.3957 x 0.4626 cm (6.455 x 0.19 in.); Material 8, aluminum

Unit 110 Aluminum Sheet with right gap

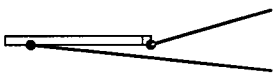

Gap; 0.3175 x 0.4626 cm (0.125 x 0.19 in.); Material 0, void

Plate; 16.3957 x 0.4626 cm (6.455 x 0.19 in.); Material 8, aluminum

Unit 1 Aluminum Sheet

Thermal Shunt; 0.4826 cm square (0.19); Material 8, aluminum

Unit 12 Gap

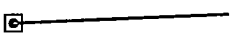

Gap; 1.1112 cm (0.4375 in.) square; Material 0, void

Unit 14 Poison Plate

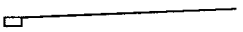

Poison Plate; 1.1112 x 0.4826 cm (0.4375 x 0.19 in.); Material 7, borated stainless steel

Unit 15, 24 Poison Plate

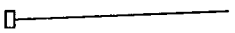

Poison Plate; 0.4826 x 1.1112 cm (0.19 x 0.4375 in.); Material 7, borated stainless steel

Figure B.6-2
KENO V.a units and Radial Cross Sections of the Model
Part 6 of 20 - (all units 381.00 cm (150 inches) long)

Unit 16 Aluminum Sheet

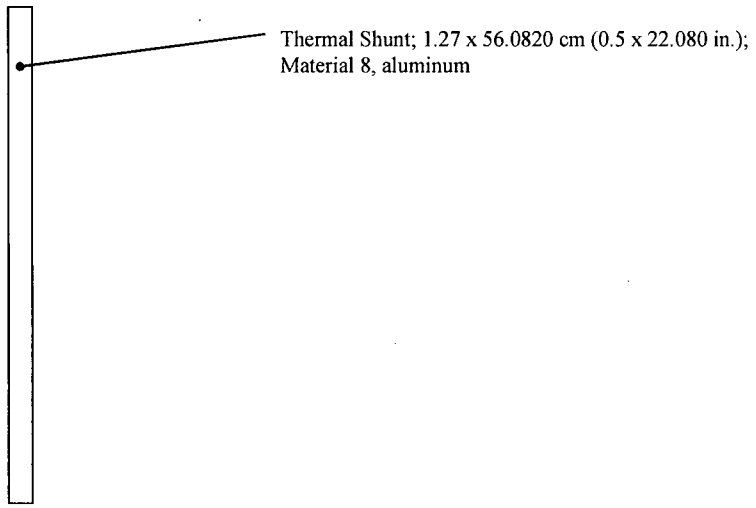

Unit 17 Aluminum Sheet

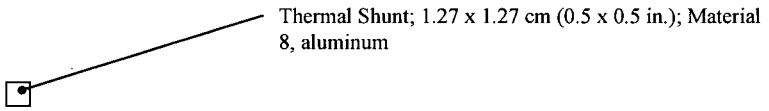

Unit 18 Aluminum Sheet

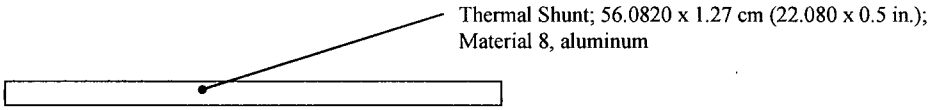

Figure B.6-2
KENO V.a units and Radial Cross Sections of the Model
Part 7 of 20 - (all units 381.00 cm (150 inches) long)

Unit 21 Aluminum Sheet

Thermal Shunt; 1.1112 x 16.7132 cm (0.4375 x 6.58 in.); Material 8, aluminum

Unit 22, 23 Aluminum Sheet

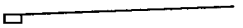

Thermal Shunt; 1.1112 x 0.4826 cm (0.4375 x 0.19 in.); Material 8, aluminum

Unit 25 Aluminum Sheet with gap on both ends

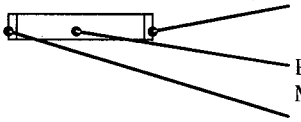

Gap; 0.3175 x 1.5874 cm (0.125 x 0.625 in.); Material 0, void

Poison Plate; 16.0782 x 1.5874 cm (6.33 x 0.625 in.); Material 8, aluminum

Gap; 0.3175 x 1.5874 cm (0.125 x 0. 625 in.); Material 0, void

Unit 26 Poison Plate

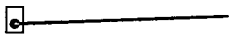

Poison Plate; 1.1112 x 1.5874 cm (0.4375 x 0.625 in); Material 7, borated stainless steel

Unit 27 Aluminum Sheet with gap on both ends

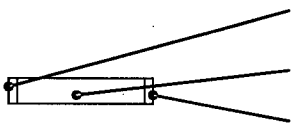

Gap; 0.3175 x 1.27 cm (0.125 x 0.5 in.); Material 0, void

Plate; 16.0782 x 1.27 cm (6.33 x 0.5 in.); Material 8, aluminum

Gap; 0.3175 x 1.27 cm (0.125 x 0.5 in.); Material 0, void

Unit 28 Poison Plate

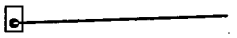

Poison Plate; 1.1112 x 1.27 cm (0.4375 x 0.5 in); Material 7, borated stainless steel

Figure B.6-2
KENO V.a units and Radial Cross Sections of the Model
Part 8 of 20 - (all units 381.00 cm (150 inches) long)

Unit 31Aluminum Sheet

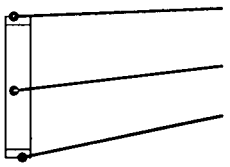

Unit 32 Aluminum Sheet with gap on both ends

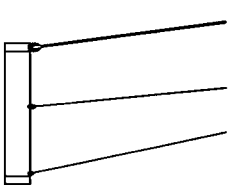

Unit 33 Poison Plate

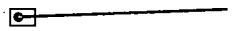

Unit 34 Poison Plate

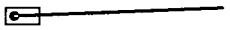

Figure B.6-2
KENO V.a units and Radial Cross Sections of the Model
Part 9 of 20 - (all units 381.00 cm (150 inches) long)

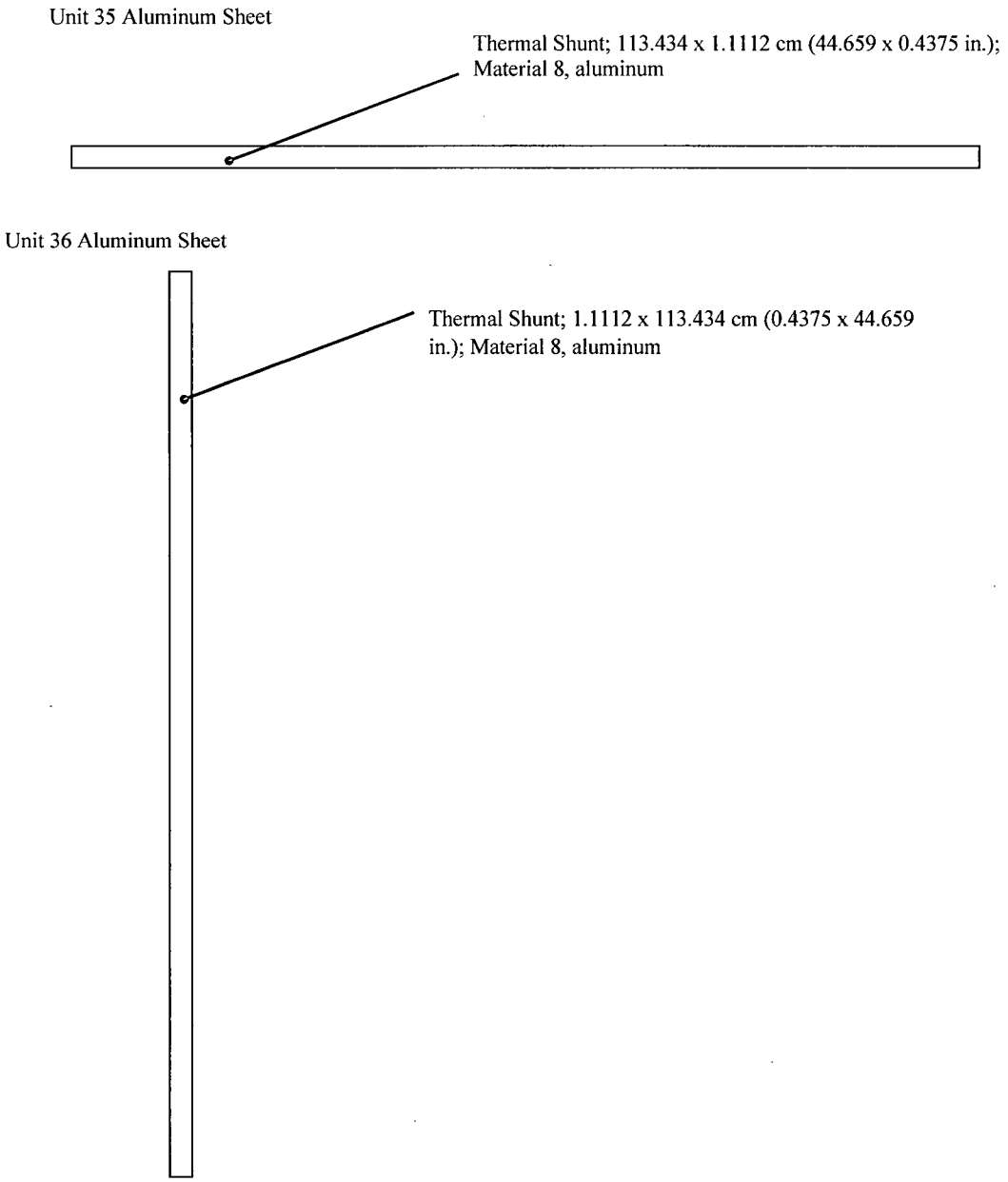

Figure B.6-2
KENO V.a units and Radial Cross Sections of the Model
Part 10 of 20 - (all units 381.00 cm (150 inches) long)

Array 2 Top Left 3x3 Array

Unit numbers shown for each row from left to right)

7, 24 poison; 107 poison w/ Lf gap; 117

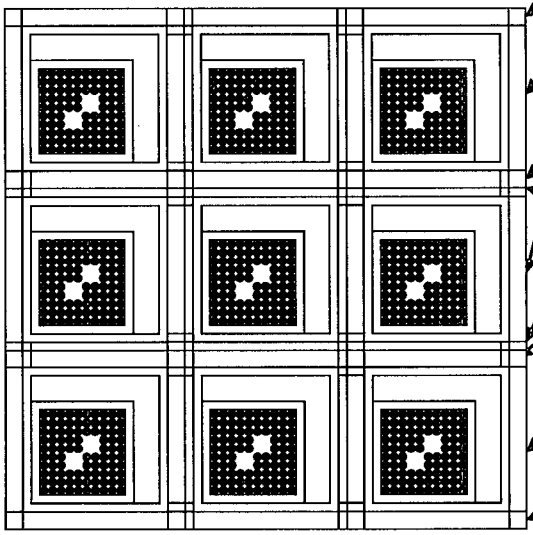

Units: 12, 7, 5, 15, 7, 15, 5, 7, 12 (Unit 12 void; rest poison)

Units: 6, 2, 106, 108, 2, 108, 106, 2, 6 (Unit 6 poison; Unit 2 fuel compartment; Unit 106 poison with gaps; Unit 108 al with gaps)

Units: 5, 107, 5, 24, 7, 24, 5, 117, 5 (Units 5, 7, 24 poison; 107 poison w/ Lf gap; 117 poison w/ Rt gap)

Units: 14, 100, 23, 11, 10, 11, 23, 110, 14 (Unit 14, poison; 100 al w/ Lf gap; 110 al w/ Rt gap; Unit 23, 11, 10 al)

Units: 5, 107, 5, 24, 7, 24, 5, 117, 5 (Units 5, 7, 24 poison; 107 poison w/ Lf gap; 117 poison w/ Rt gap

Units: 6, 2, 106, 108, 2, 108, 106, 2, 6 (Unit 6 poison; Unit 2 fuel compartment; Unit 106 poison with gaps; Unit 108 al with gaps)

Units: 12, 4, 3, 13, 4, 13, 3, 4, 12 (Unit 12 void; rest al)

Unit 70 3x3 with stainless wrap

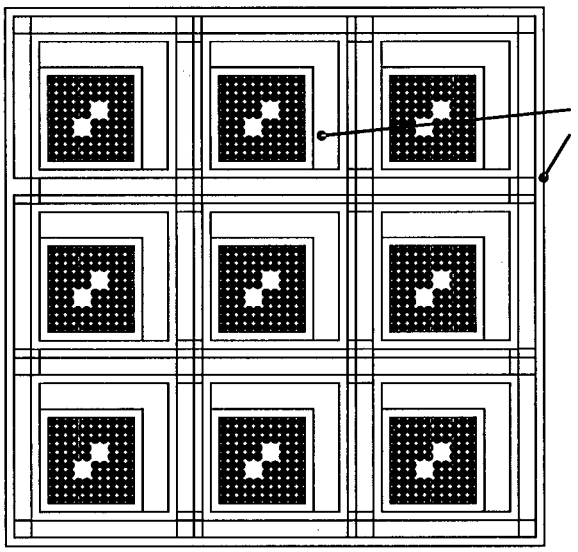

3x3 Assembly; Array 2 inside wrap Wrap; 56.082 cm (22.080 in.) square (0.105 in. thick); Material 4, stainless steel

Figure B.6-2
KENO V.a units and Radial Cross Sections of the Model
Part 11 of 20 - (all units 381.00 cm (150 inches) long)

Array 3 Top Right 3x3 Array

Unit numbers shown for each row from left to right

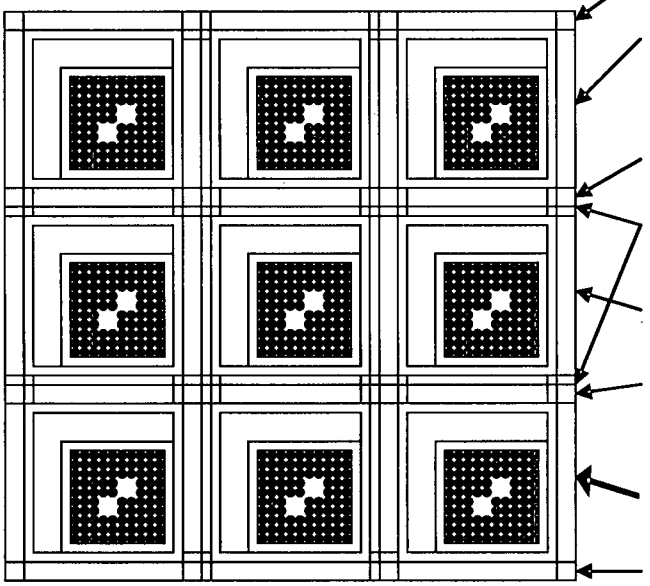

Units: 12, 7, 5, 24, 7, 24, 5, 7, 12 (Unit 12 void; rest poison)

Units: 6, 20, 56, 58, 20, 58, 56, 20, 21 (Unit 6 poison, Unit 20 fuel compartment; Unit 56 poison w/ top gap; Unit 58 al w/ top gap; 21 al)

Units: 5, 67, 5, 9, 67, 9, 5, 67, 3 (Unit 5 poison; 67 poison w/ end gaps; 9 al; 3 al)

Units: 14, 60, 14, 11, 60, 11, 14, 60, 22 (Unit 14 poison; 60 al w/ end gaps; 11, 22 al)

Units: 6, 20, 6, 8, 20, 8, 6, 20, 21 (Unit 6 poison, Unit 20 fuel compartment; 8, 21 al)

Units: 5, 67, 5, 9, 67, 9, 5, 67, 3 (Unit 5 poison; 67 poison w/ end gaps; 9 al; 3 al)

Units: 6, 20, 66, 68, 20, 68, 66, 20, 21 (Unit 6 poison, Unit 20 fuel compartment; Unit 66 poison w/ bottom gap; Unit 88 al w/ bottom gap; 21 al)

Units: 12, 7, 5, 15, 7, 15, 5, 7, 12 (Unit 12 void; rest poison)

Unit 71 3x3 with stainless wrap

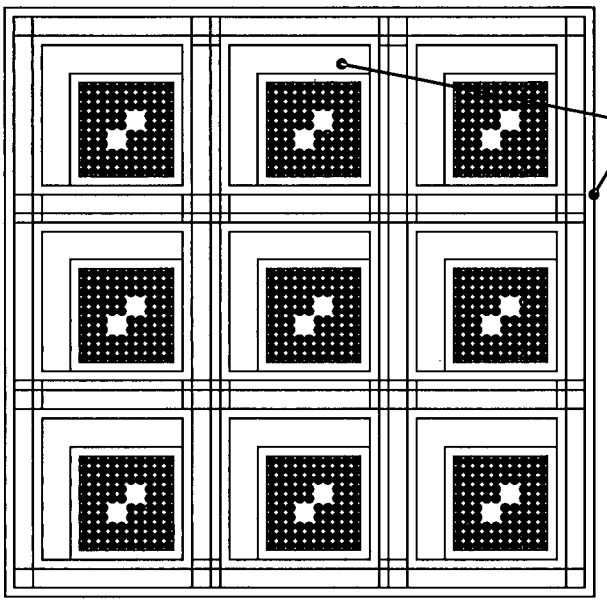

3x3 Assembly; Array 3 inside wrap

Wrap; 56.082 cm (22.080 in.) square (0.105 in. thick); Material 4, stainless steel

Figure B.6-2
KENO V.a units and Radial Cross Sections of the Model
Part 12 of 20 - (all units 381.00 cm (150 inches) long)

Array 4 Bottom Left 3x3 Array

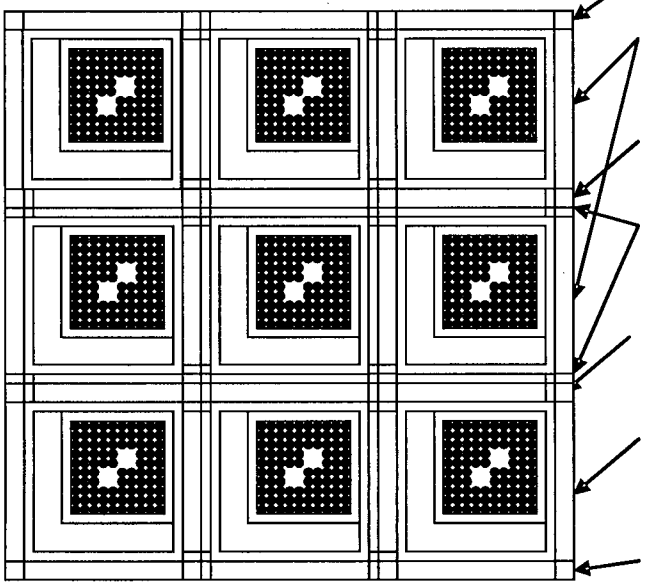

Unit numbers shown for each row from left to right

Units: 12, 4, 3, 13, 4, 13, 3, 4, 12 (Unit 12 void; rest al

Units: 6, 30, 106, 108, 30, 108, 106, 30, 6(Unit 6 poison; Unit 30 fuel compartment; Unit 106 poison with gaps; Unit 108 al with gap

Units: 5, 107, 5, 24, 7, 24, 5, 117, 5 (Units 5, 7, 24 poison; 107 poison w/ Lf gap; 117 poison w/ Rt gap)

Units: 14, 100, 23, 11, 10, 11, 23, 110, 14 (Unit 14, poison; 100 al w/ Lf gap; 110 al w/ Rt gap; Unit 23, 11, 10 al)

Units: 5, 107, 5, 24, 7, 24, 5, 117, 5 (Units 5, 7, 24 poison; 107 poison w/ Lf gap; 117 poison w/ Rt gap)

Units: 6, 30, 106, 108, 30, 108, 106, 30, 6 (Unit 6 poison; Unit 30 fuel compartment; Unit 106 poison with gaps; Unit 108 al with gaps

Units: 12, 7, 5, 15, 7, 15, 5, 7, 12 (Unit 12 void; rest poison)

Unit 72 3x3 with stainless wrap

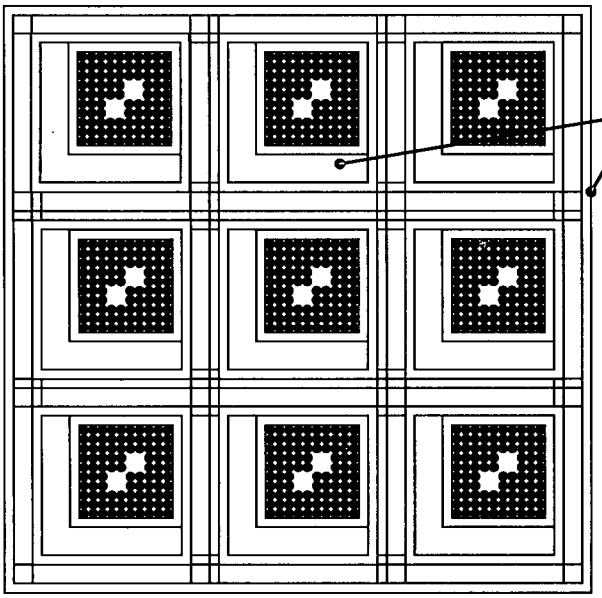

3x3 Assembly; Array 4 inside wrap Wrap; 56.082 cm (22.080 in.) square (0.105 in. thick); Material 4, stainless steel

Figure B.6-2
KENO V.a units and Radial Cross Sections of the Model
Part 13 of 20 - (all units 381.00 cm (150 inches) long)

Array 5 Bottom Right 3x3 Array

Unit numbers shown for each row from left to right)

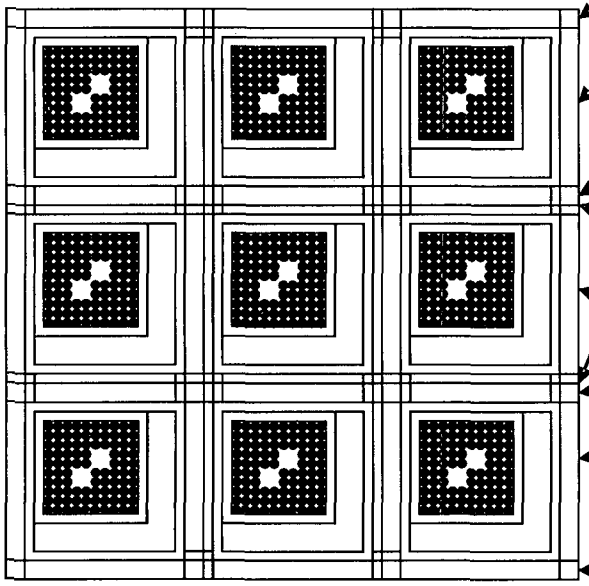

Units: 12, 7, 5, 24, 7, 24, 5, 7, 12 (Unit 12 void; rest poison

Units: 21, 40, 56, 58, 40, 58, 56, 40, 6 (Unit 6 poison; Unit 40 fuel compartment; Unit 56 poison w/ top gap; Unit 58 al w/ top gap; 21 al

Units: 3, 67, 5, 9, 67, 9, 5, 67, 5 (Unit 5 poison; 67 poison w/ end gaps; 9 al; 3 al)

Units: 22, 60, 14, 11, 60, 11, 14, 60, 14 (Unit 14 poison; 60 al w/ end gaps; 11, 22 al)

Units: 21, 40, 6, 8, 40, 8, 6, 40, 6 (Unit 6 poison, Unit 40 fuel compartment; 8, 21 al)

Units: 3, 67, 5, 9, 67, 9, 5, 67, 5 (Unit 5 poison; 67 poison w/ end gaps; 9 al; 3 al)

Units: 21, 40, 66, 68, 40, 68, 66, 40, 6 (Unit 6 poison, Unit 40 fuel compartment; Unit 66 poison w/ bottom gap; Unit 88 al w/ bottom gap; 21 al)

Units: 12, 7, 5, 15, 7, 15, 5, 7, 12 (Unit 12 void; rest poison)

Unit 73 3x3 with stainless wrap

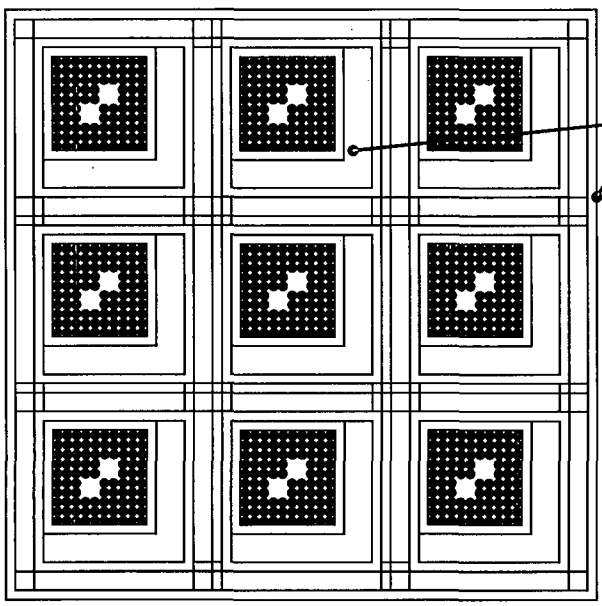

3x3 Assembly; Array 5 inside wrap

Wrap; 56.082 cm (22.080 in.) square (0.105 in. thick); Material 5, stainless steel

Figure B.6-2
KENO V.a units and Radial Cross Sections of the Model
Part 14 of 20 - (all units 381.00 cm (150 inches) long)

Array 7 Right 1x2 Array

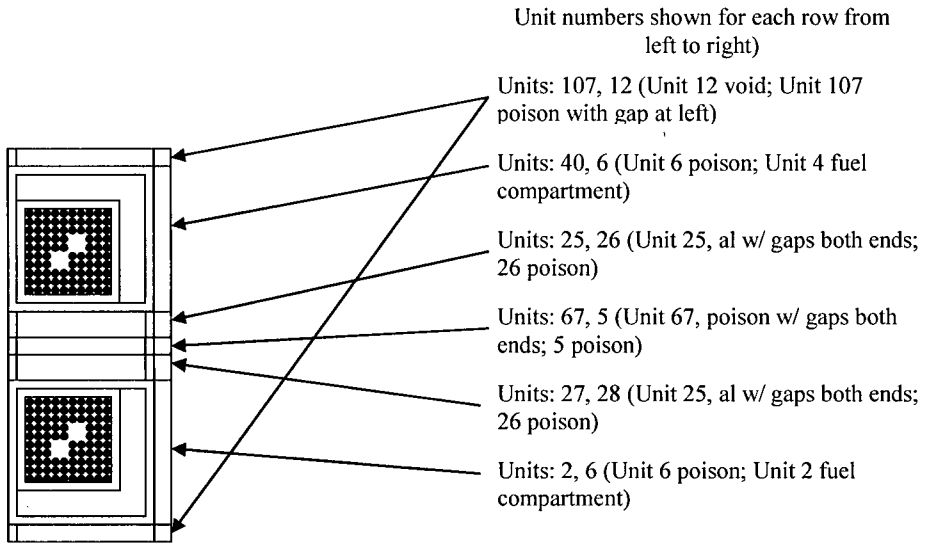

Unit 74 1x2 with stainless wrap

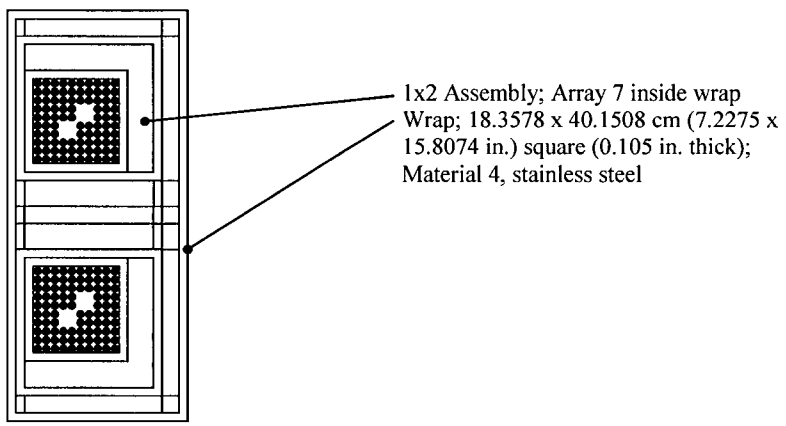

Figure B.6-2
KENO V.a units and Radial Cross Sections of the Model
Part 15 of 20 - (all units 381.00 cm (150 inches) long)

Array 8 Top 2x1 Array

Unit numbers shown for each row from left to right)

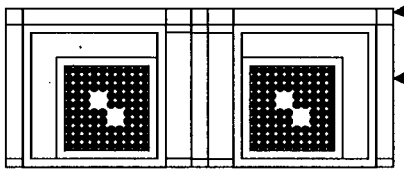

Units: 12, 7, 33, 5, 34, 7, 12 (Unit 12 void; Rest poison;)

Units: 66, 20, 31, 106, 32, 2, 66 (Unit 66 poison w/ bottom gap; Units 2, 20 fuel compartment; Units 31, 32 al w/ gap both ends; Unit 106 poison w/ gap both ends)

Unit 75 2x1 with stainless wrap

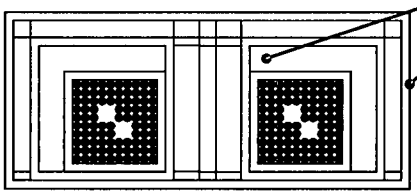

2x1 Assembly; Array 8 inside wrap Wrap; 40.1508 x 18.3578 cm (15.8074 x 7.2275 in.) square (0.105 in. thick); Material 4, stainless steel

Figure B.6-2
KENO V.a units and Radial Cross Sections of the Model
Part 16 of 20 - (all units 381.00 cm (150 inches) long)

Array 9 Left 1x2 Array

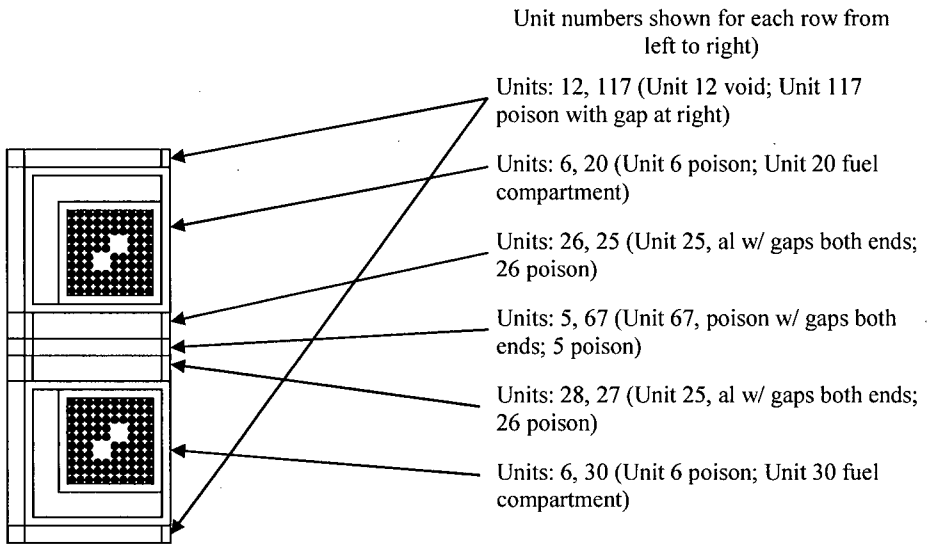

Unit 76 1x2 with stainless wrap

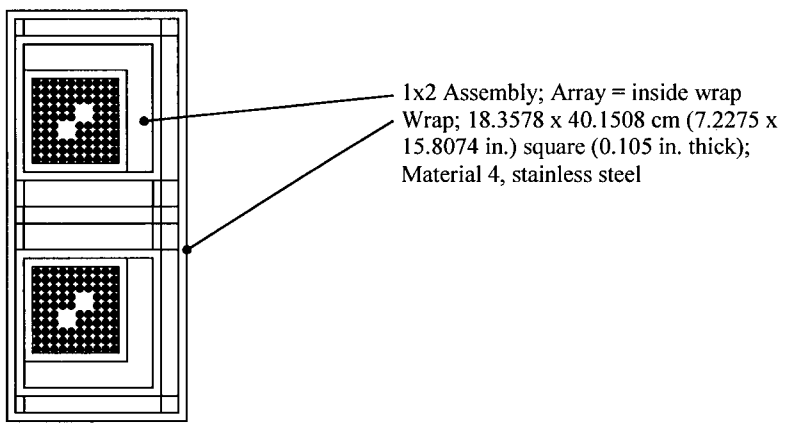

Figure B.6-2
KENO V.a units and Radial Cross Sections of the Model
Part 17 of 20 - (all units 381.00 cm (150 inches) long)

Array 10 Bottom 2x1 Array

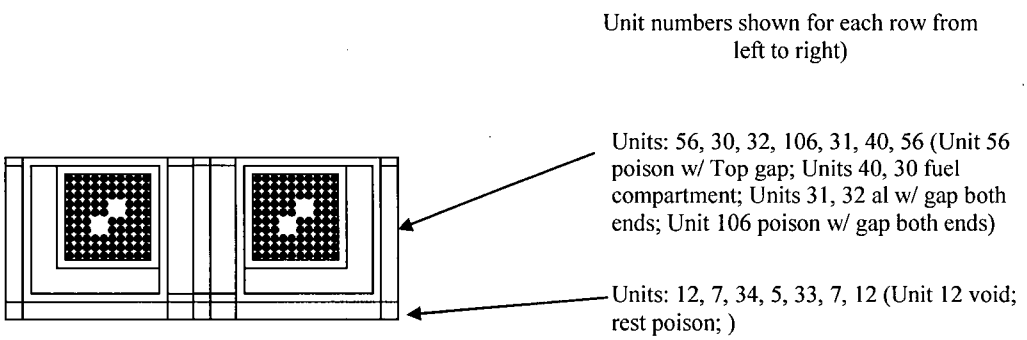

Unit 77 2x1 with stainless wrap

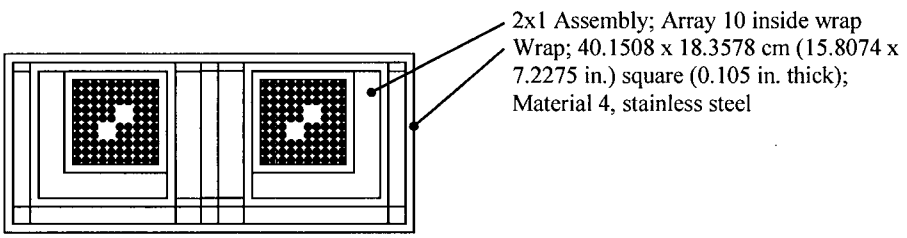

Figure B.6-2
KENO V.a units and Radial Cross Sections of the Model
Part 18 of 20 - (all units 381.00 cm (150 inches) long)

Array 6 Collection of 3x3 Arrays with Al

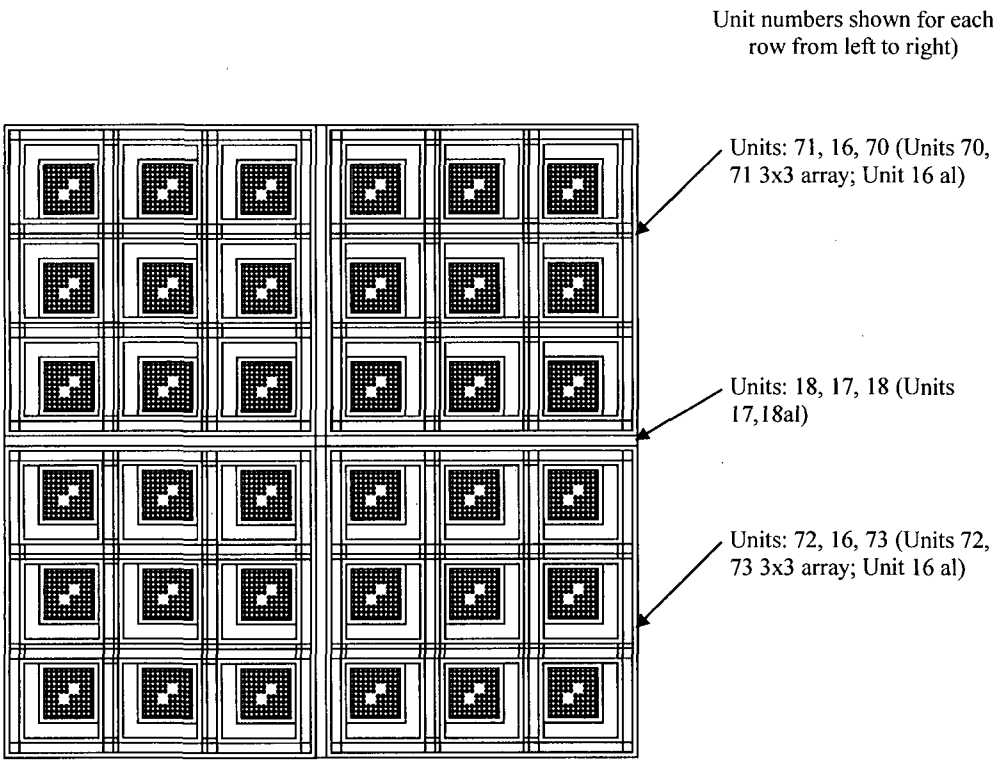

Figure B.6-2
KENO V.a units and Radial Cross Sections of the Model
Part 19 of 20 - (all units 381.00 cm (150 inches) long)

Global Unit 90 Cask and Canister

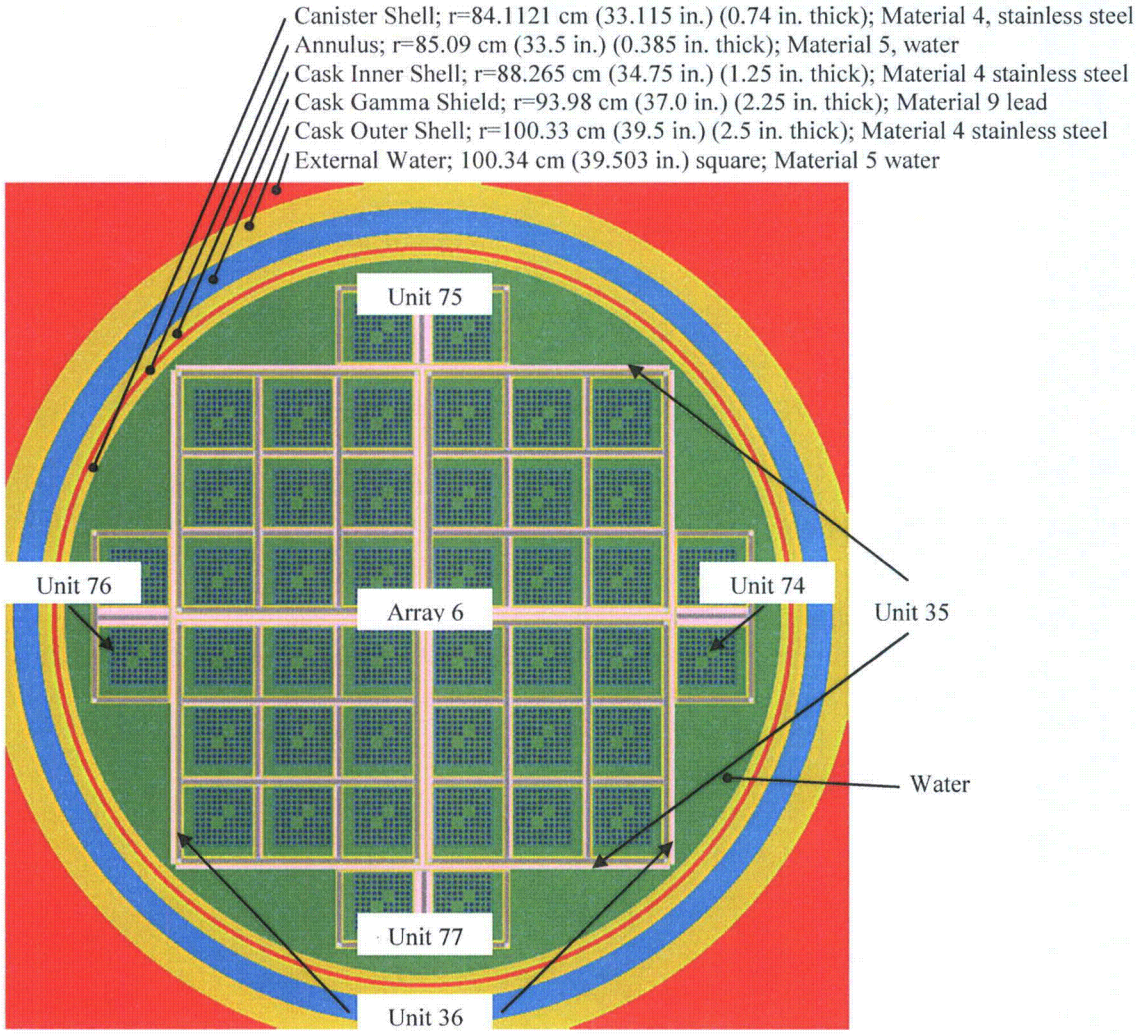

Figure B.6-2
KENO V.a units and Radial Cross Sections of the Model
Part 20 of 20 - (all units 381.00 cm (150 inches) long)

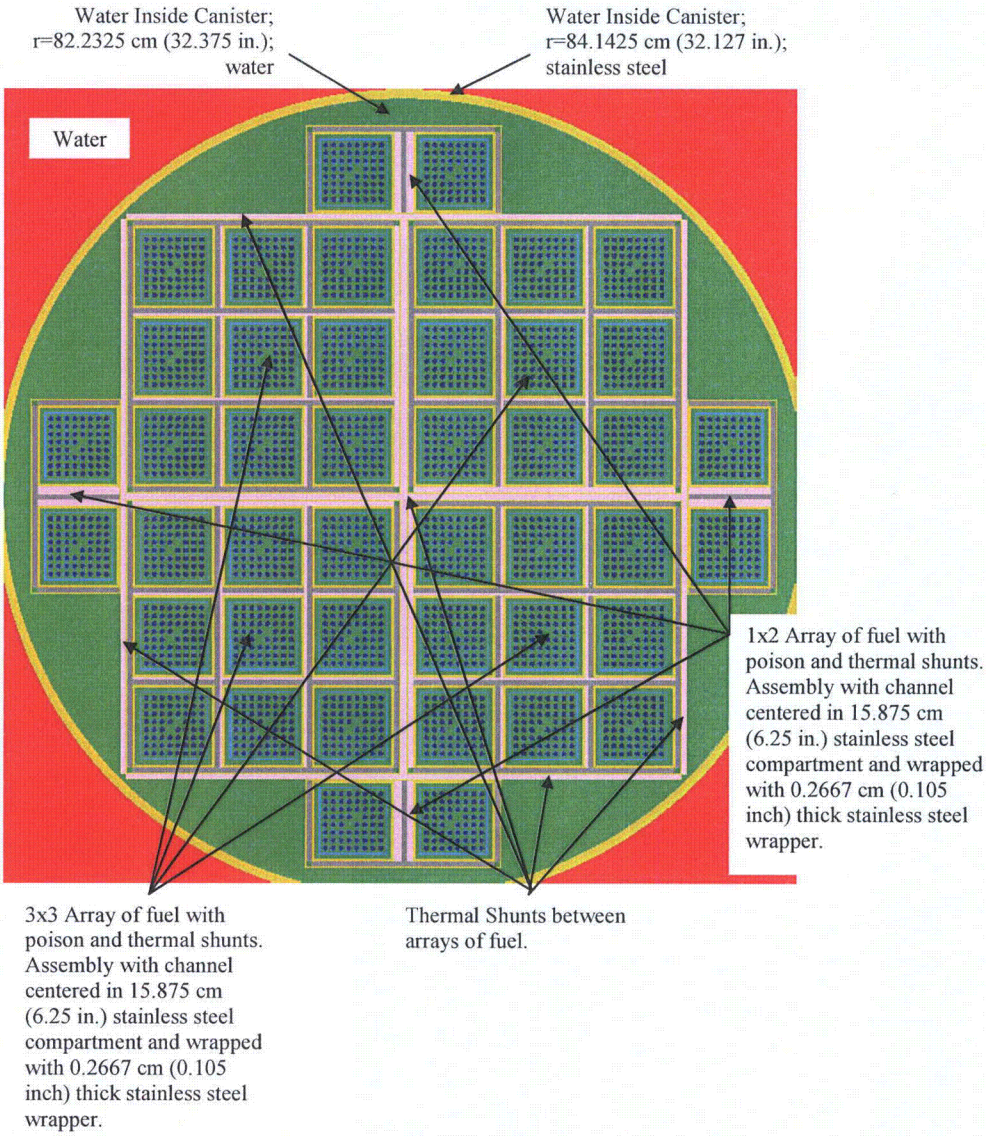

Figure B.6-3
Representative KENO V.a Model Cross Section – Most Reactive Fuel

1	1	1	1	1	1	1
1	1	1	1	1	1	1
1	1	1	1	1	1	1
1	1	1	1	1	1	1
1	1	1	1	1	1	1
1	1	1	1	1	1	1
1	1	1	1	1	1	1

GE1, GE2, GE3, ENC-IIIA
7x7 Array
1 = Fuel Rod

1	1	1	1	1	1	1
1	1	1	1	1	1	1
1	1	1	1	1	1	1
1	1	1	88	1	1	1
1	1	1	1	1	1	1
1	1	1	1	1	1	1
1	1	1	1	1	1	1

ENC-III,
7x7 Array
1 = Fuel Rod
88 = Water Rod

1	1	1	1	1	1	1	1
1	1	1	1	1	1	1	1
1	1	1	1	1	1	1	1
1	1	1	88	1	1	1	1
1	1	1	1	1	1	1	1
1	1	1	1	1	1	1	1
1	1	1	1	1	1	1	1
1	1	1	1	1	1	1	1

GE4,
8x8 Array
1 = Fuel Rod
88 = Water Rod

1	1	1	1	1	1	1	1
1	1	1	1	1	1	1	1
1	1	1	1	1	1	1	1
1	1	1	88	88	1	1	1
1	1	1	88	88	1	1	1
1	1	1	1	1	1	1	1
1	1	1	1	1	1	1	1
1	1	1	1	1	1	1	1

ENC Va,b,
GE8 Type II, GE9
8x8 Array
1 = Fuel Rod
88 = Water Rod or Zirc Rod

1	1	1	1	1	1	1	1
1	1	1	1	1	1	1	1
1	1	1	1	1	1	1	1
1	1	1	88	1	1	1	1
1	1	1	1	88	1	1	1
1	1	1	1	1	1	1	1
1	1	1	1	1	1	1	1
1	1	1	1	1	1	1	1

FANP8, GE5, GE8
8x8 Array
1 = Fuel Rod
88 = Water Rod

1	1	1	1	1	1	1	1
1	1	1	1	1	1	1	1
1	1	1	88	1	88	1	1
1	1	1	1	88	1	1	1
1	1	1	88	1	88	1	1
1	1	1	1	1	1	1	1
1	1	1	1	1	1	1	1
1	1	1	1	1	1	1	1

GE4, 59 rods, Config. 2
8x8 Array
1 = Fuel Rod
88 = Water Rod

1	1	1	1	1	1	1	1
1	1	1	1	1	1	1	1
1	1	1	1	88	1	1	1
1	1	1	88	88	88	1	1
1	1	1	1	88	1	1	1
1	1	1	1	1	1	1	1
1	1	1	1	1	1	1	1
1	1	1	1	1	1	1	1

GE4, 59 rods, Config. 3
8x8 Array
1 = Fuel Rod
88 = Water Rod

1	1	1	1	1	1	1	1
1	88	1	1	1	1	88	1
1	1	1	1	1	1	1	1
1	1	1	1	1	1	1	1
1	1	1	1	88	1	1	1
1	1	1	1	1	1	1	1
1	88	1	1	1	1	88	1
1	1	1	1	1	1	1	1

GE4, 59 rods, Config. 4
8x8 Array
1 = Fuel Rod
88 = Water Rod

1	1	1	1	1	1	1	1
1	1	88	1	1	1	1	1
1	1	1	1	1	1	1	1
1	1	1	88	88	1	1	1
1	1	1	88	1	1	1	1
1	1	1	1	1	1	1	1
1	1	1	1	1	88	1	1
1	1	1	1	1	1	1	1

GE4, 59 rods, Config. 1
8x8 Array
1 = Fuel Rod
88 = Water Rod

Figure B.6-4
Fuel Assembly Layouts

1	1	1	1	1	1	1	1
1	1	1	1	1	1	1	1
1	1	1	1	1	1	1	1
1	1	1	88	88	1	1	1
1	1	1	88	88	1	1	1
1	1	1	1	1	1	1	1
1	1	1	1	1	1	1	1
1	1	1	1	1	1	1	1

GE4, 60 rods
8x8 Array
1 = Fuel Rod

1	1	1	1	1	1	1	1
1	1	1	1	1	1	1	1
1	1	1	1	1	1	1	1
1	1	1	88	88	1	1	1
1	1	1	1	88	1	1	1
1	1	1	1	1	1	1	1
1	1	1	1	1	1	1	1
1	1	1	1	1	1	1	1

GE4, 61 rods
8x8 Array
1 = Fuel Rod
88 = Water Rod

1	1	1	1	1	1	1	1
1	1	1	1	1	1	1	1
1	1	1	1	1	1	1	1
1	1	1	88	1	1	1	1
1	1	1	1	88	1	1	1
1	1	1	1	1	1	1	1
1	1	1	1	1	1	1	1
1	1	1	1	1	1	1	1

GE4, 62 rods
8x8 Array
1 = Fuel Rod
88 = Water Rod

1	1	1	1	1	1	1	1
1	1	1	1	1	1	1	1
1	1	1	1	1	1	1	1
1	1	1	88	1	1	1	1
1	1	1	1	1	1	1	1
1	1	1	1	1	1	1	1
1	1	1	1	1	1	1	1
1	1	1	1	1	1	1	1

GE4, 63 rods
8x8 Array
1 = Fuel Rod
88 = Water Rod

1	1	1	1	1	1	1	1
1	1	1	1	1	1	1	1
1	1	1	1	1	1	1	1
1	1	1	1	1	1	1	1
1	1	1	1	1	1	1	1
1	1	1	1	1	1	1	1
1	1	1	1	1	1	1	1
1	1	1	1	1	1	1	1

GE4, 64 rods
8x8 Array
1 = Fuel Rod
88 = Water Rod

1	1	1	1	1	1	1	1	1
1	1	1	1	1	1	1	1	1
1	1	1	1	1	1	1	1	1
1	1	1	88	88	1	1	1	1
1	1	1	88	88	88	1	1	1
1	1	1	1	88	88	1	1	1
1	1	1	1	1	1	1	1	1
1	1	1	1	1	1	1	1	1
1	1	1	1	1	1	1	1	1

GE11, GE13
9x9 Array
1 = Fuel Rod
88 = Water Rod

1	1	1	1	1	1	1	1	1
1	1	1	1	1	1	1	1	1
1	1	1	1	1	1	1	1	1
1	1	1	1	1	1	1	1	1
1	1	1	88	1	1	1	1	1
1	1	1	88	88	1	1	1	1
1	1	1	88	88	1	1	1	1
1	1	1	1	1	1	1	1	1
1	1	1	1	1	1	1	1	1

FANP9
9x9 Array
1 = Fuel Rod
88 = Water Rod

1	1	1	1	1	1	1	1	1
1	1	1	1	1	1	1	1	1
1	1	1	1	1	1	1	1	1
1	1	1	88	88	88	1	1	1
1	1	1	88	88	88	1	1	1
1	1	1	88	88	88	1	1	1
1	1	1	1	1	1	1	1	1
1	1	1	1	1	1	1	1	1
1	1	1	1	1	1	1	1	1

QFA
9x9 Array
1 = Fuel Rod
88 = Water Rod

1	1	1	1	1	1	1	1	1	1
1	1	1	1	1	1	1	1	1	1
1	1	1	1	1	1	1	1	1	1
1	1	1	1	1	1	1	1	1	1
1	1	1	1	1	1	1	1	1	1
1	1	1	1	1	1	1	1	1	1
1	1	1	1	1	1	1	1	1	1
1	1	1	1	1	1	1	1	1	1
1	1	1	1	1	1	1	1	1	1
1	1	1	1	1	1	1	1	1	1

AC LeCrosse,
10x10 Array
1 = Fuel Rod
88 = Water Rod

Figure B.6-4
Fuel Assembly Layouts
(continued)

1	1	1	1	1	1	1	1	1	1
1	1	1	1	1	1	1	1	1	1
1	1	1	1	1	1	1	1	1	1
1	1	1	88	88	88	1	1	1	1
1	1	1	88	88	88	1	1	1	1
1	1	1	88	88	88	1	1	1	1
1	1	1	1	1	1	1	1	1	1
1	1	1	1	1	1	1	1	1	1
1	1	1	1	1	1	1	1	1	1
1	1	1	1	1	1	1	1	1	1

ATRIUM-10
10x10 Array
1 = Fuel Rod
88 = Water Rod

1	1	1	1	1	1	1	1	1	1
1	1	1	1	1	1	1	1	1	1
1	1	1	1	1	1	1	1	1	1
1	1	1	88	88	1	1	1	1	1
1	1	1	88	88	1	1	1	1	1
1	1	1	1	1	88	88	1	1	1
1	1	1	1	1	88	88	1	1	1
1	1	1	1	1	1	1	1	1	1
1	1	1	1	1	1	1	1	1	1
1	1	1	1	1	1	1	1	1	1

GE12
10x10 Array
1 = Fuel Rod
88 = Water Rod

1	1	1	1	88	1	1	1	1	
1	1	1	1	88	1	1	1	1	
1	1	1	1	88	1	1	1	1	
1	1	1	1	88	1	1	1	1	
88	88	88	88	88	88	88	88	88	
1	1	1	1	88	1	1	1	1	
1	1	1	1	88	1	1	1	1	
1	1	1	1	88	1	1	1	1	
1	1	1	1	88	1	1	1	1	

SVEA-64
4x(4x4) Array
1 = Fuel Rod
88 = Water Channel

88	1	1	1	1	88	1	1	1	1	88
1	1	1	1	1	88	1	1	1	1	1
1	1	1	1	1	88	1	1	1	1	1
1	1	1	1	1	88	1	1	1	1	1
1	1	1	1	88	88	88	1	1	1	1
88	88	88	88	88	88	88	88	88	88	88
1	1	1	1	88	88	88	1	1	1	1
1	1	1	1	88	1	1	1	1	1	1
1	1	1	1	88	1	1	1	1	1	1
1	1	1	1	88	1	1	1	1	1	1
1	1	1	1	88	1	1	1	1	1	1

SVEA-92
4x(5x5-2) Array
1 = Fuel Rod
88 = Water Channel

1	1	1	1	1	88	1	1	1	1	1
1	1	1	1	1	88	1	1	1	1	1
1	1	1	1	1	88	1	1	1	1	1
1	1	1	1	1	88	1	1	1	1	1
1	1	1	1	88	88	88	1	1	1	1
88	88	88	88	88	88	88	88	88	88	88
1	1	1	1	88	88	88	1	1	1	1
1	1	1	1	1	88	1	1	1	1	1
1	1	1	1	1	88	1	1	1	1	1
1	1	1	1	1	88	1	1	1	1	1
88	1	1	1	1	88	1	1	1	1	88

SVEA-96
4x(5x5-1) Array
1 = Fuel Rod
88 = Water Channel

1	1	1	1	1	88	1	1	1	1	1
1	1	1	1	1	88	1	1	1	1	1
1	1	1	1	1	88	1	1	1	1	1
1	1	1	1	1	88	1	1	1	1	1
1	1	1	1	88	88	88	1	1	1	1
88	88	88	88	88	88	88	88	88	88	88
1	1	1	1	88	88	88	1	1	1	1
1	1	1	1	1	88	1	1	1	1	1
1	1	1	1	1	88	1	1	1	1	1
1	1	1	1	1	88	1	1	1	1	1
1	1	1	1	1	88	1	1	1	1	1

SVEA-100
4x(5x5) Array
1 = Fuel Rod
88 = Water Channel

Figure B.6-4
Fuel Assembly Layouts
(concluded)

68	67	67	67	68	68	69
67	1	1	1	1	67	68
1	1	1	1	1	1	68
1	1	1	1	1	1	67
1	1	1	1	1	1	67
67	1	1	1	1	1	67
67	67	1	1	1	67	68

GE2
7x7 Array
1 = Fuel Rod, w/ 5.39 wt.%
67 = Fuel Rod, w/3.57 wt. %
68 = Fuel Rod, w/3.11 wt. %
69 = Fuel Rod, w/2.45 wt.%

67	68	68	68	68	68	67	1
68	69	69	69	69	69	68	67
69	69	69	69	69	69	69	68
69	69	69	88	69	69	69	68
69	69	69	69	88	69	69	68
69	69	69	69	69	69	69	68
69	69	69	69	69	69	69	68
68	69	69	69	69	69	68	67

GE5
8x8 Array
1 = Fuel Rod, w/ 2.44 wt.%
67 = Fuel Rod, w/3.15 wt. %
68 = Fuel Rod, w/3.73 wt. %
69 = Fuel Rod, w/5.07 wt.%

Figure B.6-5
Variable Enrichment Fuel Assembly Layouts

Listing of Disk Numbering and Contents for Computer Files
(all files are Proprietary)

Disk ID No. (size)	Discipline	File Series (topics)	Number of Files
Disk 1 (DVD) (1.98 GB)	Structural	000-README.txt (Summary List of Files)	001
	Structural (Canister)	001-ttn44b_sdep14.inp to 003-ttn44b_sdep14.rst (B.2.13.7–Canister Side Drop Analysis for NCT)	001 to 003 for a total of 3
	Structural (Canister)	004-ttn44b_sdep12.inp to 006-ttn44b_sdep12.rst (B.2.13.7–Canister Side Drop Analysis for HAC)	004 to 006 for a total of 3
	Structural (Basket)	007-44b_0sde4r10.inp to 009-44b_0sde4r10.rst (B.2.13.8 – Basket Side Drop Analysis for NCT)	007 to 009 for a total of 3
	Structural (Basket)	010-44b_10sdcr.inp to 012-44b_10sdcr.rst (B.2.13.8 – Basket Limit Load Analysis)	010 to 012 for a total of 3
	Structural (Basket)	013-44b_0sdbr10.inp to 015-44b_0sdbr10.rst (B.2.13.8 – Basket Side Drop on Rails- HAC)	013 to 015 for a total of 3
Disk 2 and Disk 3 (DVDs) (6.69GB)	Structural (Impact Limiter)	016-TAD_BoltsEnd.k to 123-d3plot101 (B.2.13.12 – Input and output files for Impact Limiter 30 ft End Drop LS-Dyna Analysis Performed)	016 to 123 for a total of 108

Listing of Disk Numbering and Contents for Computer Files
(all files are Proprietary)

Disk ID No. (size)	Discipline	File Series (topics)	Number of Files
Disk 4 and Disk 5 and Disk 6 (DVDs) (9.41GB)	Structural (Impact Limiter)	124-TAD_BoltsSide.k to 272-d3plot142 (B.2.13.12 – Input and output files for Impact Limiter 30 ft Side Drop LS-Dyna Analysis Performed)	124 to 272 for a total of 149
	Structural (Impact Limiter)	273-TAD_BoltsEnd1Foot.k to 326-TAD_Slap20.k (B.2.13.12 – Input files for all LS-Dyna Analysis Performed)	273 to 326 for a total of 54
Disk 7 (DVD) (3.62 GB)	Structural (Fuel)	327-SVEA-92_10-2_10X10_side_drop.inp to 329-SVEA-92_10-2_10X10_side_drop.rst (B.2.13.11 – Input and output file for fuel Side Drop- NCT-HAC)	327 to 329 for a total of 3
	Structural (Fuel)	330-10x10_elem.k to 366-abb_10x10_ac.d3plot31 (B.2.13.11– Input and output file for fuel End drop- LS-Dyna analysis)	330 to 366 for a total of 37
Disk 8 (DVD) (2.75 GB)	Structural (Cask)	367-tntadcaskmod01nctsd_30G.inp to 371-tntadcaskmod01nctsd_30G.rst (B.2.13.1– Input and output file for Cask Side Drop- NCT)	367 to 371 for a total of 5
	Structural (Cask)	372-tntadcaskmod01g75top_end_ip.inp to 375-tntadcaskmod01hacg75top_end_ip.rst (B.2.13.1– Input and output file for Cask End Drop- HAC)	372 to 375 for a total of 4

Listing of Disk Numbering and Contents for Computer Files
(all files are Proprietary)

Disk ID No. (size)	Discipline	File Series (topics)	Number of Files
Disk 9 (DVD) (2.77 GB)	Structural (Cask)	376-tntadcaskmod01g75sd_ep.inp to 379-tntadcaskmod01hacg75sd_ep.rst (B.2.13.1– Input and output file for Cask Side Drop- HAC)	376 to 379 for a total of 4
	Structural (Cask)	380-tntadcaskmod01hacbot_cg10_ep.inp to 383-tntadcaskmod01hacbot_cg10_ep.rst (B.2.13.1– Input and output file for Cask 10 degree Slap Down-HAC)	380 to 383 for a total of 4
Disk 10 (DVD) (1.65 GB)	Structural (Cask)	384-tntadcaskmod01hactop_cg66_ip.inp to 387-tntadcaskmod01hactop_cg66_ip.rst (B.2.13.1– Input and output file for Cask CG Over Corner Drop-HAC)	384 to 387 for a total of 4
Disk 11 (DVD) (1.86 GB)	Thermal	Index_thermal_MP197TAD TO.xls	1 file
	Thermal	A001-TAD-TO-44B.inp to A003-TAD-TO-44B.db (MP197TAD TO Model Generation)	A001 to A003 for a total of 3
	Thermal	B001-TO-44B-NCT100.inp to B008-TO-44B-NCT100.out (MP197TAD TO with TN44B DSC and 22 kW - NCT)	B001 to B008 for a total of 8
	Thermal	C001-TO-44B-IC.inp to C010-TO-44B-IC.out (MP197TAD TO with TN44B DSC and 22 kW - Initial Temp. for HAC)	C001 to C010 for a total of 10
	Thermal	D001-TO-44B-Cr.inp to D003-TO-44B-Cr.db (MP197TAD TO Model Generation with Crash Deformations)	D001 to D003 for a total of 3

Listing of Disk Numbering and Contents for Computer Files
(all files are Proprietary)

Disk ID No. (size)	Discipline	File Series (topics)	Number of Files
Disk 12 (DVD) (3.16 GB)	Thermal	E001-TO-44B-HAC-R1.inp to E011-TO-44B-HAC-R1.out These files are zipped into E001_to_E011_files.zip file (MP197TAD TO with TN44B, 22 kW, HAC, Rear Impact Limiter Punctured)	E001 to E011 for a total of 11
	Thermal	F001-TO-44B-CD.inp to F007-TO-44B-CD.out (MP197TAD TO with TN44B, 22 kW, SS Cool-Down)	F001 to F007 for a total of 7
Disk 13 (DVD) (44.2 MB)	Shielding and Criticality	Index_nuclear_TAD_Part71.xls	1 file
	Shielding	A001-TADZ1G1 to A024-TADZ3G4mesh (MP197TAD TO with TN44B – Response function – Gamma)	A001 to A024 for a total of 24
	Shielding	A025-TADZ1n to A030-TADZ3nmesh (MP197TAD TO with TN44B – Response function – Neutron)	A025 to A030 for a total of 6
	Shielding	B001-2619.in to B010-TN_2619.out (MP197TAD TO with TN44B – Bounding source – Normal Condition)	B001 to B010 for a total of 10
	Shielding	B011-6226.in to B020-TN_6226.out (MP197TAD TO with TN44B – Bounding source – Accident Condition)	B011 to B020 for a total of 10
	Shielding	C001-TADG to C004-TADNmesh (MP197TAD TO with TN44B – Design basis fuel – Normal Condition)	C001 to C004 for a total of 4

Listing of Disk Numbering and Contents for Computer Files
(all files are Proprietary)

Disk ID No. (size)	Discipline	File Series (topics)	Number of Files
Disk 13 (continued) (DVD) (44.2 MB)	Shielding	C005 - TADGA to C008-TADNAmesh (MP197TAD with TN44B - Design basis fuel – Accident Condition)	C005 to C008 for a total of 4
	Criticality	E001-TADGE12wch1.in to E006-TADABB102wch3.out (MP197TAD with TN44B – 10x10 GE – 0.12" Channel)	E001 to E006 for a total of 6
	Criticality	F001-TADMIC3.in to F006-TADABBA.out (MP197TAD with TN44B – Natural Boron (Type A))	F001 to F006 for a total of 6
	Criticality	G001-TADMICB.in to G006-TADABBB.out (MP197TAD with TN44B – 25% Enriched Boron (Type B))	G001 to G006 for a total of 6
	Criticality	H001-TADMICC.in to H006-TADABBC.out (MP197TAD with TN44B – 35% Enriched Boron (Type C))	H001 to H006 for a total of 6